

**Characterization Of The *Drosophila melanogaster* Atypical Soluble Guanylyl  
Cyclases Gyc-88E, Gyc-89Da, And Gyc-89Db**

by

**Kristofor K. Langlais**

A DISSERTATION

Presented to the Department of Cell and Developmental Biology  
and the Oregon Health & Science University  
School of Medicine  
in partial fulfillment of  
the requirements for the degree of  
Doctor of Philosophy

September 2005

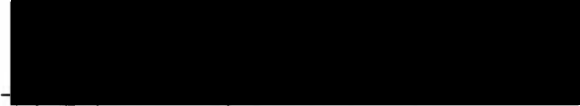
School of Medicine  
Oregon Health and Science University


---


**Certificate of Approval**

---

This is to certify that the Ph.D. Dissertation of  
**Kristofor K. Langlais**  
has been approved

  
David Morton, Ph.D., *thesis advisor*

  
Philip Copenhaver, Ph.D., *committee chair*

  
Michael Forte, Ph.D., *committee member*

  
Doris Kretzschmar, Ph.D., *committee member*

## Table of Contents

Table of contents.....	i-iii
List of figures and tables.....	iv-vii
Acknowledgements.....	viii-ix
Abstract.....	x-xi
<b>Chapter 1: Introduction and historical overview</b>	
I. Foreword .....	1
II. Guanylyl cyclases.....	2
A. Soluble guanylyl cyclases.....	2
1. Isoforms of classic soluble guanylyl cyclase subunits.....	2
2. Structure/modeling and sequence features of classic soluble guanylyl cyclase domains.....	4
a. N-Terminal domain and heme group.....	4
b. Dimerization region.....	8
c. Catalytic domain.....	9
3. Invertebrate soluble guanylyl cyclases.....	12
a. Classic NO-sensitive $\alpha/\beta$ heterodimers.....	12
b. Atypical invertebrate soluble guanylyl cyclases.....	14
4. Conserved and substituted residues in the predicted GTP-binding sites of sGCs.....	21
B. Receptor guanylyl cyclases.....	27
1. Mammalian receptor guanylyl cyclases.....	28
2. Invertebrate receptor guanylyl cyclases.....	31

III. Phosphodiesterases.....	36
IV. cGMP targets.....	40
A. cGMP-dependent protein kinases.....	40
B. cGMP-gated ion channels.....	47
V. Physiological functions/pathways in the nervous system.....	51
A. Phototransduction.....	51
B. Neuronal plasticity: long-term potentiation and long-term depression.....	52
C. Neuronal development.....	52
D. Ecdysis.....	54
E. Food search and feeding behaviors.....	57
F. Chemosensation.....	60
1. Olfaction.....	60
2. Aerotaxis and oxygen sensation in <i>C. elegans</i> and <i>Drosophila</i> .....	65
VI. Questions addressed in this dissertation.....	67

**Chapter 2: Initial cloning, characterization, and biochemical properties of Gyc-88E, Gyc-89Da, and Gyc-89Db**

Introduction.....	69
Methods.....	71
Results.....	76
Discussion.....	99

**Chapter 3: Localization of Gyc-88E, Gyc-89Da, Gyc-89Db expression in the nervous system**

Introduction.....112  
Methods.....113  
Results.....117  
Discussion.....163

**Chapter 4: Functional impairment of neurons and degradation of cGMP in cells that express Gyc-89Da and Gyc-89Db**

Introduction.....172  
Methods.....175  
Results.....181  
Discussion.....209

**Chapter 5: Summary and future directions**

Summary.....221  
Future Directions.....227

**Literature Cited.....231-267**

## List of Figures and Tables

<b>Figure 1.1.</b> Predicted catalytic domain for the soluble GCs.....	11
<b>Figure 1.2.</b> Unrooted phylogenetic tree showing the relationships between $\alpha 1$ , $\alpha 2$ , $\beta 1$ , $\beta 2$ , $\beta 3$ , and other unclassified $\beta$ -like GC subunits.....	17
<b>Figure 2.1.</b> Gene structure and variations of Gyc-88E, Gyc-89Da, and Gyc-89Db.....	79
<b>Figure 2.2.</b> ClustalW sequence alignment of the highly identical regions in the C-terminal extensions of the known Gyc-88E orthologues.....	81
<b>Figure 2.3.</b> Expression of Gyc-88E in larvae and adults.....	82
<b>Figure 2.4.</b> Expression of the atypical soluble guanylyl cyclase subunits throughout development.....	84
<b>Figure 2.5.</b> Guanylyl cyclase activity of Gyc-88E.....	85
<b>Figure 2.6.</b> Kinetic analysis of Gyc-88E-S and Gyc-88E-L.....	87
<b>Figure 2.7.</b> Guanylyl cyclase activity of two truncated versions of Gyc-88E.....	89
<b>Figure 2.8.</b> The NO donor SNP stimulates the activity of Gyc-88E.....	91
<b>Figure 2.9.</b> The NO donor SNAP stimulates the activity of Gyc-88E.....	92
<b>Figure 2.10.</b> Sodium cyanide has no effect on the guanylyl cyclase activity of Gyc-88E or the MsGC- $\alpha$ /MsGC- $\beta$ heterodimer.....	94
<b>Figure 2.11.</b> Guanylyl cyclase activity of Gyc-89Da.....	95
<b>Figure 2.12.</b> Guanylyl cyclase activity of Gyc-89Db.....	97
<b>Figure 2.13.</b> Stimulation of Gyc-88E, Gyc-89Da, and Gyc-89Db by the NO donor SNAP, in the presence of Mg.....	98
<b>Figure 2.14.</b> Heme environment.....	107

**Figure 2.15.** ClustalW sequence alignment of known and putative H-NOX (partial) domains.....110

**Figure 3.1.** Localization of *Gyc-88E* and *Gyc-89Db* expression in the central nervous system of *Drosophila* embryos.....119

**Figure 3.2.** Localization of *Gyc-88E* and *Gyc-89Db* in cells associated with the embryonic peripheral nervous system.....121,122

**Figure 3.3.** *Gyc-88E* and *Gyc-89Db* are expressed in neurons of the peripheral nervous system.....126,127

**Figure 3.4.** *Gyc-88E* expression in the stage 17 embryonic midgut.....129

**Figure 3.5.** *Gyc-89Da* was expressed in a limited pattern in the CNS and in lateral cells that appear to be associated with the PNS in stage 17 embryos.....130,131

**Figure 3.6.** Diagram illustrating the upstream genomic regions used to build promoter::*GFP* and promoter::*GAL4* constructs.....134

**Figure 3.7.** *Gyc-89Da* and *Gyc-89Db* expression in the dorsal and terminal ganglion and other peripheral neurons in the 3<sup>rd</sup> instar larval head segment.....138,139

**Figure 3.8.** Expression of *Gyc-89Da* and *Gyc-89Db* in the lateral PNS of 3<sup>rd</sup> instar larvae.....141,142

**Figure 3.9.** *Gyc-89Da* and *Gyc-89Db* are co-expressed in sensillum-innervating neurons in the larval sensory cones.....144,145

**Figure 3.10.** *Gyc-89Da* and *Gyc-89Db* were expressed in the 3<sup>rd</sup> instar larval CNS and ring gland.....149,150

**Figure 3.11.** *Gyc-89Da* and *Gyc-89Db* were co-expressed with *dimmed* in several cells in the CNS and in the corpora cardiaca cells.....152,153

<b>Figure 3.12.</b> Gyc-89Da and Gyc-89Db are not co-expressed with EH or <i>dimmed</i> anywhere in the 3 <sup>rd</sup> instar larval CNS.....	154,155
<b>Figure 3.13.</b> Gyc-89Da were not expressed in motor neurons while Gyc-89Db is expressed in a subset of motor neurons in 3 <sup>rd</sup> instar larval CNS.....	157,158
<b>Figure 3.14.</b> Gyc-89Db was expressed in the adult labellum, pharynx, and prothoracic leg.....	161,162
<b>Figure 4.1.</b> The RB PiggyBac insertion in line 17991 eliminated the Gyc-89Da transcript in larvae.....	183
<b>Figure 4.2.</b> Survival of animals during development in promoter driven tetanus toxin light chain experiments.....	186,187
<b>Figure 4.3.</b> Defects and other observations associated with p89Da::GAL4 and p89Db::GAL4 driven TNT expression in larvae.....	191,192
<b>Figure 4.4.</b> Normal eclosion behavior of control animals and eclosion failure of p89Da::GAL4, UAS::TNT (active) animals.....	197,198
<b>Figure 4.5.</b> Equipment associated with the hypoxia fleeing assays and yeast dollop-Petri dish configuration.....	200,201
<b>Figure 4.6.</b> Behavioral response of experimental larvae to a 1% oxygen environment over a five-minute time period.....	204,205
<b>Figure 4.7.</b> Hypoxia fleeing assay.....	206,207
<b>Table 1.1.</b> Species code key and database gene designations.....	18
<b>Table 1.2.</b> Conserved and substituted residues in the predicted GTP-binding sites of selected GCs.....	22,23



<b>Table 1.3.</b> Mammalian PDE families and classification of <i>Drosophila</i> predicted PDEs.....	37
<b>Table 3.1.</b> Summary of data from the riboprobe/22C10 double label and double riboprobe experiments.....	123
<b>Table 3.2.</b> Summary of Gyc-88E, Gyc-89Da,Gyc-89Db expression in the peripheral nervous system in larvae and adults.....	146

## Acknowledgements

First and foremost, I thank David Morton, who invited me into his lab and supported my graduate studies and thesis work. David was an excellent mentor, providing me with years of challenge and guidance, which served to hone my skills as a scientist and an independent thinker. My time in the Morton lab has been stimulating and extremely rewarding, and I am lucky to have found such a wonderful place to do my graduate research.

I also thank Martin Hudson, my second mentor and primary antagonist in the Morton Lab. Martin really cared about my success as a student and scientist and supplied his own special brand of encouragement in those first several years.

I thank Judy Stewart, Anke Vermehren, Caitlin Anderson, and Kate Butler for friendship, conversation, advice, and fun times in the lab.

I thank my thesis advisory committee, Philip Copenhaver, Jan Christian, and Michael Forte, for the advice and guidance that aided in the completion my thesis research.

I thank Philip Copenhaver and Karla Kent for mentoring during my rotation projects and beyond, and kindling my interest in insects. They are truly wonderful teachers. I also thank Mark Snyder, Tracy Swanson, and Laura Knittel for friendship and training during my first months at OHSU.

I thank Michael Danilchik for providing training and use of the confocal microscope. I also thank Betsy Brown, Steve Matsumoto, Agnieszka Balkowiec, and the rest of the Integrative Biosciences department for being such a great bunch of people to be around.

I thank all of those spending time to teach me fly genetics, techniques, and tricks, especially: Sarah Smolik, Michael Forte, Bill Wolfgang, Catherine Clay, Joe Weiss, and John Keen.

I thank my parents, Cynthia and Roger Langlais, for support and encouragement, throughout my life and my education.

Finally, I thank my wife Carly, who is my inspiration and my everything. I am forever grateful for her unending support, strength, and love, which guided me to the very end of this endeavor. I could not have succeeded without her.

## Abstract

Eukaryotic organisms utilize two major isoforms of guanylyl cyclase in cGMP signaling: receptor guanylyl cyclases and soluble guanylyl cyclases. Receptor guanylyl cyclases are single transmembrane-spanning proteins that function as homodimers and are activated by either extracellular peptide ligands or intracellular, calcium-regulated guanylyl cyclase activating proteins (GCAPs). Soluble guanylyl cyclases are cytoplasmic hemoproteins that have primarily been thought of as the major receptors for the freely diffusible signaling molecule nitric oxide (NO). NO-sensitive soluble guanylyl cyclases are obligate heterodimers and are composed of an  $\alpha$  subunit and a  $\beta$  subunit. The recent discovery of the *Manduca sexta* MsGC- $\beta$ 3 subunit and related atypical soluble guanylyl cyclase subunits in vertebrates and invertebrates revealed that this family of enzymes is more diverse than previously thought. In contrast to NO-sensitive soluble guanylyl cyclases but consistent with predictions based on sequence features, MsGC- $\beta$ 3 was found to form active homodimers that were not sensitive to NO. The *Drosophila melanogaster* genome was predicted to contain an MsGC- $\beta$ 3 ortholog, named Gyc-88E, and two additional atypical soluble guanylyl cyclases that were named Gyc-89Da and Gyc-89Db. This dissertation describes the cloning and characterization of the three *Drosophila* atypical guanylyl cyclases. Like MsGC- $\beta$ 3, Gyc-88E possesses a number of unusual sequence features that led to the prediction that it would be active as a homodimer and be insensitive to NO. I found that Gyc-88E yielded basal guanylyl cyclase activity in the absence of other subunits, and that this activity was only slightly stimulated by NO, compared to typical  $\alpha/\beta$  heterodimers. Gyc-89Da and Gyc-89Db were predicted to be inactive when expressed alone, which was confirmed biochemically. However, when

Gyc-89Da or Gyc-89Db was co-expressed with Gyc-88E, significantly more basal and NO donor-stimulated activity was observed than when Gyc-88E was expressed alone. The expression patterns of these guanylyl cyclases were characterized in embryos, larvae, and adults using a combination of whole mount *in situ* hybridization and promoter-driven reporter techniques. All three guanylyl cyclases were expressed in a large number of cells in the embryonic and larval CNS, including several peptidergic neurons. Gyc-88E, Gyc-89Da, and Gyc-89Db expression was also found in a number of peripheral neurons that innervate olfactory and gustatory sensilla, as well as trachea and other external sensilla of unknown function. To examine the function of the Gyc-89Da- and Gyc-89Db-expressing neurons, tetanus toxin light chain (TNT) was driven in these cells using the GAL4/ UAS transgene expression system. Guanylyl cyclase promoter-driven TNT expression caused a number of abnormalities during development, including discrete lethal defects during larval and adult ecdysis. Expression of TNT or an exogenous cGMP-specific phosphodiesterase using the promoter-GAL4 constructs also dramatically reduced the larval hypoxia escape response, which is characterized by the cessation of feeding activity and initiation of locomotion and exploratory behavior in response to sudden exposure to hypoxia. The results presented in this dissertation, combined with reports demonstrate that atypical guanylyl cyclases bind and are activated by oxygen rather than NO, support a role for Gyc-88E, Gyc-89Da, and Gyc-89Db as multipurpose oxygen sensors in *Drosophila melanogaster*.

## Chapter 1: Introduction and historical overview

### I. Foreword

Guanosine 3',5' cyclic monophosphate (cGMP) is an intracellular second messenger molecule that is utilized in wide range of signal transduction pathways throughout the animal kingdom. cGMP was first discovered in urine in 1963, soon after the discovery of cAMP. Guanylyl cyclases, which were discovered several years afterwards, are the enzymes that convert guanosine-5'-triphosphate (GTP) to cGMP, while phosphodiesterases convert cGMP to guanosine-5'-monophosphate (GMP). In the 1970's it was established that guanylyl cyclase activity could be found in both the soluble and membrane fractions of cells from various sources. However, only in the 1980's, when molecular biology techniques were developed, could the full diversity of this family of enzymes begin to be characterized. Twenty years later, new and intriguing isoforms of guanylyl cyclase continue to be discovered in a large variety of organisms in a process that has been greatly aided by the completion of numerous genome projects.

An astounding range of processes are mediated or modulated by cGMP pathways. In mammals, cGMP is well known as the primary signal in phototransduction. cGMP also mediates intestinal fluid and electrolyte homeostasis and vascular smooth muscle relaxation, and in the nervous system the NO/cGMP pathway is implicated in long-term potentiation and depression. In invertebrates, cGMP has been shown to play a major role in regulating feeding behaviors/strategies and in the mediation of several aspects of sensory transduction. Additionally, numerous lines of evidence strongly implicate a role for cGMP in the regulation of neuronal development, hormonal release in ecdysis behavior, and malpighian tubule regulation. Recent discoveries in *C. elegans* and

*Drosophila melanogaster* together with the work reported here reveal a new and exciting role for a new class of soluble guanylyl cyclases: direct oxygen sensation leading to acute behavioral modulation.

## **II. Guanylyl cyclases**

### **A. Soluble guanylyl cyclases**

Soluble guanylyl cyclases (sGCs) are hemoproteins that have been primarily thought of as the major receptors for the freely diffusible gaseous signaling molecule nitric oxide (NO), which is generated by the calcium-dependent nitric oxide synthase (NOS) (Bredt and Snyder, 1994). Classic soluble guanylyl cyclases function as obligate heterodimers, consisting of an  $\alpha$  subunit and a  $\beta$  subunit. A key feature of all known soluble guanylyl cyclases is the bound prosthetic heme group, which serves as the binding site for NO. NO binding to the ferrous iron atom in the heme group leads to conformational change and potent enzyme activation. Recent reports have identified a number of mostly invertebrate soluble guanylyl cyclases that exhibit unusual characteristics, such as homodimeric activity, relative insensitivity to NO, and activation by hypoxic environments.

#### **1. Isoforms of classic soluble guanylyl cyclase subunits**

NO-sensitive guanylyl cyclase was originally isolated by several groups from a variety of mammalian sources, such as rat and bovine lung and brain tissue. These studies identified the 73 kDa  $\alpha$ 1 and the 70 kDa  $\beta$ 1 subunits, which were cloned and sequenced (Giuli et al., 1992; Koesling et al., 1990; Koesling et al., 1988; Nakane et al., 1990; Nakane et al., 1988). The mammalian  $\alpha$ 2 subunit and  $\beta$ 2 were subsequently found (in human fetal brain and rat kidney, respectively) with a homology screening approach

(Harteneck et al., 1991; Yuen et al., 1990). It was mistakenly reported that humans also possessed subunits distinct from previously described subunits, named  $\alpha 3$  and  $\beta 3$ , as a follow-up study revealed these to be human  $\alpha 1$  and  $\beta 1$  (Giuli et al., 1993; Zabel et al., 1998). A literature search and BLAST search using the rat  $\alpha 1$  and rat  $\beta 1$  protein sequences reveal that several other vertebrates possess (predicted gene, EST, and/or demonstrated mRNA/protein) a potential NO-sensitive  $\alpha 1/\beta 1$  heterodimer, including the mouse, chicken, cow, pig (Moreno et al., 2005), *Danio rerio* (zebrafish), *Xenopus laevis* (frog), *Tetradon nigroviridis* (spotted pufferfish), *Oryzias latipes* (medaka ricefish), and *Takifugu rubripes* (Fugu pufferfish) (K. Langlais, unpublished observations).

The  $\beta 1$  subunit was identified as the dimerizing partner of both the  $\alpha 1$  and  $\alpha 2$  subunits, with the two heterodimers yielding identical basal catalytic activities, NO-stimulation, and substrate affinity (Russwurm et al., 1998). This finding was surprising because the N-terminal domains of  $\alpha 1$  and  $\alpha 2$  are only weakly homologous. It was later discovered that the  $\alpha 2$  subunit differs from  $\alpha 1$  subunit by interacting with PDZ domains via the C-terminal peptide (Russwurm et al., 2001). Specifically, the  $\alpha 2$  subunit was found to interact with the PDZ-containing protein PSD-95, and was localized to synaptic membranes (Russwurm et al., 2001).

For some time after its discovery, the functional role of the  $\beta 2$  subunit was elusive. Several groups were unable to demonstrate enzyme activity when the  $\beta 2$  subunit was co-expressed with  $\alpha$  subunits, and a heterodimer containing  $\beta 2$  never materialized. Then in 2001, a novel splice variant of this subunit (that possessed a sizable piece of the N-terminus that was apparently missing in the original  $\beta 2$ ) was isolated that yielded NO-stimulated activity in the absence of a second subunit (Koglin et al., 2001). This finding



was surprising though not wholly novel as a  $\beta$  subunit was previously found in the hawkmoth *Manduca sexta* that also yielded activity in the absence of a second subunit (atypical sGC catalytic model discussed below) (Nighorn et al., 1999). This splice variant of  $\beta$ 2 also forms a functional heterodimer with either the  $\alpha$ 1 or  $\alpha$ 2 subunit (Gibb et al., 2003).

## **2. Structure/modeling and sequence features of classic soluble guanylyl cyclase domains**

Classic sGC subunits have been assigned two or three functionally distinct domains: the N-terminal regulatory domain or heme-binding domain, a central domain that is thought (in some reports) to contain most of the region responsible for dimerization, and a C-terminal domain that functions in substrate recognition and catalytic activity (Lucas et al., 2000). The crystal structure of NO-sensitive sGC has not been solved, hindering the understanding of the mechanism of activation and catalysis. However, the crystal structure of adenylyl cyclase, which has many similarities to sGC, has been informative with regard to the catalytic domain.

### **2a. N-Terminal domain and heme group**

The N-terminal domain, which encompasses residues 1-214 in the rat  $\beta$ 1 subunit, is primarily responsible for heme-binding and enzyme regulation. This region displays lower homology with other isoforms, but does contain a number of conserved residues that are important or required for heme-binding and heme-mediated enzyme activation. The heme-group is necessary for the activation of the enzyme by NO. In contrast to other hemoproteins, such as hemoglobin or myoglobin, the heme-group in NO-sensitive sGCs does not bind oxygen. Removal of the heme group abolishes NO-activation of sGC, and

re-introduction of heme rescues activity (Craven and DeRubertis, 1978; Ignarro, 1990). The stoichiometry of heme in soluble GC heterodimers is one heme group per sGC heterodimer (absorbance peak at 431nm), which contains either a Fe<sup>2+</sup> or Fe<sup>3+</sup> ion that is coordinated in the plane of the heme by 4 nitrogen atoms (Brandish et al., 1998). The iron atom is coordinated by histidine-105, which serves as the heme proximal ligand in  $\beta$  subunits (Foerster et al., 1996; Wedel et al., 1994; Zhao et al., 1998). Histidine-105 is required for heme binding and NO-activation (as demonstrated in point mutation studies), and is conserved in all known  $\beta$  subunits to date. Histidine-105 is not conserved in  $\alpha$  subunits, supporting the finding of one heme group per heterodimer. Cysteine-78 and cysteine-214 have also been shown to be important for heme-binding and NO-activation, and are conserved in all  $\beta$ 1 and  $\beta$ 2 subunits known to date (Friebe et al., 1997). Using sequentially truncated  $\alpha$  subunits, it was demonstrated that deletion of the first 259 residues has no effect on heme-binding or NO-activation of the  $\alpha/\beta$  heterodimer (Koglin and Behrends, 2003). However, removal of residues 1-364 resulted in a NO-insensitive heterodimer with intact heme-binding. Hence, it appears that while the  $\alpha$  is not required for heme-binding to the heterodimer, the 259-364 residue region of the subunit is required for NO-sensitivity.

#### *Activation of NO-sensitive sGC by NO*

In the 1970's, NO-releasing compounds were found to be potent activators of soluble GC (Arnold et al., 1977; Bohme et al., 1978). It was also known that NO-producing nitrovasodilators such as glyceroltrinitrate and isosorbide effectively treated coronary heart disease by stimulating sGC (Ahlner et al., 1986). The physiological significance of this activation was unknown however, because a source of NO in the

body was unknown, and it was uncertain that NO was the *in vivo* activator. Then it was discovered that endothelium-derived relaxing factor (EDRF) was in fact NO (Ignarro et al., 1987; Palmer et al., 1987). EDRF was shown to form in endothelial cells in response to various vasodilatory agonists such as histamine and acetylcholine, which led to vasodilation via the activation of soluble GC in smooth muscle. Soon after EDRF was identified as NO, formation of NO was discovered in many other tissue types throughout the body.

The enzyme responsible for the production of NO was then identified and called nitric oxide synthase (NOS) (Bredt et al., 1991). Three isoforms of NOS have been found. The inducible NOS (iNOS) is regulated on the transcriptional level, is constitutively active producing high levels of NO, and is used by macrophages to exert cytotoxic effects in the nonspecific immune response (Lowenstein et al., 1992). Neuronal and endothelial NOS (nNOS and eNOS) are constitutively expressed enzymes that are regulated by intracellular calcium concentrations, catalyzing lower levels of NO compared to iNOS when activated (1 to 100 nmol/L; Janssens et al., 1992; Sessa et al., 1992). NO is not cytotoxic at these levels, and functions primarily to activate NO-activated sGC (Gross and Wolin, 1995).

Of the three redox forms of NO ( $\text{NO}^-$ ,  $\text{NO}^\bullet$ ,  $\text{NO}^+$ ), only the uncharged radical NO form ( $\text{NO}^\bullet$ ) has been shown to significantly activate NO-sensitive GC (Moncada and Higgs, 1995). NO binding to the heme group results in up to 200-fold activation of the enzyme (Humbert et al., 1990; Stone and Marletta, 1994). Activation is initiated when NO binds to the sixth-coordinating position of the heme iron. This leads to the breaking of the iron-histidine-105 bond yielding a five-coordinating nitrosyl-heme complex that

has an absorption maximum of 399nm (Gerzer et al., 1981). The conformational change in the heme group communicates an activating signal to the catalytic domain through an unknown mechanism. Substituting the heme group with the heme precursor protoporphyrin IX results stimulation of the enzyme in the absence of NO. Protoporphyrin IX lacks a central iron atom and does not interact with histidine-105, perhaps mimicking the heme conformation when the NO-histidine-105 bond in the hemoprotein is broken (Ignarro et al., 1982). While carbon monoxide (CO) can bind the heme group, this leads to only poor activation because the iron-histidine is not broken, and a six-coordinated heme iron is achieved with absorbance peak of 424nm (Friebe et al., 1996; Stone and Marletta, 1994).

Several novel substances have been found to activate and sensitize NO-sensitive sGC heterodimers. YC-1, a derivative of benzlindazole, was first reported to be an inhibitor of rabbit platelet aggregation, through the activation of sGC (Wu et al., 1995). The approximately 10-fold activation by YC-1 is not affected by the presence of NO-scavengers. In addition to acting as an NO-independent activator, YC-1 also greatly sensitized sGC to NO, and even turned CO into an effective activator on par with NO. Several YC-1 analog molecules have been found to share these remarkable properties, differing only in the  $EC_{50}$  (Stasch et al., 2002a; Stasch et al., 2001). The possible location of YC-1 binding was examined using a variety of techniques, however, these studies do not agree with each other (Denninger et al., 2000; Russwurm et al., 1998; Stasch et al., 2001). The location of this potential allosteric site remains unclear. Importantly, YC-1 was also found to inhibit various phosphodiesterases (PDEs), likely contributing to increased cGMP levels observed in many YC-1 studies (Friebe et al., 1998; Galle et al., 1999). Another remarkable molecule is Bay 58-2667, which was also found to stimulate

sGC (~40-fold) independently of NO. But in contrast to YC-1, Bay 58-2667 potently activates sGC that has been stripped of heme (~200-fold) and was additive to the effects of NO, rather than causing a potentiating effect to it. These characteristics suggest that Bay-58-2667 substitutes for the heme group or stabilizes an active, heme-free conformation. Both YC-1 and Bay 58-2667 have beneficial therapeutic effects on the cardiovascular system by displaying vasodilatory and anti-platelet abilities (Stasch et al., 2002b).

Two specific inhibitors of sGC have been identified: 1H-[1,2,4]oxadiazolo[4,3-a]-quinoxalin-1-one (ODQ) and the related NS 2028 (oxadiazolo(3,4-d)benz(b)(1,4)oxazin-1-one) (Garthwaite et al., 1995; Olesen et al., 1998). These molecules have been used to effectively inhibit sGC activity in several tissues (Abi-Gerges et al., 1997; Brunner et al., 1996; Garthwaite et al., 1995; Moro et al., 1996). ODQ has also been used in a number of guanylyl cyclase activity experiments to identify heme dependant activation and to distinguish soluble NO-sensitive GC activity from other guanylyl cyclase activity and other effects of NO (Zhao et al., 2000). ODQ interferes with sGC activation by oxidizing the heme iron, rendering it unable to bind a ligand while leaving basal activity completely intact (Schrammel et al., 1996; Zhao et al., 2000).

## **2b. Dimerization region**

The dimerization region has been postulated to occur in a region between the N-terminal heme-binding domain and the C-terminal catalytic domain. This region was first implicated in dimerization by analogy to the dimerization domains of receptor GCs (Wilson and Chinkers, 1995). An immunoprecipitation study that utilized a number of N- and C-terminal constructs identified the rat  $\beta 1$  subunit regions important for dimerization

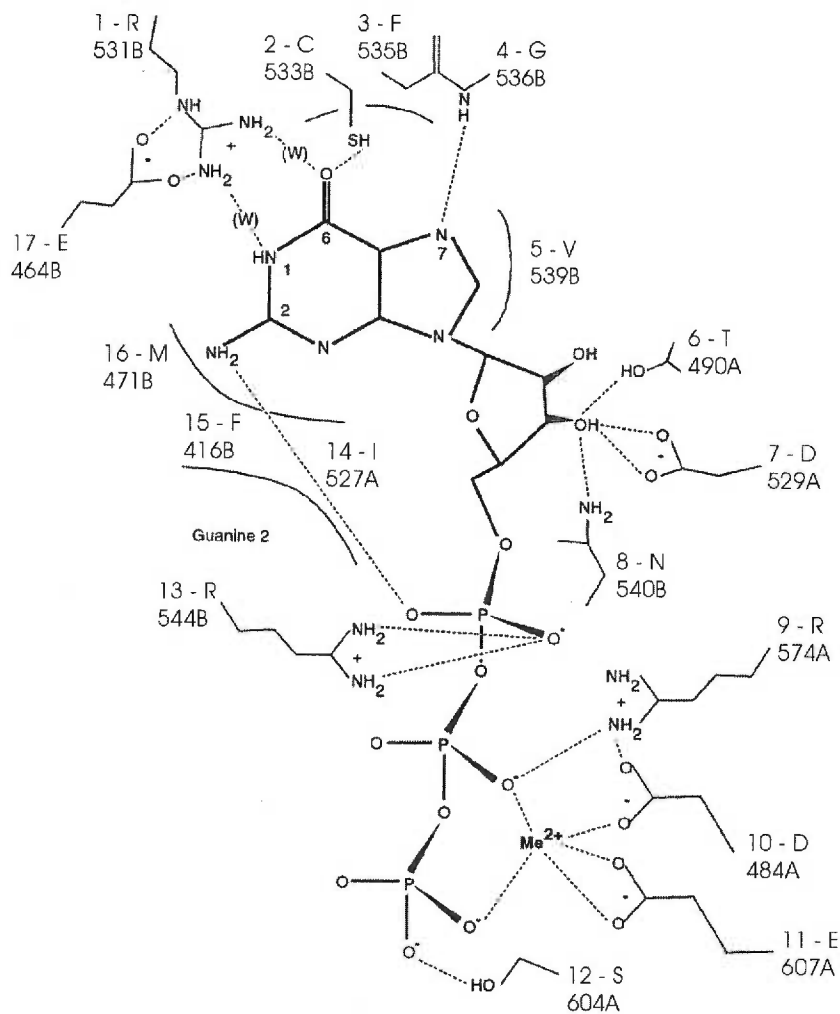
with a partner subunit (Zhou et al., 2004). It was found that a more N-terminal site covering residues 204-244 and a separate more C-terminal site covering residues 379-408 both contribute to dimer formation. It is worth noting that MultiCoil (<http://multicoil.lcs.mit.edu/cgi-bin/multicoil>) predicts with high probability the formation of a coiled-coil motif in the rat  $\beta 1$  subunit including residues ~360-400 (K. Langlais, unpublished observation) (Wolf et al., 1997). A more recent immunoprecipitation study has examined the regions of the  $\alpha$  subunit that are important for dimerization (Wagner et al., 2005). An N-terminal region (residues 61-128) and a central region (residues 367-462) were both found to be required for detectable dimerization. Matching somewhat with these findings, MultiCoil predicts the formation of two coiled-coil motif in the rat  $\alpha 1$  subunit, one with a lower probability spanning residues ~80-120 and one with high probability spanning residues ~400-450 (K. Langlais, unpublished observations) (Wolf et al., 1997). Thus, it appears that multiple regions, in both the regulatory and central “dimerization” domains of both subunit partners participate in dimerization. Another interesting finding in the Wagner study was that stable, heme-containing (but inactive)  $\beta 1$ - $\beta 1$  homodimers do form, while  $\alpha$  homodimers do not form and lone  $\alpha$ -subunits appear to be unstable and targeted for degradation.

### **2c. Catalytic domain**

The catalytic domain is the most conserved domain between the GCs and also shares significant sequence homology with the catalytic domain of adenylyl cyclase (AC), which is a similar enzyme that catalyzes cAMP from ATP in a stereochemically analogous reaction. As the crystal structure of sGC has not been solved, and much of our

understanding of the sGC catalytic domain is taken by analogy from what is known through the crystal structure of mammalian adenylyl cyclase, which has an active heterodimeric form that consists of a C<sub>1</sub> and C<sub>2</sub> subunit (Liu et al., 1997). A C<sub>2</sub>/C<sub>2</sub> homodimer with low levels of activity has also been demonstrated (Zhang et al., 1997a). The active site of AC forms a wreath-like dimer with a catalytic site together with a forskolin binding site in a deep cleft (Zhang et al., 1997b). The adenylyl cyclase active site crystal structure model was utilized in a homology modeling study to predict the structure of the active site in both heterodimeric sGCs and the homodimeric retGC-1 (Liu et al., 1997). Figure 1.1 illustrates the predicted catalytic site including residue-substrate interactions in the MsGC- $\alpha$ 1/MsGC- $\beta$ 1, the insect ortholog of the NO-sensitive sGC heterodimer (Liu et al., 1997; Morton and Hudson, 2002).

In this model, which was reworked by Morton and Hudson (2002) from the Liu et al. (1997) schematic to reflect the amino acid positions in the insect  $\alpha/\beta$  heterodimer, the  $\beta$  subunit (or B strand) binds to the guanosine moiety while the  $\alpha$  subunit (or A strand) binds to the Mg<sup>2+</sup> and triphosphate moieties. In homodimeric adenylyl cyclases or GCs, each subunit possesses all of the interacting residues needed for catalysis, and two active sites are likely formed in one cleft (Liu et al., 1997). In heterodimeric adenylyl cyclases and sGCs, both subunits contribute different critical residues to form one active site. Thus, the residues that contribute to the A strand are not required in the  $\beta$  subunit and the residues that contribute to the B strand are not required in the  $\alpha$  subunit. This model will be important in the discussion of atypical invertebrate sGCs later in this chapter.



from Morton and Hudson, 2002

**Figure 1.1.** Predicted catalytic domain for the soluble GCs. The model for the Mg-GTP binding site is derived from the crystal structure of adenylyl cyclase from Liu *et al.* (1997). The residues that are predicted to be in close association with Mg-GTP are numbered, clockwise from 1-17, starting with the arginine at position 531. The position in either the A strand or B strand is indicated and the amino acid number is given for the *Manduca* sGC, either MsGC- $\alpha$ 1 for the A strand or MsGC- $\beta$ 1 for the B strand.



A hypothetical mechanism of catalysis was proposed by Liu et al. (1997), and has been adopted to match the equivalent MsGC- $\alpha/\beta$  residues for this discussion. The proximity of the MsGC- $\alpha$ 1 D529 (A strand) to the ribose 3' hydroxyl makes it a good candidate to act as the catalytic base. The essential Asn N540, provided by the B strand, is located adjacent to the Asp (D529) and is within range to hydrogen bond with the 3' hydroxyl, suggesting a possible role in stabilizing an oxyanion-like nucleophile. The essential Arg R574 is positioned to stabilize a pentavalent transition state at the  $\alpha$ -phosphate during the nucleophilic hydroxyl attack on the  $\alpha$ -phosphate. The Asn/Arg pair is analogous to the Gln/Arg pair in GTPases, as proposed by Tang *et al.* (1995). Nucleotide substrate specificity is provided (at least in part) by Glu E464 and Cys C533, which interact directly with the guanosine moiety. In adenylyl cyclases, E464 is substituted with Lys, and C533 is substituted with Asp. When these substitutions were made in the mammalian receptor guanylyl cyclase GC-E (RetGC-1), the substrate specificity was changed from GTP to ATP, resulting in a functional adenylyl cyclase that retained the ability to be regulated by the GCAPs, which are the *in vivo* regulators of GC-E (Tucker et al., 1998). This study illustrates the similarity between the catalytic site of guanylyl cyclases and adenylyl cyclases.

### **3. Invertebrate soluble guanylyl cyclases**

#### **3a. Classic NO-sensitive $\alpha/\beta$ heterodimers**

Like the vertebrates, a wide range of invertebrate animals make use of the NO/cGMP pathway. An  $\alpha$  and  $\beta$  subunit from *Manduca sexta* and *Drosophila melanogaster* have been cloned (Liu et al., 1995; Nighorn et al., 1998; Shah and Hyde, 1995), and their sequences are similar to the mammalian  $\alpha$ 1 and  $\beta$ 1 sequences, with the

exception of the *Drosophila*  $\beta 1$  subunit, which has an additional 118 amino acids in the regulatory region that is absent in all other  $\beta$  subunits (Shah and Hyde, 1995). Expression of these subunits in heterologous cells revealed that they display similar biochemical properties with the vertebrate orthologs (Nighorn et al., 1998; Shah and Hyde, 1995). First, the  $\alpha 1$  and  $\beta 1$  subunits were not active when expressed alone, but did yield basal activity when co-expressed, displaying more activity in the presence of  $Mn^{2+}$  than  $Mg^{2+}$ . When NO-donors were applied to the heterodimers, activity was potently stimulated. Consistent with these properties, all of the amino acid residues known to be important for heme-binding, NO-activation, and catalytic activity in the vertebrate sGCs are conserved in the insect sGCs (Morton and Hudson, 2002). A BLAST search using the *Manduca*  $\alpha 1$  and  $\beta 1$  protein sequences reveal that several other insects possess an  $\alpha 1$  and  $\beta 1$  subunit (predicted or EST) and hence the NO/cGMP pathway, including *Drosophila pseudoobscura*, *Anopheles gambiae* (malaria mosquito, the  $\beta 1$  subunit has been cloned; Caccone et al., 1999), *Apis mellifera* (honeybee), and *Gryllus bimaculatus* (cricket) (K. Langlais, unpublished observations).

NO donors and cGMP immunochemistry have been used to map the location of soluble guanylyl cyclases in the nervous systems of several invertebrate species, including *Manduca sexta* (Gibson and Nighorn, 2000; Zayas et al., 2000), *Drosophila melanogaster* (Wildemann and Bicker, 1999), the lobster *Homarus americanus* (Scholz et al., 1998), and the snail *Helix pomatia* (Huang et al., 1998). ODQ, the selective sGC inhibitor (discussed above), reduced or eliminated NO-stimulated cGMP immunoreactivity, suggesting that the source of the cGMP in nervous system results from sGC activity.

### 3b. Atypical invertebrate soluble guanylyl cyclases

The first of several soluble guanylyl cyclases characterized that displayed unusual biochemical and sequence features was the MsGC- $\beta$ 3 subunit, discovered in the hawkmoth *Manduca sexta* using a degenerate primer PCR screen (Nighorn et al., 1999). In contrast to all previously known sGCs, MsGC- $\beta$ 3 was found to be active as a homodimer and was insensitive to NO when expressed in COS-7 cells (Morton and Anderson, 2003; Nighorn et al., 1999). While it showed significant similarity to other  $\beta$  subunits, sequence analysis and multiple sequence alignments of the MsGC- $\beta$ 3 protein revealed a number of unique features that suggested to its discoverers that it be placed into a novel class of sGCs, named the  $\beta$ 3's. The most obvious unusual feature of this sGC is the presence of an additional 315 amino acids tacked on at the N-terminus, after the catalytic domain. At the time, this "tail" stretch of amino acids bore little similarity to any other protein in the databases, although there is a predicted C-terminal isoprenylation site and a number of possible protein phosphorylation sites at various locations (Nighorn et al., 1999). Another very interesting feature of the MsGC- $\beta$ 3 sequence is found in the heme-binding domain. While all previously known sGCs possess Cys-78 and Cys-214 (in the rat  $\beta$ 1), residues found to be required for heme-binding and NO-activation (as discussed above), MsGC- $\beta$ 3 lacks these, consistent with the finding that it is NO-insensitive. MsGC- $\beta$ 3 does however retain histidine-105, the axial ligand for the heme group and conformational change trigger. Co-expression of MsGC- $\beta$ 3 with MsGC- $\alpha$ 1 or protoporphyrin failed to generate NO-sensitivity (Nighorn et al., 1999). YC-1, the heme-independent activator of sGC, also failed to stimulate MsGC- $\beta$ 3, further demonstrating the unusual biochemistry of this subunit (Morton and Anderson, 2003). Comparison of

the MsGC- $\beta$ 3 catalytic region residues to the predicted sGC catalytic domain (Liu et al., 1997) shows that the important residues donated by the  $\alpha$  and  $\beta$  subunits to form the catalytic binding pocket are all conserved in MsGC- $\beta$ 3, suggesting that like receptor GCs, this GC could function as a homodimer (Morton and Hudson, 2002) (discussed in more detail later).

Experiments using hexahistidine-tagged MsGC- $\alpha$ 1, MsGC- $\beta$ 1, and MsGC- $\beta$ 3 subunits demonstrated that MsGC- $\beta$ 3 does form heterodimers with the conventional sGC subunits (Morton and Anderson, 2003). It was also demonstrated, through the use of key point mutations in the catalytic region, that MsGC- $\beta$ 3/ MsGC- $\alpha$ 1 and MsGC- $\beta$ 3/ MsGC- $\beta$ 1 heterodimers were inactive. It was previously demonstrated that the mammalian  $\alpha$ 1 and  $\beta$ 1 subunits form inactive homodimers (Zabel et al., 1999). Additionally, it appears that *Manduca* sGCs can dimerize to *Drosophila* sGCs when co-expressed, with dominant-negative effects (D. Morton, unpublished observations). These interaction/activity studies suggest that sGC subunits freely dimerize with any other subunits that are present, with little or no specificity, even if the result is the formation of a non-functional enzyme.

The function of the MsGC- $\beta$ 3 $\Delta$ 338 residue C-terminus extension was examined by making a deletion mutant that lacked it. The resulting construct, named MsGC- $\beta$ 3 $\Delta$ C338 was then expressed in COS-7 cells and examined for activity (Morton and Anderson, 2003). MsGC- $\beta$ 3 $\Delta$ C338 displayed no activity differences when compared to wild type MsGC- $\beta$ 3, functioning as a NO-insensitive homodimer. However, when the kinetics of MsGC- $\beta$ 3 $\Delta$ C338 activity were examined using several concentrations of GTP substrate, an interesting difference was discovered. MsGC- $\beta$ 3 $\Delta$ C338 had a significantly

lower  $K_m$  than MsGC- $\beta$ 3 in the presence of Mg, while both versions had a similar  $K_m$  in the presence of Mn (Morton and Anderson, 2003). This data suggested that the C-terminal extension may act as an autoinhibitory domain.

The Michaelis-Menton kinetics data also revealed that MsGC- $\beta$ 3 had a Hill Coefficient of 1.0, suggesting that the homodimer only has one GTP binding site, or that the two GTP binding sites act independently of each other (Morton and Anderson, 2003). This was surprising because previously studied homodimeric GCs (receptor GCs) are thought to contain two GTP-binding sites and exhibit kinetics that indicate positive allosteric cooperativity (Lucas et al., 2000). It is notable that the homodimeric mammalian  $\beta$ 2 subunit was also found to exhibit linear Michaelis-Menton kinetics (Koglin et al., 2001).

MsGC- $\beta$ 3 orthologues have been found in other organisms, including several other insect species. These orthologues form a distinct group, separate from  $\beta$ 1 and  $\beta$ 2 subunits in a phylogenetic tree (Fig. 1.2). The *Drosophila melanogaster* gene CG4154, which we later named Gyc-88E after its chromosomal location (Langlais et al., 2004), is over 80% identical to MsGC- $\beta$ 3 (Morton and Hudson, 2002) and is one of the three GCs focused on in the following chapters. Previous to the cloning and characterization work found in this thesis, a predicted Gyc-88E sequence was available from Flybase. Sequence analysis of the predicted Gyc-88E protein revealed that some of the interesting features of MsGC- $\beta$ 3 were present in the fly ortholog. First, Gyc-88E has substitutions in place of the two critical cysteines (Cys-78 and Cys-214) that are critical for NO-activation, but retains histidine-105, the axial ligand for the heme group. A C-terminal tail similar to MsGC- $\beta$ 3 was not predicted for Gyc-88E.

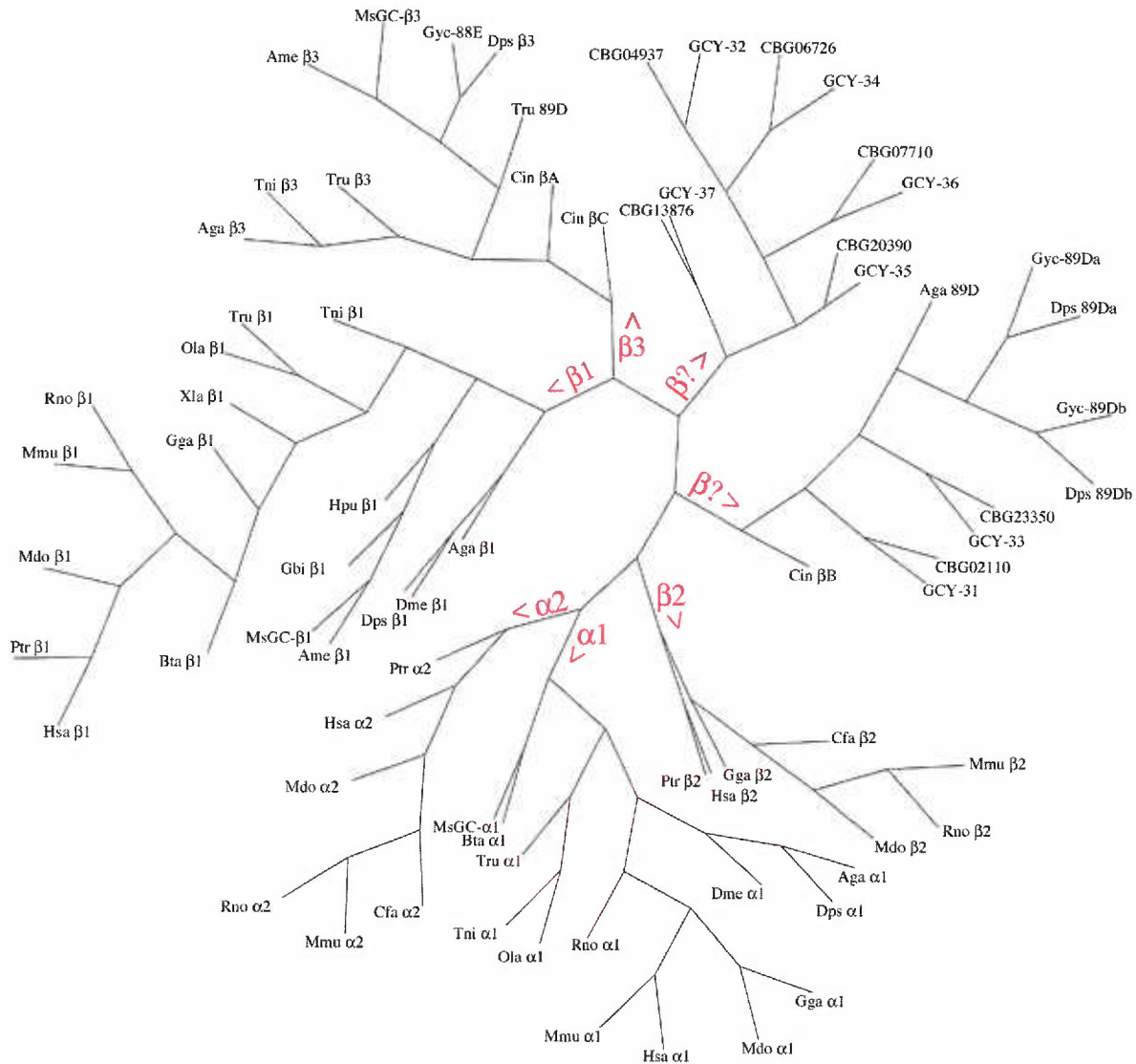


**Figure 1.2.** Unrooted phylogenetic tree showing the relationships between  $\alpha 1$ ,  $\alpha 2$ ,  $\beta 1$ ,  $\beta 2$ ,  $\beta 3$ , and other unclassified  $\beta$ -like GC subunits, generated with ClustalW analysis. Two main branches hold the  $\alpha$  subunits, while five main branches hold the more diverse family of  $\beta$  subunits. The  $\beta 1$ ,  $\beta 2$ , and  $\beta 3$ -like subunits fall into separate groupings, while one unclassified branch contains only nematode  $\beta$  subunits and another unclassified branch holds several nematode and Gyc-89D-like subunits. Many gene designations here have been simplified with a species code and subunit type. Refer to Table 1.1 for species code key and database designations/official gene symbols.

**Table 1.1.** Species code key and database gene designations

Code	Species and common name	GC genes and database designations
Aga	<i>Anopheles gambiae</i> mosquito	$\alpha$ 1=GA15127, $\beta$ 1=Q17010, $\beta$ 3=ENSANGG00000015966, 89D=XP_313866
Ame	<i>Apis mellifera</i> honeybee	$\beta$ 1= XM_392410.1 $\beta$ 3= BAD89804
Bta	<i>Bos taurus</i> cow	$\alpha$ 1= GCYA1_BOVIN, $\beta$ 1= GCYB1_BOVIN
CBG	<i>Caenorhabditis briggsae</i> nematode	CBG04937, CBG06726, CBG07710, CBG20390, CBG23350, CBG02110, CBG13876
GCY	<i>Caenorhabditis elegans</i> nematode	GCY-31, GCY-32, GCY-33, GCY-34, GCY-35, GCY-36, GCY-37
Cin	<i>Ciona intestinalis</i> ascidian, sea squirt	$\beta$ A= Ci0100131817, $\beta$ B= Ci0100142223 $\beta$ C= Ci0100146224
Cfa	<i>Canis familiaris</i> dog	$\alpha$ 2= ENSCAFG00000014739, $\beta$ 2=XP_542553.1
Dme	<i>Drosophila melanogaster</i> fruit fly	$\alpha$ 1=Gyc $\alpha$ -99B", $\beta$ 1=Gyc $\beta$ -100B, Gyc-88E, Gyc-89Da, Gyc-89Db
Dps	<i>Drosophila pseudoobscura</i> fruit fly	$\alpha$ 1=GA15127, $\beta$ 1= GA13187 $\beta$ 3=predicted/assembled from raw nucleotide data (K.Langlais), 89Da=GA13322 89Db=GA13323
Gga	<i>Gallus gallus</i> chicken	$\alpha$ 1= ENSGALG00000009354 $\beta$ 1= ENSGALG00000009361, $\beta$ 2=XP_426684
Gbi	<i>Gryllus bimaculatus</i> field cricket	$\beta$ 1=BAD91320
Hpu	<i>Hemicentrotus pulcherrimus</i> sea urchin	$\beta$ 1=BAB58877
Hsa	<i>Homo sapiens</i> human	$\alpha$ 1= GUCY1A1, $\alpha$ 2 = GUCY1A2, $\beta$ 1= GUCY1B1, $\beta$ 2= GUCY1B2
Mdo	<i>Monodelphus domestica</i> opossum	$\alpha$ 1= Q02108, $\alpha$ 2= Q7T040, $\beta$ 1= Q02153, $\beta$ 2=Q9BI80
Mmu	<i>Mus musculus</i> mouse	$\alpha$ 1= Gucyl1a1, $\alpha$ 2= Gucyl1a2, $\beta$ 1= Gucyl1b1, $\beta$ 2= Gucyl1b2
Ms	<i>Manduca sexta</i> tobacco hornworm	MsGC- $\alpha$ 1, MsGC- $\beta$ 1, MsGC- $\beta$ 3
Ola	<i>Oryzias latipes</i> medaka fish	$\alpha$ 1=BAA19198 $\beta$ 1=BAA19199
Ptr	<i>Pan troglodytes</i> chimpanzee	$\alpha$ 2= GUCY1A2, $\beta$ 1=GUCY1B1, $\beta$ 2=GUCY1B2
Rno	<i>Rattus norvegicus</i> rat	$\alpha$ 1= GCYA1_RAT $\alpha$ 2= Q8R5L4_RAT $\beta$ 1= GCYB1_RAT $\beta$ 2= Q920Q1_RAT
Tni	<i>Tetraodon nigroviridis</i> Spotted pufferfish	$\alpha$ 1= GSTENG00023239001 $\beta$ 1= GSTENG00023239001, $\beta$ 3= GSTENG00011672001 (Note: $\alpha$ 1 and $\beta$ 1 included on same transcript)
Tru	<i>Takifugu rubripes</i> fugu pufferfish	$\alpha$ 1=Q90VV5 $\beta$ 1= Q90VY5 $\beta$ 3= SINFRUG00000143617
Xla	<i>Xenopus laevis</i> African clawed frog	$\beta$ 1=AAH72271

The first and second columns match the species code used in Figure 1.2 with the full species name. Subunits in rightmost column are matched with the GenBank accession code, Ensembl gene ID, Uniprot/SPTREMBL ID, or official symbol.

As discussed in the next chapter, the prediction was incorrect and the experimentally derived Gyc-88E sequence has a C-terminal extension of similar length to MsGC- $\beta$ 3, and shares with it a short, highly identical stretch of residues. Insect MsGC- $\beta$ 3 orthologs have been predicted in the genomes of *Anopheles gambiae* (agCP12881), *Apis mellifera* (Apm- $\beta$ 3, cloned but report unpublished) and *Drosophila pseudoobscura* (not yet annotated, K. Langlais, unpublished observations) (Morton, 2004b). All three of these GCs are highly identical to MsGC- $\beta$ 3 and Gyc-88E, lack the two critical cysteine residues required for NO-activation, retain His-105, and have a lengthy C-terminal extension.

The *Drosophila melanogaster* genome, in addition to the Gyc $\alpha$ -99B ( $\alpha$ 1), Gyc- $\beta$ 100B ( $\beta$ 1), and Gyc-88E genes, was found to possess two more predicted sGCs originally designated CG14885 and CG14886 (Morton and Hudson, 2002), renamed Gyc-89Da and Gyc-89Db respectively after their chromosomal location (Langlais et al., 2004). The characterization of these two GCs, together with Gyc-88E, are the focus of this dissertation. Gyc-89Da and Gyc-89Db are more similar to other atypical  $\beta$  subunits than  $\beta$ 1 or  $\alpha$  subunits. These two genes are located adjacently 2 kb apart in the genome and are highly identical (82%). It is likely that one of these genes is the result of a recent gene duplication of the other. Both of these predicted sGCs have substitutions in place of Cys-78 and Cys-214 and retain Histidine-105. However, Gyc-89Da and Gyc-89Db do not have C-terminal extensions and are similar in length to  $\beta$ 1 subunits (Morton and Hudson, 2002). These genes are about 40% identical to Gyc-88E and under 30% identical to Gyc $\beta$ -100B, and appear to be yet another distinct sGC isoform. A Gyc-89D ortholog has not been found in *Manduca sexta*, but orthologs have been predicted in the genomes of *Anopheles gambiae* and *Apis mellifera* and *Drosophila psuedoobscura*. These subunits



form a distinct grouping, separate from the  $\beta 3$ ,  $\beta 1$ , and  $\beta 2$  groups in a phylogenetic tree (Fig. 1.2). Interestingly, only one Gyc-89D ortholog can be found in *Apis* and *Anopheles* (ebiP3998), while two tandem orthologs are predicted in *D. psuedoobscura*, supporting the notion of a recent gene duplication in a *Drosophila* ancestor. Gyc-89D and its orthologs have all been predicted to be inactive as homodimers, requiring another subunit to complement missing key residues in the catalytic pocket (Morton, 2004b), like  $\beta 1$  subunits (discussed in more detail below).

The family of known soluble guanylyl cyclases became even more diverse with the completion and analysis of the *C. elegans* genome. Seven soluble GCs were predicted to occur, all of them more similar to the  $\beta$  subunits from other organisms (Morton et al., 1999). GCY-32, GCY-34, GCY-35, GCY-36, and GCY-37 form a distinct group in the phylogenetic tree, while GCY-31 and GCY-33 fall into the Gyc-89D grouping (Fig. 1.2). Comparison of these GCs with known NO-sensitive GCs revealed that all seven *C. elegans* sGCs had substitutions in place of the two cysteines that are critical for NO-activation, like MsGC- $\beta 3$ , Gyc-88E, and their orthologs. This observation, taken with the fact that *C. elegans* has no identifiable nitric oxide synthase gene, led to the prediction that these GCs are all NO-insensitive and that *C. elegans* does not utilize the NO/cGMP signaling pathway (Morton et al., 1999). This prediction has not been testable, however, as the *C. elegans* sGCs have not yielded even basal activity when expressed in COS-7 cells, in any pairwise combination or by themselves (Hudson et al., 2000; Morton, 2004b). This is in contrast to insect sGCs, all of which have yielded activity when expressed in COS-7 cells with their proper partners or alone if homodimeric (Morton, 2004b). It will be important to develop a system in which the *C. elegans* sGCs can be

functionally expressed in order to examine the biochemical properties of these interesting invertebrate sGCs. Orthologs of each of the seven *C. elegans* sGCs were found in the recently sequenced *C. briggsae* genome (Fig. 1.2).

#### **4. Conserved and substituted residues in the predicted GTP-binding sites of sGCs**

By consulting the model of interacting residues of the predicted sGC catalytic site (see Fig. 1.1 above), one can make predictions about which subunits would interact, as heterodimers or homodimers, to form an active catalytic/GTP-binding site (Liu et al., 1997; Morton, 2004b). Table 1.2 summarizes the conserved and substituted residues in the predicted GTP-binding sites of selected sGCs from several species. Each subunit in a homodimer or heterodimer contributes critical residues that interact with the GTP substrate. In Table 1.2, *Manduca sexta*  $\alpha$ 1 and  $\beta$ 1 (MsGC- $\alpha$ 1 and MsGC- $\beta$ 1) are used as the model subunits for sequence comparisons. MsGC- $\alpha$ 1 and MsGC- $\beta$ 1 have identical residues in equivalent positions to mammalian  $\alpha$  and  $\beta$  subunits, respectively (Liu et al., 1997; Tucker et al., 1998). In the NO-sensitive *Manduca*  $\alpha$ 1/ $\beta$ 1 heterodimer, the  $\alpha$  subunit has substitutions in place of the  $\beta$  residues, including two residues known to be required for catalytic activity, Asn-540 and Arg-544. Conversely, the  $\beta$  subunit has substitutions in place of several  $\alpha$  residues, including one known to be required for catalytic activity, Asp-484. The *Drosophila melanogaster*  $\alpha$  and  $\beta$  subunits have the same substitutions as MsGC- $\alpha$ 1 and MsGC- $\beta$ 1 respectively, with the  $\alpha$  subunit having one additional substitution at another required residue, Arg-531.

**Table 1.2.** Conserved and substituted residues in the predicted GTP-binding sites of selected GCs. The  $\alpha$  subunits from both *Manduca* and *Drosophila* have identical residues in the equivalent positions to the mammalian  $\alpha$  subunits predicted in models for the catalytic sites (Liu et al., 1997). Similarly, the  $\beta$  subunits residues are also 100% conserved. The MsGC- $\alpha$ 1 and MsGC- $\beta$ 1 subunits are used as the model subunits in this table, and the conserved  $\alpha$  and  $\beta$  subunit residues are shown in bold boxes. Residues shown in bold have been demonstrated to be crucial for GC activity. Residues in other subunits that match the boxed residues are depicted with a “-“, and residues that are different from the boxed residues are depicted with the one letter amino acid abbreviation of what residue is substituted. While the  $\beta$ 1 subunits possess the full complement of the  $\beta$  residues found in mammalian  $\beta$ 1 subunits,  $\beta$ 1 subunits have substitutions in place of several of the conserved  $\alpha$ 1 residues. Similarly, while the  $\alpha$ 1 subunits possess all of the conserved  $\alpha$  residues, they have substitutions in place of several conserved  $\beta$  residues. Hence,  $\alpha$ 1 subunits need to dimerize with  $\beta$ 1 subunits to form an active site. Some subunits, such as the rat- $\beta$ 2 subunit (Rno  $\beta$ 2), Gyc-88E, and MsGC- $\beta$ 3, possess all of the conserved  $\alpha$  and  $\beta$  residues, allowing them to form active homodimers with theoretically two complete active sites. Refer to Table 1.1 for species code key and database designations/official gene symbols.

	$\alpha$ subunit residues	$\beta$ subunit residues
MsGC- $\beta$ 3	- - - - -	- - - - -
MsGC- $\alpha$ 1	<b>D T I D R E</b>	- - C - - T N K
MsGC- $\beta$ 1	G A V - T -	<b>F E M R C N S R</b>
Gyc-88E	- - - - -	- - - - -
Dme $\alpha$ 1	- - - - -	- - C K - T N K
Dme $\beta$ 1	G G V - T -	- - - - -
Gyc-89Da	E Y V M - -	- - - - -
Gyc-89Db	E Y V M - -	- - - - -
Dps $\beta$ 3	- - - - -	- - - - -
Dps 89Da	E Y V M - -	- - - - -
Dps 89Db	E Y V M - -	- - - - -
Aga $\beta$ 3	- - - - -	- - - - -
Aga 89D	E I V K K -	- - - - -
Tni $\beta$ 3	- N - - -	- - - - -
Tru $\beta$ 3	- N - - -	- - - - -
Tru 89D	- - - - -	H - - - G H - A
Cin $\beta$ A	- - - - -	- - - - -
Cin $\beta$ B	- A V - - -	- - - Q - H - K
Cin $\beta$ C	- A V - - -	- - - - - K
GCY-31	- - - - -	- - - - Y N K
GCY-32	- Q V - - -	- - - K - T - Q
GCY-33	R S - E K -	- - - - -
GCY-34	- Q V - - -	- - - - T - Q
GCY-35	- - - - -	- - - - N K
GCY-36	- Q V - - -	- - - - -
GCY-37	- F L - - C	- L L - - K S
Rno $\beta$ 2	- - - - -	- - - - -
DAF-11	- - - - -	Y I C - A I K -
ODR-1	Q N T E - Q	- - - - -

Two  $\beta$  subunit isoforms are predicted to be active as homodimers, like most receptor GCs.  $\beta 2$  subunits, such as the rat  $\beta 2$ , and  $\beta 3$  subunits, such as MsGC- $\beta 3$  and Gyc-88E (examined in chapter 2), possess all of the  $\alpha 1$  and  $\beta 1$  GTP-interacting residues on one subunit (Table 1.2). Backing up these predictions, both the Rat- $\beta 2$  and MsGC- $\beta 3$  have been shown to form functional homodimers (Koglin et al., 2001; Morton and Anderson, 2003; Nighorn et al., 1999). However, it isn't certain that the fish (*Tetroodon* and *Takifugu*)  $\beta 3$ -like subunits would be active as homodimers, as they both have an Asn substitution at the Thr-490 in the  $\alpha$  residue complement (Table 1.2) (K. Langlais, unpublished observations). While Thr-490 has been predicted to interact with the substrate (Fig.1.1), it has not been demonstrated to be crucial for catalysis, so it is still possible that these sGCs could form active homodimers. Also included in Table 1.2 is a predicted *Ciona intestinalis* (primitive chordate, ascidian, sea squirt)  $\beta$  subunit tentatively called Cin  $\beta A$ , also predicted to be functional as a homodimer (K. Langlais, unpublished observations). Cin  $\beta A$  falls into the  $\beta 3$  grouping in the phylogenetic tree (Fig. 1.2).

Another predicted *Takifugu*  $\beta 3$ -like subunit, tentatively named Tru 89D is unusual in that it has several substitutions in place of interacting  $\beta$  residues (including the crucial Asn-540 and Arg-544), and yet it most identical to other  $\beta 3$ -like subunits and falls into that grouping in the phylogenetic tree (K. Langlais, unpublished observations) (Fig. 1.1). It is predicted to form an active GC with the Tru  $\beta 3$ -like subunit and the Tru  $\alpha 1$  subunit (not shown).

Gyc-89Da, Gyc-89Db, and their insect orthologs are similar to  $\beta 1$  subunits in that they have substitutions in place of several interacting  $\alpha$  residues, while all of the interacting  $\beta$  residues are conserved. Similar to the  $\beta 1$  subunits, Gyc-89D subunits are

predicted to be inactive when expressed alone, requiring a subunit partner that has all of the interacting  $\alpha$  subunits. The predicted partners for the insect Gyc-89D-like subunits are the corresponding  $\beta$ 3-like and  $\alpha$  subunits. Despite the prediction that a  $\beta$ 3/ $\alpha$ 1 heterodimer would have a complete binding site and would be catalytically active, it has been demonstrated that while the MsGC- $\beta$ 3 and MsGC- $\alpha$ 1 subunits can heterodimerize, the result is an inactive GC (Morton and Anderson, 2003). Whether or not other  $\beta$ 3-like subunits form active heterodimers with  $\alpha$ 1 subunits is unknown at this time. A *Manduca sexta* ortholog of Gyc-89D has not yet been identified (although one is present in the *Bombyx* genome, K. Langlais, unpublished observation), so this pairing has not been tested. The *Drosophila melanogaster* Gyc-89Da and Gyc-89Db subunits are examined in chapter 2, and the predictions are put to the test.

Two other *Ciona intestinalis*  $\beta$ -subunits are predicted to occur, tentatively named Cin  $\beta$ B and Cin  $\beta$ C (K. Langlais, unpublished observations). Cin  $\beta$ C is more identical to the  $\beta$ 3-like subunits and falls into the  $\beta$ 3 grouping in the phylogenetic tree, despite the predicted functional differences. Cin  $\beta$ B falls into the 89D-like grouping in the phylogenetic tree. Interestingly, these two subunits have several substitutions in place of both  $\alpha$  and  $\beta$  GTP-interacting residues. It would be predicted that even if Cin  $\beta$ B and Cin  $\beta$ C heterodimerized with Cin  $\beta$ A, which has all of the  $\alpha$  and  $\beta$  interacting residues, a non-functional GC would be formed. However, two of the substituted residues in the  $\alpha$  complement, Thr-490 and Ile-527, have not been demonstrated to be crucial for activity, so it is possible these heterodimers could be functional, with Cin  $\beta$ B and Cin  $\beta$ C acting as  $\alpha$  subunits. Additionally, in the Cin  $\beta$ C subunit, the only  $\beta$  residue substituted is the crucial Arg-544. Arg-544 has been substituted with lysine, a functionally conserved

residue, quite possibly allowing it to form an active GC with Cin  $\beta$ A playing the role of a  $\alpha$  subunit.

A similar situation is observed with 3 of the 7 *C. elegans* sGC subunits. GCY-32, GCY-34, and GCY-37 all have several substitutions in place of both  $\alpha$  and  $\beta$  GTP-interacting residues, leading to the prediction that these GCs would be inactive even if they heterodimerized with a subunit that had all  $\alpha$  and  $\beta$  GTP-interacting residues conserved (which *C. elegans* lacks). However, in the  $\alpha$  complement, all three of these subunits have substitutions in place of residues that have not been demonstrated to be crucial for catalytic activity, Thr-490 and Ile-527, like Cin  $\beta$ B and Cin  $\beta$ C. GCY-32 has  $\alpha$  and  $\beta$  substitutions in the same positions as the Cin  $\beta$ B subunit. If Thr-490 and Ile-527 are indeed not necessary for catalysis, then GCY-32, GCY-34, and GCY-37 would be predicted to form active heterodimers with GCY-33 or GCY-36, in which all of the complementing  $\beta$  residues are conserved. GCY-33 and GCY-36, in a more clear-cut prediction, should interact with GCY-31 and GCY-35 to form active heterodimers. GCY-31 and GCY-35 have several substitutions in the  $\beta$  complement of residues (including the critical Arg-544), but have all of the  $\alpha$  complement of residues conserved, like conventional  $\alpha$  subunits. It is also possible that GCY-36 forms active homodimers, since the only GTP-interacting residues that are not conserved are again the Thr-490 and Ile-527 in the  $\alpha$  complement. Confirming one of these predictions, it has been demonstrated genetically that GCY-35 and GCY-36 form heterodimers, with GCY-35 acting as an  $\alpha$  subunit and GCY-36 acting as a  $\beta$  subunit (Cheung et al., 2004). A critical aspartate residue that is thought to act as the catalytic base in  $\alpha$  subunits (Asp-529 in Fig. 1.1) and a critical asparagine residue in  $\beta$  subunits that is thought to stabilize an oxyanion-like

nucleophile (Asn-540 in Fig. 1.1) were point mutated separately in GCY-35 and GCY-36, and tested for the ability to rescue a feeding behavior phenotype in mutants (Cheung et al., 2004). A GCY-35 mutant with a substituted  $\alpha$  Asp-529 residue was not able to rescue the phenotype in a GCY-35 mutant background, while a GCY-36 mutant with this substitution was able to rescue the phenotype in a GCY-36 mutant background. Conversely, a GCY-35 mutant with a substituted  $\beta$  Asn-540 residue was able to rescue the phenotype in a GCY-35 mutant background, while a GCY-36 mutant with this substitution failed to rescue the phenotype in a GCY-36 mutant background. These experiments support an  $\alpha$ -like subunit role for GCY-35 and a  $\beta$ -like subunit role for GCY-36 in a heterodimeric sGC complex that regulates a feeding behavior.

It will be very interesting to see if the other predictions hold true, and to see if Thr-490 and Ile-527 really are necessary for activity. The development of a cell culture system that generates active *C. elegans* sGCs will greatly facilitate the biochemical study of these atypical sGCs.

## **IIB. Receptor guanylyl cyclases**

The second major family of guanylyl cyclases, the receptor guanylyl cyclases (rGCs), are single transmembrane-spanning proteins that function as dimers and are activated by either extracellular peptide ligands or intracellular, calcium-regulated guanylyl cyclase activating proteins (GCAPs). Receptor guanylyl cyclases, which exist as several isoforms, have been found to occur throughout the vertebrate and invertebrate phyla. While the structure, ligand-activation, and physiological functions of several mammalian rGCs have been characterized in detail, the invertebrate rGCs remain largely understudied.



## 1. Mammalian receptor guanylyl cyclases

Seven isoforms of receptor guanylyl cyclase have been identified in mammals, named GC-A through GC-G. All mammalian receptor guanylyl cyclases share a basic topology, which consists of an extracellular ligand-binding domain, a transmembrane domain, a kinase-like domain, a hinge domain, and a C-terminal intracellular catalytic domain. GC-C, GC-E, and GC-F also possess a C-terminal tail. Based on the ligand specificities of the extracellular domain, the rGCs have been classified as natriuretic peptide receptors (GC-A and GC-B), intestinal peptide-binding receptors (GC-C), and orphan receptors (GC-D, GC-E, GC-F, and GC-G). Functional expression experiments, catalytic sequence analysis, and other interaction studies show that rGCs function as homodimers, in contrast to classic soluble GCs.

GC-A binds to and is activated by atrial natriuretic peptide (ANP) and B-type natriuretic peptide (BNP), while the primary ligand and activator of GC-B is C-type natriuretic peptide. ANP begins as a prepro-polypeptide of 151 amino acids in which the C-terminal segment contains biologically active sequences (Inagami et al., 1987). The active form of ANP is the mature 28-residue peptide which consists of a 17-residue loop that is stabilized by a single interchain disulfide bridge and N- and C-terminal extensions, all of which are required for biological activity. The active form of BNP is a 26-residue peptide that has the same structure as the bioactive ANP. CNP is a 22-residue peptide that also contains the 17-residue disulfide bond-stabilized loop like ANP and BNP, but is missing a C-terminal extension and possesses different N-terminal residues.

GC-C binds to and is activated by heat-stable enterotoxins and the structurally similar guanylin and uroguanylin. Heat-stable enterotoxin is produced by the bacteria that colonize the intestine, including *Escherichia coli*, *Enterobacter* sp., *Klebsiella* sp., and

*Yersinia enterocolitica* (Rao et al., 1979). This peptide possesses 6 cysteine residues that form 3 interchain disulfide bonds that stabilize the biologically active tertiary structure and confer the heat stable property (Guerrant et al., 1980).

Extracellular ligands have not been identified for the rGCs termed the orphan rGCs. Even though GC-E is considered an orphan receptor, its role and regulation in visual transduction has been studied in great detail (Lucas et al., 2000). In this process, the activity of GC-E is regulated by the intracellular, EF hand calcium-binding guanylyl cyclase activating proteins (GCAPs) (Palczewski et al., 2000). Three GCAPs have been discovered in mammals, named GCAP1, GCAP2, and GCAP3, which are expressed in the rods and/or cones and are thought to be permanently associated with retinal rGCs. When the intracellular calcium concentration drops during phototransduction, GCAPs assume an active form and interact with the rGC kinase-like and catalytic domains, causing GC activation. Less is known about GC-F, which is expressed with GC-E in retinal cells (and is also regulated by GCAP2 and GCAP3), and GC-G, which is expressed in skeletal muscle, lung, and intestine. The extracellular domain of GC-G is homologous to the natriuretic rGC extracellular domains, raising the possibility that its ligand is similar to the natriuretic peptides (Schulz et al., 1998).

The catalytic domain of rGCs is related to and shares significant homology with the catalytic domains of sGCs and adenylyl cyclases. The GC catalytic site model discussed above (Fig. 1.1) also applies to the rGCs and can be used to make dimer activity predictions. CG-A possesses all of the residues predicted to interact with GTP, including the residues known to be critical for catalysis. Thus, GC-A is predicted, and has been shown to be active as a homodimer (Garbers, 1990). All of the other mammalian

rGCs also possess all of the predicted GTP-interacting residues and are predicted to form active homodimers. GC-B, GC-C, GC-D, GC-E, GC-F, and GC-G all yielded at least basal activity when expressed in a heterologous cell expression system in the absence of other subunits (Schulz et al., 1990; Schulz et al., 1989; Schulz et al., 1998; Yang et al., 1995; Yang and Garbers, 1997). Similar to homodimeric soluble GCs such as MsGC- $\beta$ 3 and the rat  $\beta$ 2 GCs, mammalian receptor GCs are predicted to contain two active GTP-binding sites because each subunit in the dimer possesses the full complement of A strand and B strand GTP-interacting residues (Figure 1.1 and Table 1.2), allowing two complete separate active sites to form. In contrast, heterodimeric soluble  $\alpha/\beta$  GCs contain only one GTP-binding site because the  $\alpha$  subunit possesses all of the A strand residues but is missing some of the B strand residues, while the  $\beta$  subunit possesses all of the B strand residues but is missing some of the A strand residues. The result of this is the formation of one complete catalytically active site and one psuedo-site, that may bind nucleotides but cannot cyclize them. In the case of the heterodimeric adenylyl cyclases, this psuedosite binds molecules that regulate the enzyme activity, such as forskolin. Soluble GCs exhibit linear Michaelis-Menton kinetics with Hill coefficients of 1.0, consistent with the existence of one active site (Chrisman et al., 1975; Garbers, 1979; Wolin et al., 1982). In contrast rGCs exhibit curvilinear Michaelis-Menton kinetics with Hill coefficients of  $>1.0$ , indicating the existence of two catalytic sites that interact in a positively cooperative manner (Wong et al., 1995).

Ligand binding to the extracellular domain of GC-A, GC-B, and GC-C greatly stimulates GC activity. Presumably, ligand binding results in a conformational change that is transduced to the catalytic domain, perhaps shifting key residues to more effective

relative positions. However, the specific conformation changes that occur in this process are completely unknown at this time.

## **2. Invertebrate receptor guanylyl cyclases**

While an impressive number of rGCs are predicted to occur in the genomes of a wide range of invertebrates, thanks to numerous genome projects, relatively few of these have been cloned and characterized. In arthropods, at least 6 distinct isoforms appear to occur. BLAST analysis of the *Drosophila melanogaster* genome revealed 6 genetic loci that are predicted to code for rGCs (Morton, 2004b). *Anopheles gambiae* is predicted to have an ortholog to each of these, and whole cDNAs or cDNA fragments of some of these rGCs have been isolated in other arthropods (for review see Morton, 2004). Structurally, all of these arthropod rGCs have same overall similarities to mammalian rGCs, with an extracellular domain that may bind ligands, a single transmembrane domain, a KHD domain, a dimerization domain, and a highly conserved catalytic domain that lies at the C-terminal end (Morton, 2004b; Morton and Hudson, 2002). Analysis of the catalytic domain residues revealed that these arthropod rGCs should form active homodimers (Morton, 2004b; Morton and Hudson, 2002). In terms of sequence similarities/identity to the mammalian rGCs (BLAST analysis), the *Manduca sexta* rGC MsGC-II is most closely related to GC-F, while the other 5 are most closely related to GC-A or GC-B. The extracellular domains in rGCs share little similar to each other (within a given organism and across species), which makes direct sequence identity comparisons of little value when considering possible activators and cellular function. However, the characterization of specific sequence features of a family of ligand-binding

domains related to the ANP binding domain enables one to identify possible ANP binding domains in the extracellular portion of other proteins (Morton, 2004b). All of the arthropod rGCs, except for MsGC-II, have a predicted ANP-like binding domain in the extracellular portion (Morton, 2004b), which is consistent with the BLAST analysis finding that these rGCs are most similar to GC-A or GC-B, which bind ANP, BNP, and/or CNP. While insects do not appear to have peptides that are similar (in terms of sequence identity) to ANP, there exists several peptides that are proposed to be possible ligands for these rGCs (Morton and Hudson, 2002). Two of the *Drosophila melanogaster* natriuretic receptor-like rGCs have been cloned and their expression patterns characterized, but no biochemical studies were carried out (Gigliotti et al., 1993; Liu et al., 1995; McNeil et al., 1995). These rGCs remain classified as orphan receptors.

Clear evidence of a specific ligand/rGC interaction has been found in crustaceans. A peptide hormone called crustacean hypoglycemic hormone (CHH) has been shown to activate a rGC in lobster muscle (Goy, 1990). Additionally, crab neurohemal gland extracts that contain a peptide similar to CHH elevated cGMP levels in a specific subset of neurons in the stomatogastric nervous system. A full length rGC from crayfish muscle and a fragment of a similar rGC from blue crab Y organ are most similar to the *Drosophila* Gyc76C and its *Manduca* ortholog (Hazelett and Weeks, unpublished data/sequence), both of which were also found to be expressed in muscle tissue (McNeil et al., 1995). CHH-like peptides are also found in insects, but it remains to be seen if these peptides interact with and activate any insect rGCs (Morton and Hudson, 2002).

The insect rGC that does not contain a predicted ANP-binding site, the *Manduca sexta* MsGC-II, has been studied in some detail. MsGC-II was found to be expressed in

the several regions of the central nervous system and is most similar to a retinal GC (GC-F), which is regulated by intracellular calcium sensing proteins (Morton and Nighorn, 2003). Transient expression in COS-7 cells generated guanylyl cyclase activity that was inhibited by high levels of calcium, in the absence of exogenous calcium binding proteins. When the mammalian guanylyl cyclases activating protein 2 (GCAP2) or the *Drosophila melanogaster* frequenin (an insect neuronal calcium sensing protein) was added to the assay, in the presence of low calcium levels, an increase in the level of activity was observed. Thus, the regulation of MsGC-II activity shares similarities to the regulation of GC-E and GC-F activity, namely, by calcium levels and calcium binding proteins.

The *Manduca sexta* MsGC-I is an unusual GC found during the degenerate PCR screen that identified MsGC- $\beta$ 3 in the nervous system (Nighorn et al., 2001; Simpson et al., 1999). The primary amino acid sequence of MsGC-I revealed that it is most closely related to receptor guanylyl cyclases, but it lacked the extracellular and transmembrane domains. Specifically, the dimerization and catalytic domains showed greater than 75% similarity to the mammalian GC-B (Simpson et al., 1999). Northern and Western blots demonstrated a transcript and protein size that is consistent with the isolated cDNA, showing that MsGC-I is a bonafide transcript and not a cloning artifact. Transient transfection in COS-7 cells showed that MsGC-I likely forms homodimers, as it is active in the absence of other subunits and present in the soluble fraction of COS-7 cells, as expected of a protein lacking a transmembrane domain. Gel filtration data confirmed the formation of homodimers. It appeared that *in vivo*, MsGC-I interacted directly or indirectly with a membrane-bound protein, as it was located in the particulate fraction of

CNS homogenates (Simpson et al., 1999). Orthologues of MsGC-I or MsGC-I-like GCs appear to exist in other invertebrates and in mammals. Searches of the annotated genome *C. elegans*, *Drosophila melanogaster*, and *Anopheles gambiae* identified predicted receptor-like guanylyl cyclases that lacked extracellular and transmembrane domains, although none of these have been confirmed through cloning (Morton, 2004b). In the rat, a receptor-like GC that lacked a transmembrane domain was isolated and named ksGC. The ksGC transcript appeared to be alternatively spliced variant of GC-G (Kojima et al., 1995). A subsequent report suggested ksGC was an artifactual truncation of CG-G and not a true splice variant, although Northern blots from both reports show both a large band that represents GC-G and smaller bands that could represent the soluble form (Kojima et al., 1995; Schulz et al., 1998). Supporting the presence of this form of GC in rodents, two mouse cDNAs were found in a GenBank search that appear to code for mouse versions of ksGC that also lack the extracellular and transmembrane domains (Morton, 2004b). Thus it seems possible that the MsGC-I isoform is widespread throughout the animal kingdom.

Despite its relatively small size, the genome of *C. elegans* contains an astounding 25 predicted rGCs, compared to the 7 isoforms found in vertebrates and 6 identified so far in arthropods (Morton, 2004b). These rGCs also share the same primary structural characteristics with other rGCS (Morton, 2004b). However, analysis of catalytic domain residues revealed that many (but not all) of the *C. elegans* rGCs are likely to be inactive as homodimers, requiring a different subunit partner to form a complete catalytic site, in contrast to all other known or predicted rGCs but similar to classic sGCs (Morton, 2004b). An example of possible subunit heterodimerization is observed with two of these

rGCs, DAF-11 and ODR-1. DAF-11 has all of the residues contributed by typical  $\alpha$  subunits (A strand), but has substitutions in place of several of the residues contributed by typical  $\beta$  subunits (B strand), including some that have been shown to be crucial for catalytic activity (see Table 1.2). ODR-1 on the other hand, has all of the residues contributed by typical  $\beta$  subunits, but has substitutions in place of several  $\alpha$  subunit residues. Only when these two subunits form a dimer together should a complete active site be formed. Evidence of heterodimerization *in vivo* and participation in the same pathway does exist with DAF-11 and ODR-1. Both DAF-11 and ODR-1 were found to be expressed in AWC chemosensory neurons, although both are found other non-overlapping locations (Birnby et al., 2000; L'Etoile and Bargmann, 2000). Importantly, a phenotype of DAF-11 mutants overlaps with the phenotype of ODR-1 mutants, namely defective chemotaxis to several odorants sensed by the AWC neurons (L'Etoile and Bargmann, 2000). Interestingly, DAF-11 mutants are also defective in regulated dauer formation (an alternate developmental stage; Riddle et al., 1997) while ODR-1 mutants are not, indicating that ODR-1 may also form heterodimers with another subunit in other cells to regulate dauer formation. Biochemical studies using a heterologous cell expression system are needed to clearly demonstrate the requirement of ODR-1 and DAF-11 co-expression to generate guanylyl cyclase activity.

Functional or biochemical studies have not been published for any of the other *C. elegans* rGCs. However, the expression patterns of all the rGCs have been mapped with green fluorescent protein (GFP) that was driven in worms with the non-coding sequence that lies 5' of the open reading frame (the predicted promoter) of each rGC. Using this method, many of the *C. elegans* rGCs in addition to DAF-11 and ODR-1 were found to



be expressed in a small number of chemosensory neurons, with several of these co-expressed in the same cells (Yu et al., 1997). Clearly we have only scratched the surface of guanylyl cyclase function and regulation in *C. elegans*.

### **III. Phosphodiesterases**

The duration and amplitude of cGMP levels in a cell are regulated by guanylyl cyclases, which catalyze its formation, and cyclic nucleotide phosphodiesterases (PDEs), which catalyze its degradation to GMP. PDEs are a diverse family of enzymes that are regulated by a variety of interactions, with members that can both control the levels of cGMP and act as downstream effectors in the cGMP pathway. Different combinations of PDEs and GCs expressed in a given cell could provide a wide range of temporal cGMP regulation strategies in order to control both very rapid and very slow processes.

Eleven different PDE gene families have been identified in mammalian tissues thus far, differing in their substrate specificity and regulatory domains (Table 1.3) (Morton and Hudson, 2002; Rybalkin et al., 2003). PDE families 1, 2, 3, 10, and 11 display no specificity towards cAMP or cGMP, and are regulated by a cGMP-binding domain (GAF), or a calcium/calmodulin-binding domain (PDE 1 only). A specific regulatory domain has not been identified in the PDE3 family. PDE families 4, 7, and 8 are specific for cAMP, and are regulated by upstream conserved regions (UCRs) (PDE4) or a PAS (Per, ARNT, and Sim proteins) domain (PDE 8). A specific regulatory domain has not been identified in the PDE 7 family. Finally, PDE families 5, 6, and 9 are specific for cGMP, and are regulated by GAF domains (PDE5 and 6). A specific regulatory domain has not been identified in PDE family 9.

**Table 1.3.** Mammalian PDE families and classification of *Drosophila* predicted PDEs

PDE family	Substrate specificity	Regulatory domains	Regulation by cGMP	<i>Drosophila</i> orthologs
1	cAMP/cGMP	Ca/CAM	-	CG14940
2	cAMP/cGMP	GAF	Stimulation	-
3	cAMP/cGMP	-	Inhibition	-
4	cAMP	UCR1 and 2	-	Dunce
5	cGMP	GAF	Stimulation	CG10231*
6	cGMP	GAF	-	CG8729**
7	cAMP	-	-	-
8	cAMP	PAS	-	CG5411
9	cGMP	-	-	CG1627, CG3765
10	cAMP/cGMP	GAF	-	
11	cAMP/cGMP	GAF	-	CG8729* CG10231**

The substrate specificities for the mammalian PDEs are given and are classified into three classes: cAMP specific, cGMP specific, and those with no substrate specificity (Francis et al., 2001). The regulatory domains include the calcium/calmodulin-binding domain (Ca/CAM), the cGMP binding domain (GAF), the upstream conserved regions (UCR1 and 2), and the PAS domain (named after the Per, ARNT, and Sim proteins). *Drosophila* PDE homologue assignments differ slightly depending on method of comparison (genes in disagreement indicated with asterisks). Morton and Hudson (2002) used BLAST analysis for PDE family placement (single asterisk). Day et al. (2005) compared sequence similarity and the presence of certain important sequence features (double asterisk).

Until very recently, only one *Drosophila* PDE, Dunce, had been cloned and studied. Genome analysis revealed the presence of 6 more loci that were predicted to encode for PDEs (Morton and Hudson, 2002). BLAST analysis placed each of these predicted PDEs into one of the 11 PDE families (Morton and Hudson, 2002; Table 1.3). Dunce (mutant displays defects in learning and memory) and CG5411 appeared to be specific for cAMP, falling into PDE families 4 and 8 respectively. CG14940 and CG8729 are predicted to show no substrate specificity as they fall into PDE families 1 and 11 respectively. CG10231, CG1627, and CG3765 were predicted to be specific for cGMP as they fall in PDE families 5, 9, and 9 respectively. The recent report from the Davies lab described ESTs or a cloned cDNA for 5 of these predicted PDEs, confirming their expression in *Drosophila* (Day et al., 2005). This report also confirmed biochemically that CG14940 and CG8729 hydrolyze both cAMP and cGMP as predicted by their orthology. CG10231, which the Davies group considered more PDE11-like than PDE5-like, (using percent similarity and the presence of important sequence features, rather than BLAST analysis) also hydrolyzed both cAMP and cGMP, supporting their classification of this PDE. They failed to measure significant activity from the other two PDEs examined.

At least two other studies support the existence of different PDE family members in insects, with varying cyclic nucleotide specificities and regulatory mechanisms. In *Hyalophora cecropia* (silkworm) fat body and *Manduca sexta* CNS, distinct cAMP and cGMP phosphodiesterase activities were observed (Albin et al., 1975; Fallon and Wyatt, 1977). Also, extracts from *Drosophila* heads yielded two distinct PDE activities, with one that was abolished in *dnc* (Dunce, experimentally shown to be a cAMP specific PDE)

mutants and one that remained that was activated by calcium and calmodulin (Solti et al., 1983).

GAF domains (named after the cGMP-binding PDEs, the *Anabaena* adenylyl cyclase, and the fh1A domain) are found in several of the PDE families. These domains form allosteric binding sites for cGMP at locations separate from the catalytic cGMP binding site (Soderling and Beavo, 2000). In PDE5, GAF domains bind cGMP, leading to stimulated PDE activity and invoking a negative feedback loop. Two cGMP-binding GAF domains are found in PDE5 that were found to be required for its phosphorylation by both cAMP-dependent protein kinases (PKAs) and cGMP-dependent protein kinases (PKGs) (Turko et al., 1998). PDE5 phosphorylation increases catalytic activity (Corbin et al., 2000). When cGMP levels start to rise in a cell, cGMP first binds to the catalytic site, which allosterically increases the affinity of the GAF domains for cGMP. The binding of cGMP to the GAF domains causes a conformational change that exposes the PDE5 phosphorylation site to PKA and PKG (which is also activated by cGMP), allowing phosphorylation. This phosphorylation results in increased PDE activity that drives the concentration of cellular cGMP back to basal levels (Corbin et al., 2000). PROSITE and sequence analysis shows that both CG10231 and CG8279 contain two complete GAF domains and the specific serine residue that is phosphorylated during cGMP-mediated PDE stimulation (Morton and Hudson, 2002). Like PDE5, CG10231 and CG8279 likely act as both cGMP-specific PDEs and downstream effectors that are also regulated by cGMP and possibly PKG.

A big gap in the knowledge of cGMP regulation and function exists in *Drosophila* and in the invertebrate world in general, as most research has focused on guanylyl

cyclases and the synthesis of cGMP. As we can see from vertebrate PDE studies, we may be missing half the story focusing only on the regulation of cGMP synthesis. It will be extremely interesting to see how PDEs factor into the regulation of cGMP signalling in invertebrates and in *Drosophila* in particular.

#### **IV. cGMP targets**

##### **A. cGMP-dependent protein kinases**

In addition to the PDEs, there are two more major protein families that are known to act as cGMP receptors, which are characterized by having defined cyclic nucleotide binding sites. These families are the cGMP-dependent protein kinases, or PKGs, and the cGMP-gated ion channels. A recent review reported on the results of a Protein family (Pfam) database search for cyclic nucleotide (cNMP) binding sites in insects (Morton and Hudson, 2002). 17 unique protein sequences were found, and all but one (a voltage and cyclic nucleotide-gated channel in *Heliothis virescens*) came from *Drosophila melanogaster* databases. In summary, two PKA regulatory subunits, three PKG regulatory proteins, nine ion channels, two cAMP-dependent guanine exchange factor-like proteins, and one other protein were found to contain one or more cyclic nucleotide binding sites. The last one was the product of the *swiss cheese* (*sws*) gene (Kretzschmar et al., 1997), which has three N-terminal cNMP binding domains that share similarities to the cNMP binding domains in both PKA (Kretzschmar et al., 1997) and PKG (Morton and Hudson, 2002). The relative affinities for cAMP and cGMP of the *sws* protein product are not known. *Sws* mutants show age-dependent neurodegeneration, and one of *sws* alleles contains a point mutation that results in a substitution in the cNMP binding site at a residue that is present in all 17 insect cNMP binding sites, indicating the

functional importance of this site. The *sws* protein product may represent an additional target for cGMP.

Two structurally distinct families of cyclic nucleotide-activated protein kinases exist both in mammals and in insects. One family is specifically activated by cGMP while the other is activated only by cAMP. These families differ by more than just cyclic nucleotide specificity, which is governed by several key residues at the binding site. cAMP-dependent protein kinases are tetrameric proteins that are composed of two catalytic subunits and two cAMP-binding subunits, while cGMP-dependent protein kinases are homodimers, with each monomeric subunit containing both the catalytic and cGMP regulatory domains (Scott, 1991). Cyclic nMP binding to the regulatory domain leads to kinase activation and transfer of the  $\gamma$ -phosphate from ATP to a serine or threonine residue on the target protein.

In addition to holding two cNMP binding sites, the N-terminal domain of PKGs contain 5 other regulatory sites: the subunit dimerization site (which consists of an  $\alpha$ -helix with a conserved leucine/isoleucine heptad repeat), several autoinhibitory sites (which inhibit the enzyme in the absence of cGMP), several autophosphorylation sites (which increase basal activity in the presence of cGMP), a site that regulates the affinity and cooperative behavior of the cGMP binding sites, and finally an intracellular localization site, which determines the interaction of the enzyme with particular subcellular structures. The catalytic domain, which is located at the C-terminus of PKGs, contains the binding sites for  $Mg^{2+}$ -ATP and the target protein (Lincoln et al., 2001; Lucas et al., 2000; Pfeifer et al., 1999).

Two PKG genes have been identified thus far in mammals. One gene encodes for two (alternatively spliced) isoforms of PKG (Tamura et al., 1996), while the other encodes for PKG II (Orstavik et al., 1996). PKG I was shown to exist as a cytosolic 76-kDa homodimer that is expressed in many tissues, particularly in cerebellum, platelet, and smooth muscle (Lohmann et al., 1997). The two isoforms of PKG I have different N-terminal domains, conferring different binding affinities for cGMP. PKG II was shown to be an 86-kDa membrane-bound homodimer. The main sequence differences between PKG I and PKG II occur in the N-terminal region, and one of these differences is responsible for subcellular localization. PKG I contains an acetylated site, while PKG II contains a myristoylated site that causes it to be anchored in membranes (Lohmann et al., 1997). PKG II is absent from the cardiovascular system but is abundant in brain and intestine, and is also found in lung, kidney, and bone (Jarchau et al., 1994; Lohmann et al., 1997).

cGMP-dependent protein kinase activity has been demonstrated to occur in a wide range of insect tissues indicating that these enzymes are utilized throughout the insect world. Examples include *Hyalophora cecropia* body wall and fat body (Filburn et al., 1977), fat body from *Antheraea polyphemus*, *Manduca sexta*, and the cockroach *Blaberus discoidalis* (Kuo et al., 1971), eggs and pupae from *Bombyx mori* (Kuo and Greengard, 1974; Kuo et al., 1971), *Manduca sexta* CNS (Morton and Truman, 1986), and whole body extracts from *Drosophila melanogaster* (Kuo et al., 1971).

Two PKG genes have been cloned in *Drosophila melanogaster*, and a third PKG gene is predicted in its genome (MacPherson et al., 2004). A BLAST analysis revealed that the two cloned PKG genes, Pkg21D (or DG1) and *foraging* (*for*, or DG2) are most

similar to mammalian PKG I, while the predicted gene, CG4839, shares the most similarity with PKG II (Morton and Hudson, 2002). All three of these PKGs share the same overall domain structure with the mammalian PKGs, with an N-terminal regulatory and a C-terminal catalytic domain both in one subunit. Again the N-terminal regulatory domains of the *Drosophila* PKGs share the least similarity with each other and other PKGs, but all contain at least the two cNMP binding sites and the dimerization domain (Foster et al., 1996). Like PKG I, *for* mRNA is produced as multiple splice variants, two of which likely result in a regulatory domain with only one cGMP binding site (Kalderon and Rubin, 1989).

The biochemical properties of *pkg21D* were shown to be similar to that of the mammalian PKGs (Foster et al., 1996). Recombinant *pkg21D* formed homodimers, was preferentially activated by cGMP, and was autophosphorylated in the presence of cGMP (Foster et al., 1996). The positive cooperativity observed in cGMP-stimulated activity indicated the presence of two functional cGMP binding sites (Foster et al., 1996). No direct biochemical studies have been carried out on *for*, but there is evidence that it does encode a functional PKG. Two naturally occurring alleles of the *for* gene are correlated with different levels cGMP-dependent kinase activity. Animals with one *for* allele (*rover*) express more PKG and tissues from these animals have more PKG activity. Animals with the other *for* allele (*sitter*) have less PKG expression and tissue from these animals display less PKG activity (Osbourne et al., 1997).

Exciting findings have been reported recently on a number of behaviors (discussed later) mediated by a *C. elegans* PKG called EGL-4 (Stansberry et al., 2001). The EGL-4 kinase is 46% identical over its C-terminal domain to the mouse PKG I



(L'Etoile et al., 2002). Like the mammalian PKGs and known *Drosophila* isoforms, EGL-4 consists of a divergent N-terminal domain that contains two cGMP-binding motifs and a C-terminal serine/threonine kinase domain (L'Etoile et al., 2002). Recombinant EGL-4 was shown to have cGMP-dependent serine/threonine kinase activity *in vitro* (Stansberry et al., 2001).

A wide range of mammalian proteins have been shown to be phosphorylated by PKGs *in vitro*, but phosphorylation of only a few of these have been shown to occur *in vivo*. Many examples of PKG phosphorylation *in vitro* may represent artifacts of using cell culture systems, which often poorly match actual cellular environments found *in vivo*. Some of the protein groups that are widely recognized as bonafide PKG I substrates are the IP<sub>3</sub> receptors, phospholamban, the vasodilator-stimulated phosphoprotein, vimentin (involved with platelet and neutrophil activation), the G substrate (phosphatase inhibitor in Pukinje cells), and the thromboxane A<sub>2</sub> receptor, which is inactivated by PKG phosphorylation in platelets (Komalavilas and Lincoln, 1996; Raeymaekers et al., 1990) (Aszodi et al., 1999; Endo et al., 1999; Lawrence and Pryzwansky, 2001; Wang et al., 1998). The vasodilator-stimulated phosphoprotein (VASP) is also a substrate for PKG in smooth muscle and vascular endothelium, playing a role in the relaxation of the these tissues (Smolenski et al., 1998). Less established PKG I substrates include the L-type Ca<sup>2+</sup> channel and the Ca<sup>2+</sup>-activated K<sup>+</sup> channel, which upon phosphorylation, contribute to smooth muscle tone and cardiac contractility (Fukao et al., 1999; Jahn et al., 1988). A recent study demonstrated that NO-activated sGC in gastric smooth muscle was phosphorylated and inhibited by PKG activity (Murthy, 2004). A large number of other PKG I substrates have been suggested with only circumstantial evidence for support.

Only one protein has been shown definitively to be a substrate of PKG II. The fibrosis transmembrane conductance regulator (CFTR), which is located in the intestinal mucosal cells, is phosphorylated by PKG II in response to activation of GC-C which leads to electrogenic chloride current and subsequent water secretion in the intestine (Vaandrager et al., 1997).

It appears that many PKG substrates are also PKA substrates, and that cGMP acts in concert with cAMP in some pathways. For example, both PKG and PKA inhibit IP<sub>3</sub>-dependent release of Ca<sup>2+</sup> and induce relaxation in cultured rabbit and guinea pig muscle cells, presumably through the phosphorylation of the IP<sub>3</sub> receptor (Francis and Corbin, 1999). Crosstalk between pathways may also occur through PKA activation by cGMP. The cAMP binding sites of PKA are not completely selective for cAMP and can also bind cGMP, although with a 50-fold lower selectivity (Francis and Corbin, 1994). This relevancy and occurrence of this crosstalk has not been well established *in vivo*.

In many insect studies, specific PKG substrates have been difficult to document because of the apparent overlap of PKG and PKA substrate specificities. Furthermore, both PKG and PKA are often expressed in the same tissues, and the levels of PKA usually considerably higher than PKG, making it difficult to access how much PKG contributed to a particular phosphorylation event. An example of cyclic nucleotide-dependent phosphorylation comes from silkworm eggs. The egg protein vitellin was shown to be phosphorylated by purified preparations of both PKG and PKA, with a similar K<sub>m</sub> for both enzymes (Corbin et al., 1988). Both PKA and PKG were found in the egg samples, and it was not possible to determine if one or both kinases were responsible for substrate phosphorylation *in vivo* (Corbin et al., 1988). Specific and potent PKG

inhibitors have been developed more recently, and were not available for the numerous early “classical” studies on cNMP-dependent protein kinases. These substances provide the means to help identify the specific kinase involved in cNMP-dependent phosphorylation events in future cell culture experiments and will greatly enhance our understanding of cGMP and cAMP pathways and regulation. Elegant and powerful genetic methods are now being used to study PKG pathways *in vivo*, especially in insect and nematode model systems.

An early invertebrate example PKG substrate phosphorylation was demonstrated in *Manduca sexta*. In ventral nerve cords, two proteins called the EGPs (EH and cGMP regulated phosphoproteins) are phosphorylated specifically in response to cGMP, following the release and action of eclosion hormone (EH) *in vivo* (Morton and Truman, 1986). EH release in animals has no effect on the levels of cAMP. This cGMP-dependent phosphorylation was reproduced in intact ventral nerve cords that had been removed from the animals. cAMP was not as effective as cGMP in these experiments. Interestingly, in homogenized nerve cord samples cAMP was more effective than cGMP at stimulating the phosphorylation of the EGPs. It was shown that both PKA and PKG can phosphorylate the EGPs, and that PKA levels are 10-fold higher than that of PKG in homogenates (Morton and Truman, 1986). It seems likely that in intact nerve cords, PKA is not found at high levels in the cells that contain the EGPs, and the homogenization of tissue releases the abundant stores of PKA in other cells. In this case, and likely in many other cases, substrates for PKGs are not specific because of binding affinity, but because of cellular colocalization with PKG and the selective production cGMP by upstream pathway activation.

## B. cGMP-gated ion channels

The final major group of proteins that are known to be cNMP targets are the cNMP-gated ion channels (CNGs) (Kaupp and Seifert, 2002). CNGs are non-selective cation channels that poorly discriminate between positively-charged ions, allowing even divalent cations such as  $\text{Ca}^{2+}$  to pass. CNGs are directly activated through the binding of cGMP or cAMP to specific sites in C-terminal region that share significant sequence homology to the cNMP-binding domains of PKA and PKG. The dependence of channel activation on the ligand concentration is steep, indicating that several (most likely four) molecules of cNMP are required to fully open the channels. All studied CNG channels appear to respond to some extent to both cGMP and cAMP, with some channels responding equally well to both cNMPs, but there are several examples where the CNG is highly selective for one or the other cNMP. An aspartate residue was identified near the C-terminal end of the cNMP binding site that determines the selectivity of cGMP in the bovine rod CNG (Varnum et al., 1995). Point-mutating this residue to an uncharged polar residue eliminated ligand specificity, while mutating it to a non-polar residue switched specificity from cGMP to cAMP, consistent with sequences and ligand specificities of other characterized CNGs (Varnum et al., 1995).

CNG channels function as hetero- or homo-multimers, and genes encoding several different subunits exist in a given organism. Based on sequence comparisons, CNG channel genes fall into different subfamilies. In mammals, two subfamilies can be distinguished, with the peptides encoded by these genes classified as either “A” or “B” subunits. A total of six mammalian CNG subunit genes have been identified and cloned. Members of the “A” subfamily can form functional channels on their own, with the

exception of CNGA4. The first of these subunits, called CNGA1, was first identified in retinal rods (Kaupp and Altenhofen, 1992). The major subunit found in olfactory sensory neurons is CNGA2 (Kaupp and Seifert, 2002), and the major subunit found in cones is CNGA3 (Bonigk et al., 1993). These three CNGs are highly identical (~77%) (Kaupp and Seifert, 2002). CNG4, which was also found in olfactory sensory neurons, is a modulator of CNGA3, and does not form functional channels on its own (Bradley et al., 1994). CNGA4 interacts with CNGA3 to make a channel that displays increased sensitivity to cAMP (Bradley et al., 1994).

The “B” subfamily is comprised of two subunits in mammals. CNGB1 was originally found in rod photoreceptors, and CNGB3 was first identified in cone photoreceptors (Chen et al., 1993; Gerstner et al., 2000; Korschen et al., 1999). These are modulatory subunits, as they do not form functional channels on their own and are known to modify the characteristics of homomeric channels composed of “A” subfamily members when co-expressed with them in heterologous cell systems. Hetero-multimers that contain “B” subfamily members are altered in ligand sensitivity and selectivity, gating, pharmacology, ion selectivity, and modulation by Ca<sup>2+</sup>/CaM, compared to homomeric “A” channels (reviewed in Kaupp and Seifert, 2002).

The current topological model for the CNG channel has been arrived at through protein structure/ membrane interaction predictions and experimental evidence obtained through electron microscopy (with immunogold labeling) and gene fusion approaches using enzyme reporters (reviewed in Kaupp and Seifert, 2002). The core structural unit of CNG channels consists of six membrane spanning segments, designated S1-S6, followed by a cNMP binding domain near the C-terminus. A pore region of ~20-30 residues is

located between S5 and S6. The S4 segment in CNG channels is similar (yet functionally different) to the voltage-sensor motif found in the S4 segment of voltage-gated K<sup>+</sup>, Na<sup>+</sup>, and Ca<sup>2+</sup> channels. These features indicate that CNGs and voltage gated channels evolved from a common ancestral channel (Heginbotham et al., 1992). Both the N-terminal and the C-termini of each subunit is located on the cytoplasmic side of the cell membrane, at least for homomeric channels composed of “A” subunits (Henn et al., 1995; Molday et al., 1991).

The pore region architecture and sequence of CNGs is highly similar to that of K<sup>+</sup> channels. However, the sequence similarities diverge exactly at the region known to mediate ion selectivity (reviewed in Kaupp and Seifert, 2002). Where a key tyrosine residue occurs in the selectivity filter of K<sup>+</sup> channels, hydrophilic or negatively charged residues occur in most CNGs. These residues contribute to the strong channel selectivity for cations over anions.

In *Drosophila melanogaster*, four predicted genes have been identified in the genome that appear to code for cNMP-gated ion channels (Littleton and Ganetzky, 2000). Two of these CNGs have been cloned and characterized, and were named *cyclic nucleotide-gated ion channel (cng)* and *cng-like (cngl)* (Baumann et al., 1994; Miyazu et al., 2000). The other two, designated CG3536 and CG17922, have not been cloned as of yet. The cng subunit has been expressed in heterologous cells and does form functional cGMP-gated non-specific cation channels that are 50-fold more sensitive to cGMP than cAMP (Baumann et al., 1994). The ligand specificity of cng for cGMP is consistent with the presence of a key aspartate in the cNMP-binding site, like the bovine rod BNG discussed above. In contrast, when the cngl subunit was expressed in heterologous cells,

functional channels did not form, indicating that functionally this subunit is like a “B” subunit, modulating the function of homomeric “A” channels (Miyazu et al., 2000). The *cngl* subunit, if it formed homomeric channels, should be specific for cAMP-gating as it possesses a non-polar valine residue instead of an aspartate (Morton and Hudson, 2002). CG3536 and CG17922 should not display ligand specificity, as they have a tyrosine and an asparagine respectively, in place of the key aspartate (Morton and Hudson, 2002). It is not known if these subunits interact *in vivo*, although it appears that *cng* and *cngl* do not interact as they are expressed in different tissues. *Cng* was found in antennae and in eyes, while *cngl* was found to be expressed in the antennal lobes, mushroom bodies, thoracic ganglion neurons, and in muscle fibers (Baumann et al., 1994) (Miyazu et al., 2000).

There are two other families of channels that possess cNMP-binding sites, in addition to CNG channels, called the hyperpolarization-activated ( $I_h$ ) channels and the ether-a-go-go (*eag*) family of voltage activated potassium channels. In mammals, the  $I_h$  channels are activated by hyperpolarizing currents and the presence of cGMP or cAMP causes the channels to open at more positive voltages (Ludwig et al., 1998). Two insect  $I_h$  channels have been identified: one in *Heliothis virescens* and one in *Drosophila melanogaster* (Krieger et al., 1999)(Marx et al., 1999). The *Heliothis*  $I_h$  channel was shown to behave like the mammalian  $I_h$  channels when expressed in heterologous cells. The insect  $I_h$  channels are expressed several sensory tissues, such as the eye, antennae, and auditory organs in *Drosophila* and in antennal sensory neurons in *Heliothis* (Krieger et al., 1999; Marx et al., 1999). The voltage-gated potassium channels that are encoded by the ether-a-go-go gene subfamily are modulated (not gated) by cAMP only, and will not be discussed further here.

## V. Physiological functions/pathways in the nervous system

### A. Phototransduction

One of the most well-studied functions of cGMP is its primary role in mammalian phototransduction (Stryer, 1991; Stryer, 1996). The visual signal begins when rhodopsin, a seven-pass transmembrane protein that contains an 11-cis-retinal chromophore, is struck by photon(s), causing its photoisomerization. This photoexcited form of rhodopsin activates transducin, a member of the G-protein family, catalyzing the exchange of GTP for bound GDP of the G protein  $\alpha$  subunit. The active G protein then stimulates a potent PDE, which rapidly hydrolyzes cGMP. In the absence of light,  $\text{Na}^{2+}$  and  $\text{Ca}^{2+}$  enter freely through a cGMP-gated CNG that is held open by a constant level of cGMP. The light induced decrease of cGMP levels closes the CNGs, which hyperpolarizes the plasma membrane and generates the neural impulse as a cation gradient is formed. The dark state is regained through the inactivation of PDE and activation of the receptor guanylyl cyclase GC-E. Recoverin and the GCAPs, all members of the calcium-binding EF-hand family, detect decreased cytoplasmic  $\text{Ca}^{2+}$  levels after channel closing and activate GC-E. The GTPase activity of the transducin  $\alpha$  subunit catalyzes the hydrolysis of GTP, inactivating the G-protein and blocking PDE activity.

In *Drosophila* visual transduction, the primary signal has been shown to be inositol 1,4,5-trisphosphate ( $\text{IP}_3$ ) rather than cGMP. However, cGMP may play a modulatory or adaptive role, as GCs and other components of the cGMP pathway have been located to insect photoreceptors. NO-sensitive GC activity has been found to occur in locust eyes, and a GC  $\alpha$  subunit was shown to be expressed in the photoreceptors, possibly playing a role in dark adaptation (Elphick and Jones, 1998). Also in locust eyes,



electroretinogram (ERG) recordings demonstrated that cGMP and NO donors increased the response of photoreceptors to light (Schmachtenberg and Bicker, 1999). Downstream cGMP pathway components, such as CNG and Ih channels have been shown to occur in *Drosophila melanogaster* photoreceptors, and application of exogenous cGMP induced membrane currents and also enhanced light-induced currents (Bacigalupo et al., 1995; Baumann et al., 1994; Marx et al., 1999).

### **B. Neuronal plasticity: long-term potentiation and long-term depression**

Many lines of evidence support a role for the NO/cGMP pathway in several forms of long-term potentiation (LTP) and depression (LTD) (reviewed in Prast and Philippu, 2001). LTP and LTD are activity-dependent forms of modified transmission efficacy at synapses. In hippocampal and cortical LTP, NO appears to act as a retrograde messenger that is synthesized postsynaptically and acts on presynaptic terminals, where cGMP is generated by sGC. In cerebellar and striatal LTD, NO seems to be generated presynaptically or in interneurons, acting postsynaptically. The pathway downstream of cGMP is poorly understood, but PKG is a likely target. The NO/cGMP pathway has also been shown to modulate the release of a host of neurotransmitters, such as acetylcholine, excitatory and inhibitory amino acids, catecholamine, histamine, and serotonin (Prast and Philippu, 2001).

### **C. Neuronal development**

A large number of studies in a variety of *in vivo* and *in vitro* settings implicate cGMP signaling in several types of neuronal development, particularly axonal pathfinding and synapse formation. Axonal pathfinding events are guided at least in part by secreted attractant/repellent molecules and cell surface markers that lead axons to

target regions or act as guideposts can alter or support axonal behavior (reviewed in Tessier-Lavigne and Goodman, 1996). Gradients of guidance molecules and cell surface markers along neuronal pathways are perceived by receptors localized to the growth cones, relaying guidance cues to the dynamic cytoskeletal machinery. When axons reach their targets, they receive signals instructing them to stop and form the appropriate synapses (Tessier-Lavigne and Goodman, 1996).

Several studies have shown that NOS, sGCs, and/or NO-stimulated cGMP immunoreactivity is localized to neurons at precise developmental stages where they are traveling to and nearing their targets in insect systems. These studies have examined synapse formation in *Drosophila melanogaster* photoreceptors (Gibbs and Truman, 1998), locust motor neuron (Ball and Truman, 1998; Truman et al., 1996) and antennal pioneer neuron pathfinding (Seidel and Bicker, 2000), and *Manduca sexta* enteric (Wright et al., 1998) and olfactory neuron pathfinding (Gibson and Nighorn, 2000). In addition to examining temporal and spatial cGMP localization, some of these studies also demonstrated that NO/cGMP was directly involved with axon pathfinding and synapse formation (Gibbs et al., 2001; Seidel and Bicker, 2000)

In some cases it appears that cGMP dramatically alters the behavior of growth cones responding to certain guidance cues. For example, the growth cones of *Xenopus* spinal neurons turn toward microgradients of the secreted guidance protein Semaphorin III. The attraction of the growth cone to Semaphorin IIIa (Sema IIIa), a member of a large family of guidance molecules, switches to repulsion when cGMP analogues and NO-donors are added to the cultures (Song et al., 1998). Another study revealed that the dendrites of pyramidal neurons are attracted to Sema IIIa while simultaneously the axon

of the same neuron is repulsed by Sema IIIa (Polleux et al., 2000). It was shown that sGC is concentrated in the dendrites compared to the axons, and blocking sGC activity in the cultures inhibited dendrite outgrowth and collapsed growth cones but had no effect on axonal outgrowth (Polleux et al., 2000). These results suggest that cGMP in the dendrites mediated the attractive behavior toward Sema IIIa. Semaphorin family members also occur in invertebrates and have been shown to play crucial roles in various axonal pathfinding and neuromuscular junction formation events (Kolodkin et al., 1992; Winberg et al., 1998). In at least one case, a receptor GC was found to mediate Semaphorin function (Ayoob et al., 2004).

In *C. elegans*, knockouts of the cGMP-gated ion channels *tax-2* and *tax-4* yielded animals with abnormal axonal projection patterns in those neurons that express these channels (Coburn et al., 1998). Animals that lack the *Daf-11* receptor GC, which is normally found in a subset of the same neurons, display similar axonal defects, further supporting the role of cGMP signalling in this process (Coburn et al., 1998). The recent focus on axonal guidance questions using the powerful *Drosophila melanogaster* and *C. elegans* genetic systems will undoubtedly provide many insights into the role of cGMP in the development of the nervous system, especially the downstream signaling pathway, of which little is known.

#### **D. Ecdysis**

A well characterized function for cGMP in insects is its role in the regulation of ecdysis behavior. Insects outgrow their rigid cuticles (exoskeletons) as they increase in size throughout the life cycle. At the junction of defined larval stages called instars, the insect will replace the old cuticle with a new, larger cuticle that is secreted between the

epidermis and the old cuticle in a process called molting. The removal of the old cuticle is accomplished by a stereotypical behavior called ecdysis. A related behavior, called adult ecdysis or eclosion, occurs when the adult form of the insect emerges from the pupal case, which forms at the end of the larval life. The initiation of ecdysis, and a preparatory behavior called pre-ecdysis, is controlled by several interacting neuropeptides which tightly coordinate these events. Work done mostly in *Manduca sexta*, but also in *Drosophila melanogaster* and other insects, revealed that three of the major neuropeptides that control these behaviors are eclosion hormone (EH), ecdysis triggering hormone (ETH), and crustacean cardioactive peptide (CCAP), which are broadly conserved in insects and perhaps other arthropods (reviewed in Morton and Hudson, 2002 and (Ewer and Reynolds, 2002). The most dominant model of neuropeptide action proposes that EH, a 62 residue peptide which is found in one or two pairs of cells (the Vm cells) in the insect brain, is the key peptide that initiates the events leading to ecdysis. First, EH is released into the CNS and the hemolymph, triggered by an unknown signal. EH acts on the Inka cells in the epitracheal glands (located peripherally on the trachea in a segmental pattern), which release their stores of ETH into the hemolymph. ETH then acts on the VM cells in the brain to cause more EH release, forming a positive feedback loop with the epitracheal glands (Ewer, 2005; Ewer et al., 1997; Ewer and Reynolds, 2002). In contrast to the widely accepted model resulting from endocrinological studies in *Manduca*, cell ablation and gene knockout experiments in *Drosophila* indicate that ETH initiates the positive feedback loop with EH. EH released into the CNS acts on about 50 neurons containing CCAP, causing its release into the CNS (Ewer et al., 1994).

CCAP is believed to directly activate the ecdysis motor program (Gammie and Truman, 1997; Gammie and Truman, 1999).

In *Manduca*, the ecdysis-triggering action of EH has been shown to be mediated by an increase of cGMP levels in the ventral ganglia of the CNS, specifically in the CCAP cells (Gammie and Truman, 1999; Truman et al., 1979). It was also shown that EH-mediated release of ETH from the Inka occurs with an increase in cGMP levels in the Inka cell, further supporting the role of cGMP as the mediator of EH action (Kingan et al., 1997; Zitnan et al., 1996). A final population of cells that increase cGMP levels in response to EH are the sub-transverse nerve region (STNR) cells, which appear to have nothing to do with ecdysis behavior and are non-neuronal. At the end of the 5<sup>th</sup> larval instar, following EH exposure and the subsequent increase in cGMP immunoreactivity, the STNR cells mobilize and become part of sheet-like tissues that become the ventral diaphragm muscles in the adult (Hesterlee and Morton, 2000).

In *Manduca*, the most likely GC candidate that produces cGMP in Inka cells and STNR cells neurons is the atypical GC MsGC- $\beta$ 3, which is expressed in both locations (Morton, 2000; Nighorn et al., 1999). A series of studies provided strong evidence that EH acts through an increase in cGMP by activating an NO-insensitive GC (Kingan et al., 1997; Morton, 1996; Morton and Giunta, 1992; Morton and Truman, 1985). These observations, along with the fact that MsGC- $\beta$ 3 is the only known NO-insensitive GC in *Manduca*, provides circumstantial evidence that this GC mediates EH action. However, MsGC- $\beta$ 3 immunoreactivity was not observed in the CCAP cells, which also show an increase in cGMP levels upon EH release (D. Morton, unpublished data). EH may work through an alternate mechanism to cause cGMP production in these cells.

EH is not likely to activate MsGC- $\beta$ 3 directly, as sGCs lack a transmembrane domain capable of receiving extracellular peptide signals. A number of studies attempted to identify components of the pathway downstream from EH to the activation of an NO-insensitive soluble GC. The identity of the EH receptor currently remains unknown. However, several studies provide evidence that suggest that a phospholipase C (PLC) is activated directly or indirectly by the EH receptor upon EH binding, and that the downstream sGC is activated by a lipid messenger (Morton and Simpson, 2002). Identification of the EH receptor and which receptor family it belongs to will greatly aid in the elucidation of this pathway. Recent studies of the *Drosophila melanogaster* ortholog of MsGC- $\beta$ 3 and related atypical sGCs in *C. elegans* have shed much light on the nature of at least one of the ligands that activate these sGCs. These findings are relevant to the work presented in this dissertation and will be discussed later.

#### **E. Food search and feeding behaviors**

The involvement of cGMP has been well documented in several food search and feeding behaviors in *Drosophila melanogaster* and *C. elegans* (Sokolowski, 1998). In *Drosophila*, two naturally occurring alleles of the *foraging* (*for*) gene have been found to regulate two different feeding behaviors. In the absence of food, both alleles show similar levels of locomotor activity (Sokolowski, 1980). In the presence of food however, larvae with the sitter allele do not travel far and tend to stay in one patch of food while feeding. In contrast, larvae with the rover allele continuously forage, traveling to different patches of food while feeding. Nearly 20 years after these feeding behaviors were first described, the *for* gene was mapped to the *dg2* locus, which codes for a previously known PKG (Osborne et al., 1997). An unrelated fly line that contained a P-element insertion that

disrupted the open reading frame of one of the three PKG transcripts displayed a sitter phenotype (Osborne et al., 1997). A clean excision of this P-element yielded flies with a rover phenotype, further demonstrating the role of this PKG in the behavioral polymorphism. PKG transcript expression was examined and it was found that sitter flies had lower levels of PKG transcript expression than rover flies. Next, the levels of total PKG enzyme activity was accessed in extracts made from sitter flies and rover flies, and it was found that the rover flies possessed more PKG activity than sitter flies. To further examine the possibility that the levels of PKG activity regulation the feeding strategy, Osbourne and co-workers (1997) transformed sitter flies with a cDNA encoding the PKG. The transformants displayed a rover phenotype, and exhibited more PKG activity compared to the control sitter flies.

Preliminary experiments found that the *dg2* PKG is expressed in subsets of tissues involved in olfaction, taste, gut, and central brain function (Sokolowski, 1998). This finding suggests a number of possible points where PKG could cause modulation of behavior. First, PKG could directly modulate olfactory food sensation in the sensory organs neurons, reducing signals indicating the presence of food in rovers or increasing these signals in sitters. At least two sGCs are expressed in the main olfactory organ of *Drosophila* larvae (see Chapter 3), and cGMP is known to be involved with olfaction and taste (Breer et al., 1992). Second, PKG might control foraging by modulating feedback from the gut, which influences feeding depending on how full of food it is (Sokolowski, 1998). Third, PKG modulation of foraging behavior may occur in the CNS, where the interpretation of, or response to environmental cues could be altered. Much more work is needed to determine how and where PKG activity modulates foraging behavior. Of

particular importance is the identification of which GC produces the cGMP that activates PKG, and what substrates are targeted by PKG upon its activation.

A naturally occurring behavioral polymorphism that is regulated by cGMP has also been reported in *C. elegans*. In the wild, races of *C. elegans* either feed alone (“solitary”) or as part of groups of worms that stay in tight contact (“social”) (de Bono and Bargmann, 1998). The behavioral variation between solitary feeding and social feeding is associated with two natural isoforms of a G-protein coupled receptor called NPR-1 (NPY receptor resemblance-1), which was discovered through mutagenesis screens aimed at transforming solitary feeders into social feeders (de Bono and Bargmann, 1998). A single amino acid difference in NPR-1 was found to be responsible for the two behaviors. The two NPR-1 isoforms have different ligand responses (Rogers et al., 2003). NPR-1 is co-expressed with the cGMP-gated ion channel TAX-2/TAX-4 in a limited number of neurons, including some that are directly exposed to the body fluid and one that has dendritic extensions to the tip of the nose (Coates and de Bono, 2002; Gray et al., 2004). Mutations in the TAX-2 or TAX-4 channel subunit genes also affect group feeding behavior, disrupting social feeding (Coates and de Bono, 2002). More recently it was demonstrated that two atypical guanylyl cyclases, GCY-35 and GCY-36 (related to MsGC- $\beta$ 3 and Gyc-88E), are also expressed in a subset of the cells (neurons exposed to the body cavity fluid) that express NPR-1 and the TAX-2/TAX-4 channel. Null mutations in either GCY-35 or GCY-36 (which likely form heterodimers) revert the social feeding behavior of NPR-1 mutants back to the solitary feeding behavior (Cheung et al., 2004). These GC mutations also suppressed the preference of NPR-1 mutants for the edge of the *E. coli* food lawn, where the bacteria grow the thickest (Cheung et al.,



2004). Taken together, these findings suggest that activation of GCY-35/GCY-36 leads to the opening of the TAX-2/TAX-4 channel, depolarization of neurons, and modulation of feeding behaviors regulated by NPR-1. An activating gaseous ligand of GCY-35/GCY-36 has been identified, and will be discussed in the next section.

## **F. Chemosensation**

### **1. Olfaction**

Both vertebrates and invertebrates possess an impressive number genes that code for odorant receptors, which tend to be G protein-coupled transmembrane receptors (GPCRs) (Gibson and Garbers, 2000). Over 1000 members of this receptor family, comprising about 1% of the genome, are expressed in the rodent olfactory epithelium (Buck and Axel, 1991; Levy et al., 1991). In addition to GPCRs, invertebrates (especially *C. elegans*) also appear to make use of a very large number of soluble odorant binding proteins (OBPs), which are secreted into the lymph that bathes olfactory (and also gustatory) dendrites and are thought help solublize hydrophobic molecules or regulate odorant binding to receptors (Vosshall, 2000). In *C. elegans*, it is estimated that 3-5% of the genome codes for OBPs and transmembrane receptors involved in olfaction or chemosensation (Bargmann, 1998). In the *Drosophila melanogaster* genome, 100-200 candidate seven transmembrane domain odorant receptors and about 35 candidate soluble OBPs have been identified (Galindo and Smith, 2001; Vosshall, 2000). The most established model of odorant detection derives from work done in vertebrate systems . Olfaction is initiated when the odorant molecule binds to its G protein-coupled receptor, which activates an associated G protein. This G protein then activates a specific adenylyl cyclase, resulting in the elevation of cAMP levels and the activation/opening of a CNG,

which leads to neuronal depolarization. There is also evidence in rat olfactory cilia that for some odorants inositol 1,4,5-trisphosphate (IP<sub>3</sub>) acts as the primary transduction signal instead of cAMP (Boekhoff et al., 1992).

Although the model involving cAMP is considered to be the most typical mechanism for olfactory transduction in vertebrates, in *C. elegans* and insects, a mixture of cAMP, IP<sub>3</sub>, and alternative transduction pathways may be in operation. In some of these pathways, cGMP may act as the primary transduction signal, or play a modulatory role, and GCs may even directly bind odorants and initiate the transduction process. One of the earliest putative odorant receptor GCs proposed was the rat GC-D which was found to be specifically expressed in cilia of a subpopulation of olfactory sensory neurons (Fulle et al., 1995). This expression is dispersed in a seemingly random set of neurons within one topological zone, a pattern that closely resembles the expression of individual odorant-binding G protein-coupled receptors. Particulate GC activity was measured in rat and pig olfactory cilia that was not stimulated by NO donors or several known odorant molecules (Steinlen et al., 1990). To date however, the odorant ligand for this putative receptor remains unknown, and it is still even unclear if GC-D actually acts as a odorant receptor, or plays a modulatory role in the cAMP pathway. Rather than acting as a receptor, it is possible that GC-D is regulated by calcium-binding GCAPs in a manner similar to GC-E and GC-F. Downstream IP<sub>3</sub> pathways typically involve the release of calcium from intracellular stores, which would likely inhibit GCAP-mediated activation of the GC.

Clear demonstrations of GC/cGMP involvement with olfaction comes from invertebrate studies, especially in *C. elegans*. Compared to the seven receptor GCs found

in vertebrates, the genome of *C. elegans* contains an amazing 25 receptor GC subunits, most of which share the same domain structure and predicted disulfide linkages as their vertebrate counterparts (Bargmann, 1998). In an early study, the expression patterns of several of these rGCs were mapped out by driving green fluorescent protein (GFP) expression with the predicted promoter regions of the rGC genes in transformed animals (Yu et al., 1997). All 8 of the orphan receptors that were examined in this way were found to be expressed in a small number of sensory neurons known to be involved with chemosensation. A GFP fusion construct was made for one of these GCs (GCY-10). Expression of GFP in animals transformed with this fusion construct was localized in the cilia of the sensory neuron, a location consistent with a role in chemosensation.

Mutations in two of the *C. elegans* rGCs have been isolated and described thus far, and both mutants have defects in chemosensation. ODR-1 was found to be expressed in the AWC neuron cilia and *odr-1* mutant animals are unable to sense all of the 5 known volatile odorants normally sensed by this sensory neuron (L'Etoile and Bargmann, 2000). All of the AWC odorants are thought to elicit chemotaxis through the TAX-2/TAX-4 CNG channel, suggesting that cGMP produced by ODR-1 is responsible for channel opening and neuron depolarization. It was also found that the ODR-1 GC domain but not the extracellular domain was needed for olfaction, further suggesting that this GC is not a direct odorant receptor, but plays an intermediary function shared by the odorant receptors (probably G protein-coupled receptors). Interestingly, overexpression of ODR-1 in AWC neurons causes defects in the documented discrimination between odorants sensed by this neuron (Bargmann et al., 1993; L'Etoile and Bargmann, 2000). Adaptation to the odorants was also impaired. The rGC DAF-11 was also found to be expressed in

AWC neurons and is also required for sensing all odorants sensed by this neuron (Birnby et al., 2000). DAF-11 and ODR-1 are likely to form obligate heterodimers as discussed previously, and this would explain the highly similar phenotypes. Later work discovered that a PKG called EGL-4 is also expressed in AWC neurons (as well as many other sensory neurons) and regulates short- and long-term odorant adaptation (L'Etoile et al., 2002). It was found that short term adaptation was likely attributed to TAX-2/TAX-4 phosphorylation by EGL-4, and that long-term adaptation is related to a nuclear localization signal within EGL-4. EGL-4 may mediate long-term adaptation by regulating gene expression. These findings clearly support important second messenger and modulatory roles for cGMP in several aspects of olfaction, even within a single cell. It is still unknown if G proteins, activated by G protein-coupled receptors, directly activate ODR-1/DAF-11 in a manner homologous to adenylyl cyclase activation in the more established vertebrate olfactory transduction pathway.

Similar to what has been reported in vertebrates and in *C. elegans*, cGMP does not appear to be the primary transduction molecule in most olfaction in insects. While it is generally believed that insects primarily utilize G protein-coupled receptors to detect odorants (Clyne et al., 1999; Vosshall, 2000), one report suggests that IP<sub>3</sub> is the primary downstream signal in olfaction rather than cAMP, at least in the *Drosophila melanogaster* maxillary palps. *Drosophila* adults possess two pairs of olfactory organs, the maxillary palps and the third antennal segments, and numerous other individual olfactory sensilla occur in other locations, such as on the wings. *NorpA* mutants, which are null for a specific phospholipase C (PLC), display a highly reduced ability to sense all odorants tested. Interestingly, the *NorpA* PLC is also used to generate the IP<sub>3</sub> in fly

phototransduction, and *norpA* mutants are effectively blind. Antennal responses to odorants in *norpA* mutants were normal however, indicating that the olfactory transduction machinery in other locations utilizes another PLC, or a different second messenger molecule. One other report found that  $IP_3$  is generated when silkworm antennae are exposed to pheromone (Ziegelberger et al., 1990). Much more work is still needed to gain a more complete picture of how odorant detection is transduced to the CNS in insects.

While olfactory transduction pathways are still poorly understood in insects, several studies suggest that cGMP is involved with several modulatory aspects of this process. Both soluble and particulate GC enzyme activity have been measured in insect olfactory tissue, such silkworm antennae (Ziegelberger et al., 1990). MsGC-I has been detected in *Manduca sexta* olfactory neurons (Nighorn et al., 2001) and a receptor GC has been found to be expressed in silkworm antennal sensory neurons (Tanoue et al., 2001). Other components of the cGMP pathway have also been shown to be localized to olfactory tissue. For example, a *Drosophila* CNG,  $I_h$ , and a *Heliothis*  $I_h$  channel have been shown to be expressed in antennae (Baumann et al., 1994; Krieger et al., 1999; Marx et al., 1999).

In the case of silkworm, pheromone stimulation of antennae resulted in an increase of cGMP levels (Ziegelberger et al., 1990). However, this increase was slow compared to the observed increase of  $IP_3$  levels, suggesting a role for cGMP in adaptation (Ziegelberger et al., 1990). Also, the pheromone-stimulated increase in cGMP was found in whole antennae but not olfactory dendrites, further supporting a modulatory role rather than a primary role for cGMP.

In addition to the possible modulatory roles in olfactory neurons themselves, cGMP signalling also appears to be involved in olfactory and other sensory signal processing in insects, mammals and fish. Most of the evidence supporting this comes from studies that show GC or NOS expression in interneurons and higher order centers such as the antennal lobes (Muller, 1997; Nighorn et al., 1998; Nighorn et al., 2001). A few functional studies have been carried out (Bicker, 2001). For example, inhibition of NOS in honeybees impaired a specific form of long-term memory (Muller, 1996).

## **2. Aerotaxis and oxygen sensation in *C. elegans* and *Drosophila***

Recent findings in *Drosophila melanogaster* and *C. elegans* have vastly improved our understanding of how molecular oxygen is acutely sensed. Animals that live in soil, freshwater, marine, and decomposition environments face conditions where oxygen concentration can differ drastically from one place to the next, forming steep oxygen gradients (Wannamaker and Rice, 2000; Wu, 2002). In order to navigate these environments and avoid hypoxic or hyperoxic conditions, it has been thought that these animals use fast-acting oxygen sensors capable of precisely distinguishing oxygen concentrations and perceiving gradients. Another environment where oxygen concentration is monitored is the mammalian cardiovascular system, by the glomus cells in the carotid body (Hoshi and Lahiri, 2004). In the most favored model, hypoxia results in the inhibition of the BK channel (a calcium- and voltage-gated potassium channel) activity, which lead to depolarization of the glomus cells. The oxygen sensor in this model is thought to be hemeoxygenase-2, which indirectly activates the BK channel by producing excitatory CO. Hypoxia disrupts CO production leading to BK channel inhibition (for details see Hoshi and Lahiri, 2004). Long-term exposure to hypoxia is

thought to exert transcriptional changes through the hypoxia-inducible transcription factor HIF-1 to affect several physiological processes (Semenza, 2000).

Acute oxygen sensation in *C. elegans* occurs in a much more direct fashion. In a landmark paper from the Bargmann lab, it was demonstrated that worms exhibit a strong preference for 5-12% oxygen and avoid higher and lower oxygen levels. Interestingly, avoidance of high oxygen levels required the TAX-2/TAX-4 CNG channel and the atypical guanylyl cyclase GCY-35, which are co-expressed in the same four sensory neurons that mediate solitary or social feeding behavior. Social feeding was found to occur when oxygen exceeded the preferred level, a response that required GCY-35. It was also demonstrated that the GCY-35 heme domain binds oxygen, unlike any other native sGC or sGC heme-domain tested to date. However, bacterial hemoproteins have been described that bind oxygen and mediate aerotaxis to preferred oxygen concentrations (Hou et al., 2000; Jain and Chan, 2003). Although this report clearly demonstrates that an sGC acts as a molecular oxygen sensor that rapidly mediates behavior, it remains to be shown biochemically that GCY-35 activity is directly regulated by oxygen. As discussed previously, the *C. elegans* sGCs have not yielded measurable activity in heterologous cell expression systems, so it has not been possible to perform these experiments.

In *Drosophila*, evidence from one study implicates an NO-sensitive pathway in larval avoidance of hypoxia as well as cellular and developmental responses (Wingrove and O'Farrell, 1999). When 3<sup>rd</sup> instar larvae feeding in a pile of yeast were exposed to a hypoxic atmosphere, they rapidly exited the food and continuously moved about. Feeding the larvae a NOS inhibitor reduced this response and overexpression of NOS using a

transgene potentiated the hypoxia escape response. Further evidence that supports a role for the NO/sGC/cGMP pathway in hypoxia avoidance behavior has been lacking however.

## **VI. Questions addressed in this dissertation**

The discovery of atypical soluble guanylyl cyclases opens a new chapter in GC research. The intriguing biochemical properties and tissue localization of MsGC- $\beta$ 3, the first atypical sGC described, raises a number of important questions. First, if NO is not the endogenous activator of MsGC- $\beta$ 3, what is? Does MsGC- $\beta$ 3 participate in a novel signaling pathway? What is the precise function of MsGC- $\beta$ 3 in the Inka cells of the epitracheal glands and in the STNR cells, and does it play a role in ecdysis or any other physiological or developmental processes? In order to examine the function of atypical sGCs and answer questions pertaining to function, I decided to utilize the *Drosophila melanogaster* model system, which has the advantage of a completed genome and genetic manipulation. Not only was *Drosophila* predicted to have a highly identical MsGC- $\beta$ 3 ortholog, it was predicted to possess two other atypical sGCs, named Gyc-89Da and Gyc-89Db. The initial goals of this thesis project were to clone and characterize Gyc-88E, Gyc-89Da, and Gyc-89b, and determine their biochemical properties and expression patterns. Is Gyc-88E active as a homodimer and insensitive to NO like MsGC- $\beta$ 3? How does co-expression of Gyc-89Da and Gyc-89Db affect the GC activity of Gyc-88E? When and where are these sGCs expressed at various stages in the life cycle? The results of these experiments that address these questions are reported in Chapters 2 and 3. Once this initial work was accomplished I then planned on determining the function of these genes using a P-element disruption or alternate approach. Does eliminating the function



of these sGCs affect ecdysis or any other developmental or physiological process? If these sGCs are expressed in neurons, what is the effect of disrupting the function of these neurons? These questions are explored in Chapter 4.

## Chapter 2: Initial cloning, characterization, and biochemical properties of Gyc-88E, Gyc-89Da, and Gyc-89Db

### Introduction

Guanylyl cyclases, the enzymes that catalyze the synthesis of cGMP, generally fall into one of two classes: the integral membrane receptor guanylyl cyclases (rGCs) and the cytoplasmic soluble guanylyl cyclases (sGCs). Soluble guanylyl cyclases are classically obligate heterodimers composed of an  $\alpha$  subunit and a  $\beta$  subunit (Lucas et al., 2000). The  $\alpha/\beta$  heterodimers are potently activated by the gaseous messenger nitric oxide (NO) via a prosthetic heme group that binds to the heterodimer in the N-terminal regulatory domain (Lucas et al., 2000). Receptor guanylyl cyclases, by contrast, are homodimeric proteins that are activated by extracellular ligands or intracellular calcium binding proteins (Lucas et al., 2000).

Recent reports have described a number of soluble guanylyl cyclases that exhibit significantly different properties compared to the conventional  $\alpha/\beta$  heterodimers (Morton, 2004b). One of these, MsGC- $\beta$ 3 was identified in the insect, *Manduca sexta* (Nighorn et al., 1999). Expression of MsGC- $\beta$ 3 in COS-7 cells yielded moderate levels of guanylyl cyclase activity in the absence of additional subunits. This basal activity was not stimulated by NO donors (Nighorn et al., 1999). Gel filtration experiments confirmed that MsGC- $\beta$ 3 forms homodimers (Morton and Anderson, 2003). The rat  $\beta$ 2-subunit was also found to be active in the absence of other subunits, although this activity was slightly stimulated by NO (Koglin et al., 2001).

Atypical sGCs similar to MsGC- $\beta$ 3 have been identified in the genomes of *C. elegans*, *Drosophila melanogaster*, and a number of other organisms (Morton, 2004)(Chapter 1). The *C. elegans* genome contains 7 sGCs, all of which have been predicted to be NO-insensitive (Morton et al., 1999). In addition to the previously studied conventional  $\alpha$  and  $\beta$  subunits, the *Drosophila* genome contains three additional soluble cyclase subunits that have been predicted to be insensitive to NO (Morton and Hudson, 2002)(Morton, 2004). One of these, CG4154, is over 80% identical to MsGC- $\beta$ 3 and was predicted to form active homodimers (Morton and Hudson, 2002). The other two, CG14885 and CG14886, have been predicted to require an additional subunit for activity (Morton and Hudson, 2002).

Rather than continuing to use the CG numbers, these guanylyl cyclases were given the following designations based on their chromosomal locations: Gyc-88E (CG4154), Gyc-89Da (CG14885) and Gyc-89Db (CG14886). This nomenclature is consistent with the names of the *Drosophila* NO-sensitive subunits, Gyc $\alpha$ -99B and Gyc $\beta$ -100B. In this chapter, I describe the cloning, initial characterization, and temporal expression patterns of Gyc-88E, Gyc-89Da, and Gyc-89Db. I also test the above biochemical predictions (also see Chapter 1) and examine enzyme activity utilizing a heterologous cell expression system and cGMP assay. The majority of the material covered in this chapter has been published (Langlais et al., 2004; Morton, 2004a; Morton et al., 2005).

## **Methods and Materials**

### **Animals**

*Drosophila melanogaster* stocks (Canton-S) were propagated in fly jars using standard procedures (Sullivan et al., 2000) at 25° C.

### **RNA collection**

Animals were staged according to the method described by Campos-Ortega and Hartenstein (1997). Animals of selected stages were frozen and pulverized in liquid nitrogen in a pestle and mortar. Total RNA was isolated from the resulting powder with Trizol Reagent (Invitrogen, Carlsbad, CA, USA) according to the manufacturer's instructions. Poly(A)<sup>+</sup> RNA was isolated from total RNA using oligo (dT) cellulose (Ambion, Inc., Austin, TX, USA) according to the supplied protocol.

### **RT-PCR cloning of Gyc-88E and Gyc-89Da, and splice variant analysis**

Superscript II RNase H- reverse transcriptase (Invitrogen) was used in a reverse transcription (RT) reaction using an oligo (dT)<sub>12-18</sub> primer (Invitrogen) to synthesize cDNA that was used in subsequent PCRs. The composition of the reaction mixture was: 50mM Tris-HCl (pH 8.3), 75mM KCl, 5mM MgCl<sub>2</sub>, 10mM DTT, 0.5µg total RNA (from a mix of larval and pupal animals), 1µl Oligo (dT)<sub>12-18</sub> primer (500µg/ml), 1µl dNTP mix (10mM each) in a total volume of 20µl. The RT reaction was carried out at 50°C for 50 minutes, followed by a 15 minute inactivation step at 70°C. Three primers were designed

utilizing the *Drosophila* genomic sequence located at FlyBase (accession number: AE003707, AE002708, AE014297) and used in two semi-nested PCR reactions to clone the entire open reading frame (outer primer set: 5'-CAATGTCAGCCAAGTGAAG-3', 5'-TACATATACCCTCTCATTAGC-3'; inner primer set: 5'-GAGGAAGTGGATCCATG-3', 5'-TACATATACCCTCTCATTAGC-3') in two rounds of PCR using the Expand High Fidelity PCR System (Roche Applied Science, Indianapolis, IN, USA) consisting of 30 cycles with an annealing temperature of 51°C for 25s. A 0.5µl aliquot of the PCR was used as template for subsequent amplification with the inner primers. The resulting 3kb product was cloned into the TOPO II vector (Invitrogen). Sequencing of multiple clones revealed the existence of two splice variants (Gyc-88E-L and Gyc-88E-S) that differed by 21 bp, depending how the 10<sup>th</sup> and 11<sup>th</sup> exons are spliced together. To determine if the splice variants were expressed in other stages, RT reactions were performed as described above on total RNA prepared from mixed larval stages or adults. Two nested sets of primers that were designed to amplify across the junction between the 10<sup>th</sup> and 11<sup>th</sup> exons were used in two rounds of PCR to produce a 70 bp or 91 bp band corresponding to Gyc-88E-S and Gyc-88E-L respectively. The outer set of primers: 5'-GCACCAGCCAGAGAAACG-3', 5'-TACATATACCCTCTCATTAGC-3'; the inner set of primers: 5'-GCAGTGCATCATTGGATC-3', 5'-GCAGTTGGAGTGGTTGCA-3'. The composition of the reaction mixture was: 20mM Tris-HCl (pH 8.4), 50mM KCl, 1.5mM MgCl<sub>2</sub>, 200µM each dNTP, 500 nmol of each primer, 0.5µl reverse transcription reaction, and 2.5 units of *Taq* DNA polymerase (Invitrogen) in a 50µl reaction for 30 cycles with an annealing temperature of 51°C for 25s. A 0.5 µl aliquot of the PCR was used as the

template for subsequent amplification with the inner primers using the same reaction conditions. A 3% NewSieve GQA agarose gel (ISC BioExpress, Kaysville, UT, USA) was used to distinguish the two PCR products.

The Gyc-89Da ORF that was used in all biochemical assays was cloned using the same PCR conditions used above to clone Gyc-88E, but instead of using an RT reaction for the template a single stranded unpackaged embryonic cDNA library (Clonetech, Palo Alto, CA, USA) was used with the following primer set: 5'-TTTAATCGTCCATTGTTTCC-3', 5'-ATCAGAACATGGTGCTATAAA-3'.

The Gyc-89Da UTR (partial) was elucidated by predicting the exon-intron structure in part by using two web services at the Berkeley Drosophila Genome Project: Neural Network Transcription Start site prediction ([http://www.fruitfly.org/seq\\_tools/promoter.html](http://www.fruitfly.org/seq_tools/promoter.html)) and Neural Network Splice Acceptor/Donor Prediction ([http://www.fruitfly.org/seq\\_tools/splice.html](http://www.fruitfly.org/seq_tools/splice.html)). It appeared that Gyc-89Da might have the same intron-exon structure as Gyc-89Db with a first exon containing all UTR, a large intron, and a final second exon containing some UTR and all of the ORF. Several 5' primers were designed to amplify off of this putative first exon, with the 3' primers lying just outside the stop codon. A product was obtained using an outer set of primers: 5'-AAGTCCTGTTTAACCGTTAT-3' and 5'-ACTCCTCCTGCACGTAGT-3' and an inner set of primers for round 2: 5'-CATCACTCCTGCAAGGAAT-3' and 5'-GCACACTCTCATACAGCAT-3'. Gyc-89Db was obtained as an expressed sequence tag (EST) (clone ID: GH09958) from the Berkeley Drosophila Genome Project (BDGP).

### **Generation of Gyc-88EΔC74 and Gyc-88EΔC341**

A shortened tail and tailless version of Gyc-88E was generated by performing PCR on the previously acquired Gyc-88E-S clone in TOPO II using primers designed with a stop codon addition. The 5' primer used for both versions was: 5'-CAATGTCAGCCAAGTGAAG-3'. The 3' primer used for Gyc-88EΔ74 (removed residues 883-957) was: 5'-TTACAGCCGGTTCTCTC-3'. The 3' primer used for Gyc-88EΔ341 (removed residues 616-957) was: 5'-TACTTGGTCGCCTTGTC-3'.

### **Northern Blots**

Poly(A)<sup>+</sup>-selected RNA (1.5μg) from selected stages was separated on a 1% denaturing formaldehyde agarose gel as previously described (Sambrook, 1989) and transferred to a Nytran SuperCharge nylon membrane using a Turboblotter (Schleicher and Schuell BioScience, Keene, NH, USA). A digoxigenin (DIG)-labeled RNA probe was generated using full length Gyc-88E or a portion of the ribosomal protein RP49 (used for a loading control) with the Megascript Kit (Ambion, Inc.) using DIG-UTP (Roche Applied Science). The resulting probe was hybridized to the membrane-bound transcript at 68°C using UltraHyb (Ambion, Inc.), with a final probe concentration of 0.1μM. Hybridized membranes were washed 2 x 10 minutes with low stringency wash (2 x SSC buffer, 0.1% SDS) and 2 x 15 minutes with high stringency wash (0.1 x SSC, 0.1% SDS) at 68°C. Membranes were then incubated with Fab fragments of sheep anti-DIG-AP (alkaline phosphatase) antibody (Roche Applied Science) at 1:1000 dilution in maleic acid buffer (Roche Applied Science) for one hour, followed by two 15 minute

washes with wash buffer (Roche Applied Science). AP was detected by applying CDP-Star chemiluminescent substrate (Roche Applied Science) to the membrane.

### **Transient expression of Gyc-88E and Gyc-89Db, and guanylyl cyclase assay**

To examine the enzyme activities of Gyc-88E, the full open reading frame (ORF) of Gyc-88E-L and Gyc-88E-S were subcloned into the mammalian expression vector pcDNA3.1 (Invitrogen) utilizing ApaI and KpnI restriction enzyme sites. A cDNA of Gyc-89Db that contained the full ORF was obtained as an expressed sequence tag (EST) cDNA (Clone ID: GH09958) from the Berkley Drosophila Genome Project and subcloned into pcDNA 3.1 utilizing EcoRI restriction enzyme sites. COS-7 cells were transiently transfected with constructs and extracts were collected as previously described. (Nighorn et al., 1999). When multiple guanylyl cyclases were cotransfected, the transfection efficiency was monitored by the addition of 1 mg of a  $\beta$ -galactosidase expression plasmid (Invitrogen).  $\beta$ -Galactosidase activity was determined by incubating cell extracts with 1.3mg/ml *o*-nitrophenyl- $\beta$ ,D-galactopyranoside in a 100 mM sodium phosphate buffer, pH 7.0, containing 1.5 mM MgCl<sub>2</sub> and 75 mM  $\beta$ -mercaptoethanol at room temperature for 5-20 min. The reaction was stopped by the addition of 2 mM Na<sub>2</sub>CO<sub>3</sub> and the absorbance measured at 405 nm. Guanylyl cyclase activity was measured in a buffer containing 50 mM MOPS-KOH, pH 7.5, 60 mM KCl, 8 mM NaCl, 4 mM MnCl<sub>2</sub>, 10 mM each of cGMP phosphodiesterase inhibitors dipyridamole and zaprinast and 1 mM GTP. The reaction was stopped with 0.2 M zinc acetate and excess GTP precipitated with 0.2 M Na<sub>2</sub>CO<sub>3</sub>. The amount of cGMP formed was determined using a cGMP enzyme-linked immunoassay (EIA; Kingan et al., 1997). 1H-



[1,2,4]Oxadiazole[4,3-a]quinoxalin-1-one (ODQ) was dissolved in dimethyl sulfoxide (DMSO) (Sigma-Aldrich, St. Louis, MO, USA) prior to use in guanylyl cyclase assays and was used at a final concentration of 100 $\mu$ M. NO donors were dissolved in distilled water or DMSO just prior to use in guanylyl cyclase assays. Sodium nitroprusside (SNP, Sigma-Aldrich), S-nitroso-N-acetyl-penicillamine (SNAP) (Calbiochem, San Diego, CA, USA), S-nitrosoglutathione (SNOG, Calbiochem), were used at a final concentration of 100 $\mu$ M. Sodium cyanide (Sigma-Aldrich) was dissolved in water just prior to use.

## Results

### Cloning and sequence analysis

The predicted sequence and intron/exon structure of Gyc-88E (Fig. 2.1) obtained from Flybase was consulted to design a nested set of primers with the goal of cloning the entire open reading frame (ORF) for use in an expression vector. Sequencing of several of the resulting clones revealed prediction errors in 3' end of the gene. In all clones, a splice in the message occurred just before the predicted stop codon in exon 9, resulting in an extended ORF included in a 10<sup>th</sup> and 11<sup>th</sup> exon (Fig. 2.1). Two variations were found in the splicing of exon 10 and 11. The long variant, Gyc-88E-L, includes an additional 21 base pairs, translating into an extra 7 amino acids. This extra sequence contains predicted phosphorylation sites for cGMP-dependent protein kinase (KKIT) and protein kinase C (KITFS). The last two exons of the experimentally determined ORF of Gyc-88E include the C-terminal extension, a feature absent from all classical soluble guanylyl cyclase subunits but is found in the *Manduca sexta*, *Anopheles gambiae*, *Apis mellifera* Gyc-88E orthologues, MsGC- $\beta$ 3, CP12881 (Aga  $\beta$ 3), AmsGC-beta3 (Ame  $\beta$ 3) respectively (Fig.

2.1). While the C-terminal extensions of Gyc-88E and its orthologs are of similar lengths, they bear virtually no similarity to each other except for a highly conserved stretch of about 40 amino acids (Fig. 2.2). This conserved section contains several protein phosphorylation consensus motifs, but bears little similarity with anything else in the NCBI database.

Gyc-89Db was acquired as an EST clone from the BDGP, and its sequence, including the 5' and 3' untranslated regions (UTRs) were previously available on Flybase. The entire ORF is contained on a single exon (Fig. 2.1). This exon is preceded by a smaller exon that contains almost all of the 5'UTR.

Like Gyc-88E, Gyc-89Da was cloned with the aim of generating a functional ORF, for use in an expression vector. Sequencing several clones confirmed the Flybase predicted ORF contained on one large exon, as found with Gyc-89Db. We also wished to obtain 5' UTR sequence for the generation of more specific RNA DIG-labeled probes (discussed in Chapter 3). In order to do this, I used two web-based services at the Berkeley *Drosophila* Genome Project (Neural Network promoter transcriptional start prediction and splice donor/acceptor prediction) to predict potential transcriptional start sites and likely splice donor sites. This information was used to access the possible structures of the first exon in order to design primers with the aim of amplifying a product that included most of the 5'UTR and part of the ORF. Several primers were designed to amplify the predicted UTR possibilities. A PCR product was obtained with an internal ORF primer and one that was 22 bp downstream of the (5' most) predicted transcription start site. Multiple clones of this product were sequenced. The gene structure of Gyc-89Da is very similar to Gyc-89Db, consisting of a smaller first exon

containing most of the 5'UTR and a second exon containing a small portion of UTR and the whole ORF (Fig. 2.1). A splice variation was discovered in the joining of exon 1 and 2 (Fig. 2.1). The long variant possesses 14 extra base pairs of UTR. The first exon size is either 270 bp or 284 bp. 11 bp of UTR are included in upstream of the ORF.

### **Both Gyc-88E splice variants are expressed in larvae and adults**

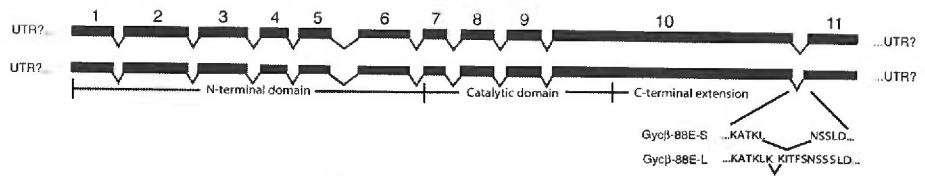
A Northern blot, using full length Gyc-88E as a probe, revealed a single Gyc-88E transcript of approximately 6 kb (Fig. 2.3A). This is about twice the size of the coding region of the transcript, indicating extensive 5' and/or 3' untranslated regions. This transcript was present in both larval and adult stages with apparently higher levels of transcript present in the adult (Fig. 2.3A).

To determine whether there was any developmental regulation of the different Gyc-88E splice variants, we used RT-PCR to examine their expression in larvae and adults (Fig. 2.3B). Two pairs of nested primers were designed to amplify a region across the splice junction to yield a 70 bp or 91 bp product, corresponding to Gyc-88E-S and Gyc-88E-L respectively. A high resolution 3% agarose gel was then used to resolve the two products. I detected PCR products corresponding to both Gyc-88E-L and Gyc-88E-S in samples from both larvae and adults (Figure 2.3B). The 140 bp fragment present in all lanes corresponds to genomic DNA contamination in the samples. No specific effort was made to amplify products in the linear range; therefore, no comparisons about the relative levels of transcripts can be made.

**Figure 2.1.** Gene structure and variations of Gyc-88E, Gyc-89Da, and Gyc-89Db. Exons are represented by boxes while introns are indicated with lines. The guanylyl cyclase functional domains are also indicated. Two Gyc-88E splice variants are generated through the use of alternative splice/donor sites to vary how exons 10 and 11 are connected to yield Gyc-88E-S and Gyc-88E-L, which includes an additional 21 bp. The extra 21 bp in Gyc-88E-L translate into a 7 amino acid stretch that contains potential PKC and PKG phosphorylation motifs, "KITFS" and "KKIT" respectively. The asterisks above exon 10 indicate the location of the highly identical region shown in Figure 2.2. Below Gyc-88E are the gene diagrams for Gyc-89Da and Gyc-89Db. Gyc-89Da was found to have a similar structure to Gyc-89Db, with a smaller 1<sup>st</sup> exon containing all UTR and a large 2<sup>nd</sup> exon containing all of the ORF. A small variation was found in the splicing of the Gyc-89Da first and second exon, affecting only the UTR. The gene structure of Gyc-89Db was previously available from Flybase, obtained from an expressed sequence tag (EST).

Gyc-88E-S (short variant) 2820 bp (ORF)

Gyc-88E-L (long variant) 2838 bp (ORF)



Gyc-89Da 2001 bp (ORF)



UTR variant 1 ...GTGCGTGAAGTTATTGGTG...intron  
UTR variant 2 ...GTGCGT...intron

Gyc-89Db 2007 bp (ORF)



Gyc-88E	722	<b>SR</b>	<b>YSPVTFKDVARRSVANSPVRSCEQFDQERRRESRSNST</b>	762
MsGC-β3	690	<b>RRM</b>	<b>YSPVTFODVARRSIANSPINR-----AERERESRSNST</b>	725
Aga β3	599	<b>RRV</b>	<b>YSPVTFEDVARRSIANSPVKLHAFG--PRGRENRSNST</b>	638
Ame β3	672	<b>RR</b>	<b>IYSPITTFODVARRSVANSPTKN-----ADSRERYRSNST</b>	706

**Figure 2.2.** ClustalW sequence alignment of the highly identical regions in the C-terminal extensions of the known Gyc-88E orthologues. The location of this sequence in the C-terminal extension of Gyc-88E is indicated by the asterisk in Figure 2.1. The region in Gyc-88E is compared with the homologous region in the *Manduca* MsGC-β3 (Nighorn et al., 1999), in the predicted orthologue CP12881 (Aga β3) in *Anopheles gambiae* (accession number EAA01162), and in the predicted orthologue (Ame β3) in *Apis mellifera* (accession number BAD89804). This region contains several protein phosphorylation consensus motifs, but bears little similarity with anything else in the NCBI database.

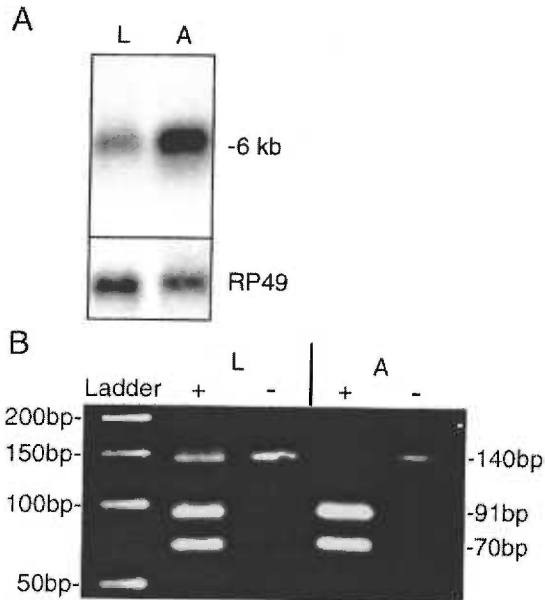


**Figure 2.3.** Expression of Gyc-88E in larvae and adults. **(A).** Northern blot showing the 6 kb transcript for Gyc-88E is present in both larvae (L) and adults (A). For a loading control, membranes were stripped and re-hybridized with a DIG-labeled riboprobe for the ribosomal protein RP49. **(B)** Both splice variants of Gyc-88E are expressed in both larvae (L) and adults (A). RT-PCR was used to amplify across the junction between exons 10 and 11 to distinguish between Gyc-88E-S and Gyc-88E-L. Both a 70 bp (Gyc-88E-S) and a 91 bp band (Gyc-88E-L) were detected in samples from both larvae (L) and adults (A) in the presence of reverse transcriptase (+). These two bands were not observed when the reverse transcriptase was omitted (-). The 140 bp band observed in all lanes results from the amplification of Gyc-88E genomic DNA contamination.

### **All three *Drosophila* atypical cyclases are expressed throughout development**

To determine the temporal expression pattern of each of the three *Drosophila* atypical guanylyl cyclases, RT-PCR was performed on mixed embryo, larval, pupal, and adult total RNA samples. Each of the subunits appeared to be expressed at similar levels in all life stages examined (Fig. 2.4). Since it was necessary to use two rounds of PCR to detect the product and no effort was made to ensure the second round of PCR ended at a linear round of amplification, there may be variations in expression levels not apparent here. However, each guanylyl cyclase is clearly expressed at some level in all stages.

### **Enzyme activity of *Drosophila* soluble guanylyl cyclases *in vitro***

To test the predictions described in Chapter 1, we subcloned the Gyc-88E, Gyc-89Da, and Gyc-89Db open reading frames into the mammalian expression vector, pcDNA3.1. These constructs were then transiently transfected in COS-7 cells and the resulting extracts assayed for guanylyl cyclase activity. As expected (see Chapter 1) Gyc-88E displayed basal activity in the absence of other subunits with both Gyc-88E splice variants yielding similar levels of activity (activity levels in equivalent conditions were not significantly different,  $p > 0.05$ , Kruskal-Wallis with Tukey-Kramer post test; Fig. 2.5). All previously described guanylyl cyclases require a metal ion co-factor (Mg or Mn) for activity, with Mn yielding higher levels of activity compared to Mg (Lucas et al., 2000). Gyc-88E exhibited similar properties, with significantly higher levels of activity measured in the presence of Mn compared to Mg (for both variants,  $p < 0.001$ , Kruskal-Wallis with Tukey-Kramer post test; Fig. 2.5).



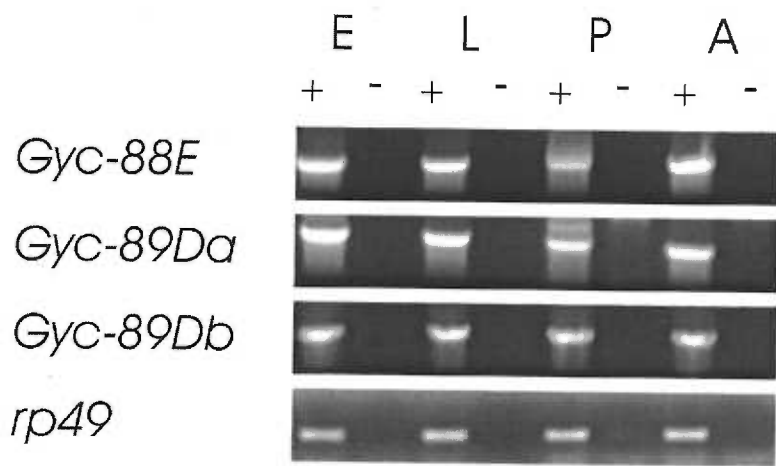


**Figure 2.4.** Expression of the atypical soluble guanylyl cyclase subunits throughout development. RNA was extracted from the stages shown and cDNA synthesis performed in the presence (+) or absence (-) of reverse transcriptase. The reaction product was then used as a substrate for PCR amplification with specific primers for *Gyc-88E*, *Gyc-89Da*, *Gyc-89Db* or ribosomal protein 49 (*rp49*).

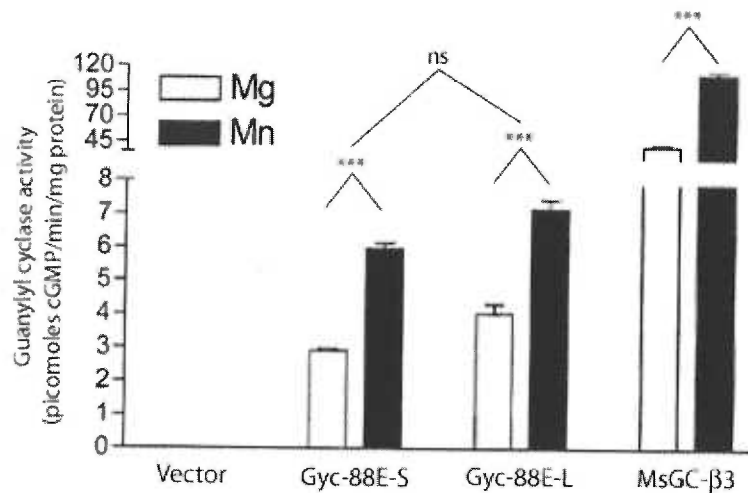


**Figure 2.5.** Guanylyl cyclase activity of Gyc-88E. COS-7 cells were transiently transfected with pcDNA3.1 vectors containing the open reading frames of various soluble guanylyl cyclase subunits and the cell extracts assayed for guanylyl cyclases activity under the conditions shown. Gyc-88E exhibits enzyme activity in the absence of additional subunits and has higher levels of activity in the presence of Mn compared to Mg. The *Manduca* guanylyl cyclase, MsGC-β3 exhibits similar properties and was included for comparison. The two splice variants of Gyc-88E, Gyc-88E-S and Gyc-88E-L yielded similar levels of activity as each other. Data shown are the mean  $\pm$  SEM of 4 determinations.

As a comparison, we also transfected COS-7 cells with a plasmid coding for the *Manduca* guanylyl cyclase, MsGC- $\beta$ 3 (Nighorn et al., 1999). The basal activity of MsGC- $\beta$ 3 was significantly higher (at least 10 fold) than Gyc-88E ( $p < 0.001$ , Kruskal-Wallis with Tukey-Kramer post test) (Fig. 2.5), but whether this was due to an intrinsically higher level of specific activity or whether it reflected higher levels of protein is not known.

To further investigate possible enzymatic differences between the two Gyc-88E splice variants, I assayed cell extracts for guanylyl cyclase activity in the presence of differing concentrations of GTP in the presence of either Mg or Mn (Fig. 2.6). Michaelis-Menton kinetics analysis was applied to the results to examine differences in the  $K_m$  or  $V_{max}$  between the splice variants. Estimates for the value of  $K_m$  for both splice variants were similar to each other in the presence of Mg (Gyc-88E-S,  $2.8 \pm 0.8$  mM; Gyc-88E-L,  $2.5 \pm 0.6$  mM) and Mn (Gyc-88E-S,  $0.03 \pm 0.02$  mM; Gyc-88E-L,  $0.02 \pm 0.02$  mM). The values for  $V_{max}$  of the splice variants were also the same as each other in the presence of Mg (Gyc-88E-S,  $6.5 \pm 0.7$  pmol cGMP/min/mg protein; Gyc-88E-L,  $6.0 \pm 0.6$  pmol cGMP/min/mg protein) and Mn (Gyc-88E-S,  $5.1 \pm 0.2$  pmol cGMP/min/mg protein; Gyc-88E-L,  $5.2 \pm 0.1$  pmol cGMP/min/mg protein). The calculated  $K_m$  of both Gyc-88E splice variants is comparable to values found in a previous study for MsGC- $\beta$ 3 (Morton and Anderson, 2003), in both Mg ( $K_m = 2.62 \pm 0.81$ ) and Mn ( $K_m = 0.13 \pm 0.07$ ). In contrast, the values for the  $V_{max}$  calculated for MsGC- $\beta$ 3 (Mg:  $V_{max} = 62.3 \pm 11.2$ , Mn:  $V_{max} = 39.0 \pm 5.0$ ) were substantially higher than the values calculated for Gyc-88E.

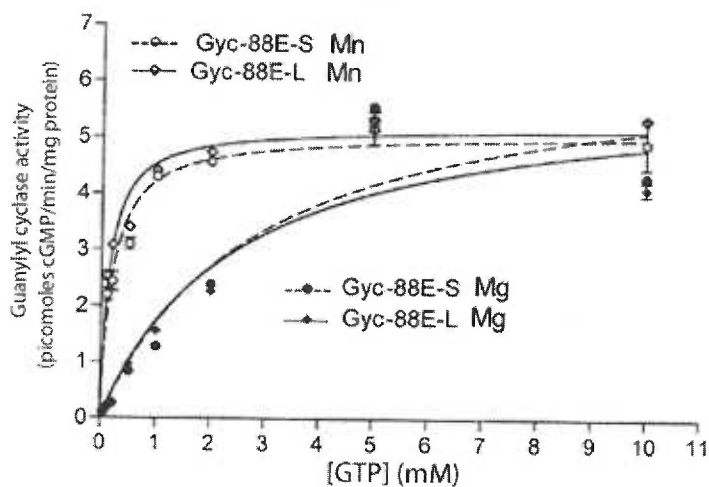


**Figure 2.6.** Kinetic analysis of Gyc-88E-S and Gyc-88E-L. Cell extracts were assayed for guanylyl cyclase activity in the presence of 0.1 to 10mM GTP in the presence of either 4mM Mg or Mn. A Michaelis-Menton curve was applied to the resulting data using Graphpad Prism 3.0. No difference in  $K_m$  or  $V_{max}$  was observed between the splice variants in the presence of Mg or Mn.

It is likely that the C-terminal extensions of Gyc-88E and its insect orthologs play a regulatory role in enzyme activity. Previously it had been demonstrated that removing the entire C-terminal extension (338 amino acids) or just 29 amino acids from the C-terminal end of MsGC- $\beta$ 3 significantly reduced the calculated  $K_m$  in the presence of Mg, using the same in vitro assay techniques used here (Morton and Anderson, 2003). This finding suggests that the C-terminal domain plays an auto-inhibitory role in enzyme activity. To determine if the C-terminal extension plays an inhibitory role in Gyc-88E, the final 341 or 74 amino acids were removed (from Gyc-88E-S) by amplifying the cDNA with 3' primers that contained a stop codon, truncating the transcript at the desired location. The 341 amino acid deletion removes the entire C-terminal extension (Fig. 2.1), including the highly identical region shown in Figure 2.2. This protein is truncated shortly after the catalytic domain (within exon 10 in Figure 2.1), where conventional  $\beta$  subunits terminate. The 74 amino acid deletion removes only exon 11 (Fig. 2.1), leaving the highly identical region intact (Fig. 2.2). The enzyme activities of the resulting constructs were compared to the full length Gyc-88E. In contrast to the results found with MsGC- $\beta$ 3, removing the C-terminal extension of Gyc-88E-S significantly decreased its activity compared to the full length protein (repeated measures by ANOVA; Fig. 2.7). However, when only 74 amino acids were removed from the end of Gyc-88E, a small but significant increase in activity was observed (repeated ANOVA).

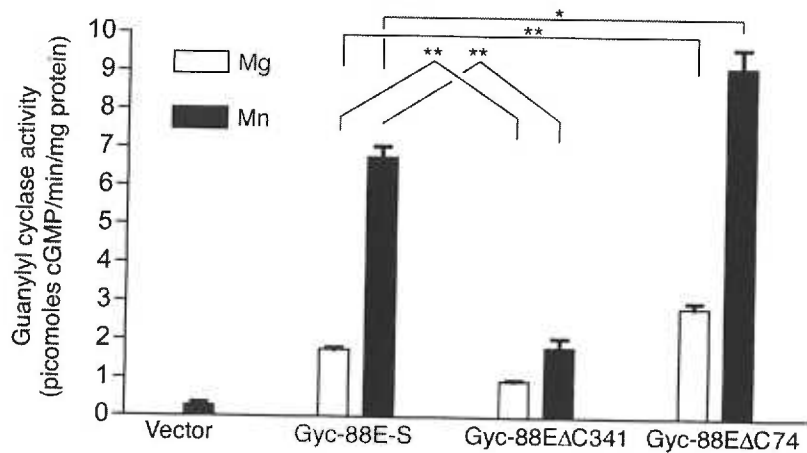


**Figure 2.7.** Guanylyl cyclase activity of two truncated versions of Gyc-88E. Truncations of Gyc-88E were made by amplifying the existing Gyc-88E cDNA using 3' primers that had a stop codon built in, as described in the methods. The resulting constructs were then subcloned back into pcDNA3.1 and tested in the guanylyl cyclase assay. Gyc-88EΔC341 yielded less activity, while Gyc-88EΔC74 yielded more activity than the unaltered Gyc-88E. Data shown are the mean  $\pm$  SEM of 2 determinations.

When the NO donor sodium nitroprusside (SNP) was applied to the extracts, a small but significant increase in activity was observed with both Gyc-88E splice variants ( $p < 0.001$  Kruskal-Wallis with Tukey-Kramer post test; Fig. 2.8). Application of S-nitroso-N-acetylpenicillamine (SNAP), an unrelated NO donor, also slightly stimulated Gyc-88E (both variants,  $p < 0.001$  Kruskal-Wallis with Tukey-Kramer post test) (Fig. 2.9). In contrast to Gyc-88E, MsGC- $\beta 3$  was not stimulated by NO donors in COS-7 cells extracts (Nighorn et al, 1999). The increase in activity of Gyc-88E was much lower (2-3 fold) than comparable samples transfected with the *Manduca*  $\alpha 1$  and  $\beta 1$  subunits (10-20 fold) (Fig. 2.8 and 2.9). Application of the soluble guanylyl cyclase inhibitor 1H-[1,2,4]oxadiazolo[4,3,-a]quinoxaline-1-one (ODQ) in the NO donor experiments failed to significantly inhibit the stimulation of Gyc-88E, in contrast to the MsGC- $\alpha 1/\beta 1$  heterodimer, where the NO-stimulation was almost completely inhibited ( $p > 0.05$ , Kruskal-Wallis with Tukey-Kramer post test; Fig. 2.8 and 2.9). Surprisingly, the basal level of activity of Gyc-88E was slightly stimulated in the presence of ODQ (not significant for both variants,  $p > 0.05$  Kruskal-Wallis with Tukey-Kramer post test), whereas the basal activity of the *Manduca*  $\alpha 1/\beta 1$  guanylyl cyclases was slightly inhibited (Fig. 2.8).

One of the breakdown products of SNP is cyanide ion ( $\text{CN}^-$ ), which has a structure similar to NO. Thus, it was possible that  $\text{CN}^-$ , rather than NO liberated from SNP breakdown that stimulated activity in the SNP experiments. To address this uncertainty, I performed guanylyl cyclase assays with Gyc-88E and the MsGC- $\alpha 1/\text{MsGC-}\beta 1$  heterodimer with the addition of two concentrations of sodium cyanide in the assay buffer.

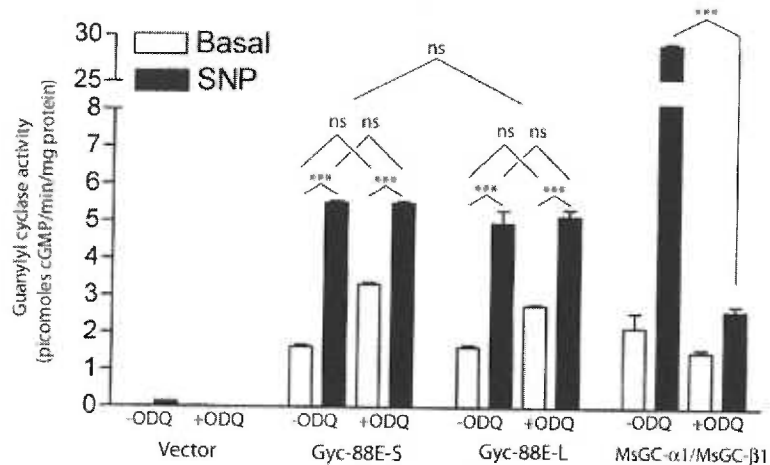


**Figure 2.8.** The NO donor SNP stimulates the activity of Gyc-88E. When the NO donor sodium nitroprusside (SNP) was included in the assay, the activity of Gyc-88E-S and Gyc-88E-L was elevated by 3- to 4-fold. By contrast, the *Manduca* guanylyl cyclases MsGC- $\alpha$ 1 and MsGC- $\beta$ 1 ( $\alpha/\beta$ ) showed a much larger increase in activity. The guanylyl cyclase inhibitor, 1H-[1,2,4]oxadiazolo[4,3,-a]quinoxaline-1-one (ODQ) eliminated the activation of the *Manduca* MsGC- $\alpha$ 1/ $\beta$ 1 heterodimer but had little effect on the stimulation of Gyc-88E. Assays were carried out in the presence of 4mM Mg. Data shown are the mean  $\pm$  SEM of 4 determinations.



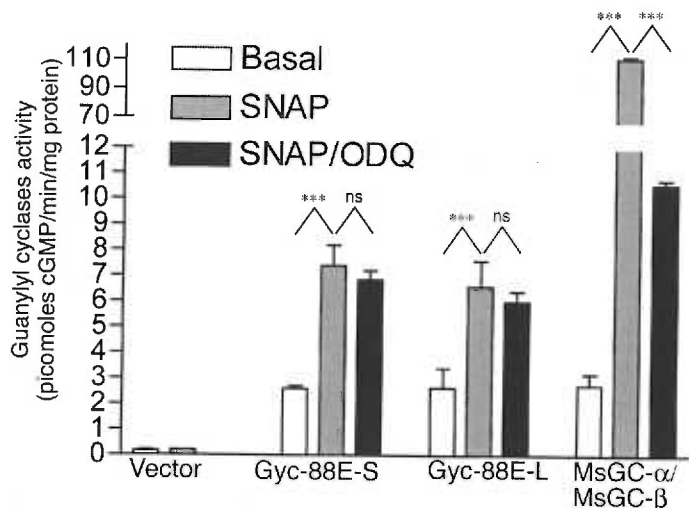


**Figure 2.9.** The NO donor SNAP stimulates the activity of Gyc-88E. When the NO donor S-nitroso-N-acetylpenicillamine (SNAP) was applied, the activity of Gyc-88E-S and Gyc-88E-L was elevated by 2-3 fold. By contrast, the *Manduca* classic soluble guanylyl cyclase MsGC- $\alpha$ 1/MsGC- $\beta$ 1 heterodimer showed a much larger increase in activity. The soluble guanylyl cyclase inhibitor, 1H-[1,2,4]oxadiazolo[4,3,-a]quinoxaline-1-one (ODQ), eliminated the activation of the *Manduca* MsGC- $\alpha$ 1/ $\beta$ 1 heterodimer but had no significant effect on the stimulation of Gyc-88E. Assays were carried out in the presence of 4mM Mg. Data shown are the mean  $\pm$  SEM of 3 determinations.

The addition of sodium cyanide failed to stimulate both Gyc-88E and MsGC- $\alpha$ 1/MsGC- $\beta$ 1 (Fig. 2.10), supporting the role of NO as the stimulator of Gyc-88E in these experiments.

To examine the guanylyl cyclase activity of Gyc-89Da and Gyc-89Db, the cloned ORF of Gyc-89Da and an EST of Gyc-89Db (obtained from the Berkeley *Drosophila* Genome Project) were subcloned into pcDNA3.1 and transiently expressed them in COS-7 cells and assayed extracts as carried out above for Gyc-88E. Gyc-89Da displayed no activity when expressed alone or when co-expressed with Gyc $\alpha$ -99B, Gyc $\beta$ -100B, or Gyc-89Db (Fig. 2.11). However, when Gyc-89Da was co-expressed with either splice variant of Gyc-88E in the presence of Mn, more activity was observed than with Gyc-88E alone. In the presence of Mg however, Gyc-88E/Gyc-89Da co-expression yielded similar activity to Gyc-88E alone.

Gyc-89Db was also inactive when expressed alone, or when co-expressed with Gyc $\alpha$ -99B (Fig. 2.12). When Gyc-89Db was co-expressed with either splice variant of Gyc-88E, in the presence of Mg or Mn, more activity was observed than when Gyc-88E was expressed alone. No significant difference in activity was observed between Gyc-88E-S/Gyc-89Db and Gyc-88E-L/Gyc-89Db.

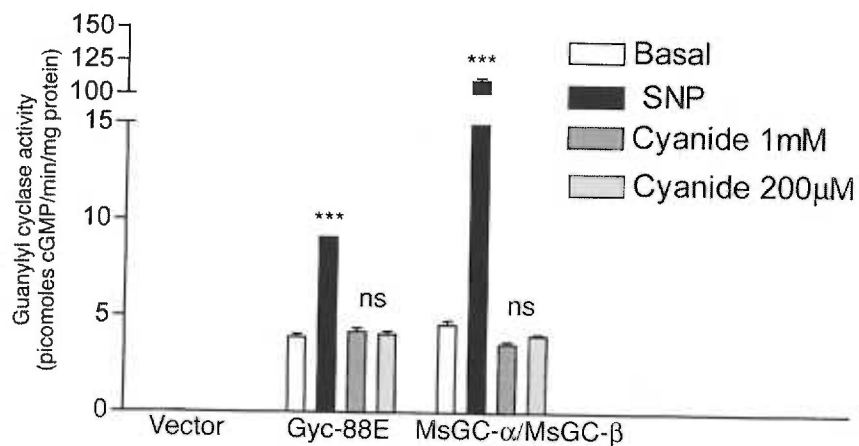


**Figure 2.10.** Sodium cyanide, a breakdown product of SNP, has no effect on the guanylyl cyclase activity of Gyc-88E or the MsGC- $\alpha$ /MsGC- $\beta$  heterodimer. SNP significantly stimulated Gyc-88E and MsGC- $\alpha$ /MsGC- $\beta$ , while two concentrations of sodium cyanide did not. Data shown are the mean  $\pm$  SEM of 2 determinations.

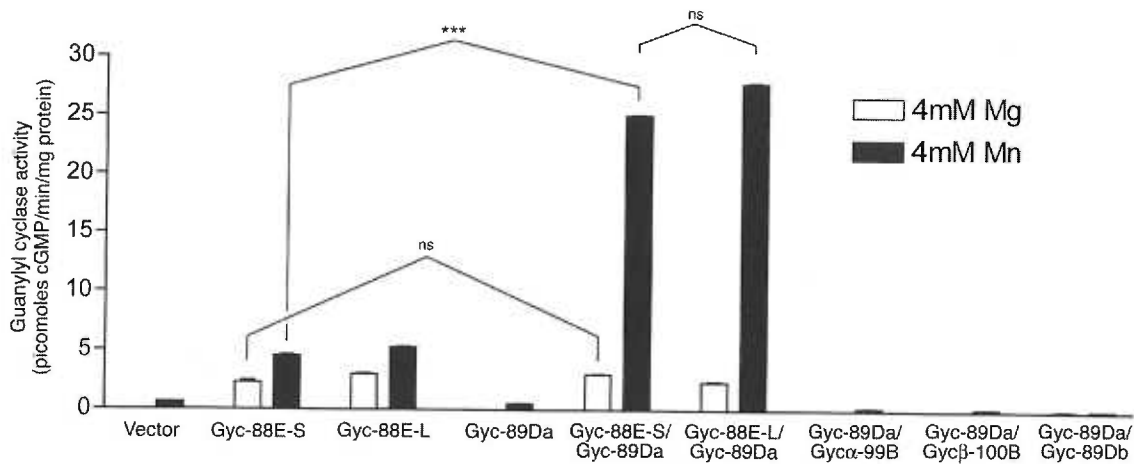


**Figure 2.11.** Guanylyl cyclase activity of Gyc-89Da. When Gyc-89Da was expressed alone, no activity was observed. However, when Gyc-89Da was expressed with either splice variant of Gyc-88E, a significant increase in activity was observed, compared to Gyc-88E expressed alone, in the presence of Mn only. Co-expression with either Gyc-88E splice variant yielded a similar level of activity. Co-expression of Gyc-89Da with Gyc $\alpha$ -99B, Gyc $\beta$ -100B, or Gyc-89Db yielded no activity. Data shown are the mean  $\pm$  SEM of 2 determinations.

To determine if Gyc-89Da or Gyc-89Db can be stimulated by NO, the NO donor SNAP was utilized in the presence of Mg. Again, Gyc-89Da and Gyc-89Db were inactive when expressed alone and no difference in activity was observed between the two Gyc-88E splice variants (Fig. 2.13). Co-expression of Gyc-89Da or Gyc-89Db with either Gyc-88E splice variant yielded more SNAP-stimulated activity than when Gyc-88E was expressed alone. The level of SNAP-stimulated activity was not significantly different between Gyc-89Da/Gyc-88E-S, Gyc-89Da/Gyc-88E-L, Gyc-89Db/Gyc-88E-S, and Gyc-89Db/Gyc-88E-L.

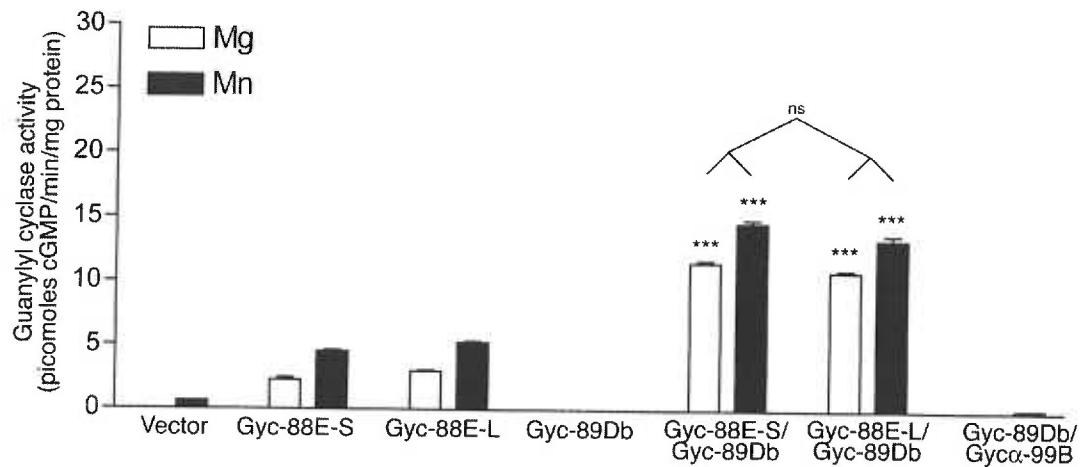


**Figure 2.12.** Guanylyl cyclase activity of Gyc-89Db. When Gyc-89Db was expressed alone, no activity was observed. When Gyc-89Db was co-expressed with either Gyc-88E splice variant, a significant increase in activity was observed, compared to the Gyc-88E variants expressed alone, in the presence of both Mg and Mn. Co-expression of Gyc-89Db with Gyc $\alpha$ -99B yielded no activity. Data shown are the mean  $\pm$  SEM of 2 determinations.

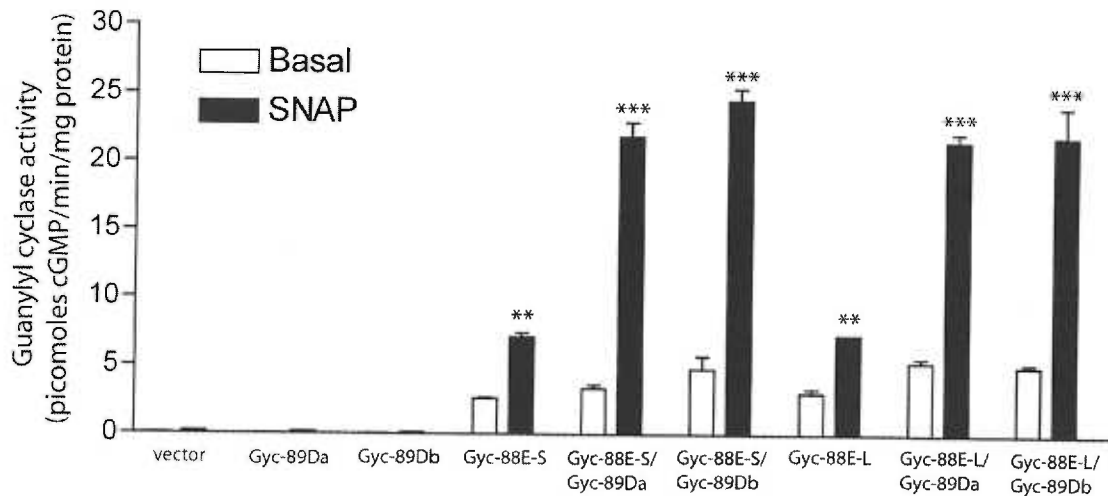


**Figure 2.13.** Stimulation of Gyc-88E, Gyc-89Da, and Gyc-89Db by the NO donor SNAP, in the presence of Mg. Gyc-89Da and Gyc-89Db alone yielded no SNOG-stimulated activity. Both splice variants of Gyc-88E were significantly activated by SNAP. Co-expression of Gyc-89Da or Gyc-89Db and Gyc-88E yielded higher levels of SNAP-stimulated activity than when Gyc-88E was expressed alone. The level of SNAP-stimulated activity was not significantly different between Gyc-89Da/Gyc-88E-S, Gyc-89Da/Gyc-88E-L, Gyc-89Db/Gyc-88E-S, and Gyc-89Db/Gyc-88E-L. Data shown are the mean  $\pm$  SEM of 2 determinations.

## Discussion

The experimentally determined sequence for Gyc-88E was found to differ from the Flybase predicted gene in the C-terminal domain. The predicted stop codon in exon 9 was bypassed by a splice site, resulting in a longer ORF contained on two additional exons. This additional sequence makes the C-terminal domain similar in length to the C-terminal domains of the insect Gyc-88E orthologues in *Manduca* (MsGC- $\beta$ 3), *Apis mellifera*, and *Anopheles gambiae*, and includes the highly conserved region of about 40 amino acids. The sequences of the C-terminal domains of these guanylyl cyclases are quite divergent but contain a highly conserved region. This region, which contains several consensus protein phosphorylation sites, likely plays an important functional role in some aspect of GC activity, cellular localization, or protein-protein interactions. Another feature found in the C-terminal domain was a splice variation, which occurs by the alternative joining of exon 10 and 11. The additional 7 amino acids found in the longer variation of the C-terminal domain contain predicted phosphorylation sites for cGMP-dependent protein kinase (KKIT) and protein kinase C (KITFS). Both of these splice variants were expressed in larval and adult stages. The experimentally determined gene structure of Gyc-89Da is similar to the structure of Gyc-89Db, further suggesting that these two highly identical guanylyl cyclases are the result of a recent gene duplication. Both genes start with a short exon containing only UTR and end with a lengthy exon that contains a small amount of UTR and the entire ORF. A splice variation was found in the 5' UTR of Gyc-89Da, occurring through alternative joining of exon 1 and 2. All three *Drosophila* atypical guanylyl cyclases were found to be expressed throughout the entire life cycle.



Gyc-88E shares a number of unusual sequence and structural features with MsGC- $\beta$ 3. First, like the receptor guanylyl cyclases and unlike all known  $\beta$ 1 subunits, both Gyc-88E and MsGC- $\beta$ 3 possess all of the residues thought to interact with the Mg-GTP substrate (see Chapter 1 and Morton and Hudson, 2002). Previous studies showed that MsGC- $\beta$ 3 does yield basal activity in the absence of other subunits (Nighorn et al., 1999) and forms homodimers (Morton and Anderson, 2003). These studies formed the basis for the prediction that Gyc-88E would also yield basal activity in the absence of other subunits, a prediction shown here to be correct. While MsGC- $\beta$ 3 yielded higher levels of basal activity than Gyc-88E, the basal activity of Gyc-88E was nevertheless similar to the basal activity levels of the *Manduca*  $\alpha/\beta$  heterodimer. Comparison of the calculated Michaelis-Menton kinetics values between Gyc-88E and MsGC- $\beta$ 3 parallel these observations. While the values for the  $K_m$  are similar between Gyc-88E and MsGC- $\beta$ 3, the values for the  $V_{max}$  are substantially higher for MsGC- $\beta$ 3 than the Gyc-88E splice variants (Morton and Anderson, 2003).

The C-terminal extension of MsGC- $\beta$ 3 was found to play an autoinhibitory role in enzyme activity: when some or all of it was removed the calculated  $K_m$  was reduced significantly in the presence of Mg, but not Mn (Morton and Anderson, 2003). The estimated values for  $K_m$  for Gyc-88E were similar to those for MsGC- $\beta$ 3, in particular the almost 20-fold reduction in the presence of Mn compared with Mg, suggesting that the C-terminal domain of Gyc-88E might also be inhibitory. In contrast to the inhibitory trend observed in MsGC- $\beta$ 3, removing the C-terminal domain of Gyc-88E resulted in significantly lowered levels of activity, although removing only part of the tail did result in significantly more activity. The kinetics of the altered tail Gyc-88E proteins was not

examined, so it is not known if the  $K_m$  was altered in either case. It is possible that removing the entire C-terminal extension in this case resulted in a globally destabilized protein, negatively affecting the catalytic domain and yielding less activity despite the absence of an autoinhibitory tail. By removing only part of the tail, perhaps the potential autoinhibitory domain was inactivated without disrupting the rest of the enzyme.

Unlike all known  $\beta 1$  subunits and the mammalian  $\beta 2$  subunits, both Gyc-88E and MsGC- $\beta 3$  have substitutions at two cysteine residues known to be crucial for heme-binding and NO-activation in the rat  $\beta 1$  subunit (Friebe et al., 1997). Extracts made from COS-7 cells transiently transfected with MsGC- $\beta 3$  yielded no increase in activity over basal levels when NO donors were applied (Nighorn et al., 1999). This observation, together with its sequence features, led to the prediction that Gyc-88E would also be NO-insensitive (Morton and Hudson, 2002). Surprisingly, we found that Gyc-88E yielded a small but significant increase in activity when sodium nitroprusside (SNP) or SNAP was applied. However, compared to the 10-20 fold stimulation of conventional  $\alpha/\beta$  heterodimers, stimulation of Gyc-88E was only 2-3 fold. Another interesting finding was that ODQ, which prevents NO-donor activation of soluble guanylyl cyclase by oxidizing the heme-group, did not block activation of Gyc-88E by SNP or SNAP. This finding illustrates possible differences between the heme groups/regulatory domain of Gyc-88E and conventional  $\alpha/\beta$  heterodimers. The region(s) that are responsible for these biochemical differences remain to be discovered.

As predicted, when Gyc-89Da or Gyc-89Db were expressed alone or when Gyc-89Da was expressed with Gyc $\beta$ -100B, no guanylyl cyclase activity was detected. In

contrast to predictions, no activity was detected when Gyc-89Da or Gyc-89Db was co-expressed with the conventional  $\alpha$  subunit, Gyc $\alpha$ -99B. It is possible that Gyc-89Da and Gyc-89Db dimerize with Gyc $\alpha$ -99B as do MsGC- $\beta$ 3 and MsGC- $\alpha$ 1 (Morton and Anderson, 2003), but possibly due to misalignment of the catalytic pockets, these heterodimers are inactive. However, when Gyc-88E was co-expressed with Gyc-89Da in the presence of Mn, more activity was measured than when Gyc-88E was expressed alone. Interestingly, when Gyc-88E and Gyc-89Da were co-expressed in the presence of Mg, no difference in activity was measured compared to Gyc-88E expressed alone. Similar results were observed when Gyc-88E was co-expressed with Gyc-89Db, although more activity was observed in the presence of both Mn and Mg compared to Gyc-88E expressed alone. These activity levels were roughly half that of Gyc-89Da/Gyc-88E in the presence of Mg. The difference in activity between these two highly identical guanylyl cyclases suggests that while one or the other of these genes may have originated from a recent gene duplication event, they may have some functional divergence *in vivo*. Both splice variants of Gyc-88E yielded similar activity levels when co-expressed with either Gyc-89Da or Gyc-89Db, suggesting that the Gyc-88E splice variation plays no functional role in the interaction with these guanylyl cyclases, at least in absence of an activator. While some differences were observed when comparing the activity levels of Gyc-88E/Gyc-89Da and Gyc-88E/89Db heterodimers in the presence of Mg and Mn, no differences in stimulated activity levels were observed between these heterodimer combinations when the NO-donor SNAP was applied. However, the SNAP-stimulated activity of Gyc-88E/Gyc-89Da and Gyc-88E/Gyc-89Db was substantially higher than the SNAP-stimulated activity levels of Gyc-88E alone. These results indicate that Gyc-89Da

and Gyc-89Db both contribute enhanced NO sensitivity to Gyc-88E, and that the potential differences in the biochemical properties between Gyc-89Da and Gyc-89Db do not involve ligand-stimulation of guanylyl cyclase activity, at least under the current conditions.

In Langlais et al. (2004), a more comprehensive selection of NO donors were tested for their ability to stimulate Gyc-88E homodimers, and Gyc-88E/Gyc-89Db heterodimers. In addition to SNP and SNAP, SNOG (an S-nitroso compound), three different NONOates and an unrelated compound, SIN-1, were applied. SNP, SNAP, and SNOG significantly stimulated soluble guanylyl cyclases in all experiments. However, SIN-1 and the three NONOates were unable to significantly stimulate the Gyc-88E homodimer, although they did raise the level of activity noticeably. Two of these NONOates and SIN-1 did significantly stimulate Gyc-88E/Gyc-89Db. It is notable that YC-1, an NO-independent activator of conventional soluble guanylyl cyclase (Friebe and Koesling, 1998), was also ineffective at stimulating Gyc-88E and Gyc-88E/Gyc-89Db activity in these experiments. These results contrast with the effect these NO-donors have on the conventional  $\alpha/\beta$  heterodimer, where all of the compounds tested were effective at stimulating guanylyl cyclase activity. The fact that several different classes of NO donors were capable of activating both Gyc-88E and the Gyc-88E/Gyc-89Db heterodimers demonstrates that NO, rather than another breakdown product of these compounds, was the active component in these experiments.

The biochemistry of Gyc-88E, Gyc-89Da, and Gyc-89Db was examined in more detail in Morton et al. (2005). To further characterize enzymatic differences between these subunits, the Michaelis-Menton kinetics of Gyc-88E, Gyc-89Da/Gyc-88E, and

Gyc-89Db/Gyc-88E were calculated using the same methods used in this chapter. No significant difference was found in the estimated value for the  $V_{\max}$  for GTP in the presence of Mg between Gyc-88E-L, Gyc-89Da/Gyc-88E-L, and Gyc-89Db/Gyc-88E-L whereas in the presence of Mn, Gyc-89Da/Gyc-88E-L yielded a significantly higher estimate for  $V_{\max}$  than either Gyc-88E-L or Gyc-89Db/Gyc-88E-L. In contrast, Mn was found to have a much greater effect (lowering values) on the  $K_m$  of Gyc-88E-L and Gyc-89Db/Gyc-88E-L than Gyc-89Da/Gyc-88E-L. These results correlate well with my findings that Gyc-89Da/Gyc-88E yields more activity than Gyc-89Db/Gyc-88E in the presence of Mn, while Gyc-89Db/Gyc-88E yields more activity than Gyc-89Da/Gyc-88E in the presence of Mg.

In Morton et al. (2005), the NO-stimulated activity of Gyc-88E-L, Gyc-89Da, and Gyc-89Db was also examined in more detail by exposing the different subunit combinations to varying concentrations of NO-donors, and comparing fold-stimulation from basal levels. BAY 41-2272, a potent, NO-independent stimulator of conventional  $\alpha/\beta$  heterodimers, failed to stimulate any of the atypical guanylyl subunit combinations. Gyc-89Da/Gyc-88E and Gyc-89Db responded similarly to SNAP and NOC-12. A difference was found between these subunit combinations with the application of DEAE-NONOate, which failed to significantly stimulate these subunits in NO-donor experiments. Lower concentrations of DEAE-NONOate than used in Langlais et al. (2004) significantly stimulated Gyc-89Db/Gyc-88E only, with a maximum 4-fold increase in activity. Higher concentrations of this NO-donor were found to be less effective for stimulation. These experiments support the possibility of different functions

and sensitivities *in vivo* for Gyc-89Da and Gyc89Db as opposed to redundant or interchangeable functions.

While I report here that ODQ was not able to significantly inhibit the SNP- or SNAP-stimulated activity of Gyc-88E, Morton et al. (2005) found that the application of ODQ completely abolished the stimulation of Gyc-89Db/Gyc-88E by DEAE-NONOate or NOC-12. Morton et al. (2005) did not examine the effect of ODQ on NO-stimulation of the Gyc-88E homodimer. Perhaps Gyc-88E heterodimers are sensitive to ODQ while the Gyc-88E homodimer is not. Alternatively, if lower concentrations of the NO donors and/or a higher concentration of ODQ were used in my experiments, a reduction in stimulation may have been observed. The results reported in Morton et al. (2005) suggest that the mechanism of activation of Gyc-88E heterodimers by NO-donors occurs through the heme-group, since ODQ inhibits NO-stimulation of soluble guanylyl cyclases by oxidizing this group (Garthwaite et al., 1995) (Zhao et al., 2000).

Evidence has recently emerged that suggests that oxygen, rather than NO, acts as the natural ligand of the *Drosophila* atypical guanylyl cyclases. First, it was found that the heme-domain of an atypical soluble guanylyl cyclase (GCY-35) in *C. elegans* binds oxygen (unlike conventional soluble guanylyl cyclase heme-domains) and is required for a social feeding behavior that is mediated by oxygen sensation (Gray et al., 2004). Next, it was reported that Gyc-88E, Gyc-88/Gyc-89Da, and Gyc-88E/Gyc-89Db were all significantly stimulated under anoxic conditions, with Gyc-88E/Gyc-89Db showing a much larger increase in activity, on par with the NO-stimulated activity levels of Gyc $\alpha$ -99B/Gyc $\beta$ -100B (which was not activated by anoxic conditions) (Morton, 2004a).

Anoxia/hypoxia-stimulated activity was induced rapidly (significant increase starting at 1

minute), showed a graded response to oxygen concentrations, and was blocked by ODQ. These results, taken along with the data that show that NO-donors are only weak activators, strongly suggest that the natural ligand of the *Drosophila* atypical soluble guanylyl cyclases is oxygen.

The sequence features that appear to characterize oxygen-sensitive GCs have been identified in a recent report. The crystal structure of an oxygen binding protein domain from the obligate anaerobe, *Thermoanaerobacter tengcongensis*, has been solved (Pellicena et al., 2004). This domain, which is part of the chemotaxis receptor Tar4, is related to the heme domain of sGCs, and was named the heme-NO and oxygen binding (H-NOX) domain. This domain was shown to have a protein fold in which a tightly packed central cavity houses an unusually distorted heme group. In contrast to sGCs, where spectroscopic studies indicate that the binding of NO breaks the proximal histidine-iron bond (resulting in a five coordinate complex), the H-NOX forms a six-coordinate ferrous-oxy complex (Karow et al., 2004). Y-140, which is fixed in specific orientation by a hydrogen-binding network, was predicted to contribute to the gas binding specificity of the protein for oxygen (Fig. 2.14A). A follow up study, using H-NOX point-mutants, demonstrated that Y-140 is necessary and sufficient for oxygen binding and is important for discrimination between oxygen and NO (Boon et al., 2005). Ser-133, and Arg-135 were determined to be very important or crucial for coordination of the heme propionate groups and form a conserved “YxSxR” motif that is invariant in all H-NOX domains (Fig. 2.14B) (Pellicena et al., 2004).

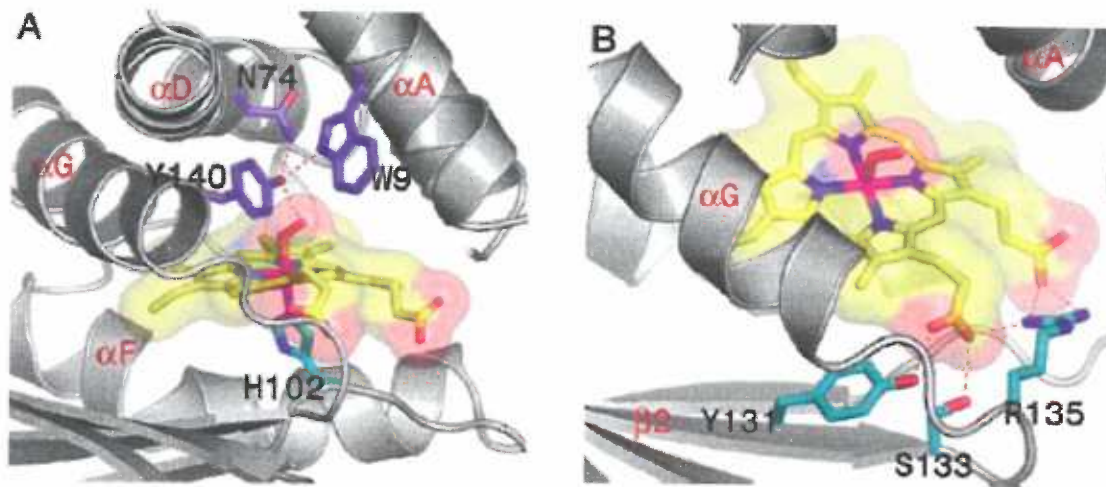


**Fig. 2.14.** Heme environment. (A) Ligand-binding pocket. Tyr-140 is shown hydrogen bonding (red dashes) to the heme-bound oxygen ligand. Trp-9 and Asn-74 interact with Tyr-140. The proximal ligand His-102 is also shown. (B) The YxRxS motif, corresponding to residues Tyr-131, Ser-133, and Arg-135, coordinates the heme propionates. *Figure and legend from Pellicena et al. (2004).*



A sequence alignment that includes the H-NOX domain of *T. tengcongenensis* and heme-binding/potential H-NOX domains of known or predicted atypical GCs reveals that the “YxSxR” motif and Tyr-140 is present in Gyc-88E, Gyc-89Da, Gyc-89Db, and a large number of other atypical sGCs (Fig. 2.15). Importantly, this Tyr residue is not found in any known NO-sensitive sGC subunit (see *Drosophila*  $\beta$ 1 example sequence in alignment). In the *T. tengcongenensis* H-NOX domain, the Tyr residue is the 5<sup>th</sup> residue following the YxSxR motif. Gyc-88E has two Tyr residues, with one in the 5<sup>th</sup> and 6<sup>th</sup> position after the YxSxR motif, while Gyc-89Da and Gyc-89Db each have one Tyr residue at 6<sup>th</sup> position. In the *C. elegans* GCY-35 and GCY-36, the Tyr is the 4<sup>th</sup> residue after the YxSxR motif. These differences indicate that there may be some degree of positional flexibility of the Tyr residue, likely reflecting the rotational position of the  $\alpha$ G helix (Fig. 2.14). The functional significance of the two Tyr residues in Gyc-88E is unclear. Several other insect species, including two more dipterans, one hymenopteran, and two lepidopterans have atypical sGCs subunits that have at least one Tyr residue in a position comparable to Tyr-140 (Fig. 2.15). It appears that all insect  $\beta$ 3-like subunits have two adjacent Tyr residues at the 5<sup>th</sup> and 6<sup>th</sup> positions, similar to Gyc-88E, while all insect Gyc-89D-like subunits have one Tyr at the 6<sup>th</sup> position. In the *C. elegans* GCY-31, GCY-32, GCY-33, GCY-34 and in the corresponding *C. briggsae* orthologs, a Tyr residue can be found in either the 4<sup>th</sup>, 5<sup>th</sup>, 6<sup>th</sup>, or both the 3<sup>rd</sup> and 6<sup>th</sup> positions after the YxSxR motif. GCY-37 and its *C. briggsae* ortholog CBG13876 do not have a Tyr residue following the YxSxR motif. Interestingly, some chordates also appear to have a Tyr residue(s) in a similar position in sGC subunits. In the primitive marine chordate *Ciona intestinalis*, three atypical sGCs have been predicted to occur. Cin  $\beta$ A and Cin  $\beta$ C, which

fall into the  $\beta$ 3-like grouping in Figure 1.2, have two Tyr residues with one at the 5<sup>th</sup> and 8<sup>th</sup> positions after the YxSxR motif. Cin  $\beta$ B, which falls into the Gyc-89D-like grouping in Figure 1.2, has two adjacent Tyr residues occurring in the 7<sup>th</sup> and 8<sup>th</sup> positions. Two different species of pufferfish also have been predicted to express  $\beta$ 3-like subunits. One of these  $\beta$ 3-like subunits in each fish species lacks a Tyr residue following the YxSxR motif, while the other  $\beta$ 3-like subunit has two Tyr residues, with one in the 3<sup>rd</sup> and 6<sup>th</sup> positions. Finally, the opossum  $\beta$ 2 subunit has a Tyr residue in the 5<sup>th</sup> position after the YxSxR motif. No other mammalian  $\beta$  subunits known at this time have a Tyr residue following the YxSxR motif.

Point mutation experiments now need to be carried out that examine the function of these Tyr residues in the GC activity of Gyc-88E, and in the Gyc-88E/Gyc-89D heterodimers. It is possible that the substitution of these Tyr residues with non-bulky/non-reactive residues will increase basal activity in normal atmospheric conditions, as other less inhibitory gas ligands may out compete inhibitory oxygen binding. Under hypoxic conditions, these mutants might display reduced activation, as other gases, which were previously excluded from the heme, may remain bound and have an inhibitory effect. It will also be interesting to see how the application of NO donors affect this mutant under normal and anoxic conditions.

		H-105	YxSxR motif	Y-140
Tte Tar4	89	-RRLVNFLMMDEVHLQLTKMIKG--ATPPRLIAKPVAKDAIEMEVVSKRK--MYDVFGLGIEGSSK-		
Gyc-88E	91	-RHMRDFLNGLDNLEHYLKFSYPRM--RAPSFCENETKQG-LTLHYRSKRR--GFVYVTMGQIREVARY		
Gyc-89Da	91	-RYFCDFLQSIDNLELIMRFTYPKM--KSPSMQLTNMDDNG-AVILYRSST--GMSKMLIGQMTEVARE		
Gyc-89Db	91	-RYFCDFLQSIDNLEHYQMRFTYPKM--KSPSMQLTNMDDDG-AVILYRSST--GMSKMLIGQMTEVAKE		
Dme β1	92	-ATPRDFLQNLDALEHDLGTLYPGMR--APSFRCETKDG--LLLHYYSERP--GLEHIVIGIVKAVASK		
Dps β3	90	-RHMRDFLNGLDNLEHYLKFSYPRM--RAPSFCENETKQG-LTLHYRSKRR--GFVYVTMGQIREVARY		
Dps 89Da	91	-RYFCDFLQSIDNLELIMRFTYPKM--KSPSMQLTNMDDDG-AVILYRSST--GMSKMLIGQMTEVAKE		
Dps 89Db	91	-RYFCDFLQSIDNLELQMRFTYPKM--KSPSMQLTNMDDDG-AVILYRSST--GMSKMLIGQMTEVAKE		
Aga β3	96	-RHMRDFLNGLDNLEHYLKFSYPRM--RAPSFCENETRHG-LTLHYRTRKR--GFVYVTMGQIREVARH		
Aga 89D	91	-RYFCDFLHSDNLELQMRFTYRKM--KSPSMQLTEVDENG-AVLVYRSTRT--GFSKMLRGQLLEIAKQ		
Ame β3	91	-RHVRDFLNGLDNLEHYLKFSYPRM--RAPSFCENETRQG-LTLHYRSKRR--GFVYVTMGQIREVARH		
MsGC β3	91	-RHMRDFLNGLDNLEHYLKFSYPRM--RAPSFCENETRQG-LTLHYRSKRR--GFVYVTMGQIREVARH		
Bmo β3	?	-RHMRDFLNGLDNLEHYLKFSYPRM--RAPSFCENETRQG-LTLHYRSKRR--GFVYVTMGQIREVARH		
Bmo 89D	?	-RYFCDFLQSIDNLELQMRFTYRKM--RSPSMQLTRAHRHG-AELVYSSGRT--GFTHYLMG-----		
GCY-31	91	-RTFPQFLNGLDNLHAYLRFTFPKL--KPSFYCEHESRTG-LTLHYRSKRR--GFLHYVQGGQIRNISQE		
GCY-32	54	-PNLKGFLDNLDLSLHYFIDHVYKANLRGSPFRCEETPDGT-LTLHYRSKRR--GFLHYVQGGQIRNISQE		
GCY-33	91	-RRFSDFIKGLDNLHAYFRFSYPKL--RAPSFCYCKSESDG-LILHYRSRRT--GLVLSYVIGQLVELARV		
GCY-34	92	-PNLKGFLDNLDLSLHYFIDHVYKANLRGSPFRCEENPDGT-LMLHYFTGRP--GLVHYVQGGQIRNISQE		
GCY-35	92	-PDLEGFLDLSLHAYFIDHVYKTKLRGSPFRCDVQADGT-LLLHYYSKRS--GLVPIVKGVVREVARR		
GCY-36	80	-PNLKGFLDNLDLSLHYFIDHVYKANLRGSPFRCEENPDGT-LTLHYRTRKR--GFVYVTMGQIREVARH		
GCY-37	92	-NNLQEFLDNLSMAYFIDQIAFKSEMKGTFQCEPFGESG-LKLLHYFSFRQ--GLFPIVKGVLREKART		
CBG02110	91	-RTFPQFLNGLDNLHAYLRFTFPKL--KPSFYCEHESRTG-LTLHYRSKRR--GFMHYVQGGQIRNIAQE		
CBG04937	24	-PNLKGFLDNLDLSLHYFIDHVYKANLRGSPFRCEENPDGT-LTLHYRTRKR--GFVYVTMGQIREVARH		
CBG23350	91	-RRFSDFIKGLDNLHAYFRFSYPKL--RAPSFCYCKSESDG-LVLHYRSRRT--GLVLSYVIGQLVELARV		
CBG06726	24	-PNLKGFLDNLDLSLHYFIDHVYKANLRGSPFRCEENPDGT-LMLHYFTGRP--GLVHYVQGGQIRNISQE		
CBG07710	24	-PNLKGFLDNLDLSLHYFIDHVYKANLRGSPFRCEENPDGT-LTLHYRTRKR--GFVYVTMGQIREVARH		
CBG13876	24	-NNLQEFLDNLSMAYFIDQIAFKSEMKGTFQCEPFGESG-LKLLHYFSFRQ--GLFPIVKGVLREKART		
Cin βA	91	-RKLCDFFINGLDNLEHYISNLYKDIK--PPSFYVEKEDDEG-LVPHYNTSRKYVGVVHYVRLIHSAAVM		
Cin βB	90	-RTRDFLNGLDNLEHFFYRFSFADI--QPPSPHISKEDVNG-LELHYRSRRTFTGFMHYVVKGLIRAIADK		
Cin βC	103	-RRFTDFLNGLDNLEHYYRFSFTEI--QPPSFHVSKEDESEG-LELHYRSRRTFTIGVHYVVKGLLLKIASK		
Tru β3	91	-RNVRDFINELDNLEHYFRFSFPPK--QPPSFCVVEECETS-LTLHYRSTRK--GFTQFVKGQLSQVGRQ		
Tru 89D	90	GRHVRDFVNGLDNLEHYLRFSYPKV--QPPTFFCQEEATG-VTLHYRSKRR--GLVHYVQGGQIRNISQE		
Tni β3	92	-RNVRDFINELDNLEHYFRFSFPPK--QPPSFCVVEECETS-LTLHYRSTRK--GFTQFVK-----		
Tni 89D	?	-----RLPLVS--ALDGRSKRK--GLVHYVQGGQIRNISQE		
Mdo β2	90	-GNLMEFIENLDALHSYLALSYQAMN--APSFVRVEKRTDGT-MLLHYYSRR--GLCYIVPGIIEAVAKD		

**Figure 2.15.** ClustalW sequence alignment of known and putative H-NOX (partial)

domains, grouped into species of origin. A portion of the *T. tengcongensis* H-NOX domain (Tte Tar4, Genbank accession 20807169) is shown at the top of the alignment.

The conserved proximal histidine (H-105) ligand, the YxSxR motif, and Y-140 are highlighted in black. The serine residue in the YxSxR motif is substituted in some

subunits with a threonine residue. Note that the *Tetroadon* 89D ysr sequence (Tni 89D)

preceding the serine residue in the YxSxR motif is incomplete. Aga=*Anopheles gambiae*,

Ame=*Apis mellifera*, Bmo=*Bombyx mori*, Cin=*Ciona intestinalis* (ascidian),

CBG=*Caenorhabditis briggsae*, Dme=*Drosophila melanogaster*, Dps=*Drosophila*

*psuedoobscura*, GCY=*Caenorhabditis elegans*, Mdo=*Monodelphis domestica*

(opossum), Ms=*Manduca sexta*, Tru=*Takifugu rubripes* (fugu pufferfish),

Tni=*Tetroadon nigroviridis* (spotted pufferfish). See Table 1.1 for more information

about these sequences.

In summary, I have cloned and characterized the three *Drosophila melanogaster* atypical soluble guanylyl cyclases. One of these, Gyc-88E, is an orthologue of a previously studied insect atypical soluble guanylyl cyclase, MsGC- $\beta$ 3. Both Gyc-88E and MsGC- $\beta$ 3 are active in the absence of other subunits (MsGC- $\beta$ 3 was shown to form homodimers) and have a novel C-terminal extension that likely plays a role in catalytic regulation. The two remaining cyclases, Gyc-89Da and Gyc-89Db, require Gyc-88E for activity and appear to be recent duplications as they are highly identical and are located 2 kb apart from each other in the genome. Orthologs of these two genes are not yet known in the unsequenced *Manduca sexta*, but one is predicted to occur in another lepidopteran, *Bombyx mori*. Co-expression of either Gyc-89Da or Gyc-89Db with Gyc-88E yielded significantly more basal or NO-stimulated activity than when Gyc-88E is expressed alone. Despite the high identity between Gyc-89Da and Gyc-89Db, my results and the results from Morton (2004a) and Morton et al. (2005) suggest that they may not be functionally interchangeable. Gyc-89Da/Gyc-88E and Gyc-89Db/Gyc-88E differ significantly in their enzyme activities in the presence of Mg and Mn. Gyc-89Db/Gyc-88E was activated faster and yielded much higher levels of activity than Gyc-88E or Gyc-89Da/Gyc-88E when exposed to anoxic conditions. Considering the differences in biochemical properties between these guanylyl cyclases *in vitro*, it will be informative to determine which cells in *Drosophila* express Gyc-88E alone, Gyc-89Da and Gyc-88E, Gyc-89Db and Gyc-88E, or all three at the same time. It will also be important to determine if these guanylyl cyclases are expressed in sensory neurons or other cells that could be in the position to detect changes in oxygen concentration. This topic is covered in Chapter 3.

### **Chapter 3: Localization of Gyc-88E, Gyc-89Da, Gyc-89Db expression in the nervous system**

#### **Introduction**

To gain insight into the possible functions of Gyc-88E, Gyc-89Da, Gyc-89Db, I set out to determine their expression patterns at several developmental stages. The sequence analysis and biochemical data presented in Chapters 1 and 2 demonstrate that Gyc-89Da and Gyc-89Db require Gyc-88E for GC activity. The related *C. elegans* atypical soluble GCs, GCY-35 and GCY-36, are predicted to form active heterodimers, have overlapping phenotypes, and are expressed in many of the same cells (Cheung et al., 2004; Gray et al., 2004). These observations and data suggest that Gyc-89Da and Gyc-89Db will be expressed in the same cells as Gyc-88E.

Several methods were utilized to determine the localization of the *Drosophila* atypical sGCs. An immunohistochemical approach was undertaken by the Morton lab, but several attempts at generating specific antibodies failed. Two other approaches were successful, however. In embryos, the expression patterns of Gyc-88E, Gyc-89Da, and Gyc-89Db were examined with RNA:RNA whole mount *in situ* hybridization, using digoxigenin (DIG)-labeled RNA probes. For the second approach, transgenic animals were generated that expressed fluorescent markers driven by the predicted promoter regions of Gyc-89Da and Gyc-89Db. The expression patterns of these animals were examined using confocal microscopy. The results of these experiments show that the *Drosophila* atypical soluble GCs are expressed widely the CNS and in several PNS locations.

## Methods and Materials

### Fly strains and genetics

All *Drosophila melanogaster* strains were propagated in fly vials using standard procedures (Sullivan, 2000) at 25°C. Canton-S (Meigen) flies were used for all *in situ* experiments. The following stocks were used for confocal experiments: c929-1 (Dimmed::GAL4, provided by P. Taghert), CCAP::GAL4 (provided by J. Ewer), C21E (EHups::GAL4, provided by J. Truman), line 6280 (UAS::DsRed, Bloomington), line 6282 (UAS::DSRED, Bloomington), line 6927 (Bloomington), UAS::mCD8-GFP (provided by W. Grueber), 109(2)80 (provided by W. Grueber), line 458 (elav::GAL4[C155], Bloomington). p89Da::GFP, p89Da::GAL4, p89Db::GFP, and p89Db::GAL4 lines were also used and are described below. Crosses and manipulations were carried out using standard genetic techniques (Greenspan, 1997). For co-localization studies, various homozygous promoter/enhancer::GAL4 lines were first crossed to line 6280, which has UAS::DsRed insertions floating on the 1<sup>st</sup>, 2<sup>nd</sup>, and 3<sup>rd</sup> chromosomes. The offspring from this cross were then crossed to either p89Da::GFP or p89Db::GFP to obtain promoter/enhancer::GAL4, UAS::DsRed, p89D::GFP animals for confocal microscopy.

### Whole-mount *in situ* hybridization of embryos and larval CNS

Whole mount *in situ* hybridization was used to identify the spatial expression pattern of Gyc-88E, Gyc-89Da, and Gyc-89Db during embryogenesis and in the larval CNS. DIG-labeled RNA probes were generated as described in Chapter 2 for the northern blots and were fragmented with a carbonate buffer (60 mM Na<sub>2</sub>CO<sub>3</sub>, 40 mM NaHCO<sub>3</sub>, pH 10.2) for

20 min at 65°C. The Gyc-89Da DIG probe used for the below experiments was not fragmented. Mixed stages of embryos were collected and fixed as described (Sullivan et al., 2000) and stored in 100% ethanol until use. Before use, the embryos were rehydrated with PBT (phosphate-buffered saline with 0.1% Tween 20) and post-fixed for 30 min with 4% formaldehyde. The larval CNS was removed and fixed in 4% paraformaldehyde for 45 min., washed 4 x 15 min. with PBT and used the same day. Samples were prehybridized with hybridization buffer [5x SSC, 50% formamide, 0.1 mg/ml heparin sulfate, 0.1 mg/ml sonicated salmon sperm DNA (Invitrogen Life Technologies, Carlsbad, CA, USA), 0.1% Tween 20, pH 5.2] for 1 hr. prior to adding probe at a final concentration of 1.5 ng/ml followed by overnight incubation at 60°C. Samples were washed for 4 x 1 hr. at 60°C in 5x SSC, 50% formamide followed by 4 x 15 min. in PBT and blocked for 1 hr. with PBT plus 10% bovine serum albumin. Fab fragments of sheep anti-DIG-AP antibody (Roche) were incubated with samples at 1:1000 with PBT overnight at 4°C and washed for 4 x 15 min with PBT. DIG labeled RNA probes were detected with NBT/BCIP one-step alkaline phosphatase substrate (Pierce, Rockford, IL, USA) and the reaction stopped with five rinses of 100% ethanol. For *in situ*/immunocytochemical double-label experiments, the neuronal marker antibody 22C10 (Developmental Studies Hybridoma Bank) was added (1:200) at the same time as the anti-DIG-AP antibody and was detected with horseradish peroxidase anti-mouse antiserum (Jackson ImmunoResearch, West Grove, PA, USA) at 1:1000 in PBT for 1 hr. After 4 x 15 min washes with PBT, 22C10 was visualized with 0.5 mg/ml diaminobenzidine (DAB; Sigma, St. Louis, MO, USA) plus 0.003% hydrogen peroxide. DAB reactions were stopped with five consecutive washes with PBT. Anti-DIG antibody

was then visualized as above. The samples were then dehydrated in ethanol, cleared in methyl salicylate and mounted in Permount (Fisher Scientific, Fairlawn, NJ, USA).

### **Gyc-89Da and Gyc-89Db promotor::GAL4 driver generation**

The region upstream from the Gyc-89Da and Gyc-89Db open reading frame start sites to the 3' end of the preceding gene was cloned. For Gyc-89Da this region was 2 kb and for Gyc-89Db this region was 3.5 kb. The primers used to amplify the upstream region of Gyc-89Da were 5'-GGGTTCTTTTTTGTAGAGAAA-3' and 5'-GGTTTATGTTTCTGAAAAAATG-3', and the primers used to amplify the region upstream of Gyc-89Db were 5'-GCACCTGTGGCTCTCTTA-3' and 5'-GATGGGGCAGGATGTGAA-3'. Standard PCR conditions were used, and the resulting PCR products were cloned into the TOPOII vector (Invitrogen Life Technologies) and subcloned into pGreen-Pelican vector (Barolo et al., 2000) and the pPTGAL vector (Sharma et al., 2002) using the BamHI and NotI restriction sites. All constructs were checked with restriction digests and sequencing. Maxipreps of these plasmid constructs, along with the  $\Delta 2-3$  helper plasmid (obtained from S. Smolick), were further purified using standard cesium chloride ultracentrifugation followed by standard phenol:chloroform extraction. The injection buffer was composed of 0.85mM NaH<sub>2</sub>PO<sub>4</sub>, 9.15mM Na<sub>2</sub>HPO<sub>4</sub>, and 5mM KCl, and was loaded with 1  $\mu$ g/ $\mu$ l of purified construct and 0.2  $\mu$ g/ $\mu$ l of helper plasmid. Injection needles were pulled on a Model P-87 Flaming/Brown micropipette puller (Sutter Instrument Co., Novato, CA, USA) using 4-inch thin-wall borosilicate glass capillaries with filament (1 mm OD/0.75 mm ID) (World Precision Instruments, Inc., Sarasota, FL, USA). Needles were loaded with 0.4  $\mu$ l of



prepared injection mixture and inserted into the injection head of a Picospritzer II (Parker Instrumentation, Chicago, IL, USA), which was attached to a Narishige micromanipulator (Narishige International USA, Long Island, NY, USA). 2 to 8 day old *yw*[1] flies raised at 18° C were allowed to lay eggs on an 8.5 cm grape juice agar plate (with two small dollops of yeast paste) at 18° C for up to 15 minutes. Embryos were collected with forceps and placed in a row on a slide coverslip with double-sided sticky tape, which was then stuck to a slide with a small strip of double-sided sticky tape. Embryos were then desiccated for 5 min. in a sealed plastic box containing a layer of Drierite (W.A. Hammond Drierite Company, LTD., Xenia, OH, USA), then covered in a thin bead of halocarbon oil 700 (Halocarbon Products Corp., River Edge, NJ, USA). The prepared embryo coverslip/slide was then placed on the stage of a Nikon Eclipse TE200 inverted microscope (Nikon USA, Melville, NY, USA). The loaded needle tip was broken finely on the edge of the slide and immediately placed in the halocarbon oil. 300 to 500 embryos were injected with ~1-10 pl of injection mixture. Completed embryo coverslips were then removed from the slide and placed on a new, yeasted, grape juice agar plate and placed in an 18° C incubator. Hatched larvae were collected from the plates with a platinum filament “worm picker” for up to 3 days post injection and placed in groups (up to 20 larvae) in standard food vials and raised at 18° C until animals eclosed. Individual adults were crossed to *yw*[1] flies in separate vials. 50-100 individual lines for each construct injection were screened for colored eye transformants, which were then individually crossed to *yw*[1] flies. Individual transformant lines were then bred homozygous. The chromosome bearing the construct insertion in each line was determined using a standard genetic mapping scheme.

## **Visualization of GFP and DsRed**

Whole animals were rinsed in water and mounted in GelMount (Sigma, St. Louis, MO) on standard slides. Larval central nervous systems or adult parts were dissected in PBS, then mounted in GelMount on Superfrost Plus slides (Fisher Scientific, Fairlawn, NJ, USA). A Nikon Eclipse E800 microscope was used in conjunction with the Bio-Rad Radiance 2100/Lasersharp 2000 (Hercules, CA, USA) confocal microscopy system to capture raw images. An argon laser with a laser line of 488nm was used to excite GFP and the emitted light was captured in the 500-530nm range. A helium/neon laser with a laser line of 543nm was used to excite DsRed and the emitted light was captured in the 570-650nm range. Raw data generated with the Bio-Rad Lasersharp 2000 software was postprocessed with ImageJ image analysis software (ver1.32j, W. Rasband, National Institutes of Health). Postprocessing in ImageJ consisted of the creation of Z-stacks, color channel merging, and contrast/brightness adjustments when needed.

## **Results**

### **Gyc-88E and Gyc-89Db are expressed in the embryonic CNS and PNS**

To determine the cellular localization of Gyc-88E and Gyc-89Db in embryos, I performed *in situ* hybridization using fragmented DIG-labeled RNA probes on whole *Drosophila* embryos. Gyc-88E expression was detected in a segmental pattern in the ventral nerve cord (VNC) and in the brain in embryos, beginning at stage 15 or 16 and continuing through stage 17 (Fig. 3.1A - horizontal view; Fig. 3.1C - lateral view). Gyc-89Db showed a similar expression pattern in the VNC and brain but could be detected as early as stage 13 (data not shown) and also continued through stage 17 (Fig. 3.1B -

horizontal view; Fig. 3.1D - lateral view). In stage 17 embryos, the total number of cells that expressed Gyc-88E was noticeably higher than the number of cells that expressed Gyc-89Db, especially in the brain (compare Fig. 3.1C and Fig. 3.1D). Stained single cells visible in the anterior and posterior of the embryo in Fig. 3.1C,D are not part of the CNS and are discussed below. Application of a sense riboprobe generated from Gyc-88E or Gyc-89Db yielded a low level of background staining throughout the embryos with no cells stained (Fig. 3.1E - Gyc-88E; Fig. 3.1F - Gyc-89Db).

In stage 17 embryos, Gyc-88E and Gyc-89Db were also expressed in a number of cells that appeared to be associated with the peripheral nervous system (Fig. 3.2). The overall pattern of this peripheral staining was very similar for probes to both Gyc-88E and Gyc-89Db. Both Gyc-88E (Fig. 3.2A - horizontal view; Fig. 3.2C - lateral view) and Gyc-89Db (Fig. 3.2B - horizontal view; Fig. 3.2D - lateral view) were expressed in two cells on each side of segments T1, T2 and T3 and in one cell on each side of A1 and A2. The cells in segment A2 often stained very weakly and were not always detected. The positions of the stained cells in the thoracic segments are similar to the locations of the embryonic/larval basiconic sensilla. As a preliminary test to determine whether both guanylyl cyclase subunits were co-expressed in the same cells, I hybridized embryos to both probes simultaneously. In these experiments, the number of lateral cells that stained was the same as when each probe was used individually: two cells on each side of segments T1, T2 and T3 and one cell on each side of A1 and A2 (Fig. 3.2E; Table 3.1). In addition to the lateral cells, both probes hybridized to cells that appeared to be associated with the ganglia that innervate the head sensory organs (Fig. 3.2F - Gyc-88E; Fig. 3.2G - Gyc-89Db).

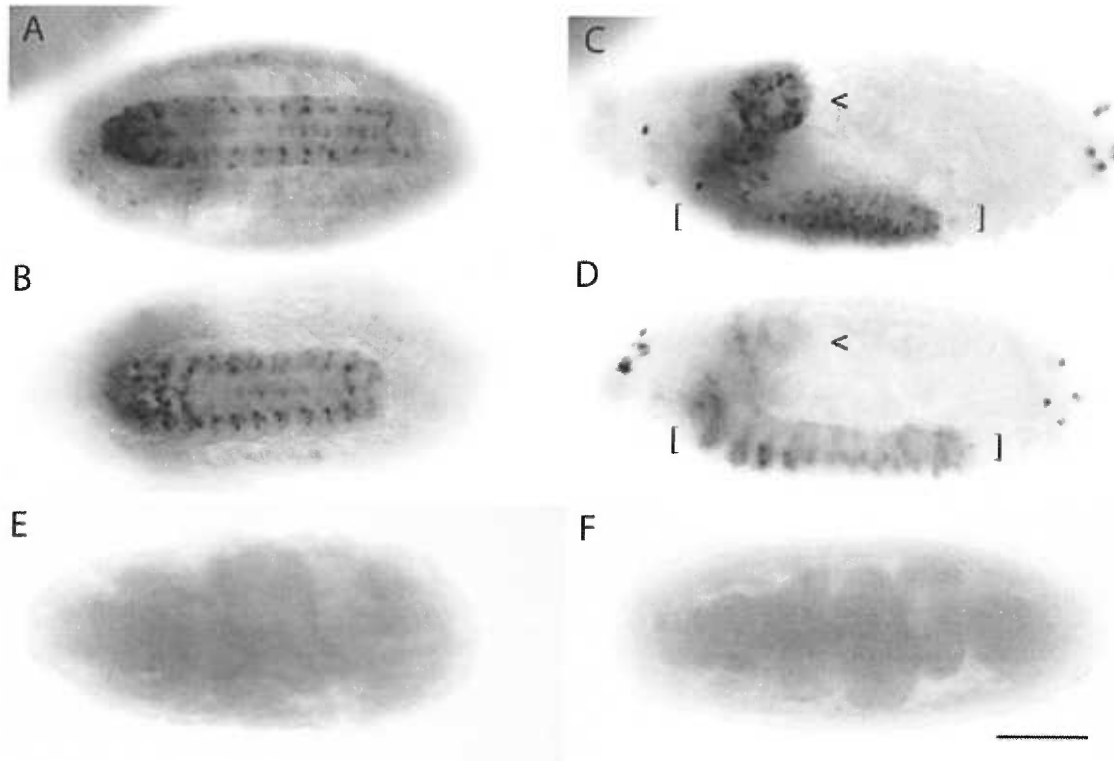


**Figure 3.1.** Localization of *Gyc-88E* and *Gyc-89Db* expression in the central nervous system of *Drosophila* embryos. *In situ* hybridization experiments were performed on whole embryos using fragmented DIG-labeled *Gyc-88E* or *Gyc-89Db* riboprobes. (**A, C**) *Gyc-88E* expression in stage 16 embryos. Expression was detected in a segmental pattern in the ventral nerve cord and throughout the brain (open arrowhead). (**B, D**) *Gyc-89Db* expression in stage 17 embryos. A similar pattern of expression was detected in the ventral nerve cord and brain, although noticeably fewer cells stain in the brain with *Gyc-89Db* (open arrowhead). (**A**) and (**B**) show the horizontal view, while (**C**) and (**D**) show the lateral view. Application of a sense probe generated from *Gyc-88E* (**E**) or *Gyc-89Db* (**F**) demonstrates that the low level of ubiquitous background staining observed reflects nonspecific hybridization. Anterior is always left and ventral is down in side views. Square brackets in (**C**) and (**D**) indicate the position of the ventral nerve cord. Scale bar= 100  $\mu$ m.

Gyc-88E hybridized to a single pair of cells whereas Gyc-89Db was expressed in 2-5 closely grouped cells on each side of the embryo. In addition, the Gyc-89Db probe stained 4-5 closely grouped cells per side located in a more posterior position (not visible in the focal plane shown in Fig. 3.2G). These cells will be described in more detail later. Finally, Gyc-88E and Gyc-89Db were also found in 12 cells in segments A8 and A9 (telson; Fig. 3.2H - Gyc-88E; Fig. 3.2I - Gyc-89Db; three focal planes shown for each probe) in an apparently overlapping pattern. These cells appear to be associated with the clusters of neurons that innervate the 10 external sensory cones found in segments A8 and A9. To determine if both probes hybridized to the same cells, we examined the preparations where both Gyc-88E and Gyc-89Db probes were used simultaneously, counted the number of cells that stained and compared these results with the number of cells stained using a single probe. I counted the same number of cells (12) in segments A8 and A9 (Fig. 3.2J; three focal planes shown) in the double-labeled embryos as in embryos labeled with Gyc-88E or Gyc-89Db probes individually. This suggests that both guanylyl cyclases were co-expressed in the same cells in these segments. In the anterior region of the embryo, where Gyc-89Db labels more cells than Gyc-88E, we never observed more labeled cells using both probes together than the maximum number of cells observed in the Gyc-89Db single probe preparations. This suggests that the cells that expressed Gyc-88E also expressed Gyc-89Db, but there were some cells that expressed only Gyc-89Db. These data are summarized in Table 3.1.

**Figure 3.2.** Localization of Gyc-88E and Gyc-89Db in cells associated with the embryonic peripheral nervous system. *In situ* hybridization on stage 17 embryos also revealed that Gyc-88E or Gyc-89Db were both expressed in several peripherally located cells. **(A, C)** Expression of Gyc-88E. **(B, D)** Expression of Gyc-89Db. **(A)** and **(B)** show the horizontal view, while **C** and **D** show the lateral view. On each side of the embryo, two cells were detected in segments T1, T2 and T3, arranged in either an upper row or a lower row of cells, and a single cell was detected in A1 and A2. Left is always anterior and down is ventral in side views. **(E)** Application of both probes simultaneously resulted in the same number of cells staining in segments T1–A2 as when each probe was applied individually. **(F, G)** Expression of Gyc-88E and Gyc-89Db in the head segment. Gyc-88E **(F)** was expressed in a pair of cells, while Gyc-89Db **(G)** was expressed in more cells (2–5 per side in the clusters in focus, and 4–5 per side in clusters located in a more posterior position and out of focus, indicated with open arrowheads). Horizontal views are shown, and anterior is up. **(H–J)** Expression of Gyc 88E and Gyc-89Db in segments A8 and A9. Three consecutive focal planes of focus are shown starting from most ventral (left) to dorsal (right) to capture all cells. Both Gyc-88E **(H)** and Gyc-89Db **(I)** are expressed in a total of 12 cells. The cells are numbered arbitrarily. **(J)** When both probes were used simultaneously, the number of cells detected remained the same. Scale bar, 200  $\mu\text{m}$ .

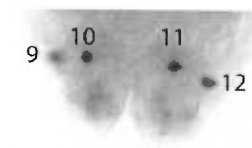
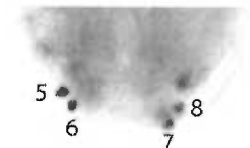
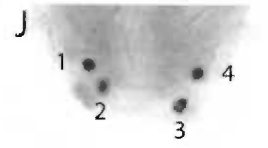
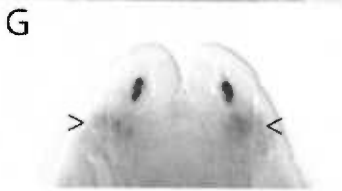
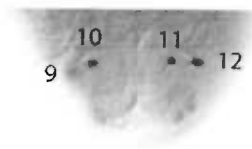
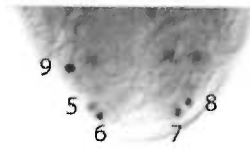
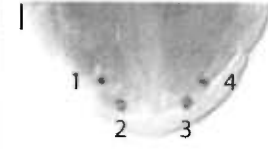
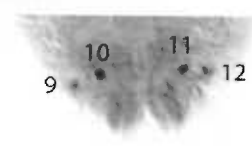
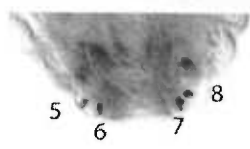
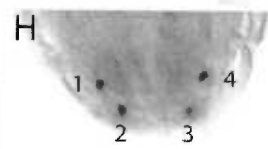
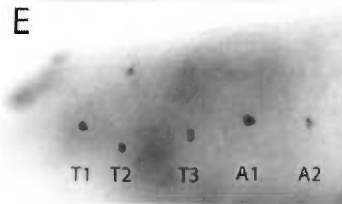
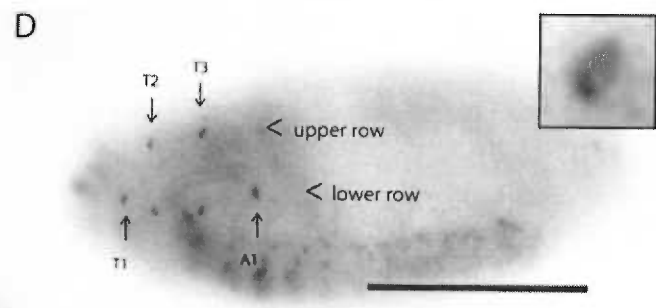
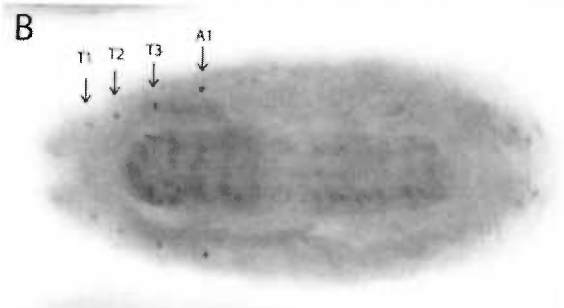
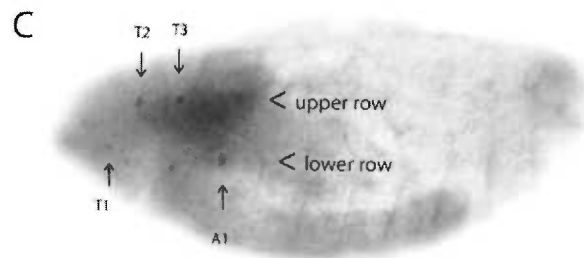
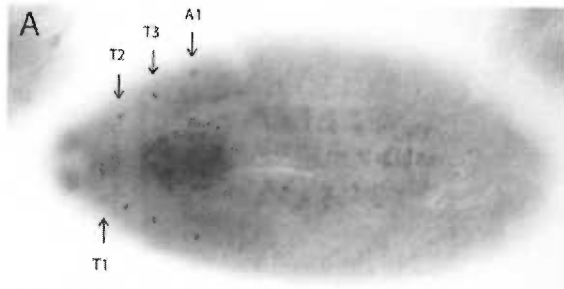


**Table 3.1.** Summary of data from the riboprobe/22C10 double label and double riboprobe experiments.

	Head segments		T1	T2 or T3	T2 or T3	A1 or A2	A8/
	dorsal ganglion	terminal ganglion		Lateral cluster	Ventral cluster	Ventral group	A9
Total neurons in ganglion or cluster per hemi-segment	~40	35+	ND	11	15	8	ND
Gyc-88E	0	1	2	1	1	1	6
Gyc-89Db	4-5	2-5	2	1	1	1	6
Both probes	4-5	2-5	2	1	1	1	6
Identity	ND	ND	ND	<i>les</i>	<i>ves</i>	<i>v'td</i>	ND
Gyc-89Da	3-5	2-3	2	1	1	0	6

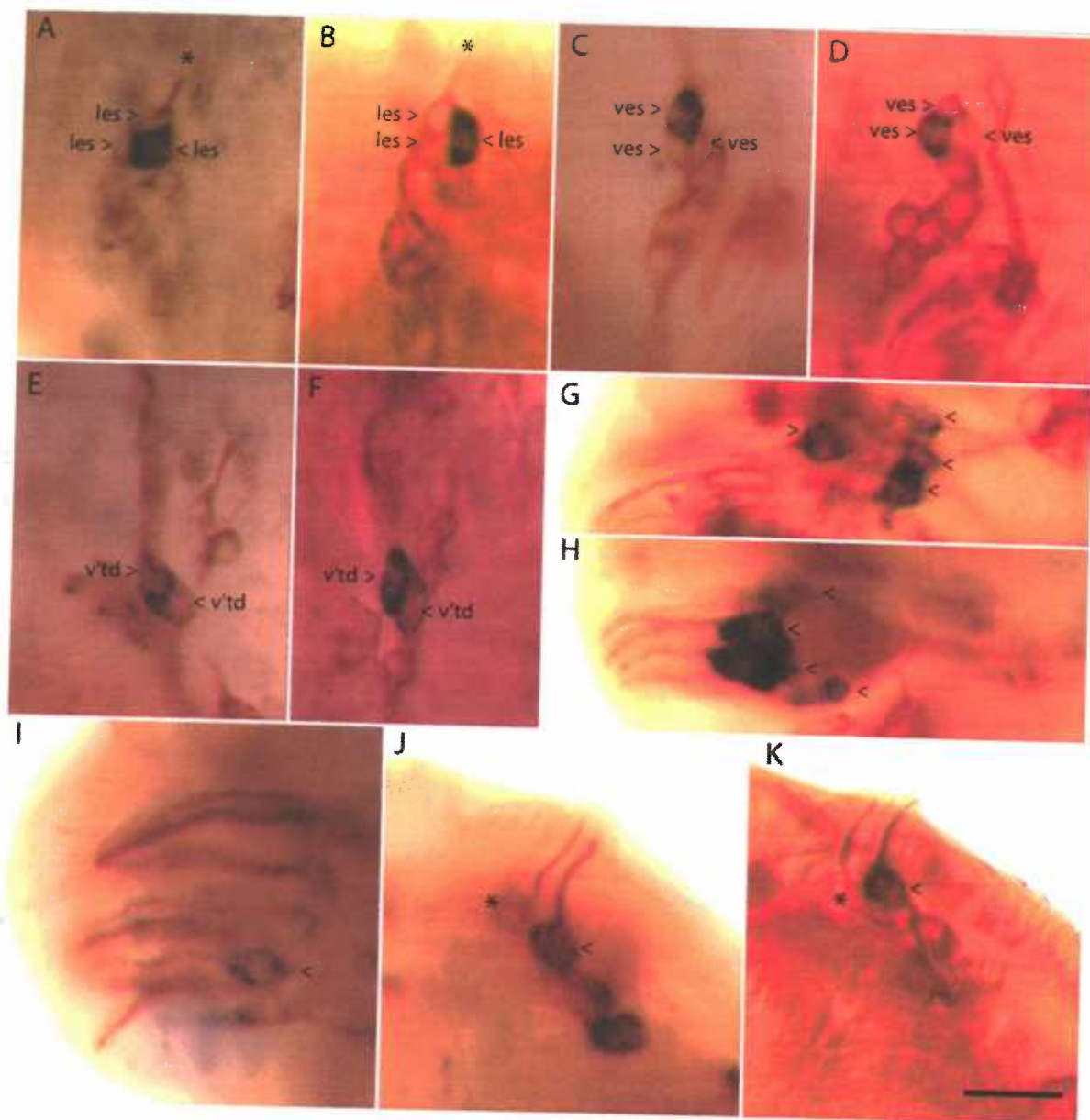
Diagrams of the *Drosophila* peripheral nervous system by Younossi-Hartenstein and Hartenstein (1997), Bodmer and Jan (1987), and Brewster and Bodmer (1995), and Stocker (1994) were used to identify the neuron cluster or ganglion location of neurons that expressed Gyc-88E, Gyc-89Da, and Gyc-89Db in stage 17 embryos. Numbers refer to each side of the animal and were obtained by examining at least 50 embryos that were labeled with a riboprobe for each guanylyl cyclase, either individually or used together, and the 22C10 antibody. Embryos treated with both riboprobes stained the same number of cells in the thoracic and abdominal segments, indicating that Gyc-88E and Gyc-89Db are co-expressed in the same neurons. The Gyc-89Da probe was not used in conjunction with any other probe or antibody. ND = not determined.



To determine if the peripheral cells that expressed Gyc-88E and Gyc-89Db in stage 17 embryos were neurons of the peripheral nervous system, I combined *in situ* hybridization with immunocytochemistry using the neuron-specific antibody 22C10 (Fig. 3.3). These experiments demonstrated that the Gyc-88E- and Gyc-89Db-expressing cells were always stained with 22C10 and by their positions were identified as peripheral neurons that innervate various external sensory organs and the trachea. Comparison of our data with detailed diagrams of the peripheral nervous system (Bodmer et al., 1987; Brewster and Bodmer, 1995; Stocker, 1994) allowed us to more specifically identify the cell or cell cluster. In segments T2 and T3, Gyc-88E and Gyc-89Db were coexpressed in one of the three neurons in the lateral and ventral clusters (Fig. 3.3A - Gyc-88E, lateral; Fig. 3.3B - Gyc-89Db, lateral; Fig. 3.3C - Gyc-88E, ventral; Fig. 3.3D - Gyc-89Db, ventral) that innervate the basiconical sensilla, which are external sensory organs with a putative chemosensory role (Stocker, 1994). In the lateral T2 and T3 clusters (upper row in Fig. 3.2C and D), Gyc-88E and Gyc-89Db were expressed in one of the three les neurons (lateral external sensilla-innervating) (Fig. 3.3A - Gyc-88E; Fig. 3.3B - Gyc-89Db). The collected dendrites from the three les neurons were observed to project upwards to the location of the basiconical sensillum (Fig. 3.3A and B). In the ventral T2 and T3 clusters (lower row in Fig. 3.3C and D), Gyc-88E and Gyc-89Db were expressed in one of the three (ves) neurons (ventral external sensilla-innervating) (Fig. 3.3C - Gyc-88E; Fig. 3.3D - Gyc-89Db). In the thoracic segments, the position of the single guanylyl cyclase expressing cell in the cluster of three external sensilla neurons was variable. In segment A1 and A2, Gyc-88E and Gyc-89Db were expressed in one of the two v'td neurons (ventral tracheal dendrite) (Fig. 3.3E - Gyc-88E; Fig. 3.3F - Gyc-89Db), which

wrap their projections around specific tracheal branches (Bodmer et al., 1987). The stained neuron in A1 and A2 was always in the anterior-most position of the two v'td neurons. In the anterior region of the embryo, Gyc-89Db was expressed in more cells than Gyc-88E. Gyc-89Db was expressed in four neurons in the dorsal ganglion (Fig. 3.3G). These cells correspond to the cells that were out of the plane of focus in the preparation shown in Figure 3.2G. The dorsal ganglion innervates a sensory structure, known as the dorsal organ, that is thought to be the main site of olfaction in larvae (Heimbeck et al., 1999; Stocker, 1994). Gyc-89Db was also expressed in two large neurons and up to three more weakly stained cells in the terminal ganglion of the maxillary organ (Fig. 3.3H), a structure that includes several types of sensilla (Stocker, 1994). Gyc-88E was also expressed in the terminal ganglion but was only expressed in a single neuron (Fig. 3.3I). The cells of the terminal ganglion that express Gyc-88E and Gyc-89Db are the same cells that are in the focal plane in preparations shown in Figure 3.2F and G. In segments A8 and A9, Gyc-88E and Gyc-89Db were expressed in a subset of neurons that innervate the sensory cones, which also have putative chemosensory roles (Stocker, 1994). The seven sensory cones (per side) are named "Sensory Organ 1" through "Sensory Organ 7" (SO1- SO7), and contain a combination of trichoid-like and basiconical-like sensilla, depending on the sensory cone (Kuhn et al., 1992). A single neuron in 6 of the 7 sensory cones was observed that expressed Gyc-88E and Gyc-89Db (Fig. 3.3J - Gyc-88E; Fig. 3.3K - Gyc-89Db). These neurons correspond to the cells numbered 2, 3 and 5-12 in Figure 3.2H-J.

**Figure 3.3.** Gyc-88E and Gyc-89Db are expressed in neurons of the peripheral nervous system. *In situ* hybridization (blue/black stain) was combined with immunohistochemical staining with the neuronal antibody 22C10 (brown stain). Stained cells are indicated with open arrowheads and are identified where possible. **(A and B)** Expression of Gyc-88E and Gyc-89Db in the lateral neuron clusters of segments T2 and T3. The example shown is segment T3 (T2 was identical). Gyc-88E (A) and Gyc-89Db (B) were expressed in one of the three les neurons that innervate a lateral external basiconical sensillum. In both of these panels, dendrites from the three les neurons can be observed to extend towards the basiconical sensillum (location marked with an asterisk). **(C and D)** Expression of Gyc-88E and Gyc-89Db in the ventral neuron clusters of segments T2 and T3. Gyc-88E (C) and Gyc-89Db (D) were expressed in one of the three ves neurons that innervate a ventral external basiconical sensillum. Again, the example shown is in segment T3 (T2 was identical). **(E and F)** Expression of Gyc-88E and Gyc-89Db in the neuron clusters of segments A1 and A2. Gyc-88E (E) and Gyc-89Db (F) were expressed in one of two v'td that innervate specific tracheal branches. The example shown is in segment A1 (A2 was identical but the staining was less intense). The stained cell was always the most anterior of the pair. **(G-I)** Expression of Gyc-88E and Gyc-89Db in the head segment. Gyc-89Db was expressed in 4-5 neurons in each of the dorsal ganglia (one on each side) (G), and in 2-5 neurons in each of the terminal (maxillary) ganglia (one on each side) (H). Gyc-88E expression was found in one neuron in each terminal ganglion (I). Note the dendrites projecting towards the head sensilla. **(J and K)** Expression of Gyc-88E and Gyc-89Db in the caudal sensory cones in the telson. Gyc-88E (J) and Gyc-89Db (K) were expressed in one of at least two neurons that innervate each of the caudal sensory cones in segment A9. The neighboring neuron that does not express guanylyl cyclase is indicated with an asterisk. In (K), the dendrite is clearly seen to extend from the neuron that expressed Gyc-89Db to the extreme tip of the sensory cone, appearing to extend past the edge of the main body of the cone as a short protrusion. Scale bar= 30  $\mu$ m.



In some cases, it was possible to trace the dendrite from the neuron that stained for Gyc-88E or Gyc-89Db to the tip of the sensory cone (Fig. 3.3K), a characteristic of chemosensory neurons (Dambly-Chaudiere et al., 1992). The remaining two neurons, numbered 1 and 4 in Figure 3.2H–J, had dendrites that projected in a posterior direction, but I could not determine their target of innervation because it was not possible to follow them to their terminus.

Gyc-88E expression was also detected in the embryonic midgut (Fig. 3.4). The Gyc-88E expression pattern in the midgut is reminiscent of the number and pattern of the cone-shaped endocrine cells that reside here. Gyc-89Db expression was not found in the midgut.

The expression pattern of Gyc-89Da was also examined in stage 17 embryos, using a full length (unfragmented) DIG-labeled RNA probe. Similar to Gyc-88E and Gyc-89Db, Gyc-89Da expression was found in the CNS and in lateral cells that appeared to be neurons associated with the PNS (Fig. 3.5 and Table 3.1). The expression of Gyc-89Da in the CNS was more restricted than Gyc-88E and Gyc-89Db, appearing in several cells only in the anterior and posterior regions (faint signal) of the VNC, several cells in the subesophageal ganglion, and in several cells in the brain lobes (Fig. 3.5A and B). In the head segment, Gyc-89Da expression was found in 2-3 cells in the terminal ganglion and in 3-5 cells in the dorsal ganglion, resembling the embryonic expression pattern of Gyc-89Db (Fig. 3.5C and Table 3.1). Similar to Gyc-88E and Gyc-89Db, Gyc-89Da expression was found in one laterally-positioned and one ventrally-positioned cell in segments T1, T2, and T3 (Fig. 3.5D and Table 3.1). Unlike Gyc-88E and Gyc-89Db, peripheral Gyc-89Da expression was not found in segments A1 and A2.

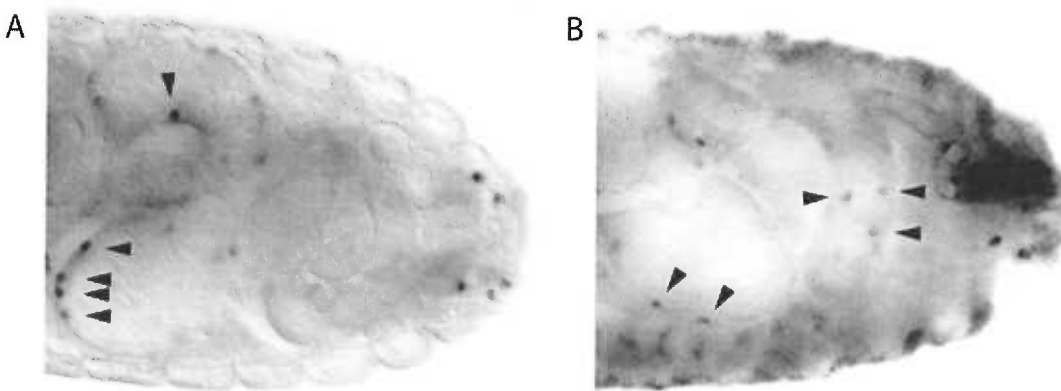
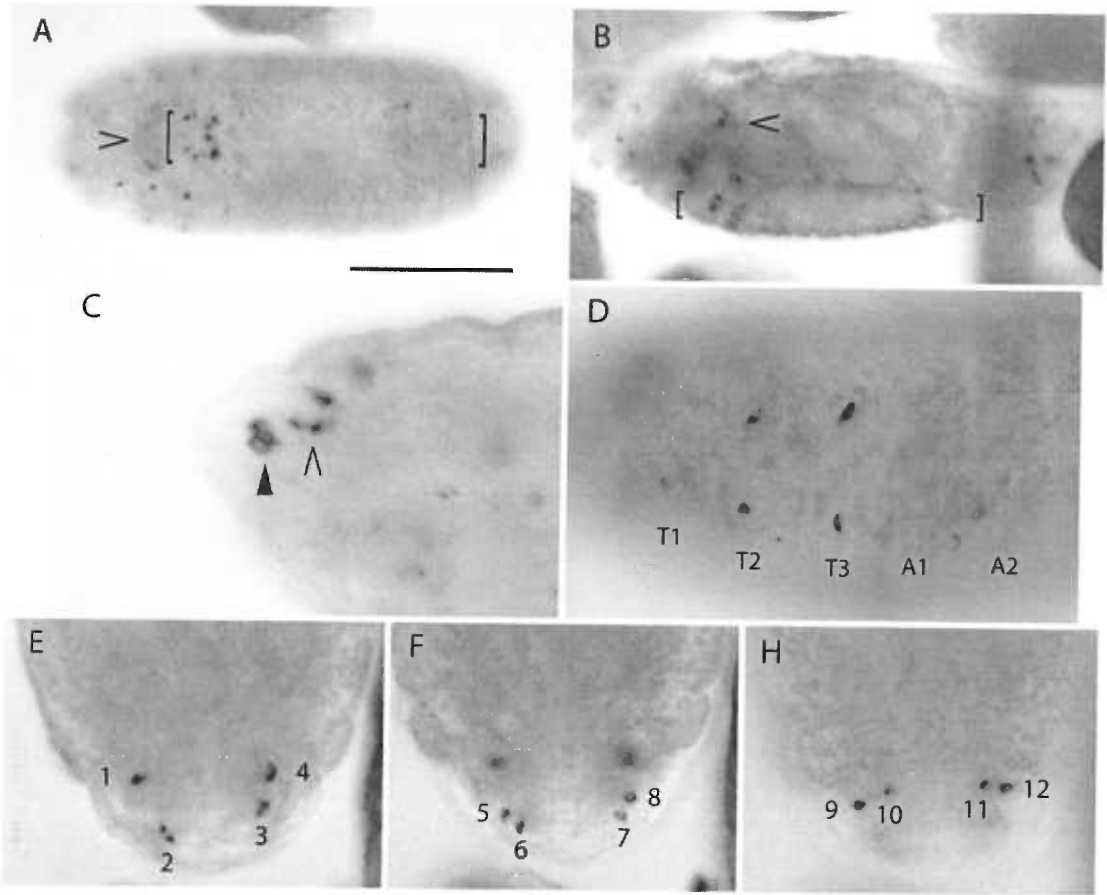


**Figure 3.4.** Gyc-88E expression in the stage 17 embryonic midgut. (A) Single Gyc-88E-positive cells are found through central midgut (closed arrows). Cells (B) Another example showing Gyc-88E-positive cells in the central midgut and late midgut, just before the hindgut. The posterior end of the embryo is in view in (A) and (B).

**Figure 3.5.** Gyc-89Da was expressed in a limited pattern in the CNS and in lateral cells that appear to be associated with the PNS in stage 17 embryos. *In situ* hybridization experiments were performed on whole embryos using unfragmented DIG-labeled Gyc-89Da riboprobes. **(A)** Bottom view of an embryo showing stronger Gyc-89Da expression in the anterior VNC (in brackets) and weaker expression in the posterior VNC. Gyc-89Da expression was also found in the subesophageal ganglion (out of focus, open arrowhead). **(B)** Side view of an embryo showing Gyc-89Da expression in the VNC (in brackets) and in the brain lobes (open arrowhead). **(C)** Side view of the anterior embryo segments showing Gyc-89Da expression in cells in the terminal ganglion (three cells visible, closed arrowhead) and the dorsal ganglion (three cells visible, open arrowhead). **(D)** Side view of an embryo showing Gyc-89Da expression in 2 cells per side in segments T1, T2, and T3 only. **(E, F, and G)** Three different focal planes of the posterior end of the same embryo, showing Gyc-89Da expression in a total of 12 cells, (numbered). In (A)-(D) left is anterior. Scale bar= 200 $\mu$ m.





Finally, Gyc-89Da expression was found in 12 cells located at the posterior end of the embryo in segments A8 and A9 (Fig. 3.5E, F, and G). The position and pattern of these cells closely match the expression pattern of Gyc-88E and Gyc-89Db in this region.

### **Gyc-89Da and Gyc-89Db expression in larvae and adults**

To examine the expression of Gyc-88E, Gyc-89Da, and Gyc-89Db in larvae and in later stages, I generated transgenic fly lines that express green fluorescent protein (GFP) or GAL4 driven by the promoter regions of the GCs. The GAL4/UAS system is a widely used targeted gene expression system that allows for the selective expression of any cloned gene in a variety of tissue and cell patterns (Brand and Perrimon, 1993). The yeast transcriptional activator GAL4 binds with high affinity to Upstream Activation Sequence (UAS) sites, activating the transcription of any gene placed behind the UAS containing promoter. A defined or potential promoter region can be used to drive GAL4 expression only in cells of interest. Crossing a promoter::GAL4 line to a UAS::reporter line results in the selective expression of the reporter (i.e. GFP) in the cells with GAL4 expression. A number of UAS::reporter lines are available from the Bloomington Stock Center. Once a potential promoter::GAL4 line has been characterized, it can also be used to express any gene or construct of choice in those cells, which was one of the reasons for constructing GAL4 lines in addition to direct promoter::GFP lines.

Three promoter-driven GFP lines were originally planned: Gyc-88E::GFP, Gyc-89Da::GFP, and Gyc-89Db::GFP. The pGreen-Pelican GFP transformation vector was used, which was specifically designed for promoter/enhancer analysis in *Drosophila* (Barolo et al., 2000). This vector was also designed with gypsy insulator elements, which

are located just 5' of the multiple cloning site and just 3' of the GFP gene and help to insulate the promoter::GFP construct from nearby endogenous regulatory elements that can influence expression patterns. In order to acquire a functional promoter capable of driving the GAL4 transgene, I cloned large regions of upstream genomic DNA to be inserted into the pGreen-Pelican vector. For the Gyc-89Da promoter, I cloned the entire 2 kb region starting at the beginning of the Gyc-89Da open reading frame (ORF) (the ATG start site was not included) to the 3' end of the preceding gene (Fig. 3.6B). Any potential 5' UTR regions and introns would have been included in these constructs. For the Gyc-89Db promoter, I cloned the entire 3.5 kb region starting at the beginning of the Gyc-89Db ORF to the 3' end of the Gyc-89Da ORF (Fig. 3.6B). The region from the start of the Gyc-88E ORF to the boundary of the preceding gene is about 6.5 kb long (Fig. 3.6A). I set out to clone the first 5 kb section of this region, beginning at the ORF, and a separate product that included an additional 5 kb, totaling 10 kb, in the event that the large introns of Zeelin1 contained Gyc-88E regulatory elements.

I successfully cloned and subcloned the 5 kb Gyc-88E upstream region into pGreen-Pelican and was successful at amplifying the 10 kb piece but was unsuccessful at cloning this long product. I proceeded with the 5 kb Gyc-88E upstream region only and subcloned it into pGreen-Pelican. The 2 kb Gyc-89Da and the 3.5 kb Gyc-89Db upstream regions were successfully cloned and subcloned into pGreen-Pelican. Three independent promoter-Gyc-88E::GFP (p88E::GFP) insertion lines, three promoter-Gyc-89Da::GFP (p89Da::GFP) insertion lines, and two promoter-Gyc-89Db::GFP (89Db::GFP) insertion lines were generated and kept as homozygous stocks.

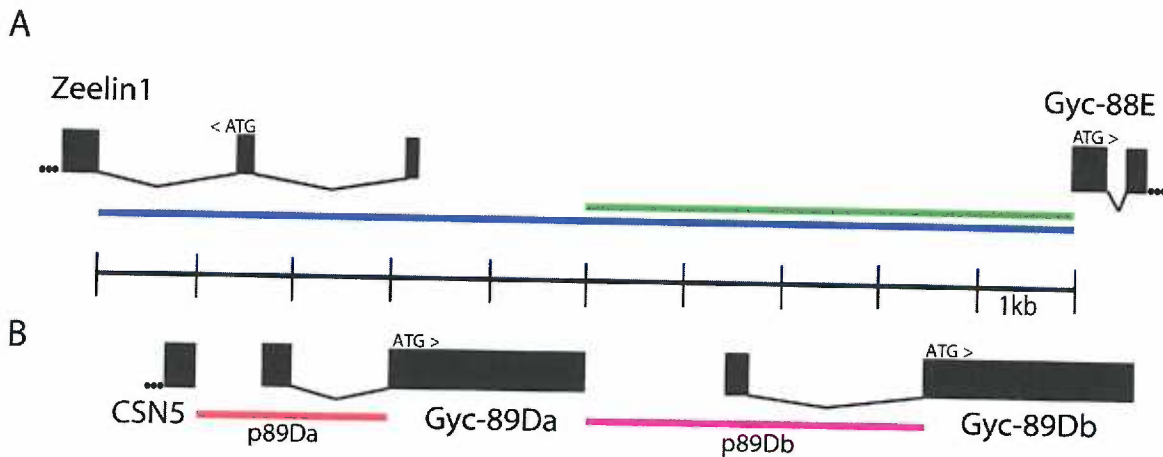


**Figure 3.6.** Diagram illustrating the upstream genomic regions used to build promoter::GFP and promoter::GAL4 constructs. **(A)** Gyc-88E upstream genomic region. A 5 kb genomic fragment (green) and a 10 kb fragment (blue) were cloned for use in ectopic expression constructs. The 10 kb fragment contained a 5' portion of the preceding gene (Zeelin1), which is located on the opposite strand from Gyc-88E. **(B)** Gyc-89Da and Gyc-89Db upstream genomic regions. The entire 2 kb region separating the beginning of the Gyc-89Da ORF and the end of the preceding gene (CSN5) was cloned (red) for use in ectopic expression constructs, including the 1<sup>st</sup> exon, which contains only UTR. The entire 3.5 kb region separating Gyc-89Db from the preceding gene (Gyc-89Da) was cloned (purple), including the 1<sup>st</sup> exon, which contains only UTR. Each segment of the scale bar separating (A) from (B) equals 1 kb.

The p88E::GFP insertion line failed to produce any GFP expression whatsoever, and the expression pattern of Gyc-88E in later larvae and adult stages remains uncharacterized. However, the p89Da::GFP and the p89Db::GFP fly lines displayed robust GFP expression in discrete populations of cells as described below. Having obtained functional promoter regions for Gyc-89Da and Gyc-89Db, I set out to generate p89Da::GAL4 and p89Db::GAL4 insertion lines. The pPTGAL vector (Sharma et al., 2002) was used as the GAL4 transformation vector, and the same cloned promoter regions used for the GFP constructs were used for the GAL4 constructs. Eleven p89Da::GAL4 insertion lines and 5 p89Db::GAL4 insertion lines were obtained and kept as homozygous stocks. Crossing these promoter::GAL4 lines to a UAS::GFP or UAS::DsRed fly line resulted in an expression pattern that closely matched the expression pattern of the promoter::GFP fly lines in the PNS and CNS (data not shown).

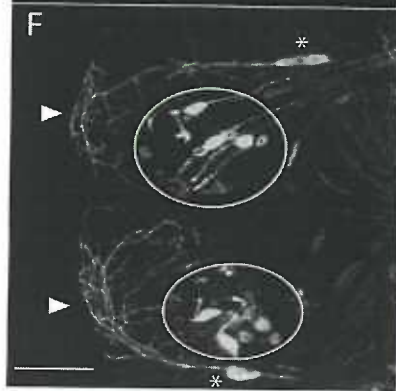
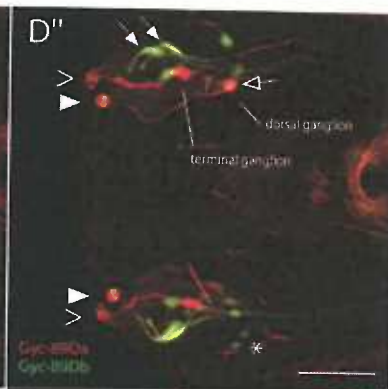
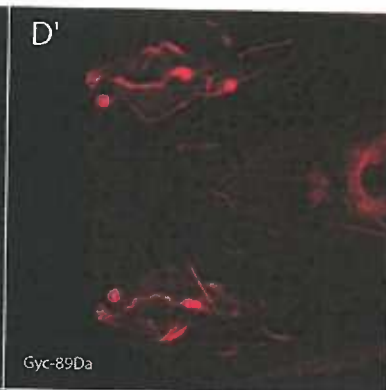
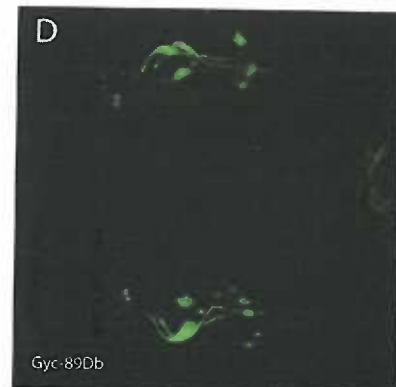
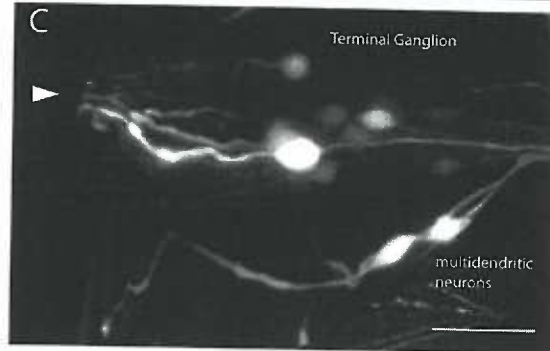
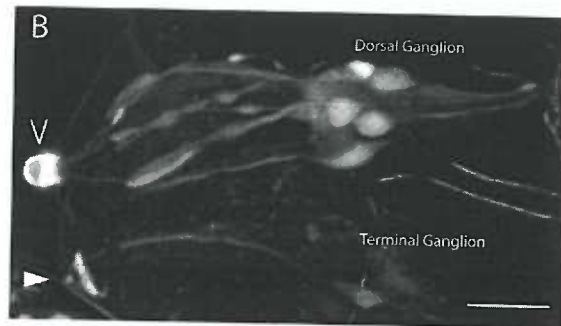
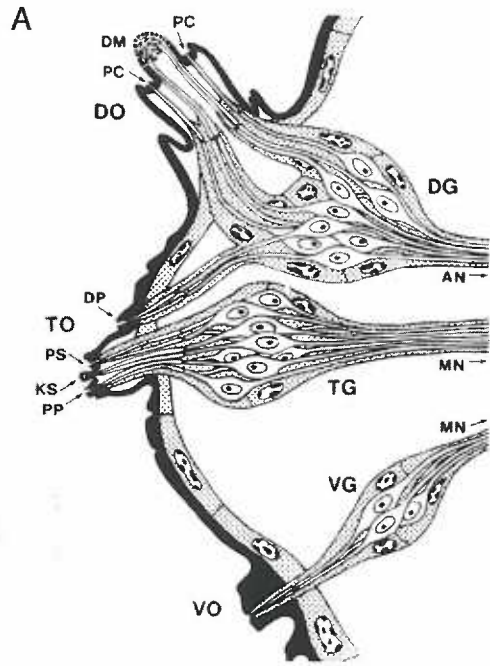
In order to determine if Gyc-89Da and Gyc-89Db were expressed in the same cells, promoter::GAL4 flies were crossed with UAS::DsRed flies (line 6280, which has UAS::DsRed insertions floating on the 3<sup>rd</sup>, 2<sup>nd</sup>, and X chromosomes). These flies were then crossed to homozygous promoter::GFP flies, resulting in offspring that expressed both GFP driven by one GC promoter and DsRed driven by the other GC promoter. All such double labeled preparations shown below use the p89Da::GFP, p89Db::GAL4, UAS::DsRed combination unless otherwise noted in the figure legend. For maximum contrast, GFP signal is shown in red (as the GFP channel tends to yield higher background autofluorescence) and the DsRed signal is shown in green unless otherwise. Using the same crossing scheme, co-expression of other genes (using promoter::GAL4 constructs obtained from other sources) with p89Da::GFP or p89Db::GFP was examined.

Both Gyc-89Da and Gyc-89Db were expressed in several cells of the terminal and dorsal ganglia of the larval head (Fig. 3.7). The dorsal ganglion is composed of about 40 neurons, most of which innervate the dorsal organ (Fig 3.7A) (Stocker, 1994). The dorsal organ is composed of a highly innervated, multipored olfactory dome structure and six peripheral pore-like sensilla that are thought to be taste or hygrosensors (Stocker, 1994). The terminal ganglion is composed of about 35 neurons, which innervate at least six types of chemosensory sensilla. Several neurons that innervate terminal organ sensilla reside in the dorsal ganglia. p89Da::GFP signal was found in several neuronal-like cells in the dorsal ganglion, all of which appear to innervate the dome structure of the dorsal organ (Fig 3.7B). A smaller number of faint cells appeared in the terminal ganglion, all of which appear to innervate the terminal organ. Gyc-89Db was expressed in several cells in terminal ganglion, including two large, adjacent cell bodies (Fig 3.7C). All of these cells appear to innervate the terminal organ. It was not possible to determine the sensilla type that was innervated. Gyc-89Db expression was also found in 2-5 neurons in the dorsal ganglion (Fig 3.7D). Examining larvae that expressed both promoter constructs revealed that Gyc-89Da and Gyc-89Db are co-expressed in only one or two cells in the dorsal ganglion and are not co-expressed in any cells of the terminal ganglion (Fig 3.7D and E). All of the Gyc-89Da- and Gyc-89Db-expressing cells in the terminal and dorsal ganglia appeared to overlap with ELAV expression (ELAV::GAL4, pan-neuronal marker), indicating that these cells are indeed neurons (Data not shown). The pattern of Gyc-89Db expression in these ganglia resemble the Gyc-89Db late embryonic *in situ* staining pattern (Fig. 3.3G and H). These data are summarized in Table 3.2.

Gyc-89Da and Gyc-89Db expression was also found in two cells on each side of the head, adjacent to each of the terminal ganglia (Fig 3.7D). These neuronal-like cells have the morphology of monoscolopidial chordotonal organ neurons, which are involved with stretch- or mechanosensation (Campos-Ortega and Hartenstein, 1997; Ghysen et al., 1986). The axons of these chordotonal-like neurons joined different nerves, with one joining the larval antennal nerve, and one joining the maxillary nerve. Finally, Gyc-89Db expression was found in a cluster of 2-3 multidendritic neurons that innervated the anteriormost regions of the larval head (Fig 3.7C and F). These Gyc-89Db expressing cells overlapped with the neurons that appear the enhancer trap line 109(2)80 (Fig 3.7G), which expresses GAL4 in most or all multidendritic neurons (Grueber et al., 2002), which are found in all segments and cover the entire larval body wall with dendritic processes. The function of the multidendritic neurons is not entirely clear, but they are thought to be involved in touch reception or thermosensation (Bodmer and Jan, 1987).

Gyc-89Da and Gyc-89Db were co-expressed in one of three neurons that innervate each of the two external sensilla on each side of larval (thoracic) segments T1 through T3 (Fig. 3.8A'', only T3 is shown) (Bodmer and Jan, 1987). This pattern is identical to the Gyc-88E and Gyc-89Db embryonic *in situ* staining observed in Figure 3.2A-E and Figure 3.3A-D. A closer view of a T2 ventral external sensilla (ves) neuron that co-expressed Gyc-89Da and Gyc-89Db reveals the knob-like structure of the sensilla (Fig. 3.8B).

**Figure 3.7.** Gyc-89Da and Gyc-89Db expression in the dorsal and terminal ganglion and other peripheral neurons in the 3<sup>rd</sup> instar larval head segment. (A) Structure of the three major larval chemosensory organs and associated ganglia. The dorsal organ (DO) is composed of a multipored dome structure (DM), and six peripheral pore channels (PC). These sensilla are innervated by neurons originating in the dorsal ganglion (DG), which connects to the CNS via the antennal nerve (AN). The terminal organ (TO) consists of several types of chemosensory sensilla: dorsolateral papilla (DP), pit sensilla (PS), knob sensilla (KS), papilla (PP). Most of these sensilla are innervated by neurons originating from the terminal ganglion (TG), but the dorsolateral papilla receives innervation from the dorsal ganglion, which connects to the CNS via the maxillary nerve (MN). The ventral organ (VO) is a simple structure that consists of 5 small pores and is innervated by a small ganglia. Diagram based on transmission EM and taken from Stocker (1994). Not drawn to scale. (B) p89Da::GFP animal. Gyc-89Da expression in the 3<sup>rd</sup> instar dorsal and terminal ganglia, innervating the dorsal organ (open arrowhead) and the terminal organ (arrowhead). Cuticular structures such as external sensilla tend to emit high autofluorescence, and often appear yellow in double labeled images. (C) p89Db::GFP animal. Gyc-89Db expression in the terminal ganglion, innervating the terminal organ (arrowhead). Gyc-89Db was also expressed in a cluster of multidendritic neurons. (D) p89Da::GFP, p89Db::GAL4, UAS::DsRed animal. Dorsal-ventral view of larval head, showing both sets of head organs/ganglia. Separate color channels in (D) and (D') are merged in (D''). Gyc-89Da and Gyc-89Db are co-expressed in one (D'', open arrow) or two (E, asterisks) neurons in the dorsal ganglion, and are non-overlapping in the terminal ganglia (D''). Open arrowheads indicate terminal organs, closed arrowheads indicate dorsal organs, asterisk indicates multidendritic neurons observed in (C), arrows indicate monoscolopidial chordotonal-like neurons. (F) p89Db::GAL4, UAS::mCD8-GFP animal. Gyc-89Db is expressed in a cluster of multidendritic neurons (asterisks) (also in D'') on each side that innervates the anteriormost portion of the head (closed arrowheads). The circled areas contain the retracted dorsal and terminal organs, and associated ganglia. (G) p89Db::GFP, 109(2)80, UAS::DsRed animal. Separate color channels in (G) and (G') are merged in (G''). Gyc-89Db is co-expressed (G'') with the multidendritic neurons in line 109(2)80. Only the cell bodies of the neurons are shown. Scale bars= (B and C) 40 $\mu$ m, (D) 50 $\mu$ m, (F) 50 $\mu$ m.

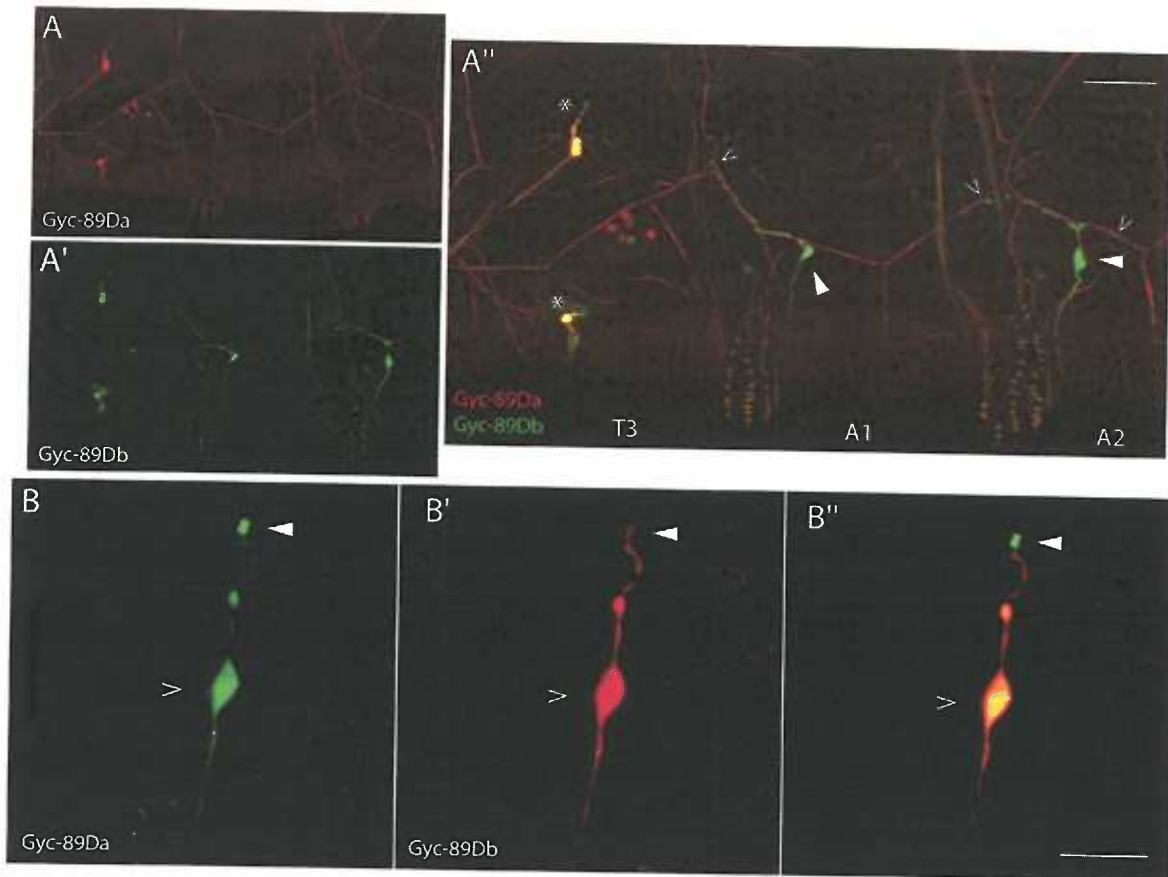




Consistent with the embryonic *in situ* experiments, only Gyc-89Db expression was found in one of the two ventral tracheal dendritic (v'td) neurons in (abdominal) segments A1 and A2 (Fig. 3.8A''). In embryos, Gyc-88E and Gyc-89Db (but not Gyc-89Da) were found to expressed the same v'td cell in segment A1 (Fig. 3.2, 3.3, and 3.5). Figure 3.8A'' also clearly illustrates the association of v'td dendrites with minor branches of the trachea, which autofluoresce. These data are summarized in Table 3.2.

Gyc-89Da and Gyc-89Db were found to be co-expressed in one neuron in each of the seven sensory cones (SO1-SO7) per side found in the caudal region of larvae (Fig. 3.9A and D), similar to what was found with Gyc-88E and Gyc-89Db expression in embryos (only 6 neurons per side were observed in late embryos) (Fig. 3.2 H-J and Fig. 3.3J and K). SO1, SO2, SO3, SO5, and SO7 (Fig. 3.9A) all have one peg-shaped external sensillum at the tip of the cone structure, in all larval stages (Fig. 3.9B)(Kuhn et al., 1992; Kuhn et al., 1995). SO1 and SO2 also have a hair-like sensillum in the 1<sup>st</sup> instar larva. In 2<sup>nd</sup> and 3<sup>rd</sup> instar larvae these hair sensilla are replaced by knob-like sensilla, which are encircled by a variable number of opposing broad-based leaflet-like bristles (Fig. 3.9C) (Kuhn et al., 1992). In SO1, SO2, SO3, and SO7, the neuron that co-expressed Gyc-89Da and Gyc-89Db clearly innervated a peg sensillum and not the knob/leaflet structure (Fig. 3.9E and F, showing SO1). SO4, SO5, and SO6 clearly contained one cone-tip innervating neuron that co-expressed Gyc-89Da and Gyc-89Db, but it was not possible to determine the sensillum type that was innervated, due to the more anterior position of these cones. As SO4 and SO6 possess only a knob/leaflet sensillum, the neuron observed in these cones likely innervates this structure.

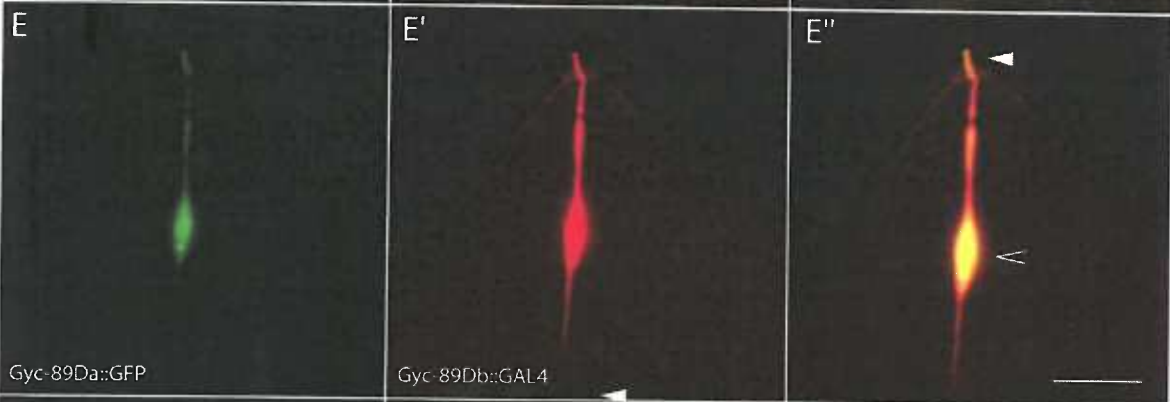
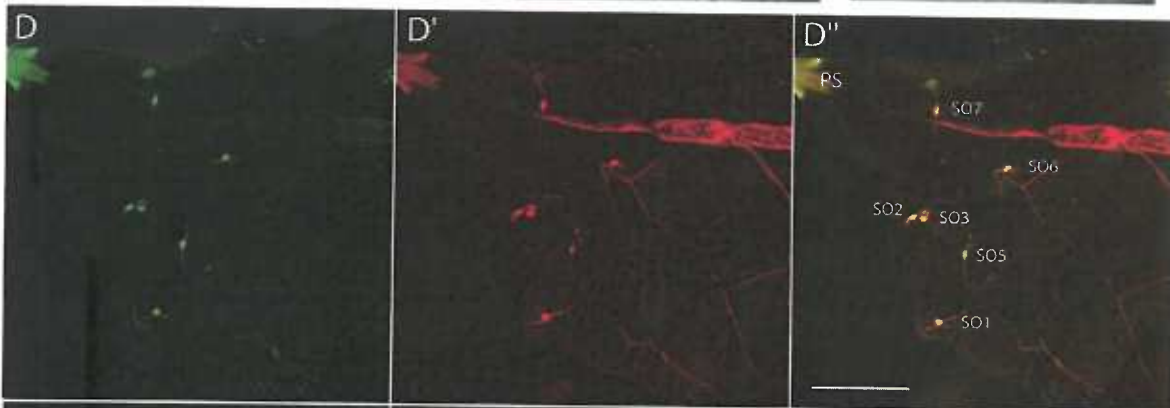
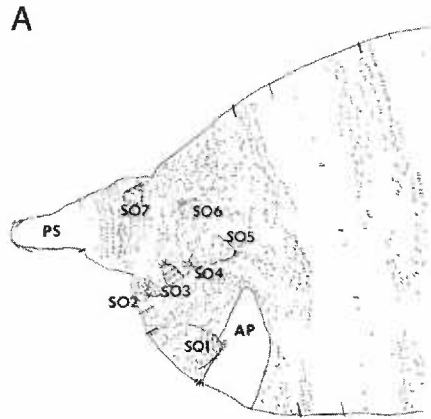
**Figure 3.8.** Expression of Gyc-89Da and Gyc-89Db in the lateral PNS of 3<sup>rd</sup> instar larvae. p89Da::GFP, p89Db::GAL4, UAS::DsRed animals were used in this figure. Double reporter experiments are split into three panels, and separate emission (color) channels in (X) and (X') are merged in (X''). (A) Gyc-89Da and Gyc-89Db are co-expressed in one of three neurons (asterisks) that innervates the lateral and ventral external sensilla (les and ves) in segments T1-T3 (only T3 shown, side view). Only Gyc-89Db is expressed in one ventral tracheal dendritic neuron (closed arrowheads) in segments A1 and A2. Open arrowheads indicate the extent of the dendritic association with the tracheal branches. (B) Close-up of a T2 ves and an innervating neuron (open arrowhead) that co-expressed Gyc-89Da and Gyc-89Db. The knob-like external sensillum (closed arrowhead) is highly autofluorescent in the GFP channel (B), revealing its structure. Only the dendritic process of the neuron (closed arrowhead) is visible in B'. Scale bars= (A) 100 $\mu$ m, (B) 25 $\mu$ m.



The fine structure and function of the both the peg and knob/leaflet sensillum is unknown at this time, although the peg sensilla closely resemble basiconical sensilla, which are known to have pores and a chemosensory function. It is also unknown how many neurons innervate the two types of sensory cone sensilla, but in my observations with the pan-neuronal marker ELAV-GAL4 line and with the whole embryo *in situ*/22C10 double label experiments it appears that both types of sensilla are innervated by only one neuron, at least in SO1 (Fig. 3.3J and K, and data not shown). These data are summarized in Table 3.2.

It should be noted that an additional cell or structure appeared in sensory cones in p89Da::GAL4 animals compared to p89Da::GFP animals. In p89Da::GFP animals, only one neuron appears in the sensory cone (Fig. 3.9E). In p89Da::GAL4 animals however, both a neuron and another cell or structure appears (Fig. 3.9F'). Crossing p89Da::GAL4 to UAS::DsRed or UAS::GFP yielded the same results. This additional cell or structure does not appear to be a neuron, and terminates well before the surface of the cone. This structure is likely a non-neuronal support or accessory cell associated with most or all external sensilla of all types. Since the same genomic region was used in the construction of both the GFP and GAL4 constructs, it is not clear what caused the additional location of expression in the p89Da::GAL4 line. It is possible that the gypsy insulator elements in the GFP line reduced the influence of endogenous regulatory elements while the GAL4 construct is susceptible to these influences. The cause is not related to insertion-specific local influences as several independent insertion lines shown the same expression pattern in the sensory cones.

**Figure 3.9.** Gyc-89Da and Gyc-89Db are co-expressed in sensillum-innervating neurons in the larval sensory cones. Double reporter experiments are split into three panels, and separate emission (color) channels in (X) and (X') are merged in (X''). (A) Diagram of the caudal region of a Canton-S 3<sup>rd</sup> instar larva (side view, dorsal is up, posterior is left). The sensory cones SO1- SO7 are arranged in an invariable pattern that is consistent throughout the larval stages. Note that SO1 is the largest and tallest cone and SO7 is positioned on the dorsal side of the posterior spiracle (PS) appendage. AP= anal pad. Figure modified from Kuhn et al (1992). (B) Visible light photograph of a 3<sup>rd</sup> instar SO1 sensory cone, showing a peg sensillum (closed arrow) and part of the knob/leaflet sensillum. (C) Different focal plane of the SO1 cone shown in (B), clearly showing the knob/leaflet sensillum (open arrowhead points to central knob). (D) p89Da::GFP, p89Db::GAL4, UAS::DsRed animal. Caudal region of a 2<sup>nd</sup> instar larva in the same orientation as (A). Gyc-89Da and Gyc-89Db are co-expressed in one neuron in each of the seven sensory cones (D'') (SO4 neuron not visible in this image). (E) p89Da::GFP, p89Db::GAL4, UAS::DsRed animal. Example of a 3<sup>rd</sup> instar SO1 sensory cone that held one neuron that co-expressed Gyc-89Da promoter driven GFP and Gyc-89Db promoter driven GAL4-DsRed (E''). Cell body indicated with open arrowhead, dendritic innervation of peg sensillum indicated with closed arrowhead. (F) p89Db::GFP, p89Da::GAL4, UAS::DsRed animal. Example of a 3<sup>rd</sup> instar SO1 sensory cone that held one neuron that co-expressed p89Da::GAL4 driven DsRed and p89Db driven GFP (F''), open arrowhead indicates cell body, closed arrowhead indicates dendritic innervation of peg). p89Da::GAL4 driven DsRed expression also appears in what is likely a non-neuronal sensillum accessory or support cell (arrow in F'). This cell terminates well before the surface of the cone (arrow in F''). The bright structures that cover the surface of the cone are autofluorescent non-sensory cuticular bristles. Scale bar= (B and C) 25µm, (D) 100µm, (E and F) 25 µm.



Tissue/ cell population	Gyc-88E	Gyc-89Da		Gyc-89Db		Overlap, p89Da+Db
		p89Da	Embr. <i>in situ</i>	p89Db	Embr. <i>in situ</i>	
<b>Larval PNS</b>						
dorsal ganglion ~40 neurons/ganglion	0	7-9	3-5	2-5	4-5	1-2
terminal ganglion ~35 neurons/ganglion	1	2-4	2-3	3-5	2-5	0
head chordotonal organs 2 monoscolopidial/side, 1 neuron each	0	2	0	2	0	2
head multidendritic arborization neurons	0	0	0	2-3	0	0
T1-T3 external sensilla 3 <i>les</i> & 3 <i>ves</i> neurons	1 <i>les</i> 1 <i>ves</i>	1 <i>les</i> 1 <i>ves</i>	1 <i>les</i> 1 <i>ves</i>	1 <i>les</i> 1 <i>ves</i>	1 <i>les</i> 1 <i>ves</i>	1 <i>les</i> 1 <i>ves</i>
A1 & A2 tracheal dendritic neurons 2 <i>v'td</i> neurons	1	0	0	1	1	0
terminal sensory cone peg sensilla 7 cones, 1-2 neurons/cone	1/cone in 6 cones	1/cone	1/cone	1/cone	1/cone	1/cone
<b>Adult PNS</b>						
Labellar taste bristles ~248 per lobe	ND	p89Da 0		p89Db 40+		-
Labellar taste pegs ~42-68 per lobe	ND	0		15+		-
Pharyngeal sensilla	ND	0		4		-
5 <sup>th</sup> seg prothoracic leg taste hairs	ND	0		4		-

**Table 3.2.** Summary of Gyc-88E, Gyc-89Da, Gyc-89Db expression in the peripheral nervous system in larvae and adults. Gyc-88E expression observations were obtained from the whole embryo *in situ* experiments only (stage 17 embryos or newly hatched 1<sup>st</sup> instar larvae). Gyc-89Da and Gyc-89Db expression observations from the whole embryo *in situ* experiments and the promoter::reporter experiments are compared in separate columns. Expression patterns of Gyc-89Da and Gyc-89Db were constant throughout the 1<sup>st</sup>, 2<sup>nd</sup>, 3<sup>rd</sup> larval instars. For the overlap column Gyc-89Db expression was compared to Gyc-89Da expression in larvae. Direct Gyc-88E/ Gyc-89Da overlap was not determined. At least 20 animals in all cases were observed to obtain the above data.

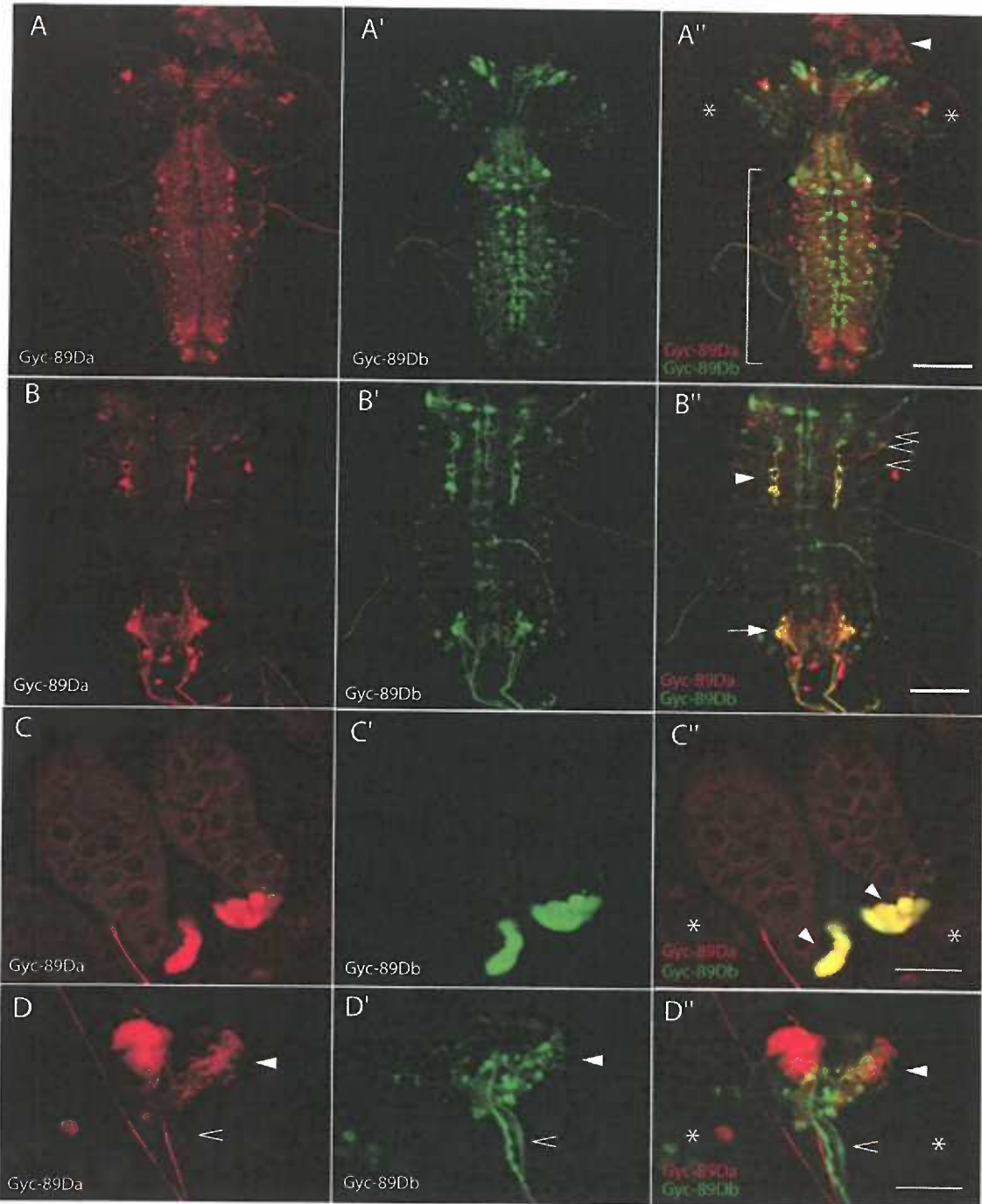
Gyc-89Da and Gyc-89Db expression was also found in many cells of the larval CNS. Interestingly, Gyc-89Da and Gyc-89Db were found to be expressed in a mostly non-overlapping pattern (Fig. 3.10A). Both Gyc-89Da and Gyc-89Db were heavily expressed in the brain lobes and the ventral nerve cord (VNC). In the VNC, two overlapping regions of expression were observed. In the posterior end of the VNC, double-labeled processes appear to arrive through nerves to make contact with the neuropil (Fig. 3.10B). By tracing these nerves posteriorly, it is apparent that these elaborations belong to the axons of the sensory cone neurons, which co-express Gyc-89Da and Gyc-89Db (Fig. 3.9). In the anterior or thoracic region of the VNC, double labeled processes appeared to arrive from lateral nerves to make contact with the neuropil (Fig. 3.10B). Following these processes laterally out through the nerves it appeared that they originated from the Gyc-89Da/Gyc-89Db expressing neurons that innervate the external sensilla found on the thoracic segments (Fig. 3.8). While Gyc-89Da and Gyc-89Db were not co-expressed in any cell bodies in the CNS, they were co-expressed in the intrinsic corpora cardiaca cells in the ring gland, which is attached to the anterior part of the CNS between the brain lobes (Fig. 3.10A and C). The ring gland also houses the corpora allatum and the prothoracic gland. The corpora cardiaca plays a crucial role in glucose homeostasis and is a producer of numerous hormones, including adipokinetic hormone (AKH), a polypeptide that mobilizes stored macromolecular energy stores when needed for high-energy activities such as flight and crawling (Kim and Rulifson, 2004; Van der Horst, 2003). The ring gland also appears to be innervated by neuronal projections that expressed Gyc-89Da or Gyc-89Db (Fig. 3.10D). These projections were



**Figure 3.10.** Gyc-89Da and Gyc-89Db were expressed in the 3<sup>rd</sup> instar larval CNS and ring gland. Double reporter experiments are split into three panels, and separate emission (color) channels in (X) and (X') are merged in (X''). p89Da::GFP, p89Db::GAL4, UAS::DsRed animals were used in this figure. (A) Gyc-89Da and Gyc-89Db are expressed in the brain lobes (asterisks) and the VNC (bracket) in a completely non-overlapping cell body pattern. Gyc-89Db expression appeared in many more cells than Gyc-89Da. The ring gland (closed arrowhead) is attached to the anterior region of the CNS. (B) In the VNC, peripheral neuron axon projections that co-express Gyc-89Da and Gyc-89Db innervate the neuropil in the thoracic region (closed arrowhead) and in the posterior abdominal region (arrow). The double labeled nerves that enter the CNS from the thoracic PNS are indicated with open arrowheads. (C) Gyc-89Da and Gyc-89Db are co-expressed in the intrinsic corpora cardiaca cells (arrowheads) in the ring gland. The CNS brain lobes are indicated with asterisks. (D) A more superficial view of the corpora cardiaca region of the ring gland shows innervation (closed arrowhead) of this region by separate Gyc-89Da- and Gyc-89Db-expressing projections (open arrowhead) that appeared to originate from the CNS (brain lobes indicated with asterisks). Bright red lines in (C) and (D) represent autofluorescent trachea. Scale bars= (A) 100 $\mu$ m, (B) 50 $\mu$ m, (C) 25  $\mu$ m, (D) 20  $\mu$ m.

mostly associated with the corpora cardiaca region of the ring gland, and contacted mutually exclusive areas (Fig. 3.10D''). The Gyc-89Da-expressing projections were weakly fluorescent, and I was unable to locate the cell bodies of origin. The Gyc-89Db-expressing projections appeared to originate from a medially located group of cells that resided near the esophageal foramen (data not shown). The position of these cells was reminiscent of the CC-MS 1 cell group reported by Siegmund and Korge (2001), which was found to contain weak allatotropin immunoreactivity (Siegmund and Korge, 2001). *In situ* hybridization experiments done with 3<sup>rd</sup> instar CNSs indicated that Gyc-88E was also expressed here at this stage (data not shown). In addition, the Gyc-89Db probe stained large number of cells in the 3<sup>rd</sup> instar CNS, confirming the results observed here with the promoter::reporter constructs (data not shown, Gyc-89Da probes were not used on 3<sup>rd</sup> instar CNS preparations).

Several of the Gyc-89Da- and Gyc-89Db-expressing cells in the CNS brain lobes and VNC resembled peptidergic neurons in morphology and/or position. To determine if any of the cells that express Gyc-89Da or Gyc-89Db are indeed peptidergic neurons, I generated larvae that contained Gyc-89Da::GFP or Gyc-89Db::GFP and Dimmed::GAL4, UAS::DsRed. *Dimmed* is a basic helix-loop-helix (bHLH) gene that has an expression pattern that corresponds precisely with most, but not all peptidergic cells in the CNS (Hewes et al., 2003). *Dimmed* was found to control the neuroendocrine fate of these peptidergic cells. I found that both Gyc-89Da and Gyc-89Db co-localized with several dimmed-positive cells in different locations. Gyc-89Da was found to be expressed in two subsets of *dimmed* positive cells in the VNC (Fig. 3.11A and B).



Co-localization occurred in a medial-lateral row of cells (Fig. 3.11A) and in a far-lateral set of larger cells (Fig. 3.11B), where several Gyc-89Da-expressing cells overlapped with several *dimmed*-expressing cells. Gyc-89Da was also colocalized with *dimmed* in the corpora cardiaca cells in the ring gland (Fig. 3.11A). No overlap was observed in the brain lobes. Gyc-89Db expression did not colocalize with *dimmed* in the VNC, but overlap was observed in the corpora cardiaca cells (Fig. 3.11C). A closer look at the ring gland/brain lobe area revealed that Gyc-89Db colocalized with *dimmed* in a cluster of 3 cells in the brain lobe (Fig. 3.11D).

The positions of the peptidergic cells in the CNS that expressed Gyc-89Da and Gyc-89Db resembles the positions of cells that were shown to express eclosion hormone (EH) and crustacean cardioactive peptide (CCAP) (McNabb et al., 1997; Park et al., 2003). CCAP is expressed in two pairs of cells in the brain lobes, and two medial-lateral rows of cells in VNC. EH is expressed only in a pair of cells in the brain lobes. The Gyc-89Da pattern in the VNC especially resembles the CCAP pattern in the VNC. To determine if Gyc-89Da or Gyc-89Db is co-expressed with EH or CCAP, flies were generated that contain both p89Da::GFP or p89Db::GFP and CCAP::GAL4, UAS::DsRed or EH::GAL4, UAS::DsRed. The Gyc-89Da expression pattern did not overlap with the CCAP or EH expression pattern anywhere in the CNS (Fig. 3.12A and B). The Gyc-89Da-expressing cells in the VNC were adjacent to the CCAP cells (Fig. 3.12A). Similarly, the Gyc-89Db expression pattern did not overlap with the CCAP or EH expression patterns anywhere in the CNS (Fig. 3.12C and D). A number of Gyc-89Db expressing cells were also just adjacent to the CCAP cells in the VNC (Fig 3.12C).

**Figure 3.11.** Gyc-89Da and Gyc-89Db were co-expressed with *dimmed* in several cells in the CNS and in the corpora cardiaca cells. Double reporter experiments are split into three panels, and separate emission (color) channels in (X) and (X') are merged in (X'').

(A) p89Da::GFP, pDimmed::GAL4, UAS::DsRed animal. Gyc-89Da was co-expressed with *dimmed* in a partially overlapping pattern in a medial-lateral row of cells (open arrowheads). Gyc-89Da was also co-expressed with *dimmed* in the corpora cardiaca cells (closed arrowheads). (B) p89Da::GFP, pDimmed::GAL4, UAS::DsRed animal. Gyc-89Da was also expressed with *dimmed* in a lateral population of large cells in the VNC (closed arrowheads). Open arrowheads point to some of the cells observed in (A). (C) p89Db::GFP, pDimmed::GAL4, UAS::DsRed animal. Gyc-89Db was coexpressed with *dimmed* in the corpora cardiaca cells in the ring gland (open arrowheads). (D) p89Db::GFP, pDimmed::GAL4, UAS::DsRed animal. A close-up of the ring gland/brain lobe area revealed that Gyc-89Db was also co-expressed with *dimmed* in a cluster of 3 cells in the brain lobe (closed arrowheads). Open arrowheads indicate the corpora cardiaca cells in the ring gland. Scale bars= (A, C, and D) 100 $\mu$ m, (B) 50 $\mu$ m.

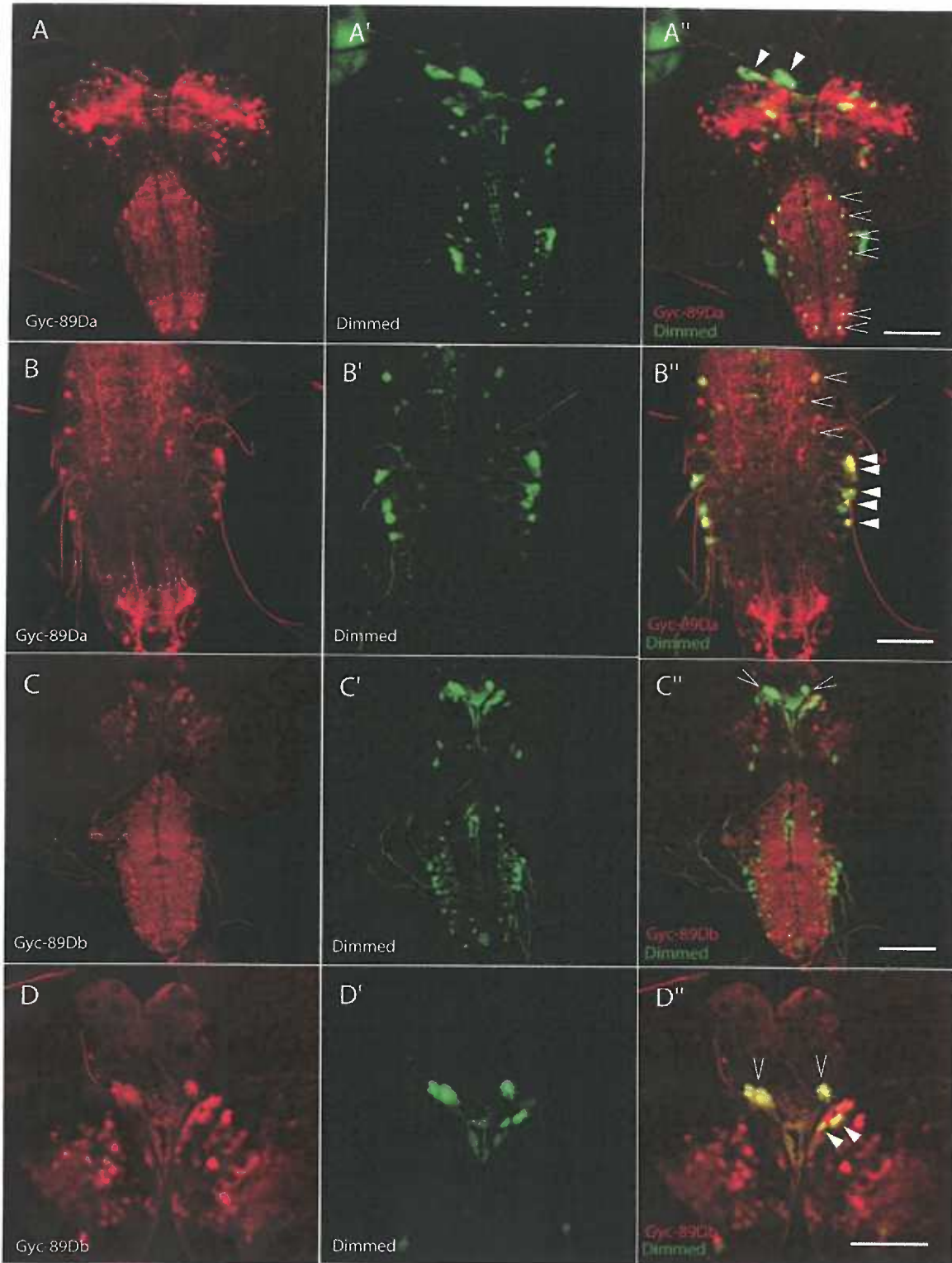
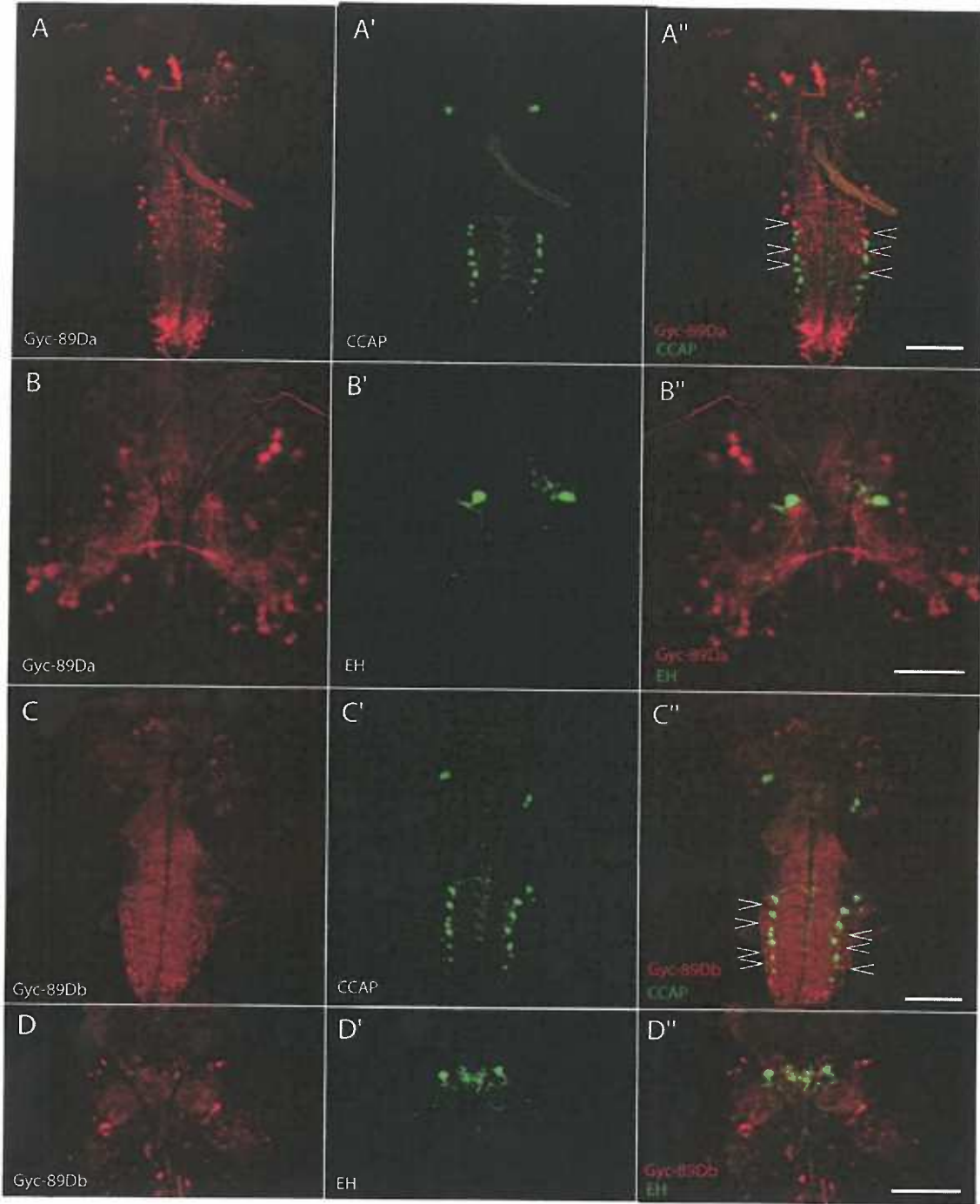


**Figure 3.12.** Gyc-89Da and Gyc-89Db are not co-expressed with EH or *dimmed* anywhere in the 3<sup>rd</sup> instar larval CNS. Double reporter experiments are split into three panels, and separate emission (color) channels in (X) and (X') are merged in (X''). (A) p89Da::GFP, pCCAP::GAL4, UAS::DsRed animal. Gyc-89Da and *dimmed* are not coexpressed in the CNS. Open arrowheads indicate Gyc-89Da-expressing cells just adjacent to *dimmed* cells. (B) p89Da::GFP, pEH::GAL4, UAS::DsRed animal. Gyc-89Da is not coexpressed with EH. (C) p89Db::GFP, pCCAP::GAL4, UAS::DsRed animal. Gyc-89Db is not coexpressed with CCAP anywhere in the CNS. Open arrowheads indicate Gyc-89Db-expressing cells just adjacent to *dimmed* cells. (D) p89Db::GFP, pEH::GAL4, UAS::DsRed animal. Gyc-89Db is not coexpressed with EH. Scale bars= (A, C, and D) 100µm, (B) 50µm.

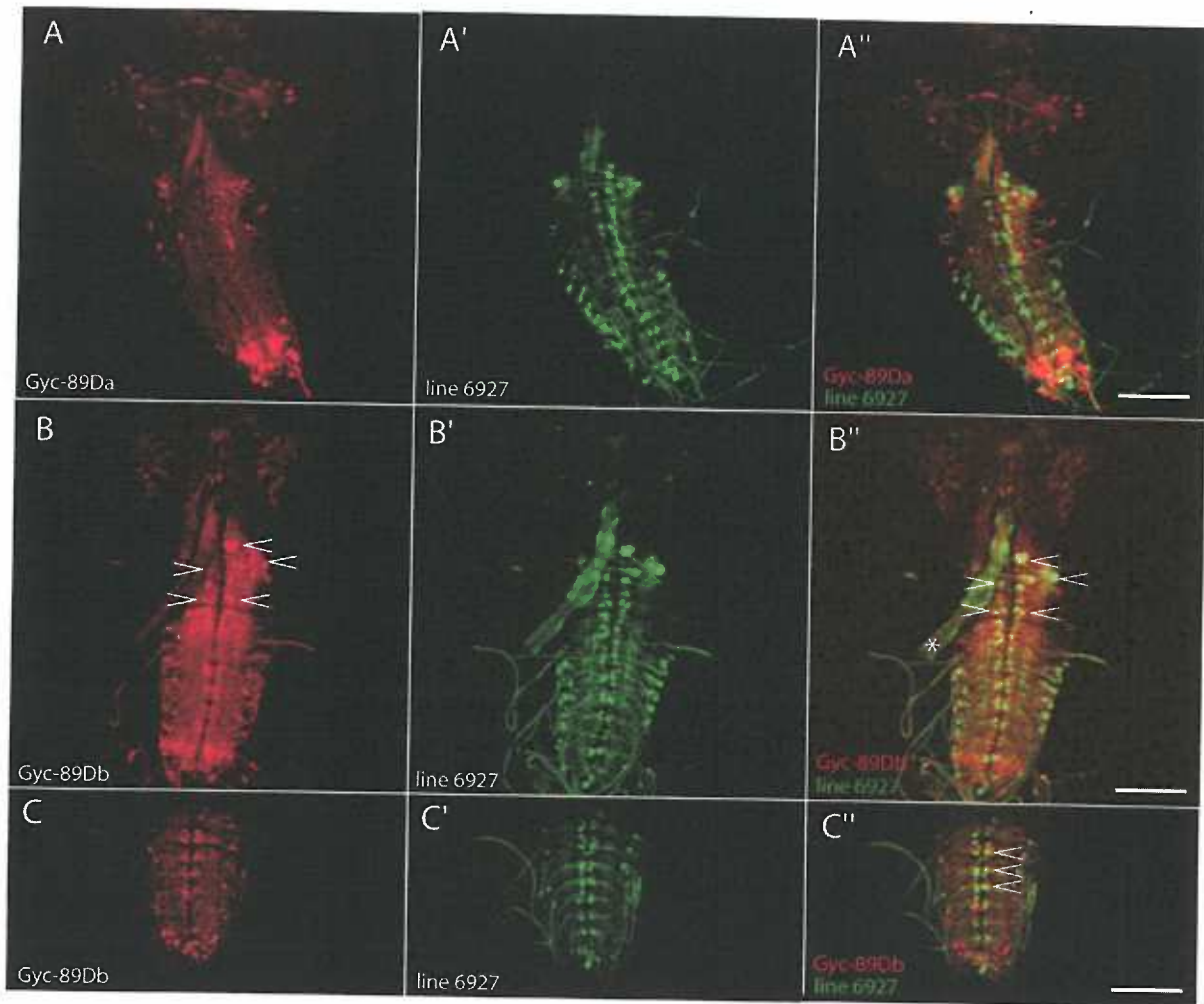




To determine if any of the cells in the CNS that expressed Gyc-89Da or Gyc-89Db are motor neurons, animals were generated that contained p89Da::GFP or p89Db::GFP and an enhancer trap driven GAL4 (from Bloomington line 6927), and UAS::DsRed. Line 6927 express GAL4 in a large subset of motor neurons in the CNS in 3<sup>rd</sup> instar larvae (Fergestad and Broadie, 2001). Gyc-89Da expression in the 3<sup>rd</sup> instar larval CNS was not colocalized with any of the cells that express GAL4 in line 6927 anywhere in the CNS (Fig. 3.13A). In contrast, expression of Gyc-89Db in a subset of VNC cells colocalized with 6927- GAL4, UAS::DsRed expression (Fig. 3.13B and C). The overlap was observed in several large cells in the anterior region of the VNC, and in a subset of midline cells that populated nearly the entire length of the VNC. No overlap was observed in more lateral regions of the VNC or in the brain lobes. These results suggest that Gyc-89Da is not expressed in motor neurons while Gyc-89Db is expressed in a small subset of motor neurons.

Gyc-89Db was also found to be expressed in several PNS locations in adult flies. Gyc-89Db expression in the labellum, which is thought of as the primary taste organ in adult flies. The labellum, a membranous bi-lobed structure that is situated on the distal end of the proboscis, is adorned with a total of 66 hair-like sensilla, 62 of which are chemosensory (Shanbhag et al., 2001) (Fig. 3.14A). A typical labellar sensillum houses one mechanoreceptor and four gustatory neurons, each of which responds to water, sugar, low salt concentration, or high salt concentration (Hiroi et al., 2002; Rodrigues and Siddiqi, 1981; Stocker, 1994). Also present on the labellum, situated in rows between the pseudotrachea (Fig. 3.14A), are about 40 short pin-like sensilla called taste pegs (Shanbhag et al., 2001).

**Figure 3.13.** Gyc-89Da was not expressed in motor neurons while Gyc-89Db is expressed in a subset of motor neurons in 3<sup>rd</sup> instar larval CNS. Double reporter experiments are split into three panels, and separate emission (color) channels in (X) and (X') are merged in (X''). (A) p89Da::GFP, 6927 GAL4, UAS::DsRed animal. Gyc-89Da was not co-expressed with GAL4 in the motor neuron marker line 6927. (B) p89Db::GFP, 6927 GAL4, UAS::DsRed animal. Gyc-89Db was coexpressed in a subset of large cells that express GAL4 in line 6927 (open arrowheads). The esophagus, which is autofluorescent in both emission channels and is sometimes retained in CNS dissections, is indicated with an asterisk. (C) p89Db::GFP, 6927 GAL4, UAS::DsRed animal. Gyc-89Db was also expressed in a subset of line 6927-GAL4-expressing cells in the midline of the VNC (open arrowheads). Scale bar= 100µm.

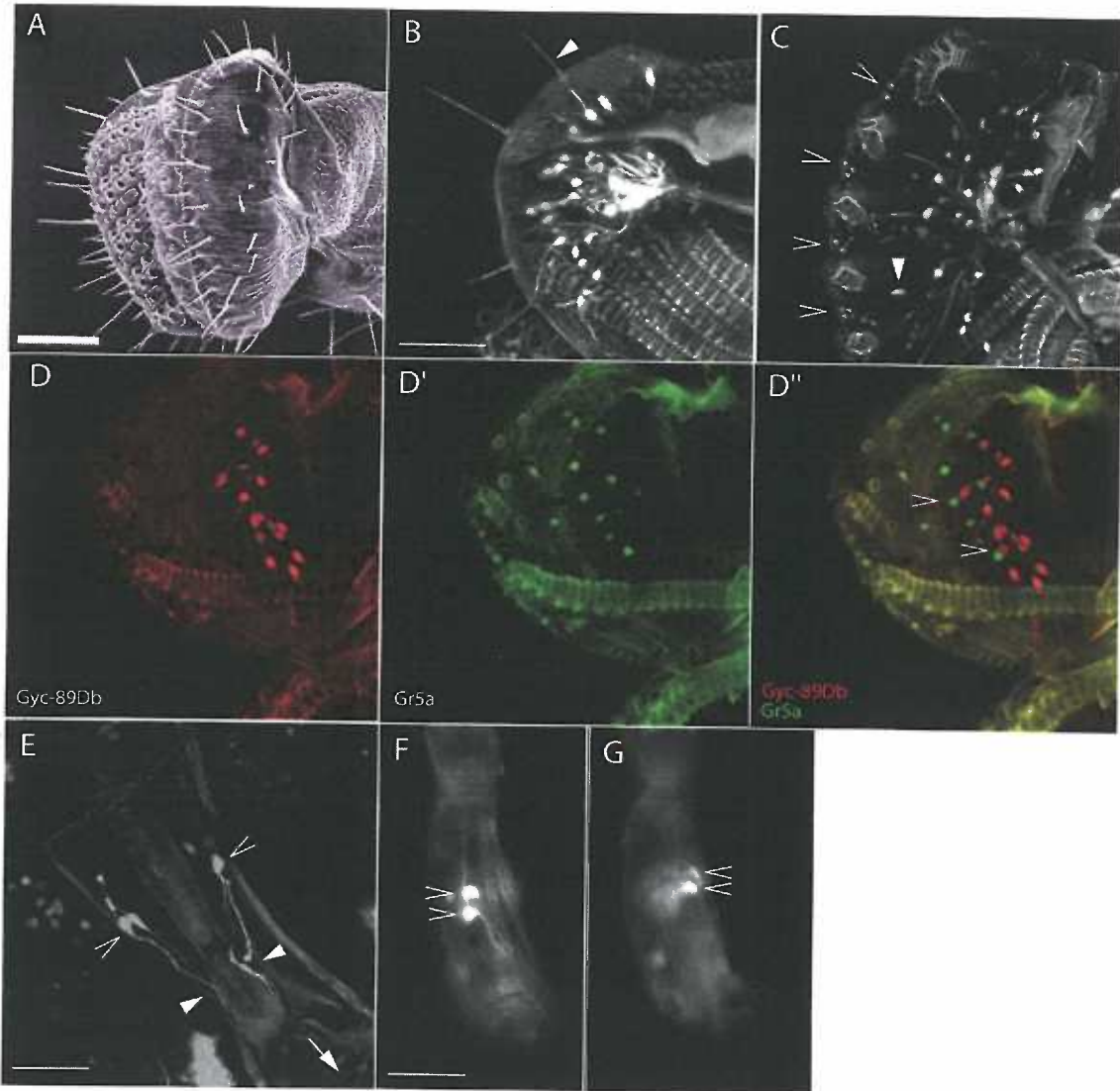


All taste peg sensilla are innervated by one putative chemosensory neuron and one mechanosensory neuron (Shanbhag et al., 2001). *Gyc-89Db* was found to be expressed in a large number of neurons in the labellum, innervating many taste bristles and taste pegs (Fig. 3.14B and C). In all cases, only one *Gyc-89Db*-expressing neuron was observed to innervate each sensillum. Over 40 *Gyc-89Db*-expressing neurons were observed per labellar lobe (Table 3.2).

The expression patterns of a dozen (of the about 60 known) gustatory receptor (*Gr*) genes have been described in the labellum (Scott et al., 2001; Thorne et al., 2004). Many of these *Gr* genes are expressed in a limited number of neurons in the labellum, ranging from 5 to about 15 neurons per lobe. One *Gr* gene however, the trehalose receptor *Gr5a*, was expressed in a large number of neurons, innervating both taste bristles and pegs (Thorne et al, 2004), similar to what was observed with the *Gyc-89Db* expression (Fig. 3.14B and C). To determine if *Gyc-89Db* is co-expressed with *Gr5a*, flies were generated that contained both *p89Db::GFP* and *Gr5a::GAL4, UAS::DsRed*. I found that *Gyc-89Db* was not co-expressed in any *Gr5a*-expressing cells (Fig. 3.14D). It appeared that the cells that expressed *Gyc-89Db* were often adjacent to the *Gr5a* neurons, indicating that these two genes were expressed in different cells in the same cluster innervating one sensillum. Co-expression of *Gyc-89Db* with other *Gr* genes was not examined. *Gyc-89Db* expression was also found in two pairs of neurons that innervate ventral cibarial sense organ, which is one of three pairs of pharyngeal sensilla (Stocker, 1994) (Fig. 3.14E). These sensilla are thought to be gustatory in function, and have been found to express at least three different *Gr* genes (Scott et al., 2001; Stocker, 1994). Finally, *Gyc-89Db* expression was found in four neurons in the 5<sup>th</sup> (Most distal) tarsal

segment of the prothoracic legs. These neurons likely innervate a subset of the 40 or so chemosensory hairs that reside on different segments of the prothoracic legs (Stocker, 1994). *Gr* genes have also been shown to be expressed in neurons that innervate these hairs, and electrophysiological recordings on two of the neurons in the 5<sup>th</sup> tarsal segment demonstrated sensitivity to bitter compounds (Meunier et al., 2003; Scott et al., 2001). Gyc-89Da was not found in any of the above locations in the adult.

**Figure 3.14.** Gyc-89Db was expressed in the adult labellum, pharynx, and prothoracic leg. (A) Scanning EM image of adult labellum. The labellum consists of two lobes, which possess 31 chemosensilla each. Rows of pseudotrachea separate the two chemosensory hair regions. Image from Hiroi et al. (2002). (B) p89Db::GFP animal. Gyc-89Db was expressed in over 40 individual neurons in each lobe of the labellum, innervating numerous chemosensory hairs (closed arrowhead). (C) p89Db::GFP animal. Labellar taste peg sensilla (open arrowheads), which reside between rows of pseudotrachea (cross-sectioned here), were also innervated by Gyc-89Db (closed arrowhead). (D) p89Db::GFP, pGr5a::GAL4, UAS::DsRed animal. Separate emission (color) channels in (D) and (D') are merged in (D''). Gyc-89Db was not coexpressed with the trehalose receptor Gr5a in the labellum. Neurons that expressed Gyc-89Db are often adjacent to neurons that express Gr5a (open arrowheads). (E) p89Db::GFP animal. Gyc-89Db was expressed in neurons (open arrowheads) that appeared to innervate the ventral cibarial sensory organ (closed arrowheads, the sensilla themselves resides inside the pharynx and are not visible here) in the pharynx. Arrow points to distal end of proboscis (F) p89Db::GAL4, UAS::DsRed animal. Gyc-89Db was expressed in four neurons in the 5<sup>th</sup> tarsal segment of the prothoracic leg. Two of the neurons are visible here (open arrowheads). (G) A different focal plane of the leg in (F) reveals the other two Gyc-89Db-expressing neurons (open arrowheads). Scale bars= (A, B, C, and D) 40 $\mu$ m, (E) 50 $\mu$ m, (F and G) 25 $\mu$ m.



## Discussion

The results presented in this chapter demonstrate that the three *Drosophila melanogaster* atypical soluble GCs, Gyc-88E, Gyc-89Da, and Gyc-89Db are expressed in the CNS and in several peripheral nervous system locations. The functional class or identity of most of the peripheral neurons and several of the central neurons was determined. Furthermore, as suggested by the catalytic sequence analysis in Chapter 1 and the *in vitro* GC activity data from Chapter 2, it was demonstrated that Gyc-88E was co-expressed with Gyc-89Db and likely Gyc-89Da in peripheral neurons.

Evidence that supports the formation of Gyc-88E and Gyc-89Db heterodimers *in vivo* was provided by *in situ* hybridization using probes to both subunits simultaneously. In these experiments, the use of both probes did not label an increased number of cells in the peripheral nervous system compared to using a single probe. The number of cells stained in thoracic and abdominal segments was identical when either probe was used individually or when both probes were used together, suggesting that all these peripheral cells expressed both Gyc-88E and Gyc-89Db (see Table 3.1). In the head segment, however, the total number of cells that I detected was more variable. Nevertheless, I never observed more stained cells in the double probe *in situ* experiments than the maximum number of cells observed when probing for Gyc-89Db alone (see Table 3.1). These experiments indicate that some of these cells express both Gyc-88E and Gyc-89Db while others express only Gyc-89Db.

In late embryos, Gyc-88E stained one large neuron in each of the two terminal ganglia while Gyc-89Db stained 2-5 neurons in each of the terminal ganglia and 4-5 neurons in each of the two dorsal ganglia. The terminal ganglion innervates the



maxillary organ, which is known to serve a gustatory function and has at least 6 different types of sensilla (Stocker, 1994; Heimbeck et al., 1999; Oppliger et al., 2000). The dorsal ganglion innervates the dorsal organ, which consists of a large dome structure and six peripheral pore sensilla, is the main olfactory organ in larval *Drosophila* (Stocker, 1994; Heimbeck et al., 1999; Oppliger et al., 2000). In all larvae stages, Gyc-89Db expression in the dorsal and terminal ganglia (number of cells) was similar to what was observed in the late embryo (Tables 3.1 and 3.2). This finding indicates that expression patterns observed in the late embryo likely represent what would be found in the larval stages. Gyc-89Da was found in a mostly non-overlapping pattern with Gyc-89Db in these ganglia, except for two overlapping cells in the dorsal ganglion. Unfortunately, I was not able to characterize Gyc-88E expression in larval stages, and it remains unknown if Gyc-88E is only expressed in one terminal ganglion neuron during the larval stages. It was not possible to determine which sensilla types in the terminal organ were innervated by the neurons that expressed Gyc-88E and Gyc-89Da, or Gyc-89Db. However, in the dorsal ganglion, all neuronal processes expressing Gyc-89Da or Gyc-89Db clearly entered the dome structure and not the peripheral pore sensilla, suggesting that these GCs play some role in olfaction at this site.

I was able to identify several of the cells staining for both guanylyl cyclases in segments T2 and T3 as one of three neurons (*les* neurons in the lateral cluster and *ves* neurons in the ventral cluster) that innervate the corresponding basiconical-like sensilla. Basiconical sensilla are external club-like structures with pore-like openings to the outside environment and have a putative hygrosensor or olfactory role (Stocker, 1994; Younossi-Hartenstein and Hartenstein, 1997). An identical expression pattern was

observed in larvae using the promoter::reporter fly lines that I generated. Gyc-89Da and Gyc-89Db were co-expressed in one neuron that clearly innervated the *les* and *ves* on segments T1, T2, and T3, from the beginning of the 1<sup>st</sup> instar to the end of the 3<sup>rd</sup> instar stage. As Gyc-89Db appeared to be coexpressed with Gyc-88E in these neurons in last embryonic stage, and Gyc-89Db expression continues here throughout larval life, it is likely that Gyc-88E, Gyc-89Da, and Gyc-89Db are all co-expressed in the observed *les* and *ves*-innervating neurons throughout larvae life (see Table 3.2).

Similarly, Gyc-89Da and Gyc-89Db were co-expressed in one neuron in each of the seven sensory cones found on the caudal regions of larvae, from the 1<sup>st</sup> instar to the end of the 3<sup>rd</sup> instar stage. As Gyc-88E and Gyc-89Db were co-expressed in one neuron in six sensory cones in late embryos, it seems likely that Gyc-88E, Gyc-89Da, and Gyc-89Db are all coexpressed in the same neuron at these locations in larvae. The neurons in this region have not been studied in detail and are not yet named. It is not clear why only 6 Gyc-88E/Gyc-89Da-expressing sensory cone neurons are observed in late embryos and 7 Gyc-89Da/Gyc-89Db-expressing neurons are observed in larvae. Perhaps GC expression in the one of the neurons only appears after the start of larval life.

The peg-like sensilla that were observed to be innervated by several of these sensory cone neurons have been described as basiconical-like, though this classification stemmed only from morphology and not from fine structure (Campos-Ortega and Hartenstein, 1997). While it is not definitively known whether the thoracic segment basiconical-like sensilla and sensory cone peg sensilla actually have pores, these sensilla, as well as the dome structure of the dorsal organs, non-specifically stain in late embryonic immunocytochemistry experiments (K. Langlais, unpublished observations).

Antibody or staining reagent may have entered pores and bound non-specifically to the non-cuticular interiors of these sensilla. Election microscopy studies are still needed to determine the fine structure of these sensilla. The function and modality of these sensilla remains to be experimentally determined.

Gyc-88E and Gyc-89Db also appeared to be co-localized in the late embryo in one of the two A1 and A2 v'td neurons (Table 3.1), which innervate or wrap their dendrites around specific minor trachea branches, avoiding overlap with other td neurons (Bodmer and Jan, 1987). In all larval stages, beginning with newly hatched 1<sup>st</sup> instars, consistent with the *in situ* results, Gyc-89Db but not Gyc-89Da was found to be expressed in one ventral group neuron in A1 and A2 that clearly associated closely with sizable lengths of tracheal branches (Fig 3.8A and Table 3.2). It is likely that Gyc-88E is expressed with Gyc-89Db in this neuron throughout larval life. The function of td neurons is not known, although it is thought that they may play a chemosensory or proprioceptor role (Bodmer and Jan, 1987). While the co-expression data presented here, combined with the sequence analysis from Chapter 1 and the biochemical data from Chapter 2, strongly support heterodimerization between Gyc-88E and Gyc-89Da or Gyc-89Db, co-immunoprecipitation experiments will be needed to definitively demonstrate subunit interaction.

Although there are many cells that appear to co-express Gyc-88E and Gyc-89Db, there are several places, at least in the embryo, where only Gyc-89Db is expressed. In addition to the peripheral neurons in the head segments, Gyc-89Db was expressed in the CNS at earlier stages than Gyc-88E (data not shown). Because Gyc-89Db was only active in the guanylyl cyclase assays co-expressed with Gyc-88E, it is not clear what the

function of Gyc-89Db is when expressed alone. It is possible that the Gyc-88E transcript was present in these cells, but was present at levels too low to be detected with *in situ* experiments or that the Gyc-89Db transcript was present, but was not translated. In the dorsal and terminal ganglia, perhaps Gyc-88E expression does not appear until after hatching, when these sensilla are actually used. Alternatively, Gyc-89Db may be playing a dominant negative role, by heterodimerizing with other soluble guanylyl cyclase subunits and thus preventing them from dimerizing with subunits that would yield an active guanylyl cyclase dimer. A similar situation has been found with MsGC- $\beta$ 3, which will form inactive heterodimers *in vitro* with MsGC- $\alpha$ 1 and MsGC- $\beta$ 1 (Morton and Anderson, 2003). Characterization of the expression pattern of Gyc-88E (and  $\alpha$ 1 and  $\beta$ 1 subunits) in the larval stages will provide clues to this question.

Gyc-88E was found to be expressed in the absence of Gyc-89Db in a individual cells scattered throughout the midgut in late embryos and newly hatched larvae. While these cells were not identified, they do resemble a population of the cone-shaped peptidergic cells that reside in the larval midgut. These cells are known to produce allostatis and FMRFamide, which regulate gut motility and contraction (Lenz et al., 2001; Merte and Nichols, 2002; Taylor et al., 2004). These are the only cells that are definitively shown here to express only Gyc-88E, which is catalytically functional without Gyc-89Da or Gyc-89Db.

Gyc-88E, Gyc-89Da, and Gyc-89Db were also expressed in many cells in the CNS. Gyc-88E was the most broadly expressed of the three GCs in the CNS in late embryos and in third instar larvae (*in situ* experiments not shown), with a large number of cells appearing in both the brain lobes and VNC. Gyc-89Da appeared to be expressed in

the lowest number of cells (3<sup>rd</sup> instar CNS only), while Gyc-89Db appeared to be expressed in an intermediate number of cells in both the embryonic and larval CNS. Interestingly, no Gyc-89Da-expressing cell bodies overlapped with Gyc-89Db-expressing cells bodies in the CNS, suggesting that these two highly identical GC subunits may function differently *in vivo*. It is not known if Gyc-88E is expressed in all Gyc-89Da- and Gyc-89Db-expressing cells, but the total number of Gyc-88E positive cells in the CNS appears to be equal to or greater than the number of Gyc-89Da and Gyc-89Db positive cells combined. It was not determined if any of these GCs are expressed in the adult CNS.

Several of the Gyc-89Da- and Gyc-89Db-expressing cells in the CNS were identified as *dimmed*-positive peptidergic neurons. These GC-expressing peptidergic neurons were not the CCAP or EH containing neurons, and their precise identity remains unknown. However, some of the Gyc-89Da/*dimmed*-expressing cells found on the lateral edges of the VNC may also express members of the RFamide family of neuropeptides, based on the position of 3 pairs of *dimmed*/PT2 (a RFamide marker)-positive cells in double label studies (Hewes et al., 2003). As several of the *dimmed*-expressing cells in the brain lobes were also PT2-positive, the Gyc-89Db-expressing peptidergic brain lobe cell cluster may also contain RFamides. Furthermore, the position of this cell cluster very closely matches the position and number of FMRFamide-positive cells in this area (Nichols et al., 1999). In *Drosophila*, members of the RFamide family have been shown to control a multitude of physiological activities in insects, with several members affecting the contraction rates of the heart (Merte and Nichols, 2002). A comprehensive immunocytochemical double label study, using the promoter::reporter constructs, anti-

GFP antisera, and anti-neuropeptide antisera (nearly 20 different insect neuropeptides have been detected with antisera), would likely provide more information pertaining to the function and identity of GC-expressing peptidergic neurons.

Gyc-89Da and Gyc-89Db were both expressed in the intrinsic cells of the corpora cardiaca, and in neuronal projections that appeared to innervate this region in the ring gland. One the primary functions of corpora cardiaca cells is the management of energy stores through the release of adipokinetic hormone (AKH), which mobilizes energy substrates such as lipids and glycogen and stimulates the synthesis of trehalose as needed for strenuous activities (Isabel et al., 2005). In *Drosophila*, AKH is also known to increase the heart rate (Baumann et al., 1990). Gyc-89Da and Gyc-89Db were also expressed in projections that innervated the ring gland, mostly in the corpora cardiaca region. Most, if not all of the peptidergic neurons that innervate the ring gland have been mapped out and named, through the examination of a dozen enhancer trap reporter lines. The secreted peptide products of several of these peptidergic neurons is known. Although the function of these peptides is not entirely clear in each case, they likely have roles in heartbeat regulation, regulation of ecdysone and juvenile hormone titers, and circadian input (Siegmund and Korge, 2001). Double label studies using the GC promoter::reporter lines and the 12 enhancer trap reporter lines reported in Siegmund and Korge (2001) could lead to the positive identification of the peptidergic neurons that innervate the ring gland, and provide clues pertaining to their function.

Finally, expression of Gyc-89Da and Gyc-89Db in the adult PNS was examined. Surprisingly, Gyc-89Db was found to be expressed in several neuronal populations known to be involved with taste, while Gyc-89Da was absent from all PNS locations

examined, which included the labellum, maxillary palps, antennae, pharynx, leg segments, and wings. In the labellum Gyc-89Db was expressed in a large number of neurons, each of which innervated a separate taste bristle or peg. Each taste bristle is innervated by 2 or 4 chemosensory neurons that detect sugars, salt, water, or bitterness through receptors likely encoded by the *Gr* gene family (Scott et al., 2001; Thorne et al., 2004). Gyc-89Db was not co-expressed with the broadly expressed trehalose receptor Gr5a, which is one of the few *Gr* genes that appears to be expressed in its own set of neurons in the absence of other *Gr* genes (Thorne et al., 2004). Neurons that do not express Gr5a tend to express multiple other *Gr* genes. Various *Gr* genes are also expressed in other gustatory neurons, such as the ones in the prothoracic leg segments and in the pharynx. Double-driver experiments using the p89Db::GFP and the *Gr* promoter::reporter lines described by Thorne et al. (2004) and Scott et al.(2001) will shed light on the integration of Gyc-89Db expression with the *Gr* expression code (Thorne et al., 2004). It will also be important to determine if Gyc-88E is expressed in these locations.

Expression of the Gyc-88E, Gyc-89Da, and Gyc-89Db in neurons that innervate various external sensilla and trachea in larvae and adults indicates that cGMP plays a direct or adaptatory role in sensory transduction. Guanylyl cyclases and cGMP have been demonstrated to play an important role in several types of sensory transduction both in vertebrates and in invertebrates (Lucas et al., 2000; Morton and Hudson, 2002)(also see Chapter 1). Based on the biochemical data in Chapter 2, in Morton (2004), and the demonstrated function of the closely related *C. elegans* atypical GCs GCY-35 and GCY-36, it is most likely that the *Drosophila* atypical GCs act as direct oxygen receptors *in*

*vivo*. It is known that *Drosophila* larvae respond immediately to hypoxic conditions by engaging in an escape response (Wingrove and O'Farrell, 1999). Such a rapid response suggests the existence of a fast-acting neuronal oxygen sensor. The location of expression of the *Drosophila* atypical sGCs in neurons that innervate basiconical-like sensilla on the thoracic segments and sensory cones, trachea, and the dorsal organ in larvae is consistent with the hypothesis that the *Drosophila* atypical sGCs act as the oxygen sensors that mediate this response. It is curious that Gyc-88E/Gyc-89Da or Gyc-89Db are also expressed in known gustatory neurons, if indeed they act as oxygen sensors in *vivo*. It is possible that *Drosophila* not only monitors the concentration of oxygen in the air, but also the dissolved oxygen content in its food substrates, possibly leading to a modulation of taste responses.

It is less clear what the role of a GC oxygen sensor in the CNS would be. It is possible that the cGMP generated by a GC oxygen sensor could regulate central neuron transcriptional activities in response to long-term exposure to low oxygen conditions. cGMP has been shown to play a role in transcriptional regulation in several cases (Lucas et al., 2000). Hypoxic conditions are known to induce transcriptional changes, although hypoxia-inducible transcription factors have been implicated in this response (Cummins and Taylor, 2005). Another potential role of a GC oxygen sensor in the CNS could occur during ecdysis, when for a brief period a pool of molting fluid resides between the old and new trachea, blocking gas exchange and possibly leading to low hemolymph and tracheal oxygen concentration. This period of low oxygen could be utilized as a signal to help coordinate CNS control of the complex events that occur leading up to the shedding of the old cuticle.



## **Chapter 4: Functional impairment of neurons and degradation of cGMP in cells that express Gyc-89Da and Gyc-89Db**

### **Introduction**

The preceding chapters described the initial characterization of the biochemical properties and expression patterns of Gyc-88E, Gyc-89Da, and Gyc-89Db. The question remained: what is the function of these sGCs *in vivo*? To answer this question, I decided to disrupt the expression of these genes using a transposable element insertion strategy, which is the most commonly employed method used to eliminate gene function in *Drosophila*. Transposable elements such as P- and PiggyBac elements are engineered constructs that at a minimum possess the P-element end regions and a marker gene, but lack an active transposase gene. These elements have been artificially introduced to the *Drosophila melanogaster* genome. P-elements can physically disrupt genes by inserting into a crucial region of a gene, such as the open reading frame or a regulatory region. PiggyBac elements act in the same manner as P-elements, but also contain additional disruption features, such as splice acceptor and donor sites (Thibault et al., 2004). A P-element insertion can be mobilized or “hopped” by crossing the insertion fly line with a line bearing an active transposase gene. Several thousand P-element and PiggyBac insertion lines are currently available that in total are predicted to disrupt over 50% of the known or predicted *Drosophila* genes, thanks to the Berkeley *Drosophila* Gene Disruption Project (GDP), Exelixis, DrosDel, and other groups (Bellen et al., 2004; Thibault et al., 2004). Several P-elements have also been designed for use in enhancer

trap analysis and contain a reporter gene that can be driven by an endogenous promoter that lies upstream of the insertion site.

A search of the project databases revealed that of the three atypical *Drosophila* sGCs, only Gyc-89Da had been hit by P-element insertion within its known or predicted gene boundaries. The Gyc-89Da PiggyBac insertion line (line 17991) contained a single PiggyBac P-element insertion in the first intron, which occurs in the cDNA untranslated region (UTR) before the ORF (see Fig 2.1). For Gyc-88E and Gyc-89Db, I searched the transposable element databases for the closest available P-element or PiggyBac insertions, with the plan of hopping these elements into the target genes. A P-element insertion (line CB-6872-3) was found in a gene located only a few hundred bases downstream of Gyc-89Db. The closest P-element insertion (line EY10895) from Gyc-88E was seven kilobases downstream. In short, I attempted to hop these P-elements into Gyc-89Db and Gyc-88E using a standard P-element hopping scheme, generating ~100 potential new insertion lines from each original insertion line. I then screened these lines for insertions into Gyc-89Db and Gyc-88E using a combination of PCR and northern blot methods, but failed to isolate any potential gene knockout insertion lines. It is possible that generating and screening more lines would have resulted in the desired insertions. Alternatively, it is possible that the Gyc-88E and Gyc-89Db gene regions are aversive to insertions, or the regions outside of these genes are insertional “hotspots”, which may draw locally mobilized elements to them. Insertional hotspots and coldspots have been described in the literature (Bellen et al., 2004; Thibault et al., 2004). Lacking potential knockout lines for Gyc-88E and Gyc-89Db, I decided on an alternative but more indirect

method of gaining information about the function of these genes, in addition to examining the potential Gyc-89Da knockout line.

Instead of directly determining the function of the *Drosophila* atypical sGCs, the function of the neurons that express Gyc-89Da and Gyc-89Db was examined. This was achieved by driving UAS controlled tetanus light chain toxin (UAS::TNT or UAS::TeTxLC) with the p89Da::GAL4 and p89Db::GAL4 lines that were characterized in chapter 3, targeting its expression to a specific population of cells. Tetanus light chain toxin has been shown to specifically degrade synaptobrevin and effectively block evoked neurotransmitter release in *Drosophila* (Sweeney et al., 1995). The heavy chain of the naturally occurring toxin, which mediates neuroselective binding, internalization, and intraneuronal sorting, is not included in the UAS::TNT construct (Sweeney et al., 1995). Promoter::GAL4 driven TNT has since been used in numerous *Drosophila* studies that demonstrate it to be extremely effective at eliminating neurotransmission. For example, Heimbeck and others (1999) drove TNT expression in the dorsal ganglion to demonstrate the role of the dorsal organ as the primary site of larval olfaction, completely abolishing larval response to several strong odorants. Suster and others drove TNT expression in central and peripheral neurons and identified discrete subsets of neurons that are involved with larval locomotion (Suster et al., 2003). Thorne and others drove TNT expression with gustatory receptor gene promoters and determined the taste modalities of two small subsets of labellar neurons in adults (Thorne et al., 2004). Yang and Kunes used TNT expression to help demonstrate that axon guidance in the development of the adult visual system requires non-vesicular release of acetylcholine (Yang and Kunes, 2004). TNT

expression in the developing photoreceptor neurons did not cause axonal pathfinding defects.

A second tool was utilized to examine the function of cGMP in the cells that express Gyc-89Da and Gyc-89Db. Recently, a cDNA encoding the bovine PDE5, a cGMP-specific phosphodiesterase, was inserted into a UAS vector and introduced to *Drosophila*, resulting in a functional UAS::bovine PDE5 line. Expression of PDE5, using a tubulin-specific GAL4 driver line, was shown to be effective at reducing the concentration of cGMP in tubules and produced a robust renal phenotype (Broderick et al., 2004). I have acquired two of these UAS::PDE5 insertion lines for use in my experiments.

This chapter focuses on and describes a number of interesting defects associated with the expression of TNT and PDE5 in the cells that express Gyc-89Da and Gyc-89Db. Importantly, the role of the Gyc-89Da-expressing neurons and cGMP in larval oxygen sensation and the hypoxia-fleeing response was determined. Line 17991 (Gyc-89Da P-element insertion) was also examined for defects.

## **Methods**

### **Fly strains and genetics**

The following strains were used: UAS::TNT active (line 1171, acquired from S. Sweeney), UAS::TNT inactive (line 1178, inactive TNT has two histidine to valine mutations, acquired from S. Sweeney), UAS::bovinePDE5 (a 2<sup>nd</sup> chromosome insertion line and a 3<sup>rd</sup> chromosome insertion line, acquired from S. Davies), p89Da::GAL4 (several individual insertion lines), p89Db::GAL4 (several individual insertion lines), line

17991 (Bloomington Stock Center), the 17991 PiggyBac insertion parental line (w[1118]), and line 7019 (UAS::GAL80). All crosses were carried out using standard methods at 25° C (Greenspan, 1997).

### **Determination of Gyc-89Da expression in line 17991**

RT-PCR was used to amplify Gyc-89Da and Gyc-89Db transcript products from homozygous PiggyBac insertion line 17991 and wild type Canton-S larval total RNA samples. Total RNA collection, reverse transcriptase reactions, and PCR (conditions) were carried out as described in the Chapter 2 methods (RT-PCR cloning of Gyc-88E and Gyc-89Da). To ensure that the RT-PCR products originate from mRNA and not genomic DNA, primers were designed that would amplify across the large intron separating the 1<sup>st</sup> and 2<sup>nd</sup> exons of both genes. As in the RT-PCR experiments carried out in Chapter 2, two rounds of PCR were required to obtain an observable product. For Gyc-89Da the outer set of primers used for the 1<sup>st</sup> round of PCR were: 5'-CGAACTCAAAGAGCACGG -3' and 5'-AAGTCCTGTTTAACCGTTAT -3'. The inner primers used for the second round of PCR were: 5' -CATCACTCCTGCAAGGAAT -3' and 5' -GCATTGGAACAAGTCCAT- 3'. The product amplified using these primers was ~1 kb in length and included most of the known UTR and the first third of the ORF. The genomic DNA product obtained with these primers was ~2kb in length (included the intron). For the amplification of Gyc-89Db, the same set of primers was used in both rounds of PCR. The primer set used was: 5' -TACCCCGACTTTACGCAT- 3' and 5' -GATGGGGCAGGATGTGAA -3'. The ~400 bp product amplified using these primers included mostly the UTR of Gyc-89Db.

### **Mortality/viability analyses**

The mortality of developing animals expressing the active or inactive forms of TNT or PDE5 was examined. Line 17991 was also examined. To determine the hatching success rate, flies were allowed to lay eggs on standard fruit plates (Sullivan, 2000) overnight at 25° C. Embryos were collected and arranged in rows on a new fruit plate and allowed to hatch for 36 hours at 25° C. Hatched and unhatched embryos were then counted. To examine the survival of 1<sup>st</sup> instar larvae to the end of the third instar stage and into the pupal stage, a known number of 1<sup>st</sup> instar larvae were placed in a standard cornmeal-agar-molasses food vial or on a custom food disc in a plastic 8.5cm Petri dish, with a few granules of Fleischmann's dried yeast (St. Louis, MO, USA). The food disc was prepared by re-melting the standard food in a flask, and pouring it onto a large plate of glass. Spacers were placed on the glass, and a second glass plate was pressed down, resulting in a 3mm thick sheet of food that was allowed to cool and solidify. Discs were then cut out of the food sheet using a medium Petri dish cover, resulting in 5.6 cm diameter food discs. Larvae placed in vials or on discs were allowed to mature at 25° C until pupariation, or about 5 days. Dead larvae and pupae were then counted, being sure to carefully pick through the food for dead larvae. The instar stage and location of larval death was recorded. To examine defects during eclosion, 7-day-old pupal animals were collected from vials and lined up on a strip of double-sided clear tape on a glass slide. Just prior to eclosion, single animals were closely observed and any eclosion defects were recorded and photographed with an Optronics MicroFire Digital Microscope Camera (Goleta, CA, USA) on an Olympus SZH binocular dissecting scope (Olympus America

Inc., Melville, NY, USA), using Optronics PictureFrame 2.2 image capture software. To determine the rate of eclosion, a known number of similarly staged pupae in vials were allowed to eclose, and the number of eclosed animals were counted. If pupae failed during development, the stage (according to Bainbridge and Bownes, 1981) of death was recorded. Images of the mouthparts and trachea of 1<sup>st</sup> instar larvae were captured on Nikon Eclipse E800 microscope using an Optronics Magnafire digital camera. 1<sup>st</sup> instar larvae were first mounted whole on standard slides in an 80% glycerol/20%PBS mounting solution.

### **Observation of pre-eclosion markers and eclosion defects**

p89Da::GAL4/ UAS::TNT (active), p89Da::GAL4/ UAS::TNT (inactive) animal, or homozygous p89Da::GAL4 animals were collected from vials at stage P15 and stuck to a glass slide in rows with double-sided sticky tape. The operculum was manually removed from each pupa with forceps. Observations of pre-eclosion markers, as described by Kimura and Truman (1990), were observed through an Olympus SZH binocular dissecting scope and a high power fiber optic light source. At least 15 experimental and control animals from three separate crosses were examined for pre-eclosion defects. Eclosion events were captured with an Optronics MicroFire Digital Microscope Camera on an Olympus SZH binocular dissecting scope, using PictureFrame 2.2 image capture software.

### **Hypoxia fleeing assays**

A modified version of the hypoxia escape behavioral assay reported by Wingrove and O'Farrell (1999) was used to determine if experimental animals responded to hypoxic conditions. A 1.5 cm diameter dollop of yeast paste (block form bakers yeast (New Seasons Market, Portland, OR, USA) thinned to a toothpaste-like consistency (with purified water) was placed on each side of a bare "T"-style Petri dish (round dish separated into two halves by a wall)(BD Biosciences, San Diego, CA, USA). Five mid-sized feeding 3<sup>rd</sup> instar experimental larvae (~100 hours old) were collected from non-crowded vials raised at 25° C, rinsed in purified water, and placed on top of each yeast dollop, with one side reserved for control larvae. Larvae were left for about three minutes to settle and burrow headlong into the yeast dollop before starting the assay. Larvae that wandered or failed to burrow after three minutes were removed and replaced. To prepare hypoxic test environments, a Plexiglas glove box (35cm X 17cm X 17cm) was used which was outfitted with a sliding top access panel, a gas input valve on one side, and a 7mm gas exit valve on the opposite side. The exit valve was fitted with an Ohmeda 5120 oxygen monitor (BOC Edwards, Santa Clara, CA, USA). Nitrogen (Airgas, Inc., Portland, OR, USA), or a controlled mixture of nitrogen (Airgas, Inc.) and oxygen was pumped into the glove box (first bubbled through a flask of water) until the desired oxygen concentration was reached (1%, 5%, or 10% oxygen). The nitrogen/oxygen mixture was controlled with two Gilmont shielded laboratory flow meters (Cole-Parmer Instrument Company, Vernon Hills, IL, USA). The prepared, uncovered Petri dish with burrowed larvae was then placed in the prepared glove box. Behavioral responses were then observed and recorded every minute for 5 minutes. Fleeing behavior was defined as any exploratory locomotion behavior, whether it was on the yeast dollop or off. Once



larvae backed out of yeast and began exploratory locomotion, re-burrowing was rarely observed.

### **GAL80<sup>TS</sup> experiments**

GAL80<sup>TS</sup> (temperature-sensitive) expression (see Zeidler et al., 2004) was used to control temporal expression of TNT in some experiments. Using standard crossing schemes (Greenspan, 1997), a homozygous fly line was created that contained the tubulin promoter (tubP)::GAL80<sup>TS</sup> insertion from Bloomington Stock Center line 7019 on chromosome 2 and the p89Da::GAL4 insertion on chromosome 3. tubP::GAL80<sup>TS</sup>;p89Da::GAL4 flies were then crossed with UAS::TNT (active) or UAS::TNT (inactive) flies, or UAS::DsRed flies, resulting in offspring that contained all three constructs, with the genotype tubP::GAL80<sup>TS</sup> /+; p89Da::GAL4/UAS::TNT or tubP::GAL80<sup>TS</sup> /+; p89Da::GAL4/UAS::DsRed. These crosses were carried out at 18° C, the permissive temperature for GAL80<sup>TS</sup>. At 18° C, GAL80<sup>TS</sup> inhibits the action of GAL4. Experimental vials, as described in the results, were switched at specific stages to an incubator set at 29° C, the non-permissive temperature for GAL80<sup>TS</sup> (Zeidler et al., 2004) that allows GAL4 to function and activate transcription of UAS controlled transgenes.

### **Locomotory experiments**

Locomotory tests were carried out on TNT (active and inactive)-expressing feeding 3<sup>rd</sup> instar larvae. For each experimental condition, 6 larvae collected from two separate crosses were placed on an 8.5cm Petri dish that had been filled with a 0.5cm thick layer of 1% agarose. A plastic dish cover was placed on the Petri dish, and larvae were allowed to travel for about 5 minutes. The paths of each larva were traced with a

marker on the dish cover, which was then digitally photographed. The distance that each larva traveled, indicated by the length of the marker path, was determined using the measure function on the ImageJ software (Wayne Rasband, NIH, USA).

## Results

### Characterization of *Gyc-89Da* and *Gyc-89Db* expression in line 17991

The release of the Exelixis PiggyBac insertion collection offered *Drosophila* researchers new opportunities to study the function of genes that had not yet been hit by P-elements. This collection, combined with the existing P-element insertion lines, brought the total number of potential gene knockouts up to more than 50% of the 13,666 predicted *Drosophila* genes. Roughly consistent with this coverage, one of the three atypical sGC genes was found to contain an insertion. Line 17991 contains a RB-type PiggyBac element, which features splice acceptor trap sites in both orientations, which aid in transcript disruption by accepting splices from an upstream exons (Thibault et al., 2004). The insertion, as mapped by Exelixis transposon project, is located near the middle of the intron lying between the first and second exons (see Fig. 2.1). The 10 kb RB PiggyBac element is in an ideal location to disrupt the *Gyc-89Da* transcript by accepting a splice from the first exon, and/or by simply creating too much distance between the first and second exons for efficient splicing. To determine the effect of the PiggyBac insertion on expression of *Gyc-89Da*, I used a standard RT-PCR method to look for the presence of transcript in homozygous and heterozygous PiggyBac insertion larvae (Fig. 4.1). *Gyc-89Da* transcript appeared to be completely eliminated, while the *Gyc-89db* transcript was retained, suggesting that line 17991 is indeed a specific *Gyc-*

89Da knockout line. A genomic DNA contamination amplification band does not appear in the 17991 sample lanes because the 10kb RB PiggyBac insertion increases the size of the gene region, making it too long to amplify under the conditions used here.

Examination of the mortality rates during the life cycle and the general morphology and behaviors of these homozygous PiggyBac insertion animals revealed no obvious defects resulting from the lack of the Gyc-89Da transcript (data not shown).

### **Examination of the functional role of neurons that express Gyc-89Da during development**

To examine the effects of blocking synaptic transmission in neurons that express Gyc-89Da and Gyc-89Db, I crossed p89Da::GAL4 and p89Db::GAL4 flies with the UAS::TNT (active) or the UAS::TNT (inactive) flies. The mutationally inactive version of the tetanus light chain toxin was used for control experiments (Sweeney et al., 1995). Each of these crosses was examined for developmental or behavioral defects throughout the life cycle. As shown in Figure 4.2, animals that expressed p89Da::GAL4- and p89Db::GAL4-driven TNT (active) displayed defects that led to a significant level of death at either the larval stages or at adult ecdysis (eclosion).

p89Da::GAL4, UAS::TNT (active) embryos displayed a reduced rate of hatching (84% hatching) compared to the cross with control embryos (p89Da::GAL4, UAS::TNT inactive) (93% hatching), but this difference was not statistically significant (Fig. 4.2A). However, a significant percentage of the hatched p89Da::GAL4, UAS::TNT (active) animals died during the 1<sup>st</sup> and 2<sup>nd</sup> larval instar stages in food vials (Fig. 4.2A).

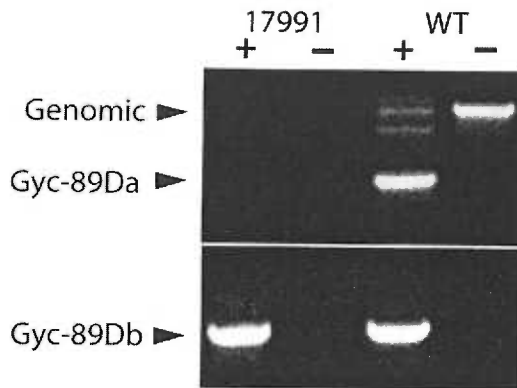


**Figure 4.1.** The RB PiggyBac insertion in line 17991 eliminated the Gyc-89Da transcript in larvae. “+” indicates the addition of reverse transcriptase to the reaction while “-” indicates no reverse transcriptase was added. The first two lanes were loaded with RT-PCR product from homozygous line 17991 larval samples and the last two lanes were loaded with RT-PCR product from wild type Canton-S larval samples. Purified RNA often retains some genomic DNA, and a larger band that represents unspliced gene product appeared in the WT lanes. The insertion of the PiggyBac element in line 17991 prevents the amplification of this genomic product. Gyc-89Db transcript was successfully amplified from the same RT reactions (bottom gel portion). These experiments were repeated 2 more times with new RNA samples, with the same results.

Most larval death occurred in the late 3<sup>rd</sup> instar, where only about 50% of the surviving p89Da::GAL4, UAS::TNT (active) 3<sup>rd</sup> instar larvae reached pupal stages, compared to high success rate of control animals. The vast majority (>90%) of dead 1<sup>st</sup>, 2<sup>nd</sup>, and 3<sup>rd</sup> instar larvae were found buried at various depths in the food, without any tunnels to connect them with the atmosphere (Fig. 4.3A). Wild type burrowing larvae normally leave behind a tunnel, enabling constant access to fresh air while feeding. Many dead 3<sup>rd</sup> instar larvae were even found at the very bottom of the vials (~3.5cm below the surface). Larvae were observed moving and feeding through the food, without tunnels, for up to 20 minutes before the cessation of movement and apparent death. Upon close examination, all dead larvae appear structurally intact, including the interior organ structures (data not shown). It seems likely that these larvae died of suffocation, lacking any contact with the atmosphere. Most of the 3<sup>rd</sup> instar larvae found buried were at the maximal larval size (>5mm long), indicating that they may have entered the wandering phase before death.

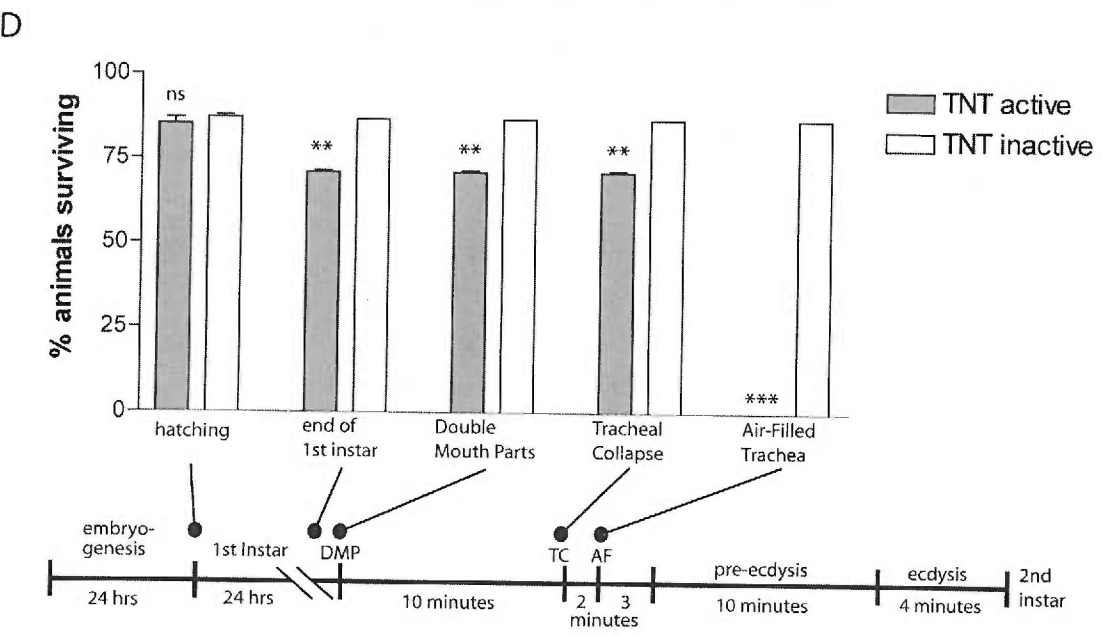
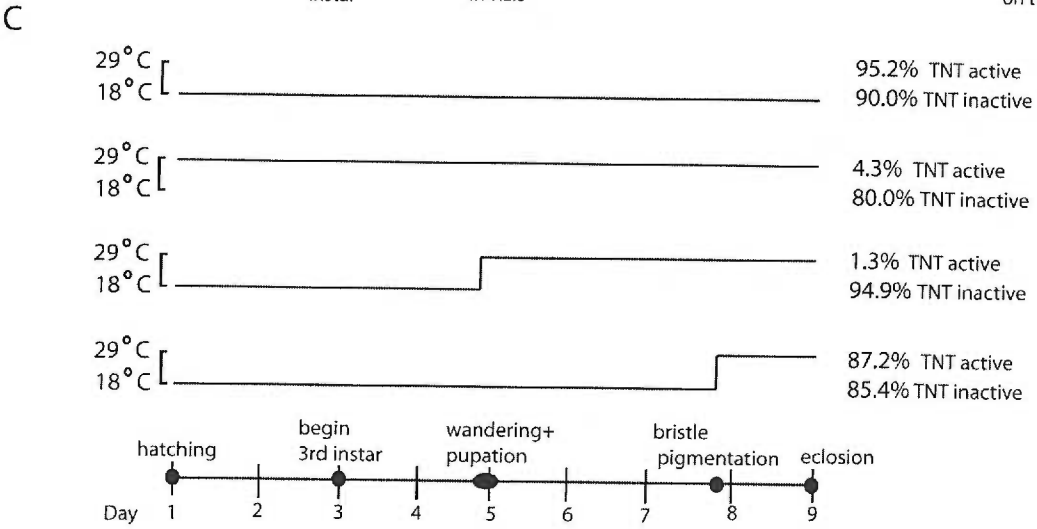
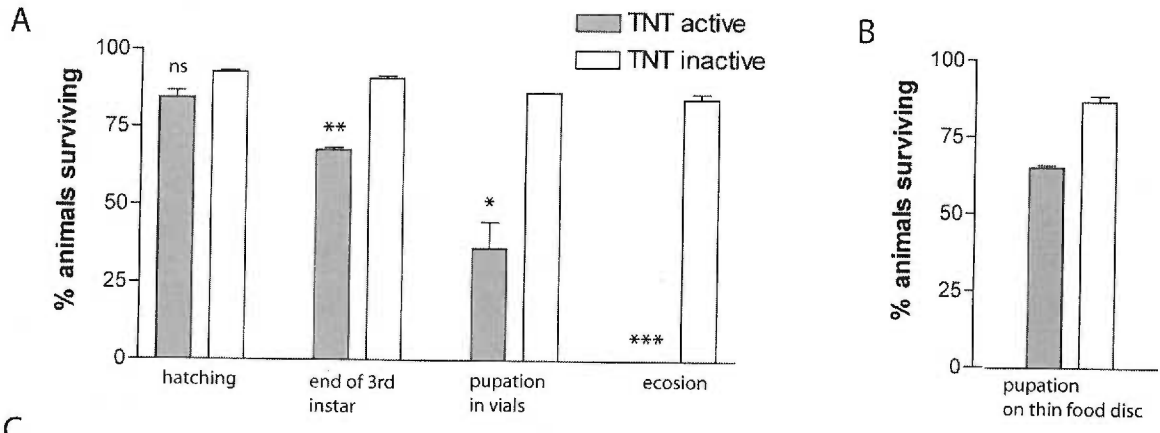
p89Da::GAL4, UAS::TNT (active) larvae described above appeared morphological normal, but displayed a “jackhammer”-like motion of the mouthparts, which was most extreme in the 3<sup>rd</sup> instar larvae. These larvae displayed the normal overall scooping motion with the mouth hooks, but as they did so, the mouthparts shivered or vibrated rapidly in an anterior-posterior direction. This “jackhammer”-like motion did not appear to inhibit feeding however, and most larvae achieved a normal maximal size and length, which was comparable to the control larvae at the equivalent stage (data not shown). No shaking motions were observed in other regions of the body, and locomotion appeared normal. The developmental time of the TNT-expressing

animals, from embryos to wandering 3<sup>rd</sup> instar larvae, was normal and comparable to control animals (data not shown).

It appeared that many p89Da::GAL4, UAS::TNT (active) larvae died, possibly from suffocation, by burying themselves without tunnels deep within anaerobic regions of the food. To further examine this defect, I designed a food arrangement that would prevent larvae from burrowing into an anaerobic environment. Instead of the standard food vials, p89Da::GAL4, UAS::TNT (active) 1<sup>st</sup> instar larvae were raised on a 3mm thick disc of food that was placed in a larger Petri dish (Fig 4.3F). These larvae burrowed into and extensively aerated the food disc (Fig. 4.3G). Before forming pupae, most (>90%) larvae wandered away from the food disc. This food arrangement completely rescued larval death and all larvae surviving to the end of the third instar successfully formed pupae (Fig. 4.2B, compare to “end of third instar” bars in Fig. 4.2A). These results support the hypothesis that the death of p89Da::GAL4, UAS::TNT (active) larvae in food vials was associated with their deep, anaerobic burial location.

The second period of mortality for p89Da::GAL4, UAS::TNT (active) larvae occurred during the pupal stage. Of the animals that survived the larval stages in food vials and of the larvae raised on food discs, over 90% proceeded to the very end of the pupal phase (stage P15) (data not shown in figure), but impressively, more than 99% of these pupae failed to eclose (Fig. 4.2A). Structurally, these animals appeared fully formed and intact, closely resembling similarly staged control pupae (data not shown).

**Figure 4.2.** Survival of animals during development in promoter driven tetanus toxin light chain experiments. Synaptic transmission was blocked in all neurons that express Gyc-89Da or Gyc-89Db by crossing the respective promoter::GAL4 line with UAS::TNT (active) flies, or with UAS::TNT (inactive) flies as the control. Survival of animals from embryogenesis through several defined stages of development is indicated in percent. **(A)** Survival of p89Da::GAL4, UAS::TNT animals through development to eclosion. The percentage of p89Da::GAL4, UAS::TNT animals that died in the embryonic stage (before hatching) was not significantly different from the control. A significant percentage of the p89Da::GAL4, UAS::TNT animals did die during the larval stages, and only about half of the surviving larvae successfully reached the pupal stages. Less than 1% of the p89Da::GAL4, UAS::TNT pupae successfully eclosed and emerged into adulthood. **(B)** If p89Da::GAL4, UAS::TNT animals were raised on thin food discs instead of in vials, all larvae that survived to the “end of the third instar” stage successfully reached the pupal stage. The percentage of larvae reaching the pupal stage in (B) is not significantly different compared to the percentage of larvae at the “end of 3<sup>rd</sup> instar” stage in (A). **(C)** Results of the GAL80<sup>TS</sup> experiment. tubP::GAL80<sup>TS</sup>; p89Da::GAL4/ UAS::TNT animals were raised at a constant 18°C, 29°C, or raised at 18°C then switched to 29°C at the stages indicated in the accompanying time line. The percentage of animals that successfully eclosed in each of the treatments is indicated at the right. **(D)** Survival of p89Db::GAL4, UAS::TNT animals during the 1<sup>st</sup> instar stage. The accompanying time line indicates major developmental events and data points examined in the graph (DMP= double mouth parts, TC= tracheal collapse, AF= air-filled trachea). All p89Db::GAL4, UAS::TNT (active) larvae die before reaching the 2<sup>nd</sup> instar. A small but significant percentage of p89Da::GAL4, UAS::TNT (active) larvae die during the feeding phase of the 1<sup>st</sup> instar (compared to the control), and all the surviving larvae die just before ecdysis, with fluid filled, collapsed inner trachea. Time line in (D) based on observations reported in Park et al. (2002). The p89Da::GAL4 experiments represent 3-4 trials using 3 independent insertion lines. A total of at least 380 animals were counted for each comparison. The tubP:: GAL80<sup>TS</sup>; p89Da::GAL4, UAS::TNT results represent a preliminary experiment, with each value representing one experimental cross and an average of 50 counted animals. The p89Db::GAL4 experiments represent 3-4 trials using 2 independent insertion lines. A total of at least 200 animals were counted for each comparison. Percent values are averages  $\pm$ S.E.M. The experimental and control groups were compared statistically using paired t-tests. NS = not significant, \* indicates P<0.05, \*\* indicates P<0.01, \*\*\* indicates P<0.001. Statistics were not applied to the GAL80<sup>TS</sup> experiment.





It is possible that TNT (active) expression interfered with a neuronal function that was required for initiation of the eclosion motor program. Alternatively, it is possible that TNT (active) expression caused a subtle developmental defect well before eclosion that resulted in the failure of eclosion machinery several days later. To examine these possibilities, I utilized the recently developed temperature-sensitive GAL80 system to control the temporal expression of TNT. The yeast GAL80 protein blocks GAL4 activity by binding to its transcriptional activation domain, a function that is retained when expressed in *Drosophila* (Yocum and Johnston, 1984; Zeidler et al., 2004). Enhancer-driven GAL80 has been used to effectively restrict expression patterns of GAL4 to small subsets of cells in *Drosophila* (Suster et al., 2004). A temperature-sensitive version of GAL80 (GAL80<sup>TS</sup>) was created by inserting a temperature-controlled yeast intein into a crucial region of the GAL80 peptide. Inteins have been described as “protein introns” and function post-translationally to autonomously and cleanly splice themselves from a host protein. A fly line was generated that contained the functional GAL80<sup>TS</sup>, driven by the ubiquitous tubulin promoter (tubP::GAL80<sup>TS</sup>) (Mcguire et al., 2003). At 18°, the permissive temperature, the intein splices itself out of GAL80<sup>TS</sup>, resulting in functional GAL80, which can then bind to and inhibit GAL4 action. At 29° C, the non-permissive temperature, the disruptive intein in GAL80<sup>TS</sup> is inactive and remains in the translated GAL80<sup>TS</sup>, allowing GAL4 activation of UAS controlled transgenes. I generated a homozygous fly line that contained both tubP::GAL80<sup>TS</sup> and p89Da::GAL4. First, to test the effectiveness of GAL80 in blocking UAS controlled transgene expression, I crossed tubP::GAL80<sup>TS</sup>; p89Da::GAL4 flies to UAS::DsRed flies and raised the offspring at either the permissive temperature (18° C) or the non-permissive temperature (29° C). The

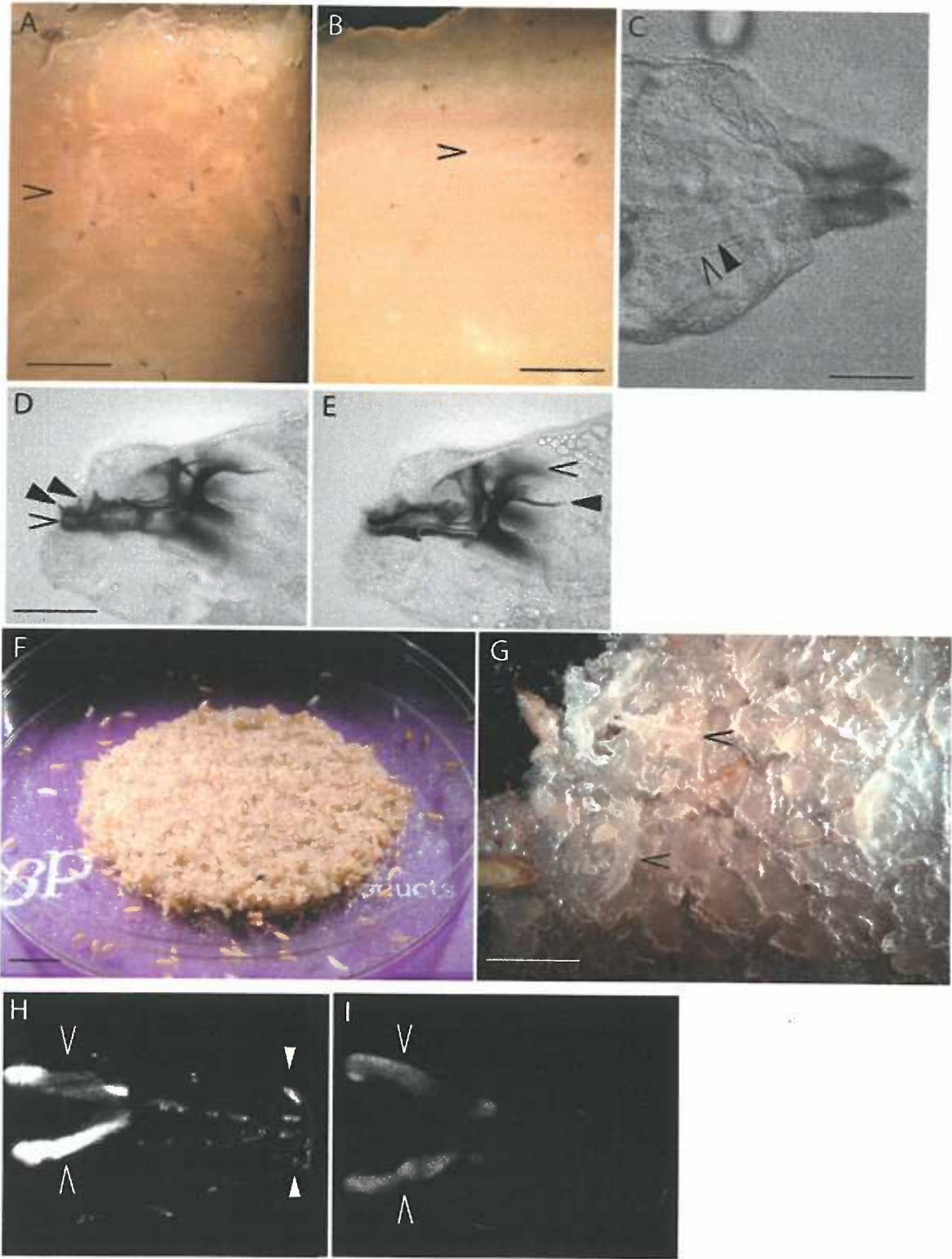
larvae raised at 29° C displayed robust DsRed expression, demonstrating that GAL80<sup>TS</sup> was not functional at the temperature (Fig. 4.3H). Larvae raised at 18° C displayed no DsRed expression in the CNS or PNS, but did retain some expression in the salivary glands, indicating that GAL80<sup>TS</sup> function was mostly inhibited at this temperature (Fig. 4.3I). This experiment confirmed the genotype of the tubP::GAL80<sup>TS</sup>; p89Da::GAL4 flies, and demonstrated the effectiveness of the GAL80<sup>TS</sup> system. Next, in a preliminary experiment, I crossed these flies to either UAS::TNT (active) or UAS::TNT (inactive), setting up three staged sets of vials at the permissive temperature (18° C) and one staged set of vials at the non-permissive temperature (29°). One set of vials raised at 18° C was switched to a 29° C incubator when larvae began the wandering stage, and another set was switched to the 29° C incubator ~30 hours before eclosion (pupal stage P10). The third set of vials raised at 18° C was kept at this temperature for the duration of the experiments. At P10, all adult structures have formed, the eyes are colored, and the bristles have begun to darken. The flies raised and kept at 18° C from both the TNT (active) and TNT control (inactive) crosses eclosed with a high success rate (Fig. 4.2C), indicating that GAL80<sup>TS</sup> inhibited GAL4 as expected. tubP:: GAL80<sup>TS</sup>; p89Da::GAL4/ UAS::TNT (active) flies that were raised at 29° C or switched to 29° C from 18° C at larval wandering displayed a very low eclosion rate, while the control flies displayed a high rate of eclosion (Fig. 4.2C). However, tubP:: GAL80<sup>TS</sup>; p89Da::GAL4/ UAS::TNT (active) flies that were switched to 29° C from 18° C at pupal stage P10 (bristle pigmentation becomes visible) displayed an eclosion rate similar to the control flies. These results indicate that the neuronal function of the Gyc-89Da-expressing cells is not required just prior to eclosion, but instead during the development of the animal in pupal

stages prior to P10. It is possible that TNT-expression caused axonal guidance or synaptic defects in circuits during adult CNS development that are important for initiation of eclosion. Alternatively, important neuropeptide or hormone release events during earlier adult development may have been blocked, leading to defects in the later peptidergic events that initiate pre-eclosion or eclosion motor program events. It is also possible that the functional GAL80 generated during the 18° C incubation period was not efficiently turned over when vials were switched to 29° C for the last 30 hours of development. This residual functional GAL80 may have kept GAL4 bound and inhibited long enough to allow the Gyc-89Da-expressing neurons to complete their function in the eclosion program. However, Zeidler and others (2004) found that relief of GAL80 inhibition and robust GAL4 activation of UAS controlled transgene expression was achieved in wing discs 30-40 hours after animals were switched to the non-permissive temperature from the permissive temperature.

#### **Examination of the functional role of neurons that express Gyc-89Db in larvae**

p89Db::GAL4, UAS::TNT (active) larvae were dramatically affected by toxin expression at an early age. p89Db::GAL4, UAS::TNT (active) embryos hatched a similar rate as the corresponding control embryos (Fig. 4.2D). Newly hatched TNT (active)-expressing larvae appeared morphological normal, but many became increasingly sluggish after a day of surface feeding. All of these larvae failed to reach the 2<sup>nd</sup> larval instar (Fig. 4.2D). About 70% of the hatched p89Db::GAL4, UAS::TNT (active) animals survived past the feeding phase to the period just before ecdysis, significantly less than the control animals.

**Figure 4.3.** Defects and other observations associated with p89Da::GAL4 and p89Db::GAL4 driven TNT expression in larvae. (A) Many p89Da::GAL4, UAS::TNT (active) 3<sup>rd</sup> instar larvae (open arrowhead indicates one larva) were found buried deep under the food, in the absence of burrowing tunnels. The surface of the food is at the top. (B) Some p89Db::GAL4, UAS::TNT (active) 1<sup>st</sup> instar larvae (open arrowhead indicates one larva) were also found buried under the food in the absence of burrowing tunnels. The surface of the food is at the top. (C) Posterior end of a p89Db::GAL4, UAS::TNT (active) 1<sup>st</sup> instar larva that died just prior to ecdysis with double mouth parts (DMP) and double trachea. The fluid-filled double trachea appear transparent, although it was possible to observe the two main tracheal branches that lead to the spiracular openings. The new, outer trachea is indicated with an open arrowhead and the old, inner tracheal lining is indicated with a closed arrowhead. (D) Anterior end of a p89Db::GAL4, UAS::TNT (active) 1<sup>st</sup> instar larva, showing the presence of double mouth hooks. Open arrowhead indicates the larger, new set of hooks and the closed arrowheads indicate the smaller, old set of hooks. (E) A different focal plane of the animal shown in (D), showing the double vertical plates. Open arrowhead indicates one of the new, larger plates and closed arrowhead indicates one of the old, smaller plates. (F) Image of the custom thin food disc in Petri dish setup used to rescue the p89Da::GAL4, UAS::TNT (active) burial death defect. The experiment shown is about halfway to completion, with 3<sup>rd</sup> instar larvae that are still feeding and some that have already wandered and pupated. Note the highly tunneled food disc. (G) Bottom of the food disc/Petri dish shown in (D), showing more closely the highly tunneled and aerated food. Open arrowheads indicate feeding 3<sup>rd</sup> instar larvae. (H) Example of a tubP::GAL80; p89Da::GAL4/ UAS::DsRed 2<sup>nd</sup> instar larva that was raised at 29° C, the non-permissive GAL80<sup>TS</sup> temperature, which allows for GAL4 activation of UAS controlled transgene expression. Expression of DsRed at 29° C is robust, comparable to what was found in p89Da::GAL4/ UAS::DsRed larvae. Open arrowheads indicate the salivary glands (always the brightest tissues) and closed arrowheads indicate the terminal and dorsal ganglia. (I) Example of a tubP:: GAL80<sup>TS</sup>; p89Da::GAL4/ UAS::DsRed 2<sup>nd</sup> instar larva that was raised at 18° C, the permissive GAL80<sup>TS</sup> temperature, which allows GAL80<sup>TS</sup> to inhibit GAL4 action on UAS targets. DsRed expression was strongly reduced in the salivary glands (open arrowheads), and was absent in all neurons, including the dorsal and terminal ganglia. Scale bar= (A) 5mm, (B) 1mm, (C and D) 50 µm, (F) 10mm, (G) 5mm.



Of the 16% of larvae that died during the feeding phase, most were found buried under the food without tunnels (63% buried vs. 37% on top) (Fig. 4.3B, not shown in Fig. 4.2), similar to what was observed with the p89Da::GAL4, UAS::TNT (active) animals raised in vials. This is surprising because 1<sup>st</sup> instar larvae do not normally even burrow, preferring to feed on top of the food. Over 99% of the p89Db::GAL4, UAS::TNT (active) larvae that survived past the 1<sup>st</sup> instar feeding phase died with transparent fluid-filled double trachea and double mouthparts (DMP) (Fig. 4.2D and Fig 4.3C, D and E). The appearance of the pigmentation of the second, larger set of mouth hooks and associated vertical plates (as a whole called double mouth parts or DMP) is one of the first signs of an impending ecdysis event (Clark et al., 2004; Park et al., 2002). About 10 minutes following the appearance of DMP, the old tracheal structures collapse (tracheal collapse or TC), leaving behind space-filling molting fluid that separates the degraded, collapsed trachea from the new, larger trachea. The trachea at this time appear optically transparent due to the presence of molting fluid. Shortly after this, the fluid is apparently reabsorbed, and the intertracheal space fills with air (air filling or AF). Only after these events occur does pre-ecdysis and ecdysis behavior proceed (Clark et al., 2004). From the time of inner tracheal collapse to the filling of the intertracheal space with air, gas exchange in tracheols is presumed to be blocked by the presence of molting fluid in the trachea. During this time, animals likely experience a period of internal hypoxia. The larvae found with DMP and transparent, fluid filled trachea likely died from suffocation and failure to initiate ecdysis.

### **Further characterization of eclosion defect in p89Da::GAL4/UAS::TNT animals**

To more precisely characterize the eclosion defect observed in p89Da::GAL4, UAS::TNT animals, late pupae (< 8 hours to eclosion) were lined up on slides and observed closely for the appearance of previously identified pre-eclosion event markers (Kimura and Truman, 1990). The operculums were removed from the pupae to facilitate the view of markers. Kimura and Truman described 6 marker stages that occur in order before the start of eclosion. The first stage is called Smooth, which occurs ~8 hours prior to eclosion and is characterized by a smooth head surface, which indicates that the molting fluid is still present between the pupal and adult cuticle. The Smooth/Grainy stage occurs ~6 prior to eclosion, and is characterized by wrinkles in the pupal cuticle, which indicates that molting fluid absorption has begun. The Grainy stage occurs 3 hours prior to eclosion, and is characterized by a grainy head surface, which indicates that molting fluid absorption is complete. The Grainy/White stage occurs ~60 minutes prior to eclosion, and is characterized by the appearance of white trachea between the eyes, which indicates that the tracheal system has filled with air. The White stage occurs ~50 minutes before eclosion, at which time the fly gains a whitish sheen because air has entered the space between the adult and pupal cuticle. About 40 minutes before eclosion, the ptilinum slowly protrudes from the front of the head and ruptures the thin pupal cuticle (extended-ptilinum or EP stage). All of these stages occurred in the proper order in both p89Da::GAL4, UAS::TNT (active) and p89Da::GAL4, UAS::TNT (inactive) animals (data not shown). Animals were also removed from the pupal cases at the Grainy/White stage and examined under a microscope to determine the extent of tracheal air filling throughout the body. The extent of tracheal air filling in p89Da::GAL4, UAS::TNT

(active) animals at this stage appeared normal and was comparable to equally staged control animals (data not shown).

These pupae were observed continuously beginning at the EP stage. Roughly 40 minutes after ptilinum extension, the p89Da::GAL4, UAS::TNT (inactive) control animals began inflating their heads and pushed forward, which serves to rupture and push open the operculum (if it was present) (Fig. 4.4A-D). After several strong head inflations occurring over 10-20 seconds, the p89Da::GAL4, UAS::TNT (inactive) control animals began the stereotyped abdominal, posteriorly directed peristalsis movements (eclosion behavior). These movements push the animal forward out of the pupal case (Fig. 4.4E and F), and with the help of the legs, the adult pulls itself completely out (Fig. 4.4G and H). The eclosion of these control animals is comparable to that of wild-type Canton-S animals (data not shown). It should be noted that the control shown in Figure 4.4 is actually a homozygous p89Da::GAL4 insertion line, which also displayed normal eclosion behavior and was chosen to be shown here for visual reasons (bright red eyes). The p89Da::GAL4/ UAS::TNT (active) animals also began head inflations about 40 minutes after ptilinum extension, but the magnitude of the inflations appeared much weaker (Fig. 4.4K-N). Indeed, these weaker head inflations rarely succeeded in completely opening the operculum, when it was left intact (data not shown). Several head inflation/deflations occurred and the animal did push forward noticeably, but the eclosion motor program was never initiated in these animals, and no abdominal peristalsis movements were observed at any time. Interestingly, head inflation/deflations occurred for at least 4 more hours. During this time, starting about an hour after the first head inflations, the antennae occasionally twitched, and the abdomen sporadically contracted



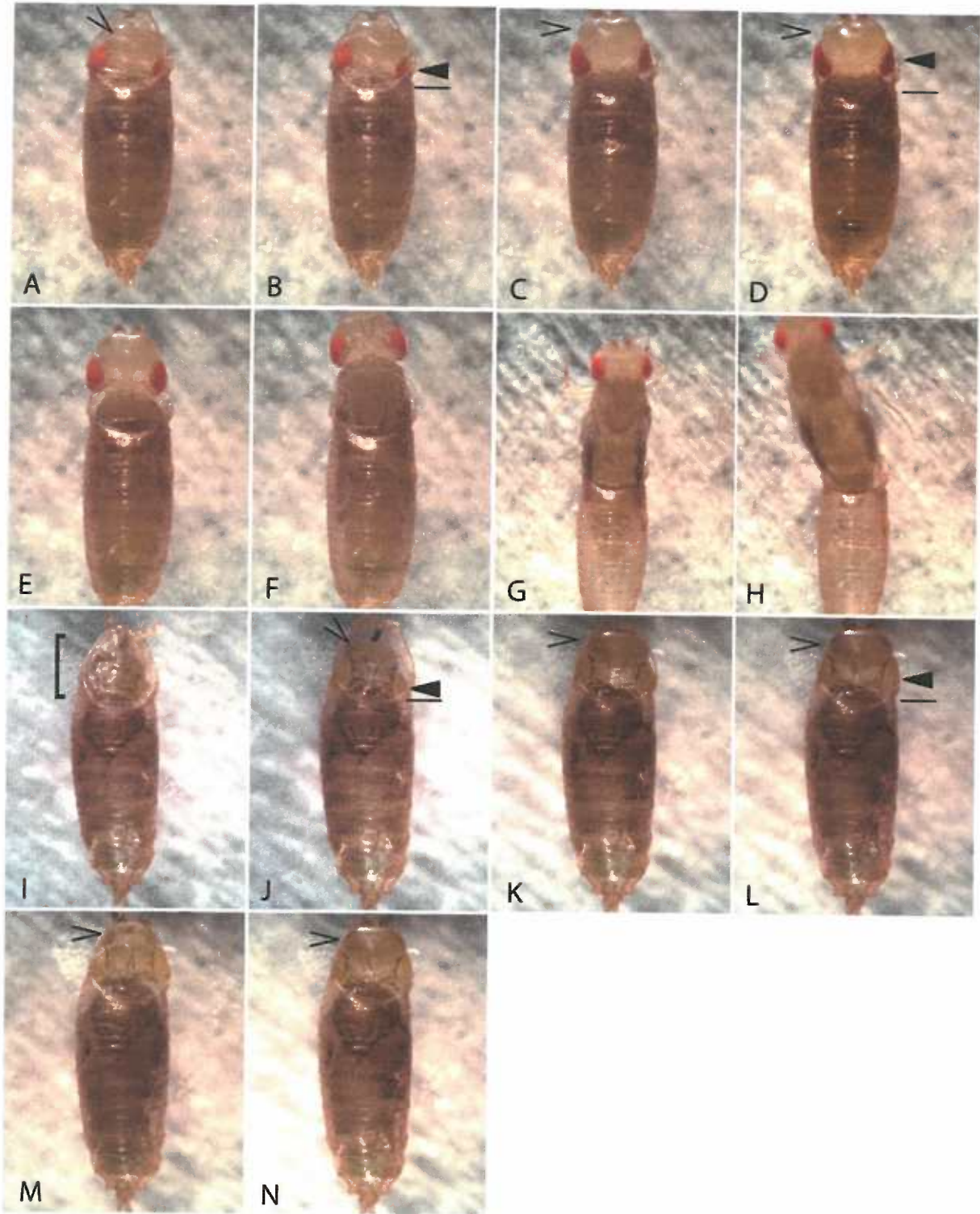
several times a minute, but these movements in no way resembled peristalsis. It appeared as though the animal was alive and functional, but was trapped in its pupal case. Manual removal of the operculum just prior to the start of eclosion always failed to rescue these animals.

### **Examination of hypoxia escape response in larvae expressing TNT or PDE5**

To examine the effects of reducing cGMP levels in the cells that express Gyc-89Da and Gyc-89Db, UAS::bovinePDE5 flies were crossed with p89Da::GAL4 and p89Db::GAL4 flies. Disappointingly, all macro-scale developmental and general behavioral aspects of these animals appeared to be normal (data not shown). Viability at all stages was comparable to that of the parental fly lines. However, sensory deficits and more subtle developmental defects would not have been obvious in these initial examinations.

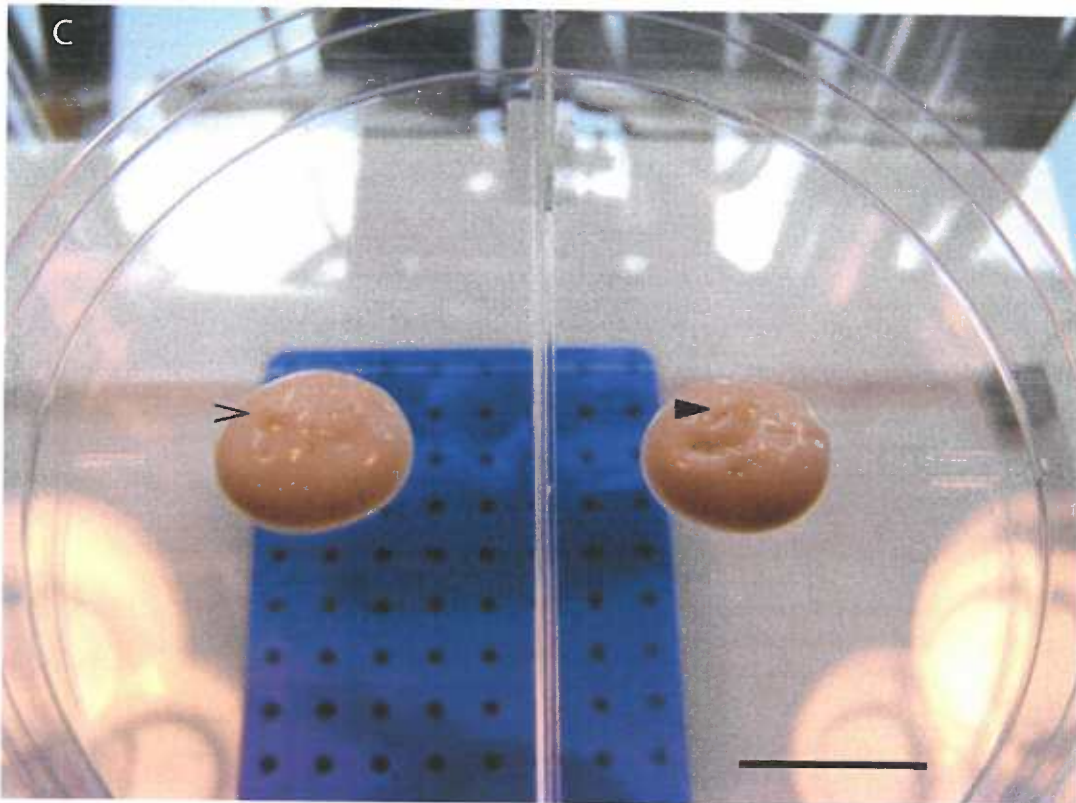
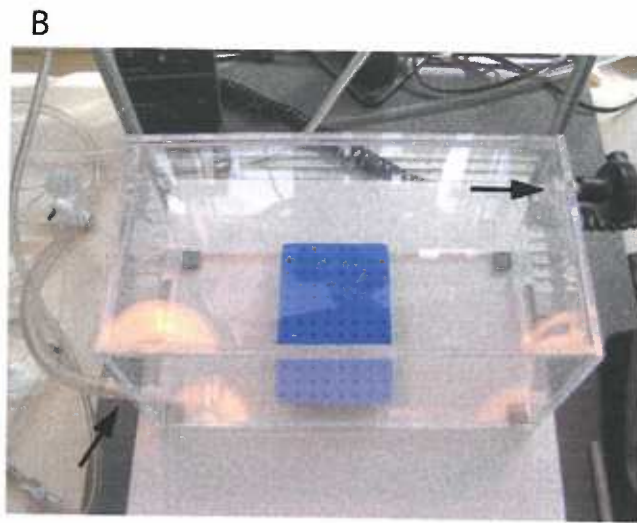
Many p89Da::GAL4/ UAS::TNT (active) and some p89Db::GAL4/ UAS::TNT (active) larvae perished deeply buried in their food, in the absence of tunnels and air. Thus, it is possible that these animals were defective in sensing hypoxic conditions, allowing themselves to remain in an airless environment until they died of suffocation. The expression of Gyc-88E, Gyc-89Da, and Gyc-89Db in neurons that innervate the dorsal organ, trachea, and putative olfactory sensilla on the thoracic segments and posterior sensory cones is consistent with a role in detecting environmental oxygen concentrations. To examine whether p89Da::GAL4, UAS::TNT (active) larvae can sense and respond to hypoxic conditions, these animals were subjected to a “hypoxia fleeing” assay.

**Figure 4.4.** Normal eclosion behavior of control animals and eclosion failure of p89Da::GAL4, UAS::TNT (active) animals. (A) A homozygous p89Da::GAL4 control animal during its 1<sup>st</sup> head inflation. Open arrowhead indicates the inflated region. (B) Control animal during its 2<sup>nd</sup> head inflation. The closed arrowhead and line indicates the distance between the back edge of the opercular opening and the middle of the eye. (C) Control animal during its third head inflation (open arrowhead). (D) Control animal during subsequent maximal head inflation (open arrowhead). At this point the animal has pushed forward. The closed arrowhead and line indicate the more anterior position of the head, compared to (B). (E) Eclosing control animal at the start of the coordinated abdominal peristalses, beginning to move forward. (F) Eclosing control animal with more forward progress. (G) Control animal has freed its legs, and is now pulling itself out of the pupal case. (H) Control animal exiting the pupal case. (I) p89Da::GAL4, UAS::TNT (active) animal after EP stage, but prior to eclosion, with the operculum still intact. (J) p89Da::GAL4/ UAS::TNT (active) animal at the same stage as (I), but with the operculum manually removed. Open arrowhead indicates the extended ptilinum. Closed arrowhead and line indicates distance of the back edge of the opercular opening from the middle of the eye. (K) p89Da::GAL4, UAS::TNT (active) animal during its 1<sup>st</sup> head inflation (open arrowhead). (L) p89Da::GAL4, UAS::TNT (active) animal during a maximal head inflation (open arrowhead), which was weak compared to (D). The closed arrowhead and line indicate the more anterior position of the head, compared to (J). (M) p89Da::GAL4, UAS::TNT (active) animal during a head deflation (open arrowhead). (N) p89Da::GAL4, UAS::TNT (active) animal during the subsequent inflation (open arrowhead), which was still weak. The above results were similar for all 15 p89Da::GAL4, UAS::TNT (active) animals examined closely for pre-eclosion defects.



When feeding third instar larvae are introduced to a penny-sized dollop of yeast paste on a grape-agarose plate, they will burrow into it and feed in a stationary vertical position (similar to what is observed in food vials), with only the very ends of their spiracles remaining exposed to the outside environment (Wingrove and O'Farrell, 1999). Upon exposure to a hypoxic environment (1% oxygen), larvae will quickly back out of the yeast and begin continuous exploration activity on the surface of the food and fruit plate (Wingrove and O'Farrell, 1999). For my "hypoxia fleeing" experiments, a plain I-style Petri dish (round dish bisected with a plastic wall) was used without fruit agarose. A dollop of yeast paste was placed on each side of the dish for the simultaneous comparison of an experimental population with a control population. A Plexiglas glove box was used to set up a 1%, 5%, or 10% oxygen environment, using a mixture of oxygen and nitrogen that was blended prior to being pumped into the glove box (Fig 4.5A and B). As reported by Wingrove and O'Farrell (1999), feeding 3<sup>rd</sup> instar larvae placed on a dollop of yeast paste burrowed into a stationary vertical feeding position, with only the very ends of the spiracular openings exposed to the outside environment (Fig 4.5C). Occasionally, p89Da::GAL4, UAS::TNT (active) larvae were observed to settle into a partially burrowed vertical feeding position, leaving 1 or 2mm of their posterior ends exposed (Fig 4.5C). Under normal atmospheric conditions, both TNT (active)- and TNT (inactive)-expressing, yeast-feeding larvae remained in the same vertical position for at least 20 minutes.

**Figure 4.5.** Equipment associated with the hypoxia fleeing assays and yeast dollop-Petri dish configuration. (A) Glove box and gas delivery system used for hypoxia fleeing assays. The nitrogen/oxygen mixture was controlled with two flow meters (attached to rack), then bubbled through a water filled flask before entering the left side of the Plexiglas glove box. (B) Close-up of the Plexiglas glove box. The gas input is visible on the lower left side and the gas output is visible on the upper right side. An oxygen meter sensor, which was used to set up and monitor the desired oxygen environment, was attached to the gas output valve (arrow). (C) An example of a prepared yeast dollop-Petri dish, with all larvae (5 per side) settled into a stationary vertical feeding position, in which only the very ends of the posterior spiracles are exposed. On the left side are the p89Da::GAL4/ UAS::TNT (active) larvae. Occasionally these larvae will leave 1 or 2mm of their posteriors exposed (open arrowhead), before the start of the assay. The positions of the other 4 larvae appear as small divots. On the right side are the control p89Da::GAL4, UAS::TNT (inactive) larvae, all of which have settled into the typical vertical feeding position. The location of one these larvae is indicated with an open arrowhead. Scale bar =1.5cm.



When yeast-feeding larvae were placed in a 1% oxygen environment, dramatic differences in behavior were observed between the p89Da::GAL4, UAS::TNT (active) and control p89Da::GAL4, UAS::TNT (inactive) animals (Fig. 4.6 and 4.7A). After 15 seconds of exposure to 1% oxygen, some of the control larvae backed out of the vertical feeding position and began to wander on top of the yeast paste (Fig. 4.6A). Larvae that backed out of the yeast and began to move about the surface were considered “fleeing” larvae. In contrast to the control larvae, all p89Da::GAL4, UAS::TNT (active) larvae remained in the vertical feeding position. After 45 seconds of exposure to 1% oxygen, many of the p89Da::GAL4, UAS::TNT (active) larvae backed out of the food slightly, but remained in the same vertical feeding position (Fig. 4.6B). After 60 seconds of exposure of 1% oxygen, all of the control larvae began fleeing behavior, while all p89Da::GAL4, UAS::TNT (active) larvae remained in the vertical feeding position (Fig. 4.6C). The average rate of fleeing of p89Da::GAL4, UAS::TNT (active) larvae, determined from numerous experiments using several independent p89Da::GAL4 insertions, was about 10% at 1 minute of exposure to 1% oxygen (Fig. 4.7A). The particular p89Da::GAL4 line used as an example for Figure 4.6, displayed a slightly weaker tendency to flee in response to hypoxia than several other lines used in these experiments, when crossed to UAS::TNT (active). After 3 minutes of exposure to 1% oxygen, the control larvae, all of which remained in a state of locomotion, began to wander off of the yeast dollop onto the Petri dish (Fig. 4.6D). All p89Da::GAL4, UAS::TNT (active) larvae remained in the vertical feeding position, although they backed even further out of the yeast dollop, with nearly half of their bodies exposed to the atmosphere (Fig. 4.6D). The average rate of fleeing of p89Da::GAL4, UAS::TNT

(active) larvae from all experiments at 3 minutes in 1% oxygen was about 45% (Fig. 4.7A). After 5 minutes of exposure to 1% oxygen, many of the control larvae wandered far from the yeast dollop, and all remained in a state of locomotion. By this time, many of the p89Da::GAL4, UAS::TNT (active) larvae had begun to wander about on top of the yeast dollop. The average rate of fleeing of p89Da::GAL4, UAS::TNT (active) larvae at 5 minutes in 1% oxygen from all experiments was about 65% (Fig. 4.7A).

Although the short term locomotory activity of p89Da::GAL4, UAS::TNT (active) larvae in food vials appeared normal, it is possible that an overall locomotory defect was responsible for the results obtained in Figure 4.7A. To address this question, these larvae were compared to control p89Da::GAL4, UAS::TNT (inactive) larvae in a standard locomotory test, which examined the distance traveled on an agarose plate over 5 minutes. The distance traveled by p89Da::GAL4, UAS::TNT (active) larvae was quite variable, averaging 10 cm in five minutes (Fig 4.7J). The control larvae on average traveled about 16cm. The difference in average distance traveled was not significant between the two crosses. Despite the more variable locomotory behavior of p89Da::GAL4, UAS::TNT (active) larvae, all traveled at least 4cm, which is a sufficient distance to back out of the vertical feeding position and begin an escape response. Also, when the hypoxia fleeing assay was continued beyond 5 minutes, all p89Da::GAL4, UAS::TNT (active) larvae did eventually begin the fleeing response. The difference in hypoxia fleeing response between the two crosses does not appear to be caused by a locomotory deficiency.



**Figure 4.6.** Behavioral response of experimental larvae to a 1% oxygen environment over a five-minute time period. Left yeast dollop contained five p89Da::GAL4/UAS::TNT (active) larvae and right yeast dollop contained five control p89Da::GAL4, UAS::TNT (inactive) larvae. In all panels, closed arrowheads indicate the location of larvae in stationary vertical feeding positions, while open arrowheads indicate fleeing larvae. **(A)** 15 seconds of hypoxia. All p89Da::GAL4, UAS::TNT (active) larvae remained in a stationary vertical feeding position while 3 of the 5 control larvae has already begun fleeing behavior. **(B)** 45 seconds of hypoxia. All p89Da::GAL4, UAS::TNT (active) larvae remained in a stationary vertical feeding position but some have backed out of the yeast slightly, leaving 1 or 2mm of their posteriors exposed (closed arrowheads). 3 of the 5 control larvae remained in a locomotory state. **(C)** 1 minute of hypoxia. All p89Da::GAL4, UAS::TNT (active) larvae remained in a stationary vertical feeding position, with 4 of the 5 slightly backed up out of the yeast. All control larvae have left the vertical feeding position and entered a locomotory state. **(D)** 3 minutes of hypoxia, side view. All p89Da::GAL4, UAS::TNT (active) larvae remained in a stationary vertical feeding position, but have backed out of the yeast even further, exposing about half of their bodies. The control larvae have begun to leave the yeast dollop and travel on the Petri dish (only 4 of 5 are visible here). **(E)** 5 minutes of hypoxia. 3 of the 5 p89Da::GAL4, UAS::TNT (active) larvae left the vertical feeding position and began to travel on top of the yeast. All control larvae remained in a locomotory state, and 2 of 5 have completely left the yeast dollop.

Scale bar =1cm.

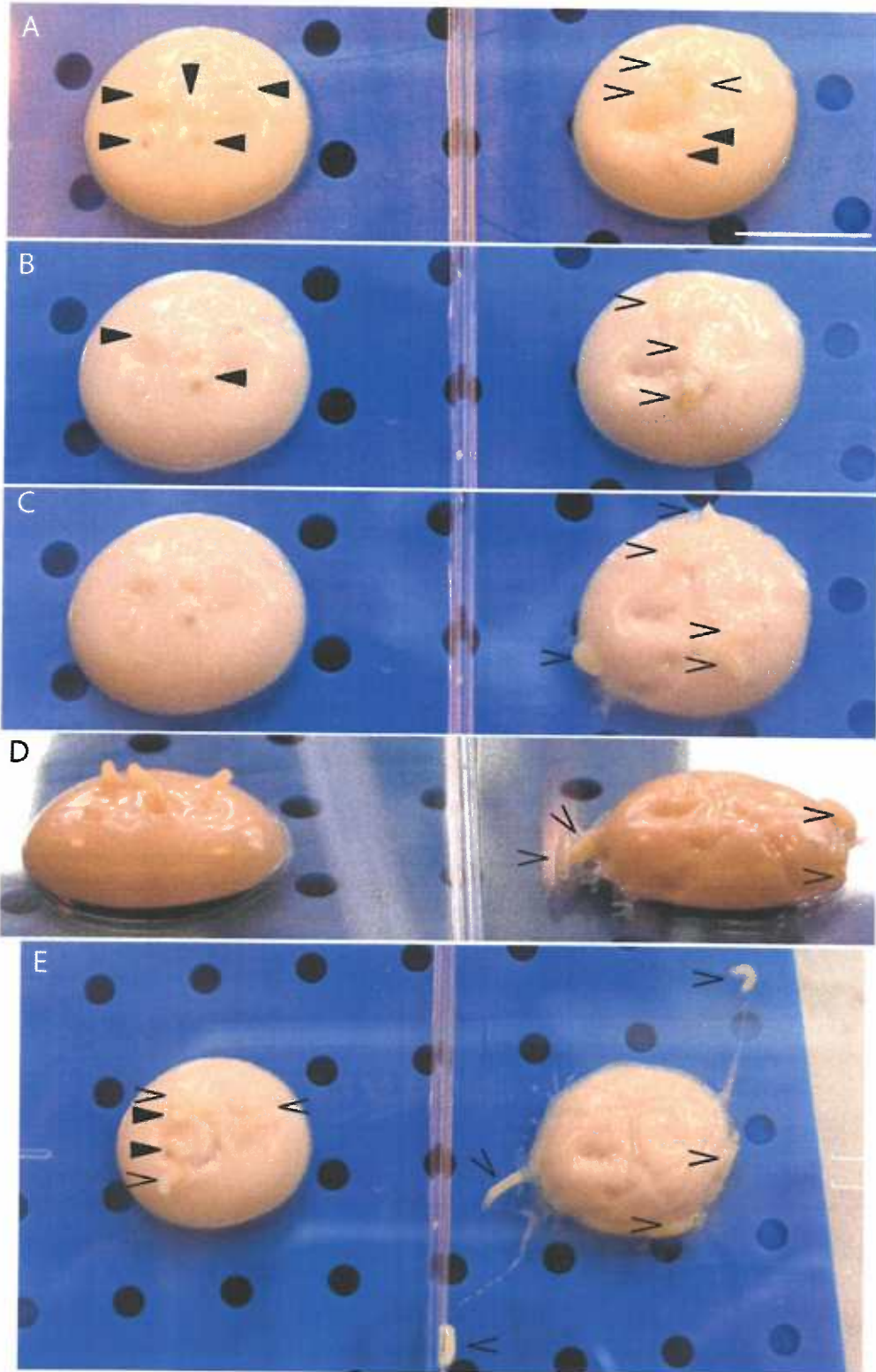
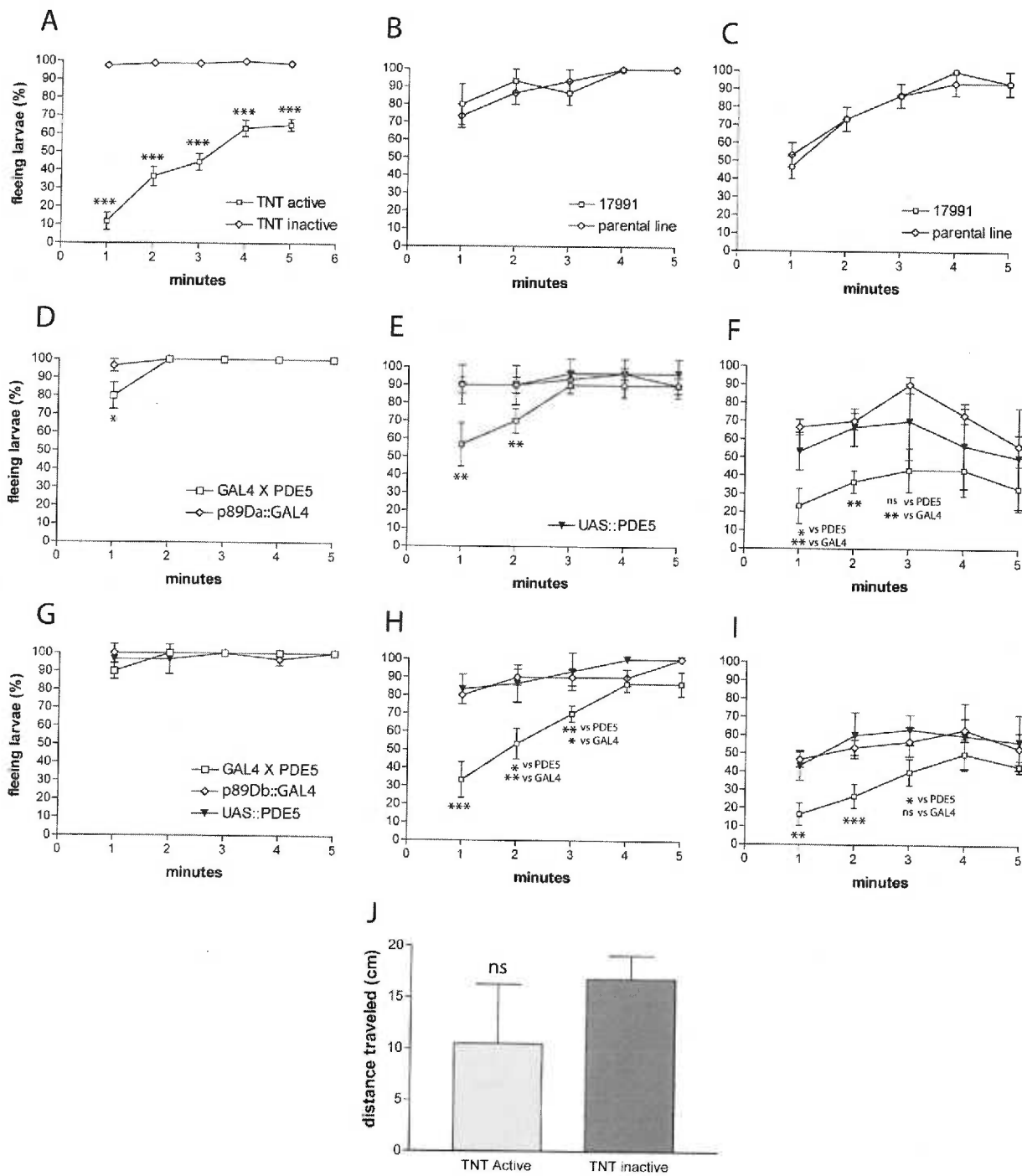


**Figure 4.7.** Hypoxia fleeing assay. Yeast-feeding 3<sup>rd</sup> instar larvae were subjected to a 1%, 5%, or 10% oxygen in nitrogen environment, and observed for the start of fleeing behavior every minute for five minutes. (A) 1% oxygen, p89Da::GAL4,UAS::TNT (active) vs. p89Da::GAL4, UAS::TNT (inactive). (B) 5% oxygen, line 17791 vs. parental line. (C) 10% oxygen, line 17991 vs. parental line. (D) 0% oxygen, p89Da::GAL4, UAS::bovPDE5 vs. p89Da::GAL4 at 0% oxygen. The UAS::bovinePDE5 line response was not examined at this concentration. (E) 5% oxygen, same animals as (D) but also with UAS::bovinePDE5. (F) 10% oxygen, same animals as (D) and (E). (G) 0% oxygen, p89Db::GAL4, UAS::bovPDE5 vs. p89Db::GAL4 vs. UAS::bovinePDE5. (H) 5% oxygen, same animals as (G). (I) 10% oxygen, same animals as (G) and (H). (J) 5 minute locomotory assay with p89Da::GAL4, UAS::TNT (active) and p89Da::GAL4, UAS::TNT (inactive) larvae. Graph in (A) represents UAS::TNT crosses with 6 independent p89Da::GAL4 insertion lines, with 3-6 trials each. All other hypoxia assay graphs represent data from at least 3 trials. Significant differences between data points at each minute are indicated with asterisks and lack of significance is indicated by a lack of asterisks. Paired two-tailed T-tests or one-way ANOVA with Tukey post-test were used to test significance between data points at each minute. \* = P<0.05, \*\* = P<0.01, \*\*\* = P<0.001.



While line 17991 (Gyc-89Da knockout) animals appeared to be normal with regard to viability and overall development and behavior, it is possible that these larvae are deficient in sensory processes. The homozygous 17991 larvae were compared to the parental line for differences in their hypoxia response behavior. No significant differences in the fleeing response were observed between the two lines at 0% oxygen (data not shown), 5% oxygen (Fig. 4.7B), and 10% oxygen (Fig. 4.7C). Higher concentrations of oxygen were used in an attempt to tease apart more subtle differences in low oxygen detection and the hypoxia fleeing response, as 1% oxygen likely induces a strong response that may obscure any such subtleties.

Similar to line 17991, p89Da::GAL4, UAS::bovinePDE5 and p89Db::GAL4, UAS::bovinePDE5 animals appeared to be generally normal. These larvae were tested for deficits in the hypoxia escape response, compared to the uncrossed GAL4 and UAS::bovinePDE5 larvae. At 1% oxygen, a small but significant difference was observed in the fleeing response between p89Da::GAL4, UAS::bovinePDE5 larvae and the uncrossed GAL4 line, at 1 minute only (Fig. 4.7D). In contrast, no significant differences were observed between the p89Db::GAL4, UAS::bovinePDE5 larvae and the uncrossed lines (Fig. 4.7G). At 5% oxygen, strong and significant differences in the fleeing response were observed between p89Da::GAL4, UAS::bovinePDE5 or p89Db::GAL4, UAS::bovinePDE5 and the parental lines at 1 and 2 minutes, and even 3 minutes for the p89Db::GAL4, UAS::bovinePDE5 cross (Fig. 4.7E and H). At 10% oxygen, significant differences in the fleeing response were observed between p89Da::GAL4, UAS::bovinePDE5 or p89Db::GAL4, UAS::bovinePDE5 and both uncrossed lines at 1 and 2 minutes only (Fig. 4.7F and I). These results suggest that the reduction of cGMP

levels in the cells that express Gyc-89Da and Gyc-89Db leads to reduced sensitivity to hypoxia and a reduced tendency to leave the feeding position to seek out a more desirable environment.

## **Discussion**

In this chapter I report the results of experiments intended to shed light on the function of the *Drosophila* atypical sGCs. The initial strategy was to create or acquire gene knockout lines for each of the three atypical sGCs, especially Gyc-88E, which was indispensable for atypical sGC activity. While only one of the three desired gene knockout lines was obtained for these studies (Gyc-89Da), the alternate approaches undertaken to gain information pertaining to function yielded intriguing and informative results.

The lack of an observable phenotype in the Gyc-89Da gene knockout line (17991) was not entirely unexpected. Gyc-89Da and Gyc-89Db required Gyc-88E for activity in biochemical studies (Chapter 2). However, Gyc-88E was active as a homodimer. In the report by Morton (2004), putative Gyc-88E/Gyc-89Da and Gyc-88E/Gyc-89Db heterodimers were potently activated by hypoxia. Gyc-88E expressed alone was still activated by hypoxia, but to a lower extent. Thus, it is possible that eliminating Gyc-89Da expression only reduced the magnitude of cGMP signaling, as Gyc-88E function was retained. While Gyc-89Da and Gyc-89Db expression in the CNS was non-overlapping, they were co-expressed in many of the same peripheral neurons. In these cases Gyc-89Db may play a redundant or partially redundant role with Gyc-89Da, making the effects of a Gyc-89Da knockout extremely subtle. Also, phenotypes

associated with sensory signaling pathways in peripheral neurons are almost never readily observable, sometimes requiring a battery of specialized tests to characterize. In the current studies, I examined line 17991 for defects in detecting and reacting to hypoxia using the hypoxia fleeing assay. No significant differences in activity were observed between line 17991 and its parental line at 1%, 5%, and 10% oxygen levels. It is likely that peripheral neurons mediate acute oxygen sensation, with the best candidates being the neurons that innervate rod sensilla in the sensory cones, which express both Gyc-89Da and Gyc-89Db. As Gyc-89Db may play a partially redundant role with Gyc-89Da, the lack of Gyc-89Da in these neurons may not reduce their ability to sense oxygen to an observable extent. Finally, the expression of Gyc-89Da and Gyc-89Db in a non-overlapping pattern in the CNS implies separate specialized roles for these subunits. Again, perhaps Gyc-88E activity alone was functionally sufficient in these cells. As the *Drosophila* atypical sGCs appear to function as oxygen sensors, perhaps in the CNS they also mediate transcriptional changes or modulate behavior in response to long-term, less severe hypoxia. A phenotype related to these possible functions in line 17991 would not have been apparent as I did not examine the effects of long term hypoxia in these studies.

The tetanus light chain toxin (TNT) and bovine PDE5 expression studies yielded several interesting results, some of which support the role of the *Drosophila* atypical sGCs as oxygen sensors. One of the most obvious defects associated with expressing active TNT in neurons that express Gyc-89Da in older larvae was the rapid, “jackhammer”-like shaking movements observed in the mouthparts during feeding. The cause of this defect was likely attributable to TNT expression in certain cells in the CNS, perhaps in interneurons that are involved in the circuitry that communicates to the motor

neurons that control the fine anterior-posterior motion of the mouth hooks. Interestingly, this “jackhammer” defect did not appear to alter the ability of the larvae to feed efficiently. Though possible, it seems unlikely that cGMP generated by atypical sGC directly controls input to these mouth part motor neurons and that Gyc-88E knockout larvae would display a similar phenotype, especially considering that p89Da::GAL4, UAS::bovinePDE5 larvae did not display this defect.

An occurrence that was observed with active TNT expression in both the Gyc-89Da and Gyc-89Db neurons was the curious burial death of larvae. Wild type larvae, when feeding vertically in food vials or jars, will quickly back out to re-establish posterior spiracular contact with the atmosphere when their burrowing tunnels collapse or become blocked by liquefied food. This response could be triggered by the sudden reduction of oxygen exposure and perhaps posterior mechanosensory stimulation. It appeared that TNT-expressing larvae were not interested in re-establishing contact with the atmosphere when burrowing tunnels collapsed, and just kept burrowing and feeding until their apparent suffocation. The failure of TNT-expressing larvae to find these anaerobic paths under the food to be aversive suggests a defect in oxygen sensation. However, a separate phenomenon also appeared to be in play here. Some p89Da::GAL4, UAS::TNT (active) and p89Db::GAL4, UAS::TNT (active) 1<sup>st</sup> instar larvae were found buried and dead under the food. However, larvae do not normally burrow completely into the food until the 2<sup>nd</sup> instar stage. The behavior of 3<sup>rd</sup> instar larvae that expressed active TNT in the Gyc-89Da neurons was even more peculiar. During the 1<sup>st</sup>, 2<sup>nd</sup>, and early 3<sup>rd</sup> instar stages the p89Da::GAL4, UAS::TNT (active) larvae displayed significantly reduced but relatively good viability, with no more than 1/5 of larvae perishing under the



food. However, at the end of the 3<sup>rd</sup> instar, when these larvae reached their maximal size and likely began the wandering phase, about half behaved normally and climbed out of the food and onto the walls of the vial to pupate. The other half however traveled downward, with many actually coming to rest at the very bottom of the vials. This defect in the wandering guidance in p89Da::GAL4, UAS::TNT (active) larvae and less penetrant abnormal burrowing tendency in 1<sup>st</sup> instar larvae in both crosses appears to be a separate problem from the potential oxygen-sensation defect. It was not determined if p89Db::GAL4, UAS::TNT (active) 3<sup>rd</sup> instar larvae also display a wandering guidance defect because these larvae do not survive past the 1<sup>st</sup> instar stage. As Gyc-89Da and Gyc-89Db are not co-expressed in the CNS, it would seem that the 1<sup>st</sup> instar burrowing tendency and apparent oxygen sensation defect is attributable to TNT expression in the peripheral neurons where both of the genes are co-expressed. Alternatively, the burrowing tendency defect could be the result of TNT expression in the CNS, if Gyc-89Da- and Gyc-89Db-expressing neurons are part of the same circuitry that controls this aspect of behavior. An oxygen-sensation defect however would likely be attributed to TNT-expression in neurons that innervate the trachea or rod sensilla on the posterior sensory cones, as these are the only sensilla/structures that make direct contact the atmosphere while feeding. It is possible however, that certain Gyc-89Da- and Gyc-89Db-expressing neurons in the CNS mediate the behavior response to external hypoxia sensed in some other manner, and the TNT expression in these neurons blocks the initiation of behavior associated with sudden hypoxia. It is not likely that CNS neurons themselves detect sudden external hypoxia in order to make rapid behavioral changes because the

hypo-oxygenation of CNS cells would likely occur too gradually to be utilized as an effective acute signal.

The “burial death” phenotype of the p89Da::GAL4, UAS::TNT (active) larvae was completely eliminated by raising the larvae on a thin plate of food, which prevented them from burrowing into an anaerobic environment. This finding indicates that buried larvae died of suffocation, and that vial-raised larvae failed to respond appropriately to a normally aversive hypoxic environment.

Most p89Db::GAL4, UAS::TNT (active) 1<sup>st</sup> instar larvae did not perish under the food, but rather died on top of the food. Most of these died during the preparatory events just prior to the 1<sup>st</sup> instar molt, with double mouthparts and fluid-filled trachea. These larvae likely died of suffocation, due to the failure of trachea to reabsorb the molting fluid and refill with air after the 1<sup>st</sup> instar tracheal lining separates from the new 2<sup>nd</sup> instar trachea shortly before ecdysis. This finding parallels what was observed in larvae that lack EH neurons, most of which die during the larval stages prior to ecdysis with double mouthparts and fluid filled trachea (McNabb et al., 1997). These results also closely resemble ecdysis-triggering hormone (ETH) knockout larvae, which all die before reaching the second instar (98% mortality) (Park et al., 2002). Ecdysis did not occur in these animals and the air filling of trachea was severely delayed (~1.5 hours).

Molting, the process of making a new cuticle, is controlled by steroid hormones. Molting cumulates with ecdysis behavior, which is controlled by an unknown number of interacting neuropeptides. Three of these neuropeptides have been identified and studied in detail in several insect systems: ecdysis-triggering hormone (ETH), eclosion hormone, and crustacean cardioactive peptide (CCAP) (for discussion of available data and the

current models in *Manduca* and *Drosophila* see Ewer (2005). The first event in the endocrine cascade that initiates ecdysis is currently unknown. However, work in *Drosophila* has shown that one of the first events leading to larval ecdysis is the release of ETH from the Inka cells (located peripherally along the two dorsal tracheal trunks), which become immunoreactive for cGMP shortly after peptide release begins.

Circulating ETH appears to act on the Vm neurons in the CNS causing the release of EH into the CNS and hemolymph, which acts on the Inka cells to release more ETH to form a positive feedback loop with the Vm neurons. ETH and EH then appear to act in concert to trigger air filling of fluid filled trachea and initiation of the pre-ecdysis program.

Following the air filling of trachea, circulating ETH and EH cause the release of CCAP from a population of neurons in the CNS. CCAP appears to inhibit the pre-ecdysis program and directly activate the ecdysis motor program. Several of the actions of ETH and EH described above are likely to be indirect.

As *Gyc-89Db* was not expressed in the EH and CCAP neurons or in the Inka cells (data not shown), it is tempting to speculate that TNT-inactivation of the dendritic neurons that innervate trachea was responsible for this failure. It is presumed that at this stage the presence of molting fluid blocks gas exchange in the tracheols, causing a brief period of hypoxia at this location and perhaps in internal tissues as well. It is possible that the function of the tracheal dendritic neurons at this time is to sense this event, and signal for the release of unknown neuropeptides that promote the reabsorption of the molting fluid and the filling of trachea with air. Importantly, this defect was not observed to occur with *p89Da::GAL4, UAS::TNT* (active) larvae, which do not express TNT in the tracheal dendritic neurons. Alternatively, the tracheal fluid reabsorption and air filling defect

could have resulted from TNT expression in the Gyc-89Db-expressing peptidergic or non-peptidergic CNS neurons alone, some of which may respond to hypoxia and act upstream of the Inka cells and Vm neurons. Recent evidence from *Manduca* indicates that a highly conserved insect peptide called corazonin causes the release of ETH from the Inka cells, which express the corazonin receptor (a GPCR) (Kim et al., 2004). In *Drosophila*, the function of corazonin has not yet been studied, but corazonin expression was found in a population of cells in the CNS in a pattern that resembles part the expression pattern of Gyc-89Db in the brain lobes and VNC (Choi et al., 2005). It is possible that Gyc-89Db is expressed in the corazonin neurons, and that TNT expression in these neurons blocks the release of corazonin, subsequent release of ETH, EH, and all following events. Double-label experiments would demonstrate if this is the case. The defects observed in p89Db::GAL4, UAS::TNT larvae are consistent with the combined defects observed in EH-cell and ETH knockout larvae, supporting the hypothesis that the Gyc-88E/Gyc-89Db heterodimer initiates the neuropeptide cascade upstream of ETH. Further studies should examine the release of ETH from the Inka cells and EH from Vm cells in p89Db::GAL4, UAS::TNT larvae or in Gyc-88E and Gyc-89Db knockout larvae (with immunocytochemistry) when available. While it is interesting that levels of cGMP are increased in the Inka cells shortly after the release of ETH begins, no atypical sGC expression was found in these cells (data not shown). It will be important to determine if the conventional  $\alpha 1$  and  $\beta 1$  subunits are expressed here.

Also intriguing was the complete failure of eclosion in p89Da::GAL4, UAS::TNT (active) pupae. Animals that made it to the end of the pupal stage completed all pre-eclosion events (including tracheal air-filling) and initiated head inflation, but then failed

to initiate the eclosion motor program, which occurs through the actions of ETH, EH, and CCAP (and likely other unknown peptides) in a neuropeptide cascade similar to the cascade used in larval ecdysis. This defect is unlike EH cell knockout animals which displayed delayed and incomplete tracheal air filling throughout the body (Baker et al., 1999; McNabb et al., 1997). Despite this defect, a third of EH cell knockout animals successfully eclosed and emerged as adults. The eclosion defect in p89Da::GAL4, UAS::TNT (active) animals was also unlike the defects observed in CCAP cell knockout animals. These animals displayed lethal defects at pupal ecdysis and only very subtle defects at larval ecdysis and eclosion (Park et al., 2003). Interestingly, several neurons and some tracheal elements in the abdominal CNS were observed to become immunoreactive for cGMP beginning at the grainy stage, before the trachea have filled with air (Baker et al., 1999). These cells were not immunoreactive for CCAP. Because the spike in cGMP production in these cells occurs at a time when the animal may be experiencing inhibited gas exchange and some level of internal hypoxia, it is possible that atypical sGCs are the source of this cGMP. Double labels studies of the CNS at the grainy stage could examine this possibility. Also needed are studies that examine the production of cGMP in these cells and the release of ETH and EH from the Inka and Vm cells in p89Da::GAL4, UAS::TNT (active) animals prior to the failed eclosion event.

The GAL80<sup>TS</sup> experiment revealed the temporal requirement for the function of Gyc-89Da-expressing neurons. When the restriction on TNT expression was lifted at the larval wandering stage, all pupae failed to eclose. Surprisingly, when the restriction on GAL4 function and TNT expression was lifted 30 hours before eclosion, most animals emerged from the pupal case. These results suggest that the activity of Gyc-89Da-

expressing neurons is not required just before eclosion to initiate the motor program. It is possible that TNT-expression in Gyc-89Da-expressing neurons early in pupal development causes axonal guidance or synaptic defects, resulting in faulty circuits that are later used for initiating the eclosion motor program. Alternatively, TNT-expression in the Gyc-89Da-expressing, dimmed-positive peptidergic neurons may block the release of neuropeptides that somehow prime the machinery that later controls the initiating of the eclosion motor program. As Gyc-89Da was not expressed in a large subset of motor neurons, these animals were likely capable of performing the characteristic abdominal peristalses associated with eclosion, if the motor program was only initiated. Although the GAL80<sup>TS</sup> system was not applied to the p89Db::GAL4, UAS::TNT (active) animals in the current studies, it would be very interesting to see if the larval death/ecdysis failure in these larvae could be bypassed, allowing TNT expression only after the last larval ecdysis to see if animals can successfully pupate and eclose.

Crossing the UAS::bovinePDE5 line with p89Da:GAL4 or p89Db::GAL4 did not result in any of the viability and behavioral defects just discussed. It is possible that PDE5 expression in the Gyc-89Da and Gyc-89Db cells does not reduce the levels of cGMP effectively enough to generate these defects. Subtle defects in the timing of pre-ecdysis events (possibly caused by reduced levels of cGMP) was not examined. Alternatively, it is possible that these defects only reflect the function of the cells themselves, and not the function of cGMP and possibly the function of the *Drosophila* atypical sGCs in these cells. However, the expression of PDE5 in Gyc-89Da- and Gyc-89Db-expressing cells did have a significant effect in the larval hypoxia behavioral response.

In the hypoxia fleeing assay, p89Da::GAL4, UAS::TNT (active) larvae displayed a much slower response to hypoxia than the control larvae, with most tending to remain feeding for several minutes in 1% oxygen before initiating the escape behavior. These results indicate that the Gyc-89Da-expressing neurons are important for oxygen-sensation. Though it is likely that oxygen sensation is mediated by the peripheral neurons that innervate tracheal and/or sensilla on the posterior sensory cones, the current experiments did not exclude the role of the CNS in this process. Future experiments could utilize the GAL80<sup>TS</sup> system to restrict TNT-expression in the just the PNS, or even a subset of neurons in the PNS. Such studies could definitively demonstrate the role of certain sets of peripheral neurons in oxygen sensation.

While the TNT-expression experiments provided interesting and informative results, they only provide circumstantial evidence of what the function of the atypical sGCs could be. The results obtained in the hypoxia fleeing assays with p89Da::GAL4, UAS::bovinePDE5 and p89Db::GAL4, UAS::bovinePDE5 larvae provide an important link that ties together hypoxia detection and the fleeing response to cGMP and likely atypical sGC activity. Larvae from both of these crosses displayed a significantly reduced tendency to leave the vertical feeding position and begin exploratory “fleeing” behavior in response to a 5 or 10% oxygen environment, compared to the uncrossed parental lines. It appeared that very low oxygen levels produced a strong fleeing response in all PDE5-expressing larvae, despite the reduction of cGMP in the potential oxygen-sensing neurons. It is possible that the potent activation of Gyc-88E/Gyc-89Db heterodimers in 1% oxygen overwhelmed the activity of PDE5, and the levels of cGMP were still high enough to generate a robust response. These results, combined with the finding that Gyc-

89Da and Gyc-89Db are not co-expressed in the CNS supports the hypothesis that it is peripheral neurons that sense oxygen levels. Future experiments could utilize the GAL80 system to restrict bovinePDE5-expression to the PNS, or in a subset of neurons in the PNS. The results of these experiments could definitively demonstrate the role of cGMP in certain sets of peripheral neurons in oxygen sensation. Immunohistological studies could also be undertaken to demonstrate that exposure of larvae to hypoxia increases the levels of cGMP in certain central and/or sensory neurons. Experiments such as this could provide a strong link between the defects reported here and the activity of the oxygen-sensitive, atypical sGCs and exclude the activity of oxygen-insensitive conventional  $\alpha/\beta$  heterodimers.

It is apparent from the results obtained from the hypoxia fleeing assays that larvae become less inclined to flee from their feeding positions as the oxygen concentration is increased. At 10% oxygen, about half of all larvae remained in or resettled into the yeast dollops after 5 minutes. These results suggest that slightly higher oxygen concentrations may not be aversive to larvae at all, and may actually be preferred to atmospheric oxygen concentrations (21%). While it is unknown if *Drosophila* larvae or flies prefer and seek out environments that contain a certain level of oxygen while feeding, it has been demonstrated that *C. elegans* actually prefers and seeks out a 14% oxygen environment, and that this preference is disrupted in GCY-35 mutants (Gray et al., 2004). Testing larvae in an oxygen gradient apparatus modeled after the one used for *C. elegans* would provide information about such a preference in *Drosophila* larvae. If larvae do in fact display a preferred oxygen concentration environment, it would be very interesting to see



if this preference is eliminated or disrupted in p89Da::GAL4, UAS::TNT (active) and p89D::GAL4, UAS::bovinePDE larvae.

In summary, the results presented here support a role for the *Drosophila* atypical sGCs in oxygen sensation and behavioral response to hypoxia. Specifically, the results from the hypoxia fleeing assay experiments indicate that the activity of the Gyc-89Da-expressing neurons is important for hypoxia detection and response, and that cGMP in both the Gyc-89Da- and Gyc-89Db-expressing cells plays a role in the mediation of this process. The observation that TNT-expressing larvae allow themselves to remain in an anaerobic environment while burrowing and feed also supports such a role. While more focused TNT- and PDE5-expression experiments could provide more detailed information and circumstantial evidence pertaining to oxygen sensation in *Drosophila*, what will ultimately be needed to demonstrate that the atypical sGCs mediate oxygen sensation is a Gyc-88E gene knockout line. It will be very interesting and important to see if the atypical sGCs actually do mediate oxygen sensation in vivo in *Drosophila*, as they do in *C. elegans* and likely many other organisms. The generation of a Gyc-88E gene knockout line will undoubtedly yield a treasure trove of insight into the mostly unknown world of atypical sGC function.

## Chapter 5: Summary and future directions

The work presented in this dissertation describes the characterization of the *Drosophila melanogaster* sGCs, Gyc-88E, Gyc-89Da, and Gyc-89Db, which belong to a recently discovered family of atypical sGCs. When I first began work on these genes in late 2000, very little was known about this curious family of sGCs. The founding family member and ortholog of Gyc-88E, MsGC- $\beta$ 3, had been cloned and characterized as an NO-insensitive, apparently homodimeric sGC (Nighorn et al., 1999). This finding broke the long-standing paradigm that all sGCs are obligate heterodimers activated by NO, and raised a large number of questions concerning the activation and function of this new type of sGC. With the explosion of genome data becoming available for researchers around the turn of the millennium, it became apparent that highly identical MsGC- $\beta$ 3 orthologs and other closely related sGCs likely existed in many other animals, including *Drosophila melanogaster* and *C. elegans*.

Consistent with the biochemical properties of MsGC- $\beta$ 3, I found that Gyc-88E yielded relatively NO-insensitive GC activity in the absence of other subunits, indicating the formation of homodimers (Chapter 2). Additionally, Gyc-88E also appeared to form heterodimers with Gyc-89Da or Gyc-89Db, which enhanced basal activity and slightly increased NO-sensitivity. Orthologs of highly identical genes Gyc-89Da and Gyc-89Db were not found in a *Manduca* degenerate PCR screen, but an ortholog of these genes appears to be present in the genomes of most organisms that are predicted to contain a Gyc-88E ortholog. The weak NO-stimulation also obtained with the *Drosophila* atypical sGCs strengthened the suspicion that NO is not the endogenous ligand that activates this family of sGCs. In 2004, three reports were published that shed much light on the

regulation and function of atypical sGCs. The first report came from the Bargmann lab, which clearly demonstrated that the *C. elegans* GCY-35 mediates the preference of a 5-10% oxygen environment and avoidance of higher or lower oxygen concentrations (Gray et al., 2004). Importantly, the GCY-35 regulatory domain was found to bind oxygen, in contrast to conventional  $\alpha$  and  $\beta$  subunit regulatory domains. Next, in a report that complemented the GCY-35 findings, Morton (2004) demonstrated that the *Drosophila* atypical sGCs are potently activated by hypoxic conditions, using a heterologous cell culture expression system. The magnitude of atypical sGC activation at 0% oxygen was on par with the activity level of the NO-stimulated *Drosophila*  $\alpha/\beta$  heterodimer. Importantly, the increase in activity was graded over a 0-21% oxygen concentration range, and could be detected after only 1 minute of exposure to anoxia. This activity was blocked by the conventional sGC inhibitor ODQ, indicating that like conventional sGCs, atypical sGC activation occurs through the heme-group. Another piece of the puzzle was provided by a study of the crystal structure of an sGC related oxygen-binding heme domain from a *Thermoanaerobacter tengcongensis* oxygen-sensing protein (Pellicena et al., 2004). A single tyrosine residue (Tyr-140) in the ligand-binding pocket was predicted to confer oxygen binding specificity to the heme group, a residue that all currently known atypical sGCs possess at an equivalent position and all conventional  $\alpha$  and  $\beta$  subunits lack. Together, these reports indicate that the *Drosophila* atypical sGCs are specific oxygen sensors.

The work presented in Chapter 3 illustrates a number of expression sites where the *Drosophila* atypical sGCs are well placed to function as sensors that sample environmental oxygen concentrations. Of particular interest are the dendritic neurons that

associate with trachea and the neurons that innervate basiconical-like sensilla on the thoracic segments and on the posterior sensory cones. During the 1<sup>st</sup> instar larval stage, animals tend to crawl about the surface of a food substrate, only burrowing after the first molt. At this time, the thoracic and posterior sensory cone sensilla could be used to detect areas of lower oxygen, which may represent desirable feeding/burrowing locations on a native food source (i.e. fruit) where there is abundant microbiological activity. During the larval burrowing stages, the only external sensilla that remain in contact with the atmosphere are the posterior sensory cone sensilla. These sensilla could be used to sense hypoxia associated with burrowing depth and tunnel collapse. The tracheal dendritic neurons are in a suitable location to detect tracheal or hemolymph oxygen concentrations at this stage. Somewhat similar to the peripheral sensory expression patterns of the *Drosophila* atypical sGCs, the *C. elegans* GCY-35 was found to be expressed in sensory neurons that have cilia exposed to the body fluid and in chemosensory neurons that project dendrites to the anterior and posterior tips of the body.

The results in Chapter 4 provide evidence that the *Drosophila* atypical sGCs play a role in oxygen sensation *in vivo*. The most important findings came from the hypoxia fleeing assays. Expression of either TNT or bovinePDE5 in cells that express Gyc-89Da or Gyc-89Db significantly reduced the normally rapid tendency of larvae to leave the vertical feeding position and enter an exploratory state when exposed to hypoxic conditions. These results indicate that both the function of these neurons and elevated levels of cGMP are important for larvae to sense and respond to hypoxia. It is likely that the atypical sGCs generate the cGMP in these neurons as they are potently activated by hypoxia while the conventional  $\alpha/\beta$  heterodimers are not. The finding that both Gyc-

89Da and the Gyc-89Db promoter-driven bovinePDE5 produced nearly identical results suggests that peripheral rather than central neurons mediate oxygen sensation, as these two cyclases are not co-expressed in CNS cells. In summary, the *Drosophila* atypical guanylyl cyclases, likely acting through a small number peripheral sensory neurons, appear to mediate oxygen sensation and hypoxia escape behavior.

A BLAST search of the current genome resources revealed that a wide range of organisms possess sGCs that are highly related to Gyc-88E and Gyc-89D. These organisms include other insects such as the honeybee and the mosquito, other nematodes, an ascidian (ancestral chordate), and even two fish species. It is apparent that sGC-mediated oxygen sensation may be widespread throughout the animal kingdom, especially in organisms that exist in aquatic habitats, decomposing material, sub-terrestrial environments and other locales where hypoxic microhabitats and rapidly changing conditions exist.

Mammals appear to utilize a different oxygen sensing system to sense acute hypoxia, at least in the circulatory system. When humans and other mammals experience low blood oxygen levels, the lung ventilation rate reflexively increases in order to restore normal oxygen tension to vital organs. This mechanism depends on the glomus cells, which are found in the carotid body, located in the carotid artery. Glomus cells respond to hypoxia with membrane depolarization, which results in the production of action potentials, influx of  $\text{Ca}^{2+}$  through voltage-gated channels, and release of dopamine, which mediates the necessary physiological changes through other neurons (Prabhakar, 2000). The complex mechanism responsible for glomus cell oxygen sensation has only recently been elucidated (Williams et al., 2004). A membrane-linked isoform of heme oxygenase

(HO-2) oxidatively breaks down heme to CO, biliverdin, and iron. This reaction requires oxygen and uses NADPH-cytochrome P450 reductase as the electron donor protein. The CO generated by HO-2 appears to act on BK channels (Ca<sup>2+</sup>- and voltage-gated potassium channel), keeping them open. When oxygen levels are low, heme breakdown and CO production is inhibited. Low levels of CO result in the closing of BK channels, which leads to membrane depolarization and dopamine release. While this mechanism may be used in all mammals to sense acute hypoxia in the circulatory system, it is possible that other fast-acting oxygen sensing mechanisms (such as atypical sGC activation) are used for other roles in mammals, and in other vertebrates.

It was interesting to find Gyc-89Da and Gyc-89Db expression in several cells in the primary olfactory (dorsal) and gustatory (terminal) organs in larvae, and Gyc-89Db expression in a large number of neurons in the primary adult gustatory (labellum) organ. A separate project in the Morton lab investigated the effects of Gyc-89Da and Gyc-89Db promoter driven bovine PDE5 expression on larval response to several well-known olfactory and gustatory attractants. p89Da::GAL4 / UAS::bovPDE5 larvae displayed a significantly reduced attraction to the odorant ethyl acetate and the sugar tastant maltose. p89Db::GAL4 / UAS::bovPDE5 larvae on the other hand were normally attracted to all odorants tested but were not attracted to the sugar tastants sucrose, glucose, and fructose. These findings suggest that cGMP and possibly the atypical sGCs mediate attraction to some odorants and sugars. The most exciting result, however, was that exposure to a 10% oxygen environment dramatically restored the attraction of p89Db::GAL4 / UAS::bovPDE5 larvae to sucrose. This finding suggests that atypical sGCs may mediate and/or modulate the attraction to sugars in response to the concentration of oxygen in the

atmosphere or dissolved in food. More specifically, the concentration of oxygen may set the sensitivity of sugar receptors.

p89Da::GAL4, UAS::TNT and p89Db::GAL4, UAS:TNT animals also displayed lethal defects that prevented larval or adult ecdysis. Through classical endocrinological manipulations using *Lepidoptera*, three neuropeptides were identified that appeared to play important roles in the initiation and timing of ecdysis: EH, ETH, and CCAP. These three peptides have also been shown to play crucial or important roles in regulating ecdysis in *Drosophila*, using cell or gene knockout animals and neuropeptide injections. ETH appears to act upstream of EH and is crucial for larval ecdysis and on-time air filling of trachea (Park et al., 2002). EH does not appear to be absolutely required for larval or adult ecdysis, but the majority of EH cell knockout animals die at the 1<sup>st</sup> larval ecdysis with fluid filled trachea (McNabb et al., 1997). Surprisingly, CCAP appears to be important for pupal ecdysis only, and CCAP cell knockout animals only show subtle defects at larval and adult ecdysis (Park et al., 2003). The lethal defects observed at the end of the 1<sup>st</sup> instar in p89Db::GAL4, UAS::TNT animals resembled the combined lethal defects observed in EH cell and ETH gene knockout animals, suggesting that the Gyc-89Db-expressing cells act upstream of these peptides. It will be interesting to see if ETH and EH are released from the Inka cells and Vm neurons in the TNT-expressing animals. p89Da::GAL4, UAS::TNT animals, on the other hand, appeared normal during larval ecdysis but displayed a lethal defect at adult ecdysis: animals completed all pre-eclosion events (including tracheal air-filling), and displayed weak head inflation events, but failed to initiate the ecdysis motor program. These results suggest that the Gyc-89Da-expressing cells are responsible for initiating the final step of ecdysis and likely act

downstream of EH and ETH. However, the results of the GAL80<sup>TS</sup> experiments suggest that the function of the Gyc-89Da-expressing cells is not required just prior to eclosion but rather much earlier in pupal development. This finding suggests that these cells could be involved with the development of the ecdysis motor program circuitry. Future experiments could examine p89Da::GAL4, UAS::TNT animals for axonal pathfinding and synaptic defects in the CNS. It was disappointing that these defects were not observed in the bovinePDE5 expression experiments. However, non-lethal timing defects could have been overlooked in casual visual observations.

### **Future Directions**

The single most important task left remaining at this time is the generation of a Gyc-88E gene knockout line, which is needed to definitively demonstrate that the *Drosophila* atypical sGCs mediate oxygen sensation and hypoxia fleeing behavior. It is also unclear if the ecdysis and eclosion defects observed in the TNT expression studies are related to cGMP signaling by atypical sGCs or only the result of eliminating the function of neurons in which these sGCs are expressed. A Gyc-88E knockout line would certainly present us with a much clearer picture of the full range of processes that the atypical sGCs mediate or modulate. It will also be important to generate a functional Gyc-88E promoter driven reporter line to characterize the Gyc-88E expression pattern in larvae and adults, and to see how this pattern overlaps with Gyc-89Da and Gyc-89Db expression.

It is also important to further characterize behavioral responses to hypoxic conditions and intermediate concentrations of oxygen. A number of situations could be



examined in detail. For example, it is currently unknown if larvae prefer an intermediate oxygen concentration range when feeding, as does *C. elegans*, or if animals adapt to previously aversive oxygen concentrations. As larvae and adults express atypical sGCs in gustatory neurons and the reduction of cGMP levels in these cells eliminates larval attraction to several sugars, it should be investigated if the levels of dissolved oxygen in the food substrate affects feeding behaviors and attraction to different tastants. Also, it would be interesting to examine the effects of various atmospheric oxygen concentrations and substrate-dissolved oxygen concentrations on the egg-laying site preferences of adults. Characterization of these behaviors will greatly aid in the investigation and interpretation of Gyc-88E gene knockout phenotypes.

Point mutation studies should be undertaken to investigate the importance and function of Tyr-140 in ligand binding and specificity. It would be very interesting to see if substituting Tyr-140 with an alternate residue eliminates or reduces oxygen sensitivity or confers increased NO-sensitivity in the heterologous cell culture expression system used in Chapter 2. A hypoxia-insensitive Gyc-88E mutant could then be used to attempt a rescue of the phenotypes found in a Gyc-88E knockout line. The success of a wild-type Gyc-88E construct but failure of a Tyr-140 Gyc-88E mutant construct to rescue a hypoxia-related phenotype would confirm the importance of Tyr-140 in selective oxygen binding to the heme group *in vivo*.

The work presented in this dissertation, together with the report from Morton (2004), provides a strong foundation on which to build a more complete and detailed picture of how *Drosophila* detects and reacts to varying environmental oxygen concentrations. Future work in *Drosophila*, *C. elegans*, and other species will

undoubtedly lead to exciting discoveries and insight into oxygen sensation and the functions of the atypical soluble guanylyl cyclases.



## Literature Cited

- Abi-Gerges, N., Hove-Madsen, L., Fischmeister, R. and Mery, P. F.** (1997). A comparative study of the effects of three guanylyl cyclase inhibitors on the L-type Ca<sup>2+</sup> and muscarinic K<sup>+</sup> currents in frog cardiac myocytes. *Br J Pharmacol* **121**, 1369-77.
- Ahlner, J., Andersson, R. G., Axelsson, K. L., Bergdahl, B., Dahlstrom, U. and Rydell, E. L.** (1986). The relaxant effect of glyceryltrinitrate on isolated human peripheral vein and its relation to cyclic GMP metabolism. *Acta Pharmacol Toxicol (Copenh)* **58**, 129-36.
- Albin, E. E., Davison, S. J. and Newburgh, R. W.** (1975). Properties of cyclic nucleotide phosphodiesterase in the central nervous system of *Manduca sexta*. *Biochim Biophys Acta* **377**, 364-80.
- Arnold, W. P., Mittal, C. K., Katsuki, S. and Murad, F.** (1977). Nitric oxide activates guanylate cyclase and increases guanosine 3':5'-cyclic monophosphate levels in various tissue preparations. *Proc Natl Acad Sci U S A* **74**, 3203-7.
- Aszodi, A., Pfeifer, A., Ahmad, M., Glauner, M., Zhou, X. H., Ny, L., Andersson, K. E., Kehrel, B., Offermanns, S. and Fassler, R.** (1999). The vasodilator-stimulated phosphoprotein (VASP) is involved in cGMP- and cAMP-mediated inhibition of agonist-induced platelet aggregation, but is dispensable for smooth muscle function. *Embo J* **18**, 37-48.
- Ayoob, J. C., Yu, H. H., Terman, J. R. and Kolodkin, A. L.** (2004). The *Drosophila* receptor guanylyl cyclase Gyc76C is required for semaphorin-1a-plexin A-mediated axonal repulsion. *J Neurosci* **24**, 6639-49.

- Bacigalupo, J., Bautista, D. M., Brink, D. L., Hetzer, J. F. and O'Day, P. M.** (1995). Cyclic-GMP enhances light-induced excitation and induces membrane currents in *Drosophila* retinal photoreceptors. *J Neurosci* **15**, 7196-200.
- Baker, J. D., McNabb, S. L. and Truman, J. W.** (1999). The hormonal coordination of behavior and physiology at adult ecdysis in *Drosophila melanogaster*. *J Exp Biol* **202** ( Pt 21), 3037-48.
- Ball, E. E. and Truman, J. W.** (1998). Developing grasshopper neurons show variable levels of guanylyl cyclase activity on arrival at their targets. *J Comp Neurol* **394**, 1-13.
- Bargmann, C. I.** (1998). Neurobiology of the *Caenorhabditis elegans* genome. *Science* **282**, 2028-2033.
- Bargmann, C. I., Hartwig, E. and Horvitz, H. R.** (1993). Odorant-selective genes and neurons mediate olfaction in *C. elegans*. *Cell* **74**, 515-27.
- Barolo, S., Carver, L. A. and Posakony, J. W.** (2000). GFP and beta-galactosidase transformation vectors for promoter/enhancer analysis in *Drosophila*. *Biotechniques* **29**, 726, 728, 730, 732.
- Baumann, A., Frings, S., Godde, M., Seifert, R. and Kaupp, U. B.** (1994). Primary structure and functional expression of a *Drosophila* cyclic nucleotide-gated channel present in eyes and antennae. *Embo J* **13**, 5040-50.
- Baumann, E., Gade, G. and Penzlin, H.** (1990). Structure-function studies on neurohormone D: activity of naturally-occurring hormone analogues. *J Comp Physiol [B]* **160**, 423-9.

**Bellen, H. J., Levis, R. W., Liao, G., He, Y., Carlson, J. W., Tsang, G., Evans-Holm, M., Hiesinger, P. R., Schulze, K. L., Rubin, G. M. et al.** (2004). The BDGP gene disruption project: single transposon insertions associated with 40% of *Drosophila* genes. *Genetics* **167**, 761-81.

**Bicker, G.** (2001). Sources and targets of nitric oxide signalling in insect nervous systems. *Cell Tissue Res* **303**, 137-46.

**Birnby, D. A., Link, E. M., Vowels, J. J., Tian, H., Colacurcio, P. L. and Thomas, J. H.** (2000). A transmembrane guanylyl cyclase (DAF-11) and Hsp90 (DAF-21) regulate a common set of chemosensory behaviors in *Caenorhabditis elegans*. *Genetics* **155**, 85-104.

**Bodmer, R., Barbel, S., Sheperd, S., Jack, J. W., Jan, L. Y. and Jan, Y. N.** (1987). Transformation of sensory organs by mutations of the cut locus of *D. melanogaster*. *Cell* **51**, 293-307.

**Bodmer, R. and Jan, Y. N.** (1987). Morphological differentiation of the embryonic peripheral neurons in *Drosophila*. *Roux's Arch Dev Biol* **196**, 69-77.

**Boekhoff, I., Schleicher, S., Strotmann, J. and Breer, H.** (1992). Odor-induced phosphorylation of olfactory cilia proteins. *Proc Natl Acad Sci U S A* **89**, 11983-7.

**Bohme, E., Graf, H. and Schultz, G.** (1978). Effects of sodium nitroprusside and other smooth muscle relaxants on cyclic GMP formation in smooth muscle and platelets. *Adv Cyclic Nucleotide Res* **9**, 131-43.

**Bonigk, W., Altenhofen, W., Muller, F., Dose, A., Illing, M., Molday, R. S. and Kaupp, U. B.** (1993). Rod and cone photoreceptor cells express distinct genes for cGMP-gated channels. *Neuron* **10**, 865-77.

**Bradley, J., Li, J., Davidson, N., Lester, H. A. and Zinn, K.** (1994).

Heteromeric olfactory cyclic nucleotide-gated channels: a subunit that confers increased sensitivity to cAMP. *Proc Natl Acad Sci U S A* **91**, 8890-4.

**Brand, A. H. and Perrimon, N.** (1993). Targeted gene expression as a means of altering cell fates and generating dominant phenotypes. *Development* **118**, 401-15.

**Brandish, P. E., Buechler, W. and Marletta, M. A.** (1998). Regeneration of the ferrous heme of soluble guanylate cyclase from the nitric oxide complex: acceleration by thiols and oxyhemoglobin. *Biochemistry* **37**, 16898-907.

**Bredt, D. S., Hwang, P. M., Glatt, C. E., Lowenstein, C., Reed, R. R. and Snyder, S. H.** (1991). Cloned and expressed nitric oxide synthase structurally resembles cytochrome P-450 reductase. *Nature* **351**, 714-8.

**Bredt, D. S. and Snyder, S. H.** (1994). Nitric Oxide: a physiologic messenger molecule. *Annu Rev Biochem* **63**, 175-195.

**Breer, H., Klemm, T. and Boekhoff, I.** (1992). Nitric oxide mediated formation of cyclic GMP in the olfactory system. *Neuroreport* **3**, 1030-2.

**Brewster, R. and Bodmer, R.** (1995). Origin and specification of type II sensory neurons in *Drosophila*. *Development* **121**, 2923-36.

**Broderick, K. E., Kean, L., Dow, J. A., Pyne, N. J. and Davies, S. A.** (2004). Ectopic expression of bovine type 5 phosphodiesterase confers a renal phenotype in *Drosophila*. *J Biol Chem* **279**, 8159-68.

**Brunner, F., Schmidt, K., Nielsen, E. B. and Mayer, B.** (1996). Novel guanylyl cyclase inhibitor potently inhibits cyclic GMP accumulation in endothelial cells and relaxation of bovine pulmonary artery. *J Pharmacol Exp Ther* **277**, 48-53.

**Buck, L. and Axel, R.** (1991). A novel multigene family may encode odorant receptors: a molecular basis for odor recognition. *Cell* **65**, 175-87.

**Caccone, A., Garcia, B. A., Mathiopoulos, K. D., Min, G. S., Moriyama, E. N. and Powell, J. R.** (1999). Characterization of the soluble guanylyl cyclase beta-subunit gene in the mosquito *Anopheles gambiae*. *Insect Mol Biol* **8**, 23-30.

**Campos-Ortega, J. A. and Hartenstein, V.** (1997). The Embryonic Development of *Drosophila melanogaster*: Springer.

**Chen, T. Y., Peng, Y. W., Dhallan, R. S., Ahamed, B., Reed, R. R. and Yau, K. W.** (1993). A new subunit of the cyclic nucleotide-gated cation channel in retinal rods. *Nature* **362**, 764-7.

**Cheung, B. H. H., Arellano-Carbajal, F., Rybicki, I. and de Bono, M.** (2004). Soluble guanylate cyclases act in neurons exposed to the body fluid to promote *C. elegans* aggregation behavior. *Curr Biol* **14**, 1105-1111.

**Choi, Y. J., Lee, G., Hall, J. C. and Park, J. H.** (2005). Comparative analysis of Corazonin-encoding genes (Crz's) in *Drosophila* species and functional insights into Crz-expressing neurons. *J Comp Neurol* **482**, 372-85.

**Chrisman, T. D., Garbers, D. L., Parks, M. A. and Hardman, J. G.** (1975). Characterization of particulate and soluble guanylate cyclases from rat lung. *J Biol Chem* **250**, 374-81.

**Clark, A. C., del Campo, M. L. and Ewer, J.** (2004). Neuroendocrine control of larval ecdysis behavior in *Drosophila*: complex regulation by partially redundant neuropeptides. *J Neurosci* **24**, 4283-92.



**Clyne, P. J., Warr, C. G., Freeman, M. R., Lessing, D., Kim, J. and Carlson, J. R.** (1999). A novel family of divergent seven-transmembrane proteins: candidate odorant receptors in *Drosophila*. *Neuron* **22**, 327-38.

**Coates, J. C. and de Bono, M.** (2002). Antagonistic pathways in neurons exposed to body fluid regulate social feeding in *Caenorhabditis elegans*. *Nature* **419**, 925-929.

**Coburn, C. M., Mori, I., Ohshima, Y. and Bargmann, C. I.** (1998). A cyclic nucleotide-gated channel inhibits sensory axon outgrowth in larval and adult *Caenorhabditis elegans*: a distinct pathway for maintenance of sensory axon structure. *Development* **125**, 249-58.

**Corbin, J. D., Cobb, C. E., Beebe, S. J., Granner, D. K., Koch, S. R., Gettys, T. W., Blackmore, P. F., Francis, S. H. and Wells, J. N.** (1988). Mechanism and function of cAMP- and cGMP-dependent protein kinases. *Adv Second Messenger Phosphoprotein Res* **21**, 75-86.

**Corbin, J. D., Turko, I. V., Beasley, A. and Francis, S. H.** (2000). Phosphorylation of phosphodiesterase-5 by cyclic nucleotide-dependent protein kinase alters its catalytic and allosteric cGMP-binding activities. *Eur J Biochem* **267**, 2760-7.

**Craven, P. A. and DeRubertis, F. R.** (1978). Restoration of the responsiveness of purified guanylate cyclase to nitrosoguanidine, nitric oxide, and related activators by heme and hemeproteins. Evidence for involvement of the paramagnetic nitrosyl-heme complex in enzyme activation. *J Biol Chem* **253**, 8433-43.

**Cummins, E. P. and Taylor, C. T.** (2005). Hypoxia-responsive transcription factors. *Pflugers Arch*.

**Dambly-Chaudiere, C., Jamet, E., Burri, M., Bopp, D., Basler, K., Hafen, E., Dumont, N., Spielmann, P., Ghysen, A. and Noll, M.** (1992). The paired box gene *pox* neuro: a determinant of poly-innervated sense organs in *Drosophila*. *Cell* **69**, 159-72.

**Day, J. P., Dow, J. A., Houslay, M. D. and Davies, S. A.** (2005). Cyclic nucleotide phosphodiesterases in *Drosophila melanogaster*. *Biochem J* **388**, 333-42.

**de Bono, M. and Bargmann, C. I.** (1998). A natural variation in a neuropeptide Y homolog modifies social behavior and feeding response in *C. elegans*. *Cell* **94**, 679-689.

**Denninger, J. W., Schelvis, J. P., Brandish, P. E., Zhao, Y., Babcock, G. T. and Marletta, M. A.** (2000). Interaction of soluble guanylate cyclase with YC-1: kinetic and resonance Raman studies. *Biochemistry* **39**, 4191-8.

**Elphick, M. R. and Jones, I. W.** (1998). Localization of soluble guanylyl cyclase alpha-subunit in identified insect neurons. *Brain Res* **800**, 174-9.

**Endo, S., Suzuki, M., Sumi, M., Nairn, A. C., Morita, R., Yamakawa, K., Greengard, P. and Ito, M.** (1999). Molecular identification of human G-substrate, a possible downstream component of the cGMP-dependent protein kinase cascade in cerebellar Purkinje cells. *Proc Natl Acad Sci U S A* **96**, 2467-72.

**Ewer, J.** (2005). Behavioral actions of neuropeptides in invertebrates: Insights from *Drosophila*. *Hormones and Behavior* **in press**.

**Ewer, J., De Vente, J. and Truman, J. W.** (1994). Neuropeptide induction of cyclic GMP increases in the insect CNS: resolution at the level of single identifiable neurons. *J Neurosci* **14**, 7704-12.

- Ewer, J., Gammie, S. C. and Truman, J. W.** (1997). Control of insect ecdysis by a positive-feedback endocrine system: roles of eclosion hormone and ecdysis triggering hormone. *J Exp Biol* **200**, 869-81.
- Ewer, J. and Reynolds, S.** (2002). Neuropeptide control of molting in insects. *Hormones, Brain, and Behavior* **3**, 1-92.
- Fallon, A. M. and Wyatt, G. R.** (1977). Cyclic nucleotide phosphodiesterases in the cricket, *Acheta domesticus*. *Biochim Biophys Acta* **480**, 428-41.
- Fergestad, T. and Broadie, K.** (2001). Interaction of stoned and synaptotagmin in synaptic vesicle endocytosis. *J Neurosci* **21**, 1218-27.
- Filburn, C. R., Karn, J. and Wyatt, G. R.** (1977). Cyclic nucleotide phosphodiesterases of *Hyalophora cecropia* silkworm fat body. *Biochim Biophys Acta* **481**, 152-63.
- Foerster, J., Harteneck, C., Malkewitz, J., Schultz, G. and Koesling, D.** (1996). A functional heme-binding site of soluble guanylyl cyclase requires intact N-termini of alpha 1 and beta 1 subunits. *Eur J Biochem* **240**, 380-6.
- Foster, J. L., Higgins, G. C. and Jackson, F. R.** (1996). Biochemical properties and cellular localization of the *Drosophila* DG1 cGMP-dependent protein kinase. *J Biol Chem* **271**, 23322-8.
- Francis, S. H. and Corbin, J. D.** (1994). Structure and function of cyclic nucleotide-dependent protein kinases. *Annu Rev Physiol* **56**, 237-72.
- Francis, S. H. and Corbin, J. D.** (1999). Cyclic nucleotide-dependent protein kinases: intracellular receptors for cAMP and cGMP action. *Crit Rev Clin Lab Sci* **36**, 275-328.

- Francis, S. H., Turko, I. V. and Corbin, J. D.** (2001). Cyclic nucleotide phosphodiesterases: relating structure and function. *Prog Nucleic Acid Res Mol Biol* **65**, 1-52.
- Friebe, A. and Koesling, D.** (1998). Mechanism of YC-1-induced activation of soluble guanylyl cyclase. *Mol Pharmacol* **53**, 123-7.
- Friebe, A., Mullershausen, F., Smolenski, A., Walter, U., Schultz, G. and Koesling, D.** (1998). YC-1 potentiates nitric oxide- and carbon monoxide-induced cyclic GMP effects in human platelets. *Mol Pharmacol* **54**, 962-7.
- Friebe, A., Schultz, G. and Koesling, D.** (1996). Sensitizing soluble guanylyl cyclase to become a highly CO-sensitive enzyme. *Embo J* **15**, 6863-8.
- Friebe, A., Wedel, B., Harteneck, C., Foerster, J., Schultz, G. and Koesling, D.** (1997). Functions of conserved cysteines of soluble guanylyl cyclase. *Biochemistry* **36**, 1194-8.
- Fukao, M., Mason, H. S., Britton, F. C., Kenyon, J. L., Horowitz, B. and Keef, K. D.** (1999). Cyclic GMP-dependent protein kinase activates cloned BKCa channels expressed in mammalian cells by direct phosphorylation at serine 1072. *J Biol Chem* **274**, 10927-35.
- Fulle, H. J., Vassar, R., Foster, D. C., Yang, R. B., Axel, R. and Garbers, D. L.** (1995). A receptor guanylyl cyclase expressed specifically in olfactory sensory neurons. *Proc Natl Acad Sci U S A* **92**, 3571-5.
- Galindo, K. and Smith, D. P.** (2001). A large family of divergent *Drosophila* odorant-binding proteins expressed in gustatory and olfactory sensilla. *Genetics* **159**, 1059-72.

**Galle, J., Zabel, U., Hubner, U., Hatzelmann, A., Wagner, B., Wanner, C. and Schmidt, H. H.** (1999). Effects of the soluble guanylyl cyclase activator, YC-1, on vascular tone, cyclic GMP levels and phosphodiesterase activity. *Br J Pharmacol* **127**, 195-203.

**Gammie, S. C. and Truman, J. W.** (1997). Neuropeptide hierarchies and the activation of sequential motor behaviors in the hawkmoth, *Manduca sexta*. *J Neurosci* **17**, 4389-97.

**Gammie, S. C. and Truman, J. W.** (1999). Eclosion hormone provides a link between ecdysis-triggering hormone and crustacean cardioactive peptide in the neuroendocrine cascade that controls ecdysis behavior. *J Exp Biol* **202**, 343-52.

**Garbers, D. L.** (1979). Purification of soluble guanylate cyclase from rat lung. *J Biol Chem* **254**, 240-3.

**Garbers, D. L.** (1990). The guanylyl cyclase receptor family. *New Biol* **2**, 499-504.

**Garthwaite, J., Southam, E., Boulton, C. L., Nielsen, E. B., Schmidt, K. and Mayer, B.** (1995). Potent and selective inhibition of nitric oxide-sensitive guanylyl cyclase by 1H-[1,2,4]oxadiazolo[4,3-a]quinoxalin-1-one. *Mol Pharmacol* **48**, 184-8.

**Gerstner, A., Zong, X., Hofmann, F. and Biel, M.** (2000). Molecular cloning and functional characterization of a new modulatory cyclic nucleotide-gated channel subunit from mouse retina. *J Neurosci* **20**, 1324-32.

**Gerzer, R., Bohme, E., Hofmann, F. and Schultz, G.** (1981). Soluble guanylate cyclase purified from bovine lung contains heme and copper. *FEBS Lett* **132**, 71-4.

**Ghysen, A., Dambly-Chaudiere, C., Aceves, E., Jan, L. Y. and Jan, Y. N.**

(1986). Sensory pathways and peripheral pathways in *Drosophila* embryos. *Roux's Arch Dev Biol* **195**, 281-289.

**Gibb, B. J., Wykes, V. and Garthwaite, J.** (2003). Properties of NO-activated

guanylyl cyclases expressed in cells. *Br J Pharmacol* **139**, 1032-40.

**Gibbs, S. M., Becker, A., Hardy, R. W. and Truman, J. W.** (2001). Soluble

guanylate cyclase is required during development for visual system function in *Drosophila*. *J Neurosci* **21**, 7705-14.

**Gibbs, S. M. and Truman, J. W.** (1998). Nitric oxide and cyclic GMP regulate

retinal patterning in the optic lobe of *Drosophila*. *Neuron* **20**, 83-93.

**Gibson, A. D. and Garbers, D. L.** (2000). Guanylyl cyclases as a family of

putative odorant receptors. *Annu Rev Neurosci* **23**, 417-39.

**Gibson, N. J. and Nighorn, A.** (2000). Expression of nitric oxide synthase and

soluble guanylyl cyclase in the developing olfactory system of *Manduca sexta*. *J Comp Neurol* **422**, 191-205.

**Gigliotti, S., Cavaliere, V., Manzi, A., Tino, A., Graziani, F. and Malva, C.**

(1993). A membrane guanylate cyclase *Drosophila* homolog gene exhibits maternal and zygotic expression. *Dev Biol* **159**, 450-61.

**Giuli, G., Roechel, N., Scholl, U., Mattei, M. G. and Guellaen, G.** (1993).

Colocalization of the genes coding for the alpha 3 and beta 3 subunits of soluble guanylyl cyclase to human chromosome 4 at q31.3-q33. *Hum Genet* **91**, 257-60.

- Giuli, G., Scholl, U., Bulle, F. and Guellaen, G.** (1992). Molecular cloning of the cDNAs coding for the two subunits of soluble guanylyl cyclase from human brain. *FEBS Lett* **304**, 83-8.
- Goy, M. F.** (1990). Activation of membrane guanylate cyclase by an invertebrate peptide hormone. *J Biol Chem* **265**, 20220-7.
- Gray, J. M., Karow, D. S., Lu, H., Chang, A. J., Chang, J. S., Ellis, R. E., Marletta, M. A. and Bargmann, C. I.** (2004). Oxygen sensation and social feeding mediated by a *C. elegans* guanylate cyclase homologue. *Nature* **430**, 317-22.
- Greenspan, R. J.** (1997). *Fly Pushing*. Plainview: Cold Spring Harbor Laboratory Press.
- Gross, S. S. and Wolin, M. S.** (1995). Nitric oxide: pathophysiological mechanisms. *Annu Rev Physiol* **57**, 737-69.
- Grueber, W. B., Jan, L. Y. and Jan, Y. N.** (2002). Tiling of the *Drosophila* epidermis by multidendritic sensory neurons. *Development* **129**, 2867-78.
- Guerrant, R. L., Hughes, J. M., Chang, B., Robertson, D. C. and Murad, F.** (1980). Activation of intestinal guanylate cyclase by heat-stable enterotoxin of *Escherichia coli*: studies of tissue specificity, potential receptors, and intermediates. *J Infect Dis* **142**, 220-8.
- Harteneck, C., Wedel, B., Koesling, D., Malkewitz, J., Bohme, E. and Schultz, G.** (1991). Molecular cloning and expression of a new alpha-subunit of soluble guanylyl cyclase. Interchangeability of the alpha-subunits of the enzyme. *FEBS Lett* **292**, 217-22.

**Heginbotham, L., Abramson, T. and MacKinnon, R.** (1992). A functional connection between the pores of distantly related ion channels as revealed by mutant K<sup>+</sup> channels. *Science* **258**, 1152-5.

**Heimbeck, G., Bugnon, V., Gendre, N., Haberlin, C. and Stocker, R. F.** (1999). Smell and taste perception in *Drosophila melanogaster* larva: toxin expression studies in chemosensory neurons. *J Neurosci* **19**, 6599-609.

**Henn, D. K., Baumann, A. and Kaupp, U. B.** (1995). Probing the transmembrane topology of cyclic nucleotide-gated ion channels with a gene fusion approach. *Proc Natl Acad Sci U S A* **92**, 7425-9.

**Hesterlee, S. and Morton, D. B.** (2000). Identification of the cellular target for eclosion hormone in the abdominal transverse nerves of the tobacco hornworm, *Manduca sexta*. *J Comp Neurol* **424**, 339-355.

**Hewes, R. S., Park, D., Gauthier, S. A., Schaefer, A. M. and Taghert, P. H.** (2003). The bHLH protein Dimmed controls neuroendocrine cell differentiation in *Drosophila*. *Development* **130**, 1771-81.

**Hiroi, M., Marion-Poll, F. and Tanimura, T.** (2002). Differentiated response to sugars among labellar chemosensilla in *Drosophila*. *Zoolog Sci* **19**, 1009-18.

**Hoshi, T. and Lahiri, S.** (2004). Cell biology. Oxygen sensing: it's a gas! *Science* **306**, 2050-1.

**Hou, S., Larsen, R. W., Boudko, D., Riley, C. W., Karatan, E., Zimmer, M., Ordal, G. W. and Alam, M.** (2000). Myoglobin-like aerotaxis transducers in Archaea and Bacteria. *Nature* **403**, 540-4.



**Huang, S., Kerschbaum, H. H. and Hermann, A.** (1998). Nitric oxide-mediated cGMP synthesis in Helix neural ganglia. *Brain Res* **780**, 329-36.

**Hudson, M. L., Karow, D. S., Marletta, M. and Morton, D. B.** (2000). Characterization of the soluble guanylyl cyclase gene family in *Caenorhabditis elegans*. In *Soc. Neurosci. Abs.*

**Humbert, P., Niroomand, F., Fischer, G., Mayer, B., Koesling, D., Hirsch, K. D., Gausepohl, H., Frank, R., Schultz, G. and Bohme, E.** (1990). Purification of soluble guanylyl cyclase from bovine lung by a new immunoaffinity chromatographic method. *Eur J Biochem* **190**, 273-8.

**Ignarro, L. J.** (1990). Haem-dependent activation of guanylate cyclase and cyclic GMP formation by endogenous nitric oxide: a unique transduction mechanism for transcellular signaling. *Pharmacol Toxicol* **67**, 1-7.

**Ignarro, L. J., Byrns, R. E., Buga, G. M. and Wood, K. S.** (1987). Endothelium-derived relaxing factor from pulmonary artery and vein possesses pharmacologic and chemical properties identical to those of nitric oxide radical. *Circ Res* **61**, 866-79.

**Ignarro, L. J., Wood, K. S. and Wolin, M. S.** (1982). Activation of purified soluble guanylate cyclase by protoporphyrin IX. *Proc Natl Acad Sci U S A* **79**, 2870-3.

**Inagami, T., Misono, K. S., Fukumi, H., Maki, M., Tanaka, I., Takayanagi, R., Imada, T., Grammer, R. T., Naruse, M., Naruse, K. et al.** (1987). Structure and physiological actions of rat atrial natriuretic factor. *Hypertension* **10**, I113-7.

**Isabel, G., Martin, J. R., Chidami, S., Veenstra, J. A. and Rosay, P.** (2005). AKH-producing neuroendocrine cell ablation decreases trehalose and induces behavioral changes in *Drosophila*. *Am J Physiol Regul Integr Comp Physiol* **288**, R531-8.

**Jahn, H., Nastainczyk, W., Rohrkasten, A., Schneider, T. and Hofmann, F.** (1988). Site-specific phosphorylation of the purified receptor for calcium-channel blockers by cAMP- and cGMP-dependent protein kinases, protein kinase C, calmodulin-dependent protein kinase II and casein kinase II. *Eur J Biochem* **178**, 535-42.

**Jain, R. and Chan, M. K.** (2003). Mechanisms of ligand discrimination by heme proteins. *J Biol Inorg Chem* **8**, 1-11.

**Janssens, S. P., Shimouchi, A., Quertermous, T., Bloch, D. B. and Bloch, K. D.** (1992). Cloning and expression of a cDNA encoding human endothelium-derived relaxing factor/nitric oxide synthase. *J Biol Chem* **267**, 14519-22.

**Jarchau, T., Hausler, C., Markert, T., Pohler, D., Vanderkerckhove, J., De Jonge, H. R., Lohmann, S. M. and Walter, U.** (1994). Cloning, expression, and in situ localization of rat intestinal cGMP-dependent protein kinase II. *Proc Natl Acad Sci U S A* **91**, 9426-30.

**Kalderon, D. and Rubin, G. M.** (1989). cGMP-dependent protein kinase genes in *Drosophila*. *J Biol Chem* **264**, 10738-48.

**Karow, D. S., Pan, D., Tran, R., Pellicena, P., Presley, A., Mathies, R. A. and Marletta, M. A.** (2004). Spectroscopic characterization of the soluble guanylate cyclase-like heme domains from *Vibrio cholerae* and *Thermoanaerobacter tengcongensis*. *Biochemistry* **43**, 10203-11.

**Kaupp, U. B. and Altenhofen, W.** (1992). Cyclic nucleotide-gated channels of vertebrate photoreceptor cells and olfactory epithelium. *Soc Gen Physiol Ser* **47**, 133-50.

**Kaupp, U. B. and Seifert, R.** (2002). Cyclic nucleotide-gated ion channels. *Physiol Rev* **82**, 769-824.

**Kim, S. K. and Rulifson, E. J.** (2004). Conserved mechanisms of glucose sensing and regulation by *Drosophila corpora cardiaca* cells. *Nature* **431**, 316-20.

**Kim, Y. J., Spalovska-Valachova, I., Cho, K. H., Zitnanova, I., Park, Y., Adams, M. E. and Zitnan, D.** (2004). Corazonin receptor signaling in ecdysis initiation. *Proc Natl Acad Sci U S A* **101**, 6704-9.

**Kimura, K. I. and Truman, J. W.** (1990). Postmetamorphic cell death in the nervous and muscular systems of *Drosophila melanogaster*. *J Neurosci* **10**, 403-1.

**Kingan, T. G., Gray, W., Zitnan, D. and Adams, M. E.** (1997). Regulation of ecdysis-triggering hormone release by eclosion hormone. *J Exp Biol* **200**, 3245-56.

**Koesling, D., Harteneck, C., Humbert, P., Bosserhoff, A., Frank, R., Schultz, G. and Bohme, E.** (1990). The primary structure of the larger subunit of soluble guanylyl cyclase from bovine lung. Homology between the two subunits of the enzyme. *FEBS Lett* **266**, 128-32.

**Koesling, D., Herz, J., Gausepohl, H., Niroomand, F., Hinsch, K. D., Mulsch, A., Bohme, E., Schultz, G. and Frank, R.** (1988). The primary structure of the 70 kDa subunit of bovine soluble guanylate cyclase. *FEBS Lett* **239**, 29-34.

**Koglin, M. and Behrends, S.** (2003). A functional domain of the alpha 1 subunit of soluble guanylyl cyclase is necessary for activation of the enzyme by nitric oxide and YC-1 but is not involved in heme binding. *J Biol Chem*.

**Koglin, M., Vehse, K., Budaues, L., Scholz, H. and Behrends, S.** (2001). Nitric oxide activates the beta 2 subunit of soluble guanylyl cyclase in the absence of a second subunit. *J Biol Chem* **276**, 30737-43.

**Kojima, M., Hisaki, K., Matsuo, H. and Kangawa, K.** (1995). A new type soluble guanylyl cyclase, which contains a kinase-like domain: its structure and expression. *Biochem Biophys Res Commun* **217**, 993-1000.

**Kolodkin, A. L., Matthes, D. J., O'Connor, T. P., Patel, N. H., Admon, A., Bentley, D. and Goodman, C. S.** (1992). Fasciclin IV: sequence, expression, and function during growth cone guidance in the grasshopper embryo. *Neuron* **9**, 831-45.

**Komalavilas, P. and Lincoln, T. M.** (1996). Phosphorylation of the inositol 1,4,5-trisphosphate receptor. Cyclic GMP-dependent protein kinase mediates cAMP and cGMP dependent phosphorylation in the intact rat aorta. *J Biol Chem* **271**, 21933-8.

**Korschen, H. G., Beyermann, M., Muller, F., Heck, M., Vantler, M., Koch, K. W., Kellner, R., Wolfrum, U., Bode, C., Hofmann, K. P. et al.** (1999). Interaction of glutamic-acid-rich proteins with the cGMP signalling pathway in rod photoreceptors. *Nature* **400**, 761-6.

**Kretzschmar, D., Hasan, G., Sharma, S., Heisenberg, M. and Benzer, S.** (1997). The swiss cheese mutant causes glial hyperwrapping and brain degeneration in *Drosophila*. *J Neurosci* **17**, 7425-32.

**Krieger, J., Strobel, J., Vogl, A., Hanke, W. and Breer, H.** (1999). Identification of a cyclic nucleotide- and voltage-activated ion channel from insect antennae. *Insect Biochem Mol Biol* **29**, 255-67.

**Kuhn, D. T., Sawyer, M., Packert, G., Turenchalk, G., Mack, J. A., Sprey, T. E., Gustavson, E. and Kornberg, T. B.** (1992). Development of the *D. melanogaster* caudal segments involves suppression of the ventral regions of A8, A9 and A10.

*Development* **116**, 11-20.

**Kuhn, D. T., Turenchalk, G., Mack, J. A., Packert, G. and Kornberg, T. B.** (1995). Analysis of the genes involved in organizing the tail segments of the *Drosophila melanogaster* embryo. *Mech Dev* **53**, 3-13.

**Kuo, J. F. and Greengard, P.** (1974). Purification and characterization of cyclic GMP-dependent protein kinases. *Methods Enzymol* **38**, 329-50.

**Kuo, J. F., Wyatt, G. R. and Greengard, P.** (1971). Cyclic nucleotide-dependent protein kinases. IX. Partial purification and some properties of guanosine 3',5'-monophosphate-dependent and adenosine 3',5'-monophosphate-dependent protein kinases from various tissues and species of Arthropoda. *J Biol Chem* **246**, 7159-67.

**L'Etoile, N. D. and Bargmann, C. I.** (2000). Olfaction and odor discrimination are mediated by the *C. elegans* guanylyl cyclase ODR-1. *Neuron* **25**, 575-86.

**L'Etoile, N. D., Coburn, C. M., Eastham, J., Kistler, A., Gallegos, G. and Bargmann, C. I.** (2002). The cyclic GMP-dependent protein kinase EGL-4 regulates olfactory adaptation in *C. elegans*. *Neuron* **36**, 1079-89.

**Langlais, K. K., Stewart, J. A. and Morton, D. B.** (2004). Preliminary characterization of two atypical soluble guanylyl cyclases in the central and peripheral nervous system of *Drosophila melanogaster*. *J Exp Biol* **207**, 2323-38.

**Lawrence, D. W. and Pryzwansky, K. B.** (2001). The vasodilator-stimulated phosphoprotein is regulated by cyclic GMP-dependent protein kinase during neutrophil spreading. *J Immunol* **166**, 5550-6.

**Lenz, C., Williamson, M., Hansen, G. N. and Grimmelikhuijzen, C. J.** (2001). Identification of four *Drosophila* allatostatins as the cognate ligands for the *Drosophila* orphan receptor DAR-2. *Biochem Biophys Res Commun* **286**, 1117-22.

**Levy, N. S., Bakalyar, H. A. and Reed, R. R.** (1991). Signal transduction in olfactory neurons. *J Steroid Biochem Mol Biol* **39**, 633-7.

**Lincoln, T. M., Dey, N. and Sellak, H.** (2001). Invited review: cGMP-dependent protein kinase signaling mechanisms in smooth muscle: from the regulation of tone to gene expression. *J Appl Physiol* **91**, 1421-30.

**Littleton, J. T. and Ganetzky, B.** (2000). Ion channels and synaptic organization: analysis of the *Drosophila* genome. *Neuron* **26**, 35-43.

**Liu, W., Yoon, J., Burg, M., Chen, L. and Pak, W. L.** (1995). Molecular characterization of two *Drosophila* guanylate cyclases expressed in the nervous system. *J Biol Chem* **270**, 12418-27.

**Liu, Y., Ruoho, A. E., Rao, V. D. and Hurley, J. H.** (1997). Catalytic mechanism of the adenylyl and guanylyl cyclases: modeling and mutational analysis. *Proc Natl Acad Sci U S A* **94**, 13414-9.

**Lohmann, S. M., Vaandrager, A. B., Smolenski, A., Walter, U. and De Jonge, H. R.** (1997). Distinct and specific functions of cGMP-dependent protein kinases. *Trends Biochem Sci* **22**, 307-12.

**Lowenstein, C. J., Glatt, C. S., Bredt, D. S. and Snyder, S. H.** (1992). Cloned and expressed macrophage nitric oxide synthase contrasts with the brain enzyme. *Proc Natl Acad Sci U S A* **89**, 6711-5.

**Lucas, K. A., Pitari, G. M., Kazerounian, S., Ruiz-Stewart, I., Park, J., Schulz, S., Chepenik, K. P. and Waldman, S. A.** (2000). Guanylyl cyclases and signaling by cyclic GMP. *Pharmacol Rev* **52**, 375-414.

**Ludwig, A., Zong, X., Jeglitsch, M., Hofmann, F. and Biel, M.** (1998). A family of hyperpolarization-activated mammalian cation channels. *Nature* **393**, 587-91.

**MacPherson, M. R., Lohmann, S. M. and Davies, S. A.** (2004). Analysis of *Drosophila* cGMP-dependent protein kinases and assessment of their *in vivo* roles by targeted expression in a renal transporting epithelium. *J Biol Chem* **279**, 40026-34.

**Marx, T., Gisselmann, G., Stortkuhl, K. F., Hovemann, B. T. and Hatt, H.** (1999). Molecular cloning of a putative voltage- and cyclic nucleotide-gated ion channel present in the antennae and eyes of *Drosophila melanogaster*. *Invert Neurosci* **4**, 55-63.

**Mcguire, S. E., Le, P. T., Osborne, A. J., Matsumoto, K. and Davis, R. L.** (2003). Temporal and regional gene expression targeting with the conventional GAL4/UAS system in *Drosophila*. In *A. Dros. Res. Conf.*

**McNabb, S. L., Baker, J. D., Agapite, J., Steller, H., Riddiford, L. M. and Truman, J. W.** (1997). Disruption of a behavioral sequence by targeted death of peptidergic neurons in *Drosophila*. *Neuron* **19**, 813-23.

**McNeil, L., Chinkers, M. and Forte, M.** (1995). Identification, characterization, and developmental regulation of a receptor guanylyl cyclase expressed during early stages of *Drosophila* development. *J Biol Chem* **270**, 7189-96.

**Merte, J. and Nichols, R.** (2002). Drosophila melanogaster FMRFamide-containing peptides: redundant or diverse functions? *Peptides* **23**, 209-20.

**Meunier, N., Marion-Poll, F., Rospars, J. P. and Tanimura, T.** (2003). Peripheral coding of bitter taste in Drosophila. *J Neurobiol* **56**, 139-52.

**Miyazu, M., Tanimura, T. and Sokabe, M.** (2000). Molecular cloning and characterization of a putative cyclic nucleotide-gated channel from Drosophila melanogaster. *Insect Mol Biol* **9**, 283-92.

**Molday, R. S., Molday, L. L., Dose, A., Clark-Lewis, I., Illing, M., Cook, N. J., Eismann, E. and Kaupp, U. B.** (1991). The cGMP-gated channel of the rod photoreceptor cell characterization and orientation of the amino terminus. *J Biol Chem* **266**, 21917-22.

**Moncada, S. and Higgs, E. A.** (1995). Molecular mechanisms and therapeutic strategies related to nitric oxide. *Faseb J* **9**, 1319-30.

**Moreno, L., Gonzalez-Luis, G., Cogolludo, A., Lodi, F., Lopez-Farre, A., Tamargo, J., Villamor, E. and Perez-Vizcaino, F.** (2005). Soluble guanylyl cyclase during postnatal porcine pulmonary maturation. *Am J Physiol Lung Cell Mol Physiol* **288**, L125-30.

**Moro, M. A., Russel, R. J., Cellek, S., Lizasoain, I., Su, Y., Darley-Usmar, V. M., Radomski, M. W. and Moncada, S.** (1996). cGMP mediates the vascular and platelet actions of nitric oxide: confirmation using an inhibitor of the soluble guanylyl cyclase. *Proc Natl Acad Sci U S A* **93**, 1480-5.



**Morton, D. B.** (1996). Neuropeptide-stimulated cyclic guanosine monophosphate immunoreactivity in the neurosecretory terminals of a neurohemal organ. *J Neurobiol* **29**, 341-53.

**Morton, D. B.** (2000). Localization of the NO-insensitive soluble guanylyl cyclase, MsGC-Beta3, to the abdominal nerves of *Manduca* suggests a role in eclosion hormone action. *Soc. Neurosci. Abstracts* **26**.

**Morton, D. B.** (2004a). Atypical soluble guanylyl cyclases in *Drosophila* can function as molecular oxygen sensors. *J Biol Chem* **279**, 50651-3.

**Morton, D. B.** (2004b). Invertebrates yield a plethora of atypical guanylyl cyclases. *Mol Neurobiol* **29**, 97-116.

**Morton, D. B. and Anderson, E. A.** (2003). MsGC- $\beta$ 3 forms active homodimers and inactive heterodimers with NO-sensitive soluble guanylyl cyclase subunits. *J. Exp. Biol.* **206**, 937-947.

**Morton, D. B. and Giunta, M. A.** (1992). Eclosion hormone stimulates cyclic GMP levels in *Manduca sexta* nervous tissue via arachidonic acid metabolism with little or no contribution from the production of nitric oxide. *J Neurochem* **59**, 1522-30.

**Morton, D. B. and Hudson, M. L.** (2002). Cyclic GMP regulation and function in insects. *Adv. Insect Physiol.* **29**, 1-54.

**Morton, D. B., Hudson, M. L., Waters, E. and O'Shea, M.** (1999). Soluble guanylyl cyclases in *Caenorhabditis elegans*: NO is not the answer. *Curr Biol* **9**, R546-7.

**Morton, D. B., Langlais, K. K., Stewart, J. A. and Vermehren, A.** (2005). Comparison of the properties of the five soluble guanylyl cyclase subunits in *Drosophila melanogaster*. *Journal of Insect Science* **5**.

**Morton, D. B. and Nighorn, A.** (2003). MsGC-II, a receptor guanylyl cyclase isolated from the CNS of *Manduca sexta* that is inhibited by calcium. *J Neurochem* **84**, 363-72.

**Morton, D. B. and Simpson, P. J.** (2002). Cellular signalling in eclosion hormone action. *J Insect Physiol* **48**, 1-13.

**Morton, D. B. and Truman, J. W.** (1985). Steroid regulation of the peptide-mediated increase in cyclic GMP in the nervous system of the hawkmoth, *Manduca sexta*. *J Comp Physiol [A]* **157**, 423-32.

**Morton, D. B. and Truman, J. W.** (1986). Substrate phosphoprotein availability regulates eclosion hormone sensitivity in an insect CNS. *Nature* **323**, 264-7.

**Muller, U.** (1997). The nitric oxide system in insects. *Prog Neurobiol* **51**, 363-81.

**Murthy, K. S.** (2004). Modulation of soluble guanylate cyclase activity by phosphorylation. *Neurochem Int* **45**, 845-51.

**Nakane, M., Arai, K., Saheki, S., Kuno, T., Buechler, W. and Murad, F.** (1990). Molecular cloning and expression of cDNAs coding for soluble guanylate cyclase from rat lung. *J Biol Chem* **265**, 16841-5.

**Nakane, M., Saheki, S., Kuno, T., Ishii, K. and Murad, F.** (1988). Molecular cloning of a cDNA coding for 70 kilodalton subunit of soluble guanylate cyclase from rat lung. *Biochem Biophys Res Commun* **157**, 1139-47.

**Nichols, R., McCormick, J., Cohen, M., Howe, E., Jean, C., Paisley, K. and Rosario, C.** (1999). Differential processing of neuropeptides influences *Drosophila* heart rate. *J Neurogenet* **13**, 89-104.

**Nighorn, A., Byrnes, K. A. and Morton, D. B. (1999).** Identification and characterization of a novel beta subunit of soluble guanylyl cyclase that is active in the absence of a second subunit and is relatively insensitive to nitric oxide. *J Biol Chem* **274**, 2525-31.

**Nighorn, A., Gibson, N. J., Rivers, D. M., Hildebrand, J. G. and Morton, D. B. (1998).** The nitric oxide-cGMP pathway may mediate communication between sensory afferents and projection neurons in the antennal lobe of *Manduca sexta*. *J Neurosci* **18**, 7244-55.

**Nighorn, A., Simpson, P. J. and Morton, D. B. (2001).** The novel guanylyl cyclase MsGC-I is strongly expressed in higher-order neuropils in the brain of *Manduca sexta*. *J Exp Biol* **204**, 305-14.

**Olesen, S. P., Drejer, J., Axelsson, O., Moldt, P., Bang, L., Nielsen-Kudsk, J. E., Busse, R. and Mulsch, A. (1998).** Characterization of NS 2028 as a specific inhibitor of soluble guanylyl cyclase. *Br J Pharmacol* **123**, 299-309.

**Orstavik, S., Solberg, R., Tasken, K., Nordahl, M., Altherr, M. R., Hansson, V., Jahnsen, T. and Sandberg, M. (1996).** Molecular cloning, cDNA structure, and chromosomal localization of the human type II cGMP-dependent protein kinase. *Biochem Biophys Res Commun* **220**, 759-65.

**Osborne, K. A., Robichon, A., Burgess, E., Butland, S., Shaw, R. A., Coulthard, A., Pereira, H. S., Greenspan, R. J. and Sokolowski, M. B. (1997).** Natural behavior polymorphism due to a cGMP-dependent protein kinase of *Drosophila*. *Science* **277**, 834-6.

**Osbourne, K. A., Robichon, A. and Burgess, E.** (1997). Natural behavioral polymorphism due to a cGMP-dependent protein kinase of *Drosophila*. *Science* **277**, 834-836.

**Palczewski, K., Polans, A. S., Baehr, W. and Ames, J. B.** (2000). Ca(2+)-binding proteins in the retina: structure, function, and the etiology of human visual diseases. *Bioessays* **22**, 337-50.

**Palmer, R., Ferrige, A. and Moncada, S.** (1987). Nitric oxide release accounts for the biological activity of endothelium-derived relaxing factor. *Nature* **327**, 524-526.

**Park, J. H., Schroeder, A. J., Helfrich-Forster, C., Jackson, F. R. and Ewer, J.** (2003). Targeted ablation of CCAP neuropeptide-containing neurons of *Drosophila* causes specific defects in execution and circadian timing of ecdysis behavior.

*Development* **130**, 2645-56.

**Park, Y., Filippov, V., Gill, S. S. and Adams, M. E.** (2002). Deletion of the ecdysis-triggering hormone gene leads to lethal ecdysis deficiency. *Development* **129**, 493-503.

**Pellicena, P., Karow, D. S., Boon, E. M., Marletta, M. A. and Kuriyan, J.** (2004). Crystal structure of an oxygen-binding heme domain related to soluble guanylate cyclases. *Proc Natl Acad Sci U S A* **101**, 12854-9.

**Pfeifer, A., Ruth, P., Dostmann, W., Sausbier, M., Klatt, P. and Hofmann, F.** (1999). Structure and function of cGMP-dependent protein kinases. *Rev Physiol Biochem Pharmacol* **135**, 105-49.

**Polleux, F., Morrow, T. and Ghosh, A.** (2000). Semaphorin 3A is a chemoattractant for cortical apical dendrites. *Nature* **404**, 567-73.

**Prabhakar, N. R.** (2000). Oxygen sensing by the carotid body chemoreceptors. *J Appl Physiol* **88**, 2287-95.

**Prast, H. and Philippu, A.** (2001). Nitric oxide as modulator of neuronal function. *Prog Neurobiol* **64**, 51-68.

**Raeymaekers, L., Eggermont, J. A., Wuytack, F. and Casteels, R.** (1990). Effects of cyclic nucleotide dependent protein kinases on the endoplasmic reticulum Ca<sup>2+</sup> pump of bovine pulmonary artery. *Cell Calcium* **11**, 261-8.

**Rao, M. C., Guandalini, S., Laird, W. J. and Field, M.** (1979). Effects of heat-stable enterotoxin of *Yersinia enterocolitica* on ion transport and cyclic guanosine 3',5'-monophosphate metabolism in rabbit ileum. *Infect Immun* **26**, 875-8.

**Riddle, D. L., Blumenthal, T., Meyer, J. and Priess, J. R.** (1997). Genetic and environmental regulation of dauer larva development. In *C. elegans II*, pp. 739-768. Plainview, NY: Cold Spring Harbor Press.

**Rodrigues, V. and Siddiqi, O.** (1981). A gustatory mutant of *Drosophila* defective in pyranose receptors. *Mol Gen Genet* **181**, 406-8.

**Rogers, C., Reale, V., Kim, K., Chatwin, H., Li, C., Evans, P. and de Bono, M.** (2003). Inhibition of *Caenorhabditis elegans* social feeding by FMRFamide-related peptide activation of NPR-1. *Nat Neurosci* **6**, 1178-85.

**Russwurm, M., Behrends, S., Harteneck, C. and Koesling, D.** (1998). Functional properties of a naturally occurring isoform of soluble guanylyl cyclase. *Biochem J* **335** ( Pt 1), 125-30.

**Russwurm, M., Wittau, N. and Koesling, D.** (2001). Guanylyl cyclase/PSD-95 interaction: targeting of the nitric oxide-sensitive alpha2beta1 guanylyl cyclase to synaptic membranes. *J Biol Chem* **276**, 44647-52.

**Rybalkin, S. D., Yan, C., Bornfeldt, K. E. and Beavo, J. A.** (2003). Cyclic GMP phosphodiesterases and regulation of smooth muscle function. *Circ Res* **93**, 280-91.

**Sambrook, J., Fritsch, E. F. and Maniatis, T.** (1989). *Molecular Cloning*. Cold Spring Harbor: Cold Spring Harbor Press.

**Schmachtenberg, O. and Bicker, G.** (1999). Nitric oxide and cyclic GMP modulate photoreceptor cell responses in the visual system of the locust. *J Exp Biol* **202**, 13-20.

**Scholz, N. L., Chang, E. S., Graubard, K. and Truman, J. W.** (1998). The NO/cGMP pathway and the development of neural networks in postembryonic lobsters. *J Neurobiol* **34**, 208-26.

**Schrammel, A., Behrends, S., Schmidt, K., Koesling, D. and Mayer, B.** (1996). Characterization of 1H-[1,2,4]oxadiazolo[4,3-a]quinoxalin-1-one as a heme-site inhibitor of nitric oxide-sensitive guanylyl cyclase. *Mol Pharmacol* **50**, 1-5.

**Schulz, S., Green, C. K., Yuen, P. S. and Garbers, D. L.** (1990). Guanylyl cyclase is a heat-stable enterotoxin receptor. *Cell* **63**, 941-8.

**Schulz, S., Singh, S., Bellet, R. A., Singh, G., Tubb, D. J., Chin, H. and Garbers, D. L.** (1989). The primary structure of a plasma membrane guanylate cyclase demonstrates diversity within this new receptor family. *Cell* **58**, 1155-62.

**Schulz, S., Wedel, B. J., Matthews, A. and Garbers, D. L.** (1998). The cloning and expression of a new guanylyl cyclase orphan receptor. *J Biol Chem* **273**, 1032-7.

**Scott, J. D.** (1991). Cyclic nucleotide-dependent protein kinases. *Pharmacol Ther* **50**, 123-45.

**Scott, K., Brady, R., Jr., Cravchik, A., Morozov, P., Rzhetsky, A., Zuker, C. and Axel, R.** (2001). A chemosensory gene family encoding candidate gustatory and olfactory receptors in *Drosophila*. *Cell* **104**, 661-73.

**Seidel, C. and Bicker, G.** (2000). Nitric oxide and cGMP influence axonogenesis of antennal pioneer neurons. *Development* **127**, 4541-9.

**Semenza, G. L.** (2000). HIF-1: mediator of physiological and pathophysiological responses to hypoxia. *J Appl Physiol* **88**, 1474-80.

**Sessa, W. C., Harrison, J. K., Barber, C. M., Zeng, D., Durieux, M. E., D'Angelo, D. D., Lynch, K. R. and Peach, M. J.** (1992). Molecular cloning and expression of a cDNA encoding endothelial cell nitric oxide synthase. *J Biol Chem* **267**, 15274-6.

**Shah, S. and Hyde, D. R.** (1995). Two *Drosophila* genes that encode the alpha and beta subunits of the brain soluble guanylyl cyclase. *J Biol Chem* **270**, 15368-76.

**Shanbhag, S. R., Park, S. K., Pikielny, C. W. and Steinbrecht, R. A.** (2001). Gustatory organs of *Drosophila melanogaster*: fine structure and expression of the putative odorant-binding protein PBPRP2. *Cell Tissue Res* **304**, 423-37.

**Sharma, Y., Cheung, U., Larsen, E. W. and Eberl, D. F.** (2002). PPTGAL, a convenient Gal4 P-element vector for testing expression of enhancer fragments in *drosophila*. *Genesis* **34**, 115-8.

**Siegmund, T. and Korge, G.** (2001). Innervation of the ring gland of *Drosophila melanogaster*. *J Comp Neurol* **431**, 481-91.

**Simpson, P. J., Nighorn, A. and Morton, D. B.** (1999). Identification of a novel guanylyl cyclase that is related to receptor guanylyl cyclases, but lacks extracellular and transmembrane domains. *J Biol Chem* **274**, 4440-6.

**Smolenski, A., Bachmann, C., Reinhard, K., Honig-Liedl, P., Jarchau, T., Hoschuetzky, H. and Walter, U.** (1998). Analysis and regulation of vasodilator-stimulated phosphoprotein serine 239 phosphorylation in vitro and in intact cells using a phosphospecific monoclonal antibody. *J Biol Chem* **273**, 20029-35.

**Soderling, S. H. and Beavo, J. A.** (2000). Regulation of cAMP and cGMP signaling: new phosphodiesterases and new functions. *Curr Opin Cell Biol* **12**, 174-9.

**Sokolowski, M. B.** (1980). Foraging strategies of *Drosophila melanogaster*: a chromosomal analysis. *Behav Genet* **10**, 291-302.

**Sokolowski, M. B.** (1998). Genes for normal behavioral variation: recent clues from flies and worms. *Neuron* **21**, 463-6.

**Solti, M., Devay, P., Kiss, I., Londesborough, J. and Friedrich, P.** (1983). Cyclic nucleotide phosphodiesterases in larval brain of wild type and dunce mutant strains of *Drosophila melanogaster*: isoenzyme pattern and activation by Ca<sup>2+</sup>/calmodulin. *Biochem Biophys Res Commun* **111**, 652-8.

**Song, H., Ming, G., He, Z., Lehmann, M., McKerracher, L., Tessier-Lavigne, M. and Poo, M.** (1998). Conversion of neuronal growth cone responses from repulsion to attraction by cyclic nucleotides. *Science* **281**, 1515-8.

**Stansberry, J., Baude, E. J., Taylor, M. K., Chen, P. J., Jin, S. W., Ellis, R. E. and Uhler, M. D.** (2001). A cGMP-dependent protein kinase is implicated in wild-type motility in *C. elegans*. *J Neurochem* **76**, 1177-87.



**Stasch, J. P., Alonso-Alija, C., Apeler, H., Dembowski, K., Feurer, A., Minuth, T., Perzborn, E., Schramm, M. and Straub, A.** (2002a). Pharmacological actions of a novel NO-independent guanylyl cyclase stimulator, BAY 41-8543: in vitro studies. *Br J Pharmacol* **135**, 333-43.

**Stasch, J. P., Becker, E. M., Alonso-Alija, C., Apeler, H., Dembowski, K., Feurer, A., Gerzer, R., Minuth, T., Perzborn, E., Pleiss, U. et al.** (2001). NO-independent regulatory site on soluble guanylate cyclase. *Nature* **410**, 212-5.

**Stasch, J. P., Schmidt, P., Alonso-Alija, C., Apeler, H., Dembowski, K., Haerter, M., Heil, M., Minuth, T., Perzborn, E., Pleiss, U. et al.** (2002b). NO- and haem-independent activation of soluble guanylyl cyclase: molecular basis and cardiovascular implications of a new pharmacological principle. *Br J Pharmacol* **136**, 773-83.

**Steinlen, S., Klumpp, S. and Schultz, J. E.** (1990). Guanylate cyclase in olfactory cilia from rat and pig. *Biochim Biophys Acta* **1054**, 69-72.

**Stocker, R. F.** (1994). The organization of the chemosensory system in *Drosophila melanogaster*: a review. *Cell Tissue Res* **275**, 3-26.

**Stone, J. R. and Marletta, M. A.** (1994). Soluble guanylate cyclase from bovine lung: activation with nitric oxide and carbon monoxide and spectral characterization of the ferrous and ferric states. *Biochemistry* **33**, 5636-40.

**Stryer, L.** (1991). Visual excitation and recovery. *J Biol Chem* **266**, 10711-4.

**Stryer, L.** (1996). Vision: from photon to perception. *Proc Natl Acad Sci U S A* **93**, 557-9.

**Sullivan, W., Ashburner, M., and Hawley, R.S.** (2000). *Drosophila* Protocols. Cold Spring Harbor: Cold Spring Harbor: Cold Spring Harbor Laboratory Press.

**Suster, M. L., Martin, J. R., Sung, C. and Robinow, S.** (2003). Targeted expression of tetanus toxin reveals sets of neurons involved in larval locomotion in *Drosophila*. *J Neurobiol* **55**, 233-46.

**Suster, M. L., Seugnet, L., Bate, M. and Sokolowski, M. B.** (2004). Refining GAL4-driven transgene expression in *Drosophila* with a GAL80 enhancer-trap. *Genesis* **39**, 240-5.

**Sweeney, S. T., Broadie, K., Keane, J., Niemann, H. and O'Kane, C. J.** (1995). Targeted expression of tetanus toxin light chain in *Drosophila* specifically eliminates synaptic transmission and causes behavioral defects. *Neuron* **14**, 341-51.

**Tamura, N., Itoh, H., Ogawa, Y., Nakagawa, O., Harada, M., Chun, T. H., Suga, S., Yoshimasa, T. and Nakao, K.** (1996). cDNA cloning and gene expression of human type Ialpha cGMP-dependent protein kinase. *Hypertension* **27**, 552-7.

**Taylor, C. A., Winther, A. M., Siviter, R. J., Shirras, A. D., Isaac, R. E. and Nassel, D. R.** (2004). Identification of a proctolin preprohormone gene (Proct) of *Drosophila melanogaster*: expression and predicted prohormone processing. *J Neurobiol* **58**, 379-91.

**Tessier-Lavigne, M. and Goodman, C. S.** (1996). The molecular biology of axon guidance. *Science* **274**, 1123-33.

**Thibault, S. T., Singer, M. A., Miyazaki, W. Y., Milash, B., Dompe, N. A., Singh, C. M., Buchholz, R., Demsky, M., Fawcett, R., Francis-Lang, H. L. et al.**

(2004). A complementary transposon tool kit for *Drosophila melanogaster* using P and piggyBac. *Nat Genet* **36**, 283-7.

**Thorne, N., Chromey, C., Bray, S. and Amrein, H.** (2004). Taste perception and coding in *Drosophila*. *Curr Biol* **14**, 1065-79.

**Truman, J. W., De Vente, J. and Ball, E. E.** (1996). Nitric oxide-sensitive guanylate cyclase activity is associated with the maturational phase of neuronal development in insects. *Development* **122**, 3949-58.

**Truman, J. W., Mumby, S. M. and Welch, S. K.** (1979). Involvement of cyclic GMP in the release of stereotyped behavior patterns in moths by a peptide hormone. *J. Exp. Biol.* **84**, 201-212.

**Tucker, C. L., Hurley, J. H., Miller, T. R. and Hurley, J. B.** (1998). Two amino acid substitutions convert a guanylyl cyclase, RetGC-1, into an adenylyl cyclase. *Proc Natl Acad Sci U S A* **95**, 5993-7.

**Turko, I. V., Francis, S. H. and Corbin, J. D.** (1998). Potential roles of conserved amino acids in the catalytic domain of the cGMP-binding cGMP-specific phosphodiesterase. *J Biol Chem* **273**, 6460-6.

**Vaandrager, A. B., Tilly, B. C., Smolenski, A., Schneider-Rasp, S., Bot, A. G., Edixhoven, M., Scholte, B. J., Jarchau, T., Walter, U., Lohmann, S. M. et al.** (1997). cGMP stimulation of cystic fibrosis transmembrane conductance regulator Cl<sup>-</sup> channels co-expressed with cGMP-dependent protein kinase type II but not type Iβ. *J Biol Chem* **272**, 4195-200.

**Van der Horst, D. J.** (2003). Insect adipokinetic hormones: release and integration of flight energy metabolism. *Comp Biochem Physiol B Biochem Mol Biol* **136**, 217-26.

**Varnum, M. D., Black, K. D. and Zagotta, W. N.** (1995). Molecular mechanism for ligand discrimination of cyclic nucleotide-gated channels. *Neuron* **15**, 619-25.

**Vosshall, L. B.** (2000). Olfaction in *Drosophila*. *Curr Opin Neurobiol* **10**, 498-503.

**Wagner, C., Russwurm, M., Jager, R., Friebe, A. and Koesling, D.** (2005). Dimerization of NO-sensitive guanylyl cyclase requires the alpha N terminus. *J Biol Chem.*

**Wang, G. R., Zhu, Y., Halushka, P. V., Lincoln, T. M. and Mendelsohn, M. E.** (1998). Mechanism of platelet inhibition by nitric oxide: in vivo phosphorylation of thromboxane receptor by cyclic GMP-dependent protein kinase. *Proc Natl Acad Sci U S A* **95**, 4888-93.

**Wannamaker, C. M. and Rice, J. A.** (2000). Effects of hypoxia on movements and behavior of selected estuarine organisms from the southeastern United States. *J. Exp. Mar. Biol. Ecol.* **249**, 145-163.

**Wedel, B., Humbert, P., Harteneck, C., Foerster, J., Malkewitz, J., Bohme, E., Schultz, G. and Koesling, D.** (1994). Mutation of His-105 in the beta 1 subunit yields a nitric oxide-insensitive form of soluble guanylyl cyclase. *Proc Natl Acad Sci U S A* **91**, 2592-6.

**Wildemann, B. and Bicker, G.** (1999). Developmental expression of nitric oxide/cyclic GMP synthesizing cells in the nervous system of *Drosophila melanogaster*. *J Neurobiol* **38**, 1-15.

**Williams, S. E., Wootton, P., Mason, H. S., Bould, J., Iles, D. E., Riccardi, D., Peers, C. and Kemp, P. J.** (2004). Hemoxygenase-2 is an oxygen sensor for a calcium-sensitive potassium channel. *Science* **306**, 2093-7.

**Wilson, E. M. and Chinkers, M.** (1995). Identification of sequences mediating guanylyl cyclase dimerization. *Biochemistry* **34**, 4696-701.

**Winberg, M. L., Mitchell, K. J. and Goodman, C. S.** (1998). Genetic analysis of the mechanisms controlling target selection: complementary and combinatorial functions of netrins, semaphorins, and IgCAMs. *Cell* **93**, 581-91.

**Wingrove, J. A. and O'Farrell, P. H.** (1999). Nitric oxide contributes to behavioral, cellular, and developmental responses to low oxygen in *Drosophila*. *Cell* **98**, 105-14.

**Wolf, E., Kim, P. S. and Berger, B.** (1997). MultiCoil: a program for predicting two- and three-stranded coiled coils. *Protein Sci* **6**, 1179-89.

**Wolin, M. S., Wood, K. S. and Ignarro, L. J.** (1982). Guanylate cyclase from bovine lung. A kinetic analysis of the regulation of the purified soluble enzyme by protoporphyrin IX, heme, and nitrosyl-heme. *J Biol Chem* **257**, 13312-20.

**Wong, S. K., Ma, C. P., Foster, D. C., Chen, A. Y. and Garbers, D. L.** (1995). The guanylyl cyclase-A receptor transduces an atrial natriuretic peptide/ATP activation signal in the absence of other proteins. *J Biol Chem* **270**, 30818-22.

- Wright, J. W., Schwinof, K. M., Snyder, M. A. and Copenhaver, P. F. (1998).** A delayed role for nitric oxide-sensitive guanylate cyclases in a migratory population of embryonic neurons. *Dev Biol* **204**, 15-33.
- Wu, C. C., Ko, F. N., Kuo, S. C., Lee, F. Y. and Teng, C. M. (1995).** YC-1 inhibited human platelet aggregation through NO-independent activation of soluble guanylate cyclase. *Br J Pharmacol* **116**, 1973-8.
- Wu, R. S. (2002).** Hypoxia: from molecular responses to ecosystem responses. *Mar Pollut Bull* **45**, 35-45.
- Yang, H. and Kunes, S. (2004).** Nonvesicular release of acetylcholine is required for axon targeting in the Drosophila visual system. *Proc Natl Acad Sci U S A* **101**, 15213-8.
- Yang, R. B., Foster, D. C., Garbers, D. L. and Fulle, H. J. (1995).** Two membrane forms of guanylyl cyclase found in the eye. *Proc Natl Acad Sci U S A* **92**, 602-6.
- Yang, R. B. and Garbers, D. L. (1997).** Two eye guanylyl cyclases are expressed in the same photoreceptor cells and form homomers in preference to heteromers. *J Biol Chem* **272**, 13738-42.
- Yocum, R. R. and Johnston, M. (1984).** Molecular cloning of the GAL80 gene from *Saccharomyces cerevisiae* and characterization of a gal80 deletion. *Gene* **32**, 75-82.
- Yu, S., Avery, L., Baude, E. and Garbers, D. L. (1997).** Guanylyl cyclase expression in specific sensory neurons: a new family of chemosensory receptors. *Proc Natl Acad Sci U S A* **94**, 3384-7.

- Yuen, P. S., Potter, L. R. and Garbers, D. L.** (1990). A new form of guanylyl cyclase is preferentially expressed in rat kidney. *Biochemistry* **29**, 10872-8.
- Zabel, U., Hausler, C., Weeger, M. and Schmidt, H. H.** (1999). Homodimerization of soluble guanylyl cyclase subunits. Dimerization analysis using a glutathione s-transferase affinity tag. *J Biol Chem* **274**, 18149-52.
- Zabel, U., Weeger, M., La, M. and Schmidt, H. H.** (1998). Human soluble guanylate cyclase: functional expression and revised isoenzyme family. *Biochem J* **335** (Pt 1), 51-7.
- Zayas, R. M., Qazi, S., Morton, D. B. and Trimmer, B. A.** (2000). Neurons involved in nitric oxide-mediated cGMP signaling in the tobacco hornworm, *Manduca sexta*. *J Comp Neurol* **419**, 422-38.
- Zeidler, M. P., Tan, C., Bellaiche, Y., Cherry, S., Hader, S., Gayko, U. and Perrimon, N.** (2004). Temperature-sensitive control of protein activity by conditionally splicing inteins. *Nat Biotechnol* **22**, 871-6.
- Zhang, G., Liu, Y., Qin, J., Vo, B., Tang, W. J., Ruoho, A. E. and Hurley, J. H.** (1997a). Characterization and crystallization of a minimal catalytic core domain from mammalian type II adenylyl cyclase. *Protein Sci* **6**, 903-8.
- Zhang, G., Liu, Y., Ruoho, A. E. and Hurley, J. H.** (1997b). Structure of the adenylyl cyclase catalytic core. *Nature* **386**, 247-53.
- Zhao, Y., Brandish, P. E., DiValentin, M., Schelvis, J. P., Babcock, G. T. and Marletta, M. A.** (2000). Inhibition of soluble guanylate cyclase by ODQ. *Biochemistry* **39**, 10848-54.

**Zhao, Y., Schelvis, J. P., Babcock, G. T. and Marletta, M. A. (1998).**

Identification of histidine 105 in the beta1 subunit of soluble guanylate cyclase as the heme proximal ligand. *Biochemistry* **37**, 4502-9.

**Zhou, Z., Gross, S., Roussos, C., Meurer, S., Muller-Esterl, W. and**

**Papapetropoulos, A. (2004).** Structural and functional characterization of the dimerization region of soluble guanylyl cyclase. *J Biol Chem* **279**, 24935-43.

**Ziegelberger, G., van den Berg, M. J., Kaissling, K. E., Klumpp, S. and**

**Schultz, J. E. (1990).** Cyclic GMP levels and guanylate cyclase activity in pheromone-sensitive antennae of the silkmoths *Antheraea polyphemus* and *Bombyx mori*. *J Neurosci* **10**, 1217-25.

**Zitnan, D., Kingan, T. G., Hermesman, J. L. and Adams, M. E. (1996).**

Identification of ecdysis-triggering hormone from an epitracheal endocrine system. *Science* **271**, 88-91.